Faculty of Energy and Environmental Engineering
Department of Air Protection

DOCTORAL DISSERTATION

Determination of the mechanism and optimization of the conditions of the process of removing colored aromatic compounds by selected Basidiomycota

Author:

M.Sc. Ruchi Manishkumar Upadhyay

Supervisor:

Prof. dr hab. inż. Wioletta Przystaś,

A doctoral dissertation submitted to
Department of Air Protection,
Faculty of Energy and Environmental Engineering,
Silesian University of Technology, Poland

Gliwice, 2026

ACKNOWLEDGEMENT

I would like to express my deepest and most sincere gratitude to my PhD supervisor - **Prof. Wioletta Przystaś** for her invaluable guidance, continuous support, and constant motivation throughout the course of this research. Her insightful suggestions, research expertise, and encouragement played a crucial role in helping me achieve this milestone. Beyond academic mentorship, she demonstrated exceptional understanding and support during my personal challenges, for which I am profoundly grateful.

I am also thankful to HOD and all the staff members of the **Department of Air Protection** for their continuous support, cooperation, and guidance throughout my doctoral studies. My sincere appreciation is extended to the **Faculty of Energy and Environmental Engineering** for providing the necessary laboratory facilities, technical resources, and financial support essential for the successful completion of this PhD research. I also gratefully acknowledge the **Joint Doctoral School** for their academic and administrative support throughout this journey.

I would like to extend my heartfelt gratitude to my research collaborators - **Prof. Grzegorz Janusz** (Maria Curie-Skłodowska University, Lublin), **Prof. Gaurav Sanghvi** (Marwadi University, Rajkot, India), **Prof. Magdalena Skonieczna**, and **Dr. Roman Turczyn** (Silesian University of Technology, Gliwice) - for providing the opportunity to undertake scientific internships and for their invaluable support with experiments, instrumentation, and scientific discussions, which significantly contributed to this work. I sincerely thank **Dr. Marcelina Jureczko** for her valuable technical assistance and timely support whenever required during the course of this research.

Finally, I would like to express my heartfelt gratitude to my parents, in-laws, family members, and friends for their patience, understanding, and constant encouragement. My deepest gratitude goes to my pillar of strength- my husband **Mr. Nisarg Mehta** - whose unwavering support and belief in me made this journey possible. I dedicate my sincere love to my son- **Advait Mehta**, whose precious time I shared for the completion of this thesis.

TABLE OF CONTENTS

ABSTRACT

Synthetic dyes constitute a major environmental and public health threat due to their extensive industrial use, chemical recalcitrance, and toxicological effects on aquatic ecosystems and human health. Approximately 100,000 tons of dyes are released annually from dye-intensive industries, and in many low- and middle-income countries up to 80% of dye-containing wastewater is discharged untreated. Conventional physicochemical treatment methods are often costly, energy-intensive, and generate secondary pollution. This doctoral research investigates white-rot fungi as a sustainable biological alternative for the remediation of synthetic dye-contaminated wastewater, with particular emphasis on mechanistic understanding, process optimization and toxicity reduction.

Decolorization of dyes representing three major structural classes-azo (Evans Blue(EB), Congo Red(CR)), triphenylmethane (Brilliant Green(BG), Crystal Violet(CV)), and anthraquinone (Remazol Brilliant Blue R (RBBR))-was evaluated using *Trametes versicolor* (CB8) and *Pleurotus ostreatus* (BWPH) strains. Dye removal occurred through biodegradation and biosorption mechanisms. Optimization of operational parameters (pH, temperature, agitation, dye concentration, carbon and nitrogen sources, immobilization carrier, and biomass formulation) revealed that sponge-immobilized *T. versicolor* grown in regular medium (CB8/S2) achieved the highest decolorization efficiencies (~96%) for RBBR, Evans Blue, and Crystal Violet, followed by *T. versicolor* under shaking conditions (~90%). *P. ostreatus* showed moderate efficiencies (82–90%) under comparable conditions. ANOVA analysis confirmed that fungal species, carbon source, and nitrogen source significantly influenced decolorization ($p < 0.05$), with nitrogen source exhibiting a highly significant effect ($F = 226.64$, $p < 0.001$). Ecotoxicological assays using *Daphnia magna* and *Spirodela polyrhiza* demonstrated significant toxicity reduction in treated effluents (from Persoone class IV to III for RBBR dye via both fungal strains). Hence, post treated samples are environmentally safer than pure dye. CB8/S2 produced the highest laccase activity (20 U/L) after 96 h incubation with RBBR. Spearman correlation analysis showed strong but statistically non-significant correlations between laccase activity and RBBR decolorization ($\rho = 0.771$, $p = 0.072$) and between MnP activity and decolorization ($\rho = 0.771$, $p = 0.072$), while LiP activity showed negligible correlation ($\rho = 0.086$, $p = 0.872$), indicating that extracellular enzyme activity alone does not fully explain dye removal efficiency.

Despite extensive research on fungal dye decolorization, the molecular mechanisms underlying dye-specific metabolic adaptation in white-rot fungi remain poorly understood, particularly at the systems biology level. In this study, integrated transcriptomic and proteomic analyses were employed to elucidate the global cellular response of *T. versicolor* during the biodegradation of structurally distinct dyes, RBBR and EB. Transcriptomic analysis revealed extensive differential gene expression response, with 1,106 and 1,830 genes differentially expressed ($|fc| \geq 2$, $p < 0.05$) in *T. versicolor* during RBBR and Evans Blue degradation, respectively. Upregulated genes included cytochrome P450 monooxygenases, NAD(P)H-dependent oxidoreductases, keto reductases, and aldehyde dehydrogenases, along with transport-related genes. Concurrent downregulation of genes involved in cell cycle progression, cytoskeletal

organization, and DNA replication indicated growth suppression under dye stress. Proteomic analysis corroborated transcriptomic trends, revealing dye-specific metabolic reprogramming, conserved stress responses involving P450s and ABC transporters, and enhanced peroxidase dependence during RBBR degradation. Collectively, this multi-omics approach provides novel mechanistic insights into fungal dye biodegradation, demonstrating that dye removal by white-rot fungi involves complex intracellular regulatory networks that have not been previously characterized at this depth.

Biosorption studies demonstrated that sponge-immobilized live biosorbents (CB8/S2-BS) exhibited superior performance for triphenylmethane dyes. CB8/S2-BS achieved maximum sorption capacities of 379.4 mg/g for BG and 48.9 mg/g for CV at 400 mg/L, removing up to 90.3% and 43.9% of dyes within 6 h, which is 3-5 times higher than self-immobilized biosorbents. FT-IR analysis confirmed hydrogen bonding and electrostatic interactions as dominant binding mechanisms, and biosorbents showed effective reusability without additional treatment. Bioreactor-scale studies confirmed operational feasibility, reduced costs, and high treatment efficiency under optimized conditions.

This research delivers integrated mechanistic insights into fungal dye remediation, effectively bridging laboratory-scale findings with industrial applicability. Importantly, this work establishes a scalable framework for incorporating white-rot fungi into wastewater treatment infrastructure while advancing understanding of intracellular detoxification and transporter-mediated processes that extend beyond traditional extracellular enzyme-centric models. The results may support the development of tailored, decentralized fungal bioreactor systems optimized for specific dye classes and contribute directly to the achievement of UN Sustainable Development Goals (SDGs 6, 12, and 14).

Keywords: mycoremediation; white-rot fungi; synthetic dyes; biodegradation; biosorption; transcriptomics; proteomics; ecotoxicology; wastewater treatment; *Trametes versicolor*; *Pleurotus ostreatus*

STRESZCZENIE

Barwniki syntetyczne stanowią poważne zagrożenie dla środowiska i zdrowia publicznego ze względu na ich szerokie zastosowanie przemysłowe, stabilność chemiczną oraz toksyczny wpływ na ekosystemy wodne i zdrowie ludzi. Około 100 000 ton barwników jest uwalnianych rocznie przez przemysły intensywnie wykorzystujące barwniki, a w wielu krajach, o niskich i średnich dochodach, nawet 80% ścieków zawierających barwniki jest odprowadzanych bez oczyszczania. Konwencjonalne fizykochemiczne metody oczyszczania są często kosztowne, energochłonne i generują wtórne zanieczyszczenia. Niniejsza rozprawa doktorska dotyczy grzybów białej zgnilizny drewna jako zrównoważonej biologicznie alternatywę dla oczyszczania ścieków zanieczyszczonych barwnikami syntetycznymi, ze szczególnym naciskiem na zrozumienie mechanizmów, optymalizację procesów i redukcję ekotoksyczności.

Odbarwianie barwników reprezentujących trzy główne klasy strukturalne - azowe (błękit Evansa (EB), czerwień Kongo (CR)), trifenylometanowe (zieleń brylantowa (BG), fiolet krystaliczny (CV)) i antrachinonowe (błękit brylantowy Remazol R (RBBR)) - oceniano przy zastosowaniu *Trametes versicolor* (CB8) i *Pleurotus ostreatus* (BWPH). Usuwanie barwników następowało poprzez mechanizmy biodegradacji i biosorpcji. Optymalizacja parametrów operacyjnych (pH, temperatura, mieszanie, stężenie barwnika, źródła węgla i azotu, nośnik do immobilizacji i rodzaj biomasy) wykazała, że immobilizowany na gąbce *T. versicolor* hodowany w standardowym podłożu (CB8/S2) osiągnął najwyższą wydajność odbarwiania (~96%) dla RBBR, błękitu Evansa i fioletu krystalicznego, a następnie *T. versicolor* w warunkach wytrząsania (~90%). *P. ostreatus* wykazał umiarkowaną wydajność (82-90%) w porównywalnych warunkach. Analiza ANOVA potwierdziła, że gatunek grzyba, źródło węgla i źródło azotu istotnie wpływały na odbarwianie ($p < 0,05$), przy czym źródło azotu wykazywało wysoce istotny wpływ ($F = 226,64$, $p < 0,001$). Badania ekotoksykologiczne z użyciem *Daphnia magna* i *Spirodela polyrhiza* wykazały istotną redukcję toksyczności w oczyszczonych ściekach (od klasy IV do III według Persoone dla barwnika RBBR przez oba szczepy grzybów). Dlatego też próbki poddane dodatkowej obróbce są bezpieczniejsze dla środowiska niż czysty barwnik. CB8/S2 wykazał najwyższą aktywność lakazy (20 U/l) po 96 godzinach inkubacji z RBBR. Analiza korelacji Spearmana wykazała silne, ale statystycznie nieistotne korelacje między aktywnością lakazy a dekoloryzacją RBBR ($\rho = 0,771$, $p = 0,072$) oraz między aktywnością MnP a dekoloryzacją ($\rho = 0,771$, $p = 0,072$), podczas gdy aktywność LiP wykazała nieistotną korelację ($\rho = 0,086$, $p = 0,872$), co wskazuje, że sama aktywność enzymów zewnątrzkomórkowych nie wyjaśnia w pełni skuteczności usuwania barwnika.

Pomimo szeroko zakrojonych badań nad dekoloryzacją barwników grzybowych, mechanizmy molekularne leżące u podstaw specyficznej dla barwników adaptacji metabolicznej grzybów białej zgnilizny drewna pozostają słabo poznane, szczególnie na poziomie biologii systemów. W niniejszym badaniu wykorzystano zintegrowane analizy transkryptomowe i proteomiczne w celu wyjaśnienia zmian odpowiedzi komórkowej *T. versicolor* podczas biodegradacji strukturalnie odmiennych barwników, RBBR i EB. Analiza transkryptomiczna ujawniła rozległą zróżnicowaną odpowiedź ekspresji genów, z różnicą ekspresji genów wynoszącą 1106 i 1830 ($|fc| \geq 2$, $p < 0,05$) u *T. versicolor* odpowiednio podczas degradacji RBBR i błękitu

Evansa. Wśród genów o podwyższonej ekspresji znalazły się monooksygenazy cytochromu P450, oksydoreduktazy zależne od NAD(P)H, ketoreduktazy i dehydrogenazy aldehydowe, a także geny związane z transportem. Jednoczesne obniżenie ekspresji genów zaangażowanych w progresję cyklu komórkowego, organizację cytoszkieletu i replikację DNA wskazało na zahamowanie wzrostu pod wpływem stresu barwnikowego. Analiza proteomiczna potwierdziła trendy transkryptomiczne, ujawniając specyficzne dla barwnika przeprogramowanie metaboliczne, konserwatywne reakcje w odpowiedzi na stres z udziałem transporterów P450 i ABC oraz zwiększoną zależność od peroksydaz podczas degradacji RBBR. Łącznie takie multiomiczne podejście dostarcza nowych spostrzeżeń na temat biodegradacji barwników z udziałem grzybów, wykazując, że usuwanie barwników przez grzyby powodujące białą zgniliznę drewna wiąże się ze złożonymi wewnątrzkomórkowymi zmianami regulacyjnymi, które dotychczas nie zostały scharakteryzowane na tak głębokim poziomie.

Badania biosorpcji wykazały, że żywa biomasa w postaci biosorbentów immobilizowanych na gąbce (CB8/S2-BS) charakteryzowała się lepszą wydajnością w przypadku barwników trifenylometanowych. CB8/S2-BS osiągnął maksymalną zdolność sorpcyjną wynoszącą 379,4 mg/g dla BG i 48,9 mg/g dla CV przy stężeniu 400 mg/l, usuwając do 90,3% i 43,9% barwników w ciągu 6 godzin, co jest wynikiem 3-5 razy lepszym niż w przypadku biosorbentów immobilizowanych bez sztucznego nośnika. Analiza FT-IR potwierdziła, że dominującymi mechanizmami są powstające wiązania wodorowe i oddziaływania elektrostatyczne, a biosorbenty można skutecznie ponownie wykorzystać bez konieczności dodatkowego oczyszczania. Badania w skali bioreaktora potwierdziły wykonalność operacyjną, obniżone koszty i wysoką wydajność oczyszczania w zoptymalizowanych warunkach.
Badania te dostarczają zintegrowanej wiedzy na temat mechanizmu eliminacji barwników z udziałem grzybów, skutecznie łącząc wyniki badań prowadzonych w skali laboratoryjnej z możliwościami zastosowania przemysłowego. Co ważne, prace te ustanawiają skalowalne ramy dla włączenia grzybów białej zgnilizny do infrastruktury oczyszczania ścieków, jednocześnie pogłębiając wiedzę na temat detoksykacji wewnątrzkomórkowej i procesów zależnych od transporterów, wykraczających poza tradycyjne modele zewnątrzkomórkowe, skoncentrowane na enzymach. Wyniki mogą wspierać rozwój dostosowanych, zdecentralizowanych systemów bioreaktorów grzybowych, zoptymalizowanych pod kątem określonych klas barwników i przyczyniają się bezpośrednio do osiągnięcia Celów Zrównoważonego Rozwoju ONZ (SDGs 6, 12 i 14).

Słowa kluczowe: mykoremediacja; grzyby powodujące białą zgniliznę; barwniki syntetyczne; biodegradacja; biosorpcja; transkryptomika; proteomika; ekotoksykologia; oczyszczanie ścieków; *Trametes versicolor*; *Pleurotus ostreatus*

PREFACE

LIST OF PUBLICATIONS

Publication 1: Upadhyay R.*, Przystaś W. An evaluation of decolorization mechanism of synthetic dyes belonging to azo, anthraquinone and triphenylmethane group, as a sustainable approach, by immobilized CB8 strain (*Trametes versicolor*), *Desalination and Water Treatment*, **2023**, 284, 268–277. doi: 10.5004/dwt.2023.29270, (MNiE: 100 points, IF- 1.2)

Publication 2: Upadhyay, R.*, Przystaś, W. & Dave, B. Myco-remediation of synthetic dyes: a comprehensive review on contaminant alleviation mechanism, kinetic study and toxicity analysis. *International Journal of Environmental Science and Technology*, **2025**, 22, 521–538. https://doi.org/10.1007/s13762-024-05793-4. (MNiE: 70 points, IF-3.0)

Publication 3: Upadhyay, R.*, Przystaś, W., Turczyn, R., & Jureczko, M. Enhanced Biosorption of Triarylmethane Dyes by Immobilized *Trametes versicolor* and *Pleurotus ostreatus*: Optimization, Kinetics, and Reusability. *Water*, **2025**, *17*(17), 2600. https://doi.org/10.3390/w17172600 (MNiE: 100 points, IF-3.0)

Publication 4: Upadhyay, R.*, & Przystaś, W. Decolorization of two dyes using white-rot fungus *P. ostreatus* (BWPH) strain and evaluation of zootoxicity of post process samples. *Architecture Civil Engineering Environment*, **2022**, *15*(3). doi: 10.2478/ACEE-2022-0033 (MNiE: 70 points, IF- 0.5)

FUNDING INFORMATION

The research was funded by Faculty of Energy and Environmental Engineering, Silesian University of Technology, Poland under project numbers:

BKM-668/RIE7/2021, BKM- 676/RIE2/2022, BKM 631/RIE2/2023, 08/020/BKM_23/0034.

LIST OF ABBREVIATIONS

Abbreviation	Full Form
A	Autoclaved/dead biomass
ANM	Ammonium Nitrate Medium
BG	Brilliant Green
BS	Biosorbents
BWPH-BS	Self-immobilized *P. ostreatus* BWPH biosorbents
BWPH/S1	Immobilized *P. ostreatus* BWPH on dishwasher
BWPH/S2	Immobilized *P. ostreatus* BWPH on sponge
BWPH/S2-BS	Immobilized *P. ostreatus* BWPH sponge biosorbents
BWPH/SH	Self-immobilized *P. ostreatus* BWPH biomass
BWPH/ST	Free *P. ostreatus* BWPH Biomass
CB8-BS	Self-immobilized *T. versicolor* CB8 biosorbents
CB8/S1	Immobilized *T. versicolor CB8* on dishwasher
CB8/S2	Immobilized *T. versicolor CB8* on sponge
CB8/S2-BS	Immobilized *T. versicolor CB8* sponge biosorbents
CB8/SH	Self-immobilized *T. versicolor* CB8 biomass
CB8/ST	Free *T. versicolor CB8* Biomass
CR	Congo Red
CV	Crystal Violet
DP	Total Decolorization Percentage
DS	Desorption percentage
EB	Evans Blue
GM	Glucose Medium
L	Live biomass
MWCO	Molecular weight cut-off
RBBR	Remazol Brilliant Blue R
RM	Regular Medium
S1	Support 1- Dishwasher
S2	Support 2- Sponge
SH	Shaking growth condition
SM	Sucrose Medium
ST	Static growth condition
WRF	White-Rot Fungi
YEM	Yeast Extract Medium

CHAPTER 1
INTRODUCTION

Rapid urbanization and industrialization have effectively met a wide range of human needs, from leather and textiles to food and medicine [1,2]. Global demand for vibrantly colored items necessitates the use of various synthetic dyes. The introduction of synthetic dyes in 1856, exemplified by William Henry Perkin's serendipitous discovery of mauve, signified a crucial turning point in dye history [3,4]. Since then, more than 10,000 different kinds of dyes have been synthesized, with a global production capacity of over 1,000,000 tons per year. The textile, rubber, leather tanning, paper, culinary, pharmaceutical, and cosmetic sectors all make extensive use of this variety of synthetic dyes [5]. The Gross Domestic Product of emerging nations is greatly boosted by the textile sector, which also generates a sizable amount of export income and job possibilities.

Nevertheless, these benefits of the industrial revolution come at a high ecological cost. About 70 billion tons of wastewater containing dyes are produced each year, and the textile industry alone uses 80% of the synthetic dyes produced [6]. Bangladesh, India, and China are among the regions with a concentrated textile sector that generate an estimated 3.5 billion tonnes of wastewater each year [7]. Only 10-15% of dye truly binds to textiles; the remainder ends up in effluents. Consequently, around 100,000 tons of dye are released into the environment every year [8]. Each year, over 280,000 tons of dye end up in surface waters. Because synthetic dyes exacerbate water contamination, wastewater containing dyes is a major environmental problem that significantly impedes sustainable development and need immediate effective treatment for dye removal due to growing water scarcity difficulties [9].

Synthetic dyes are incredibly resilient and persistent in ecosystems due to their aromatic properties and resistance to biodegradation [10]. By blocking light penetration, which prevents water plants and algae from photosynthesising, they upset food cycles. Toxic impacts, including allergies, asthma, and cancer risks, can affect both people and wildlife [11]. In low- and middle-income nations, up to 80% of dye-polluted wastewater is dumped untreated, which is alarming [12]. In recent years, elucidation of water quality management has rapidly progressed, since it has become a prime research interest due to exponentially increasing water pollution problems. As part of such efforts, the regulation and abatement of highly toxic and hazardous pollutants, such as dyes, have been recognized as pivotal tasks by major environmental agencies and organizations, including the United States Environmental Protection Agency (US EPA) [5,13]. Policy responses to this worldwide environmental disaster include the UN Sustainable Development Goals and the EU Green Deal, which place a strong emphasis on preserving ecosystems and lowering pollution in the air, water, and soil. Achieving the Sustainable Development Goals (SDGs) of the UN, which prioritize access to clean water (SDG 6) and good health (SDG 3), requires the remediation of wastewater containing dyes for safe discharge as well as the recovery of dyes and salts from wastewater.

There is an urgent requirement for developing dye containing wastewater treatment technologies. Although primary focus of current research on treating wastewater containing dyes is on the removal or degradation of dyes using traditional chemical, biological, and physical methods, there is a requirement for development of decentralized wastewater treatment specifically designed to dye containing wastewater. Traditional methods, which are generally employed for the low-risk discharge of wastewater containing dyes, include coagulation, advanced oxidation processes, microbial degradation, adsorption, and membrane filtration [14–18], however, different types of dyes require different degradation methods. When choosing appropriate removal and/or degradation methods, procedures, and operating circumstances, it is important to take into account the chemical makeup of dyes, particularly their structure and solubility. The use of natural and/or recombinant microbes to break down hazardous substances by microorganisms offers easy working conditions and a great deal of versatility in experiment design. Because this method uses microbes' natural metabolic ability to convert xenobiotic substances into innocuous compounds (such CO_2 and water) through mineralization or biotransformation [19], it is thought to be environmentally safe. Among microorganisms, attention should also be paid to fungi, the use of which has often been overlooked so far, but has many advantages. Mycoremediation is notable for its low infrastructure needs, cost-effectiveness, decentralization, and environmental friendliness [20].

Hence, research focus of this thesis is about white-rot fungi's ability to remove dyes through a synergistic mechanism of biosorption and enzymatic biodegradation needs further optimization and mechanistic insight. These fungi can be efficiently transformed into small, decentralized bioreactor systems made for particular dye types. Additionally, the ecotoxicological effects of the treated effluents is essential to examine to ensure environmental safety and regulatory compliance. To understand the relationship between gene expression and enzyme profile, which might serve as the foundation for predictive modelling of the interactions between fungal enzymes and various dye classes, multi-omics research must be explored in this field. Using multi-omics techniques such as transcriptomics, proteomics, and metabolomics can further improve the prediction and effectiveness of fungal dye removal. Predictive models of enzyme-dye interactions can be developed by using these methods to decipher the intricate regulatory networks that connect gene expression to enzyme secretion. These discoveries can direct the enzyme formulations or genetically modified fungal strains with better catalytic activity and specificity. Fungal-based wastewater treatment technologies may soon undergo a revolution if these biological systems are integrated with AI-driven process control.

CHAPTER 2
REVIEW OF LITERATURE

2.1 Cultural History of Dyes

Dyes are crucial substances utilized across multiple industries, such as textiles, printing, cosmetics, and food, to impart color to substrates [21]. Dyes are chromophoric compounds that can chemically or physically interact with substrates, causing selective absorption of specific light wavelengths and producing color [22,23]. The utilization of dyes has historically been an essential aspect of human culture. This complex domain, at the intersection of science, art, culture, and industry, has influenced communities, economies, and artistic expressions throughout history.

Dyeing techniques have been documented in numerous cultures globally, utilizing natural substances to produce vivid and long-lasting hues. These activities, grounded in tradition and necessity, established the basis for the evolution of dyeing procedures. India is known in Asia for its extensive legacy of natural dyeing. The nation generates a wide spectrum of different colors utilizing botanical sources like indigo, turmeric, and madder root [24]. Moreover, conventional techniques such as tie-dyeing and block printing are used in areas such as Rajasthan and Gujarat [25]. Kente fabric is a prominent illustration of traditional African dyeing techniques in West African nations such as Ghana [26]. Europe and the United Kingdom are also included. Renowned for its ancient tartans, Scotland possesses a history of dyeing wool with natural plant dyes such as heather, moss, and lichen [27]. The esteemed "Royal Purple" dye, extracted from the secretions of murex mollusks, was much valued and represented royalty in numerous ancient civilizations, such as the Phoenicians and Romans [28,29]. Indigenous societies in Central and South America, including the Incas and Aztecs, derived colors from cochineal insects and annatto seeds, producing red, orange, and yellow pigments [30]. These dyes were utilized not just for textiles but also for art, ceramics, and body adornment.

2.2 Natural Dyes

The development of dyes exemplifies human inventiveness in utilizing natural resources. The ancient civilizations utilized botanical, mineral, and animal-derived materials to impart color to fabrics (Figure 1), rendering them biodegradable, renewable, and environmentally sustainable [31,32]. Moreover, their production often entails minimal chemical processes, thus diminishing pollution. Regarding health issues, natural dyes are often non-toxic and hypoallergenic, rendering them safer for usage, particularly in fabrics that contact the skin [33]. Individuals with sensitivities or allergies frequently favor items containing natural dyes [34].

2.3 Synthetic Dyes: Structure, Origin and Classification

As societies expanded and networked via trade and exploration, the demand for a wider array of colors prompted the discovery of new dye sources and extraction methods [35]. These advances established the groundwork for the prosperous textile industries of the Middle Ages and the later development of a global market for dyes. The introduction of synthetic dyes in 1856, exemplified by William Henry Perkin's serendipitous discovery of mauve, signified a crucial turning point in dye history [3,4]. This scientific accomplishment changed the textile business and transformed the field of chemistry, catalyzing the development of novel synthesis procedures and advancing color theory. Synthetic dyes are produced from petrochemicals, leading to environmental contamination and containing hazardous substances, including heavy metals and carcinogens, which may provide health hazards, especially with extended exposure or ingestion [36–38]. Moreover, natural dyes typically yield distinctive, muted, and organic aesthetics, however they generally do not achieve the distinct brightness associated with synthetic colors [39,40]. Synthetic dyes are demonstrated to be more advantageous due to their durability against numerous washes, resistance to sunlight exposure, cost-effective manufacture owing to the availability of raw ingredients, and highly efficient manufacturing procedures. The cost-effectiveness of synthetic dyes renders them extensively utilized throughout multiple industries, such as textiles, printing, and cosmetics.

Synthetic dyes can be categorized primarily according to the chemical structure of their chromophore and the application method used for various fiber types, as illustrated in Figure 1. Preliminary details of classification have been published in **Publication 2** [41].

2.3.1 Classification According to Chemical Composition

The chemical composition of dyes dictates their chromophores - the molecular components responsible for color and affects their reactivity, stability, and environmental behaviour [42].

Azo dyes are the predominant category of synthetic dyes, distinguished by the presence of one or more azo bonds (-N=N-) connecting aromatic rings [43,44]. These dyes are favoured for their extensive color spectrum, especially red, orange, and yellow, as well as their economical manufacturing process [45]. For example: Congo Red, Methyl Orange, Evans Blue, Disazo Red.

Anthraquinone dyes represent a significant category characterized by an anthraquinone core, comprising a three-ring aromatic structure. These dyes are recognized for yielding distinct blue and green hues, exhibiting superior lightfastness and chemical stability[10]. Their molecular stiffness and electron distribution render them especially appropriate for coloring synthetic fabrics and polymers [46]. For example, Remazol Brilliant Blue R, Alizarin Red, Disperse Blue.

Triphenylmethane dyes feature a central carbon atom covalently bound to three phenyl groups and are recognized for their brilliant and vibrant colors, including green, violet, and blue [47].

Despite their visual appeal, they generally exhibit inadequate resistance to light and environmental deterioration. These dyes are frequently utilized in paper, cosmetics, biological stains, and occasionally textiles [48], nonetheless, certain members of this class have been identified as poisonous or mutagenic. For example, Crystal Violet and Brilliant Green.

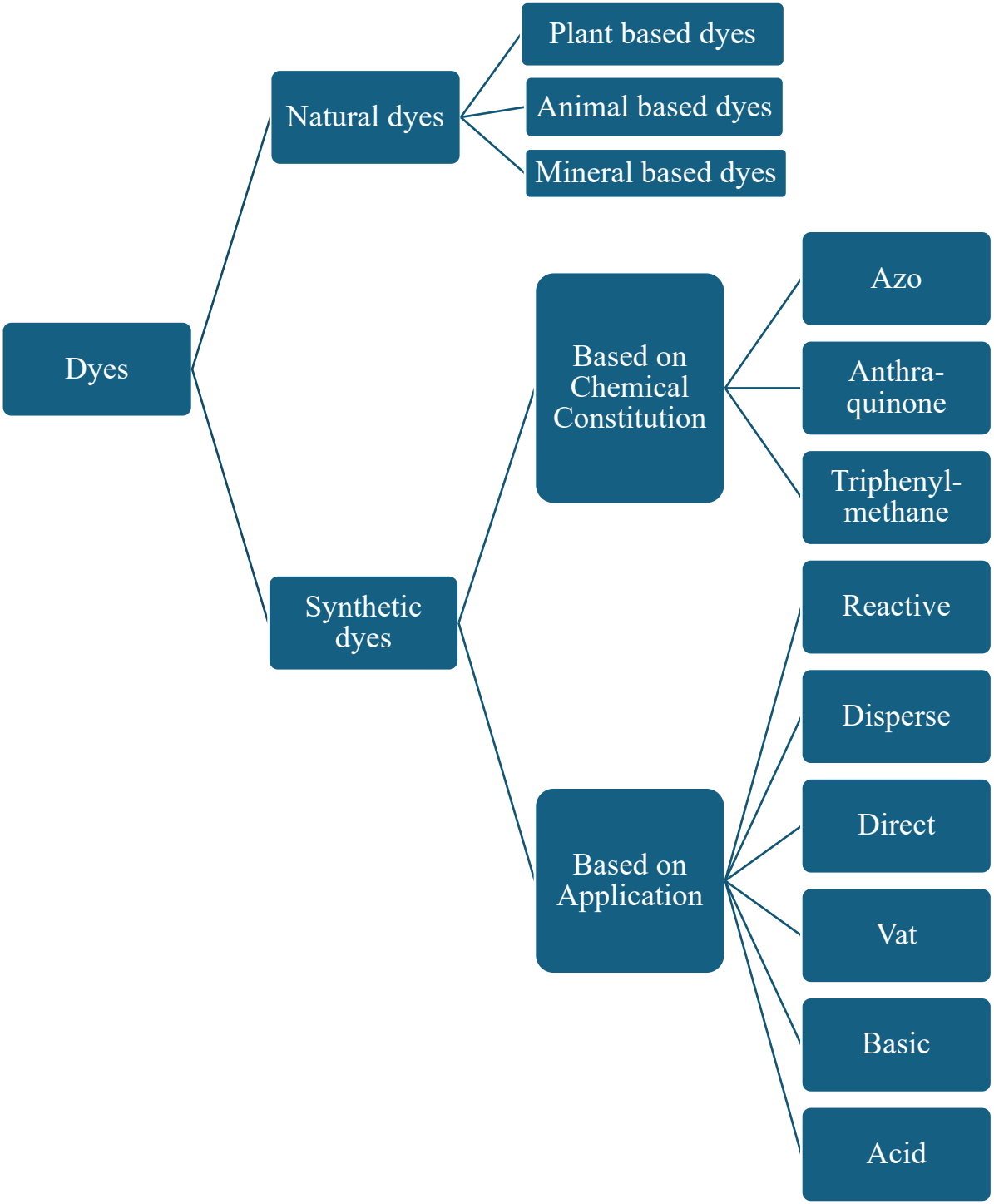

Figure 1. Classification of Natural and Synthetic dyes based on source, chemical constitution and application (Published in **Publication 2**)

2.3.2 Classification According to Application Method

The second principal classification is determined by the method of dye application to fibers, principally influenced by the dye's solubility and the chemical composition of the fiber.

Direct dyes are water-soluble pigments that can be directly applied to cellulose fibers, such as cotton, in a neutral or mildly alkaline solution. They adhere to the fiber by hydrogen bonding and Van der Waals forces, and are comparatively user-friendly [21].

Vat dyes are insoluble in water in their initial state and necessitate chemical reduction in an alkaline solution to achieve their soluble leuco form before to application. Upon the dye's infiltration into the fiber, it is re-oxidized to its initial insoluble state [49]. Vat dyes are predominantly utilized on cellulosic fibers such as cotton and are recognized for their superior light and wash fastness. An example is indigo, extensively utilized in denim manufacturing.

Basic dyes, or cationic dyes, carry a positive charge and are especially effective on materials with anionic sites, including acrylic fibers and certain protein fibers such as wool and silk [50]. These dyes yield vibrant and deep hues but frequently exhibit inadequate lightfastness, restricting their applicability in contexts necessitating high durability.

Acid dyes are anionic and are utilized from an acidic solution, rendering them appropriate for protein fibers such as wool and silk, in addition to nylon. The dye molecules adhere to the fibers via ionic interactions with the positively charged amino groups present on the fiber [51]. Acid dyes are recognized for their vibrancy and consistent coloring, however they may necessitate mordants or post-treatment to improve wash fastness.

Reactive dyes are distinctive as they establish covalent connections with fiber molecules, usually with the hydroxyl groups in cellulose or the amino groups in protein fibers. This yields superior wash fastness when the dye integrates with the fiber. Reactive dyes are prevalent in cotton dyeing and are esteemed for their vibrant hues, adaptability, and durability [52].

Disperse dyes are non-ionic and have limited solubility in water. They are utilized on hydrophobic synthetic fibers, including polyester, acetate, and nylon, as fine dispersions. The dye particles integrate into the fiber at elevated temperatures, rendering these dyes especially appropriate for thermoplastic composites [53]. They provide excellent color fastness and are widely utilized in the production of synthetic textiles.

2.4 Detrimental impacts of dyes on Ecosystem and human health

Ecosystems are significantly and extensively impacted when wastewater containing synthetic dyes is released into the environment [54]. These dyes, which mostly come from the textile, leather, paper, and plastics industries, are persistent pollutants in natural habitats because they are frequently poisonous, non-biodegradable, and chemically stable [55]. Through the transportation pathway from water and soil to food for human consumption, the discharge of untreated synthetic dyes into aquatic habitats can pose serious ecotoxicological and health

concerns to humans [5]. Preliminary data regarding adverse environmental impacts of synthetic dyes have been discussed and published as review article- **Publication 2** [41].

Even at low quantities, dye effluents that are released into rivers, lakes, and seas change the quality of the water by adding vibrant coloration. As a result, less light can reach aquatic plants and phytoplankton, which are important producers in aquatic food webs, making photosynthesis more difficult [11,56]. When high biological oxygen demand (BOD) and chemical oxygen demand (COD) are combined with the consequent decrease in oxygen production, oxygen depletion happens, resulting in hypoxic or anoxic conditions that are inappropriate for aquatic life [57,58]. Both aquatic and terrestrial organisms are poisoned by a lot of synthetic dyes and the byproducts of their degradation. They can affect fish, amphibians, and invertebrates' ability to reproduce, grow, and behave [59]. Dye deposits in fish brains, lateral lines, or gills can have toxicological effects such respiratory distress, liver damage, kidney malfunction, and uncoordinated movement. These toxicological effects impair the fish's reproductive rate in addition to lowering its fat and protein content [60,61]. Additionally, some dyes bioaccumulate in small living organisms, endangering humans and other higher-ranking predators. *Lemna gibba*, a common duckweed, has poor photosynthetic efficiency when dyes are present, and necrosis, chlorosis, and frond detachment are dye-related consequences that have also been noted [62]. Contaminated soils and sediments can also damage soil microbes, decrease microbial diversity, and hinder plant development. Sensitive species decrease and habitat deterioration are caused in part by persistent dye pollution. Fish, benthic animals, algae, and aquatic plants are especially susceptible to the harmful and light-blocking effects of dyes. This eventually causes local ecosystems to collapse and biodiversity to decline. Invasive or dye-tolerant organisms may occasionally take over, further upsetting the ecosystem. The microbial communities found in soil and water are essential to the cycling of nutrients. Synthetic dyes disrupt the nitrogen and carbon cycles by interfering with microbial metabolism and enzyme activity. The entire ecological balance, plant productivity, and soil fertility are all impacted by this disturbance [37,63].

Human exposure to synthetic dyes occurs through contaminated drinking water, consumption of aquatic organisms, dermal contact, and inhalation of dye particles. Long-term exposure to synthetic dyes can cause hormonal and reproductive disturbance, skin and respiratory disorders, and carcinogenic and mutagenic effects [64,65]. Cancers such bladder, liver, and colon cancer have been connected to specific azo dyes and the aromatic amine metabolites they produce. These substances may result in chromosomal abnormalities and genetic mutations. Textile workers and other susceptible individuals (including children and those with underlying medical conditions) are at risk for respiratory issues, dermatitis, and skin irritation due to prolonged exposure to dye dust or vapors, especially in Asia and Africa, including India, China, Bangladesh, Vietnam, Sri Lanka, Mauritius, and Nigeria [66,67]. Neurotoxicity and developmental abnormalities, particularly in children, have been linked to prolonged exposure to synthetic colors and their metabolites [68]. Particularly in female mammals, the dye gentian violet, has an innate carcinogenic nature that may result in ovarian atrophy, gland adenoma, reticulum cell sarcomas, and hepatocarcinoma in the bladder, ovaries, uterus, and vagina [69].

Different synthetic dyes typically have differing levels of cytotoxicity, neurotoxicity, genotoxicity, and carcinogenic hazards, all of which could have a negative effect on human health. Therefore, policy laws should forbid the release of wastewater that contains dyes that has not been treated. Modern wastewater treatment methods ought to be used to provide for safe discharge and protect ecosystems and people. Resolving the issue of negative impact of dyes on ecosystem corresponds with multiple United Nations Sustainable Development Goals (SDGs), particularly:

- SDG 6: Ensure the availability and sustainable management of water and sanitation for all.
- SDG 12: Guarantee sustainable consumption and production practices.
- SDG 14: Preserve and utilize oceans, seas, and marine resources sustainably.

2.5 Characteristic of dye containing wastewater and its permissible limits

A mixture of metals, dyes, and other contaminants make up the effluents released by textile or leather factories. Color, pH, suspended solids (SS), chemical oxygen demand (COD), biochemical oxygen demand (BOD), metals, temperature, and salts are all high in the dye effluents (Table 1). Therefore, before releasing the related effluent into the receiving water body, it is crucial to monitor these parameters during the treatment operations and compare them with the standard concentrations. The maximum allowable limits set by several nations for the release of textile wastewater are displayed in Table 2. Typically, BOD is controlled between 20 and 150 mg/L. The typical range for COD regulation is 8-250 mg/L. Between six and nine units is the range in which the pH is controlled. The range of 50 to 550 Pt-Co units controls the color. Some nations do not control this metric, indicating a legislative contradiction. The majority of the metrics are outside of the allowable limits (Table 2) when comparing the physicochemical properties of raw wastewater from the textile sector (Table 1). The acceptable bounds of these parameters vary depending on the regulation, and There is no control over the dye concentration.

To control such activities from the industries, the government of India through the Central Pollution Control Board (CPCB) has brought few regulations for wastewater discharge. According to the CPCB, the allowable limit of the textile dye wastewater discharge is reported as; total suspended solids (TSS): 100 mg/L, color: 5 mg/L, total dissolved solids (TDS): 2000 mg/L, chemical oxygen demand (COD): 250 mg/L, biochemical oxygen demand (BOD): 30 mg/L [70,71].

Table 1. Physicochemical characteristics of real textile wastewater

Country	Characteristics							Reference
	pH	Temp. (°C)	BOD (mg/L)	COD (mg/L)	TSS (mg/L)	Turbidity (NTU)	Color	
India	8.6-9.2	28-29	1206-1750	3880-4400	550-650	12.5-16.6	ND	[72]
Italy	9.0		9.8	1017	ND	ND	0.66	[73]
Croatia	7.28		395	1338	93	90	ND	[74]
China	7.1		ND	112	ND	ND	ND	[75]
Brazil	11.4-12.3		ND	ND		1665-2484	1180-1576	[76]
Turkey	8-9.5		ND	700-1250	ND	ND	500-1250	[77]

(ND - Not determined)

Table 2. Permissible limit of textile wastewater

Country	Standard reference	Characteristics							Refer-ence
		pH	Temp (°C)	BOD (mg/L)	COD (mg/L)	TSS	TDS	Color	
India	Central Pollution Control Board	5.5 - 9.0	NA	30	250	100	ND	5 mg/L	[71]
China	GB 4287-2012 + XG1-2015/ (MEP 2012)	6.0 - 9.0	NA	20-50	80-200	50-100	ND	50-80 U Pt-Co	[78]

Turkey	Water Pollution Control, No. 25687, 12/31/2004/ (Official News-paper 2004)	6.0 - 9.0	NA	NA	250	140	ND	NA	[78]

(ND- Not determined)

2.6 Remediation techniques for dye containing wastewater

The stability, toxicity, and intricate molecular structure of synthetic dyes make the efficient treatment of wastewater containing them a major environmental concern. This has led to the development of a number of removal tactics that can be broadly divided into three categories: physical, chemical, and biological (bioremediation) techniques. Depending on the dye type, wastewater properties, and treatment objectives, each technique has unique mechanisms, efficiency, benefit, and drawback.

2.6.1 Overview of Commonly applied Physical Remediation Methods

Using physical barriers or common forces (such as gravitational, electrical, and/or van der Waals forces) to remove chemicals from wastewater is known as physical remediation. The chemical structure of the chemicals found in water is unaffected by the application of these techniques [1]. These approaches are frequently coupled with other techniques or used as preliminary treatments.

I. Adsorption

Adsorption is an economical method of refining high-concentration dyes without producing any byproducts and allows for recovery and reuse, hence it has gained popularity. Through the processes of electrostatic interactions, hydrophobic interactions, hydrogen bonding, pore filling, and π-π interaction, the adsorbents exhibit a considerable affinity for dyes through physisorption and/or chemisorption [80]. Dye removal may be impacted by adsorption capacity, pore volume, specific surface area, and particle and pore size distribution of adsorbent. Carbon-based materials such as activated carbon, biochar, carbon nanotube, carbon nanofiber, and graphene have an intrinsically exceptional adsorption capacity for a variety of dyes when compared to other conventional absorbents (such as zeolite and clay) [81]. However, it takes a lot of energy and chemicals to regenerate them. From a techno-economic standpoint, inexpensive adsorbents for dye removal, such as natural materials, agricultural waste, household solid waste, and industrial solid by-products, are common substitutes for commercially produced adsorbents [82].

II. Membrane Separation

A semipermeable membrane is used in the conventional membrane separation method to filter impurities out of wastewater. According to Kamati et al. [80], it is a promising separation method since it enables continuous operation with a small environmental impact and less chemical usage. Based on their pore diameters, pressure-driven membranes are classified as reverse osmosis (RO), nanofiltration (NF), microfiltration, and ultrafiltration (UF). Instead of being employed as a stand-alone treatment method for advanced treatment of wastewater containing dyes, microfiltration membranes, which have pore diameters ranging from 0.1 to 10 μm, are used as a pretreatment step to remove suspended particles and colloidal dyes. Applications for UF membranes with smaller pore diameters (2-100 nm) in the direct treatment of textile wastewater containing dyes are restricted [83]. However, RO and NF membranes, which offer higher removal efficiencies, lower energy consumption, and a space-saving procedure, have been found to be the most effective methods for removing a variety of synthetic dyes from wastewater. These membranes are recent developments in membrane technology. According to Moradihamedani [84], NF and RO have inadequate water permeate flux due to their tiny pore size ranges (0.001-0.01 μm for NF and 0.001 μm for RO), even though they have strong separation efficiencies for dye removal. Larger permeate flux hence necessitates higher operating pressure, which is probably going to result in higher energy usage and operating expenses because of membrane clogging and fouling.

2.6.2 Overview of Commonly applied Chemical Remediation Methods

Chemical remediation is the process of removing dyes using chemical or electrochemical methods.

I. Chemical Coagulation and Electrocoagulation

Chemical-based coagulation has been used extensively to treat wastewater that contains dyes due to its ease of use, affordability, and scalability. There are two steps involved: coagulation and flocculation process. The crucial first step in starting the dye removal process is adding the coagulants such as Al^{3+} and Fe^{3+} based salts on to wastewater that contains dyes while vigorously mixing the mixture to create the small flocs. In order to create larger and heavier flocs that can be preferentially removed by sedimentation (a physio-chemical process), high molecular weight organic polymers are added as flocculants [85]. Due to their great solubility, water-soluble dyes (such as reactive, acidic, and direct dyes) typically coagulate ineffectively. Additionally, humans are neurotoxically affected by the residual Al^{3+} ion in concentrated sludge and/or treated water, which results in cognitive impairment. Potential solutions to reduce their environmental risks include the development of safer and more efficient flocculants and coagulants that produce less sludge and encourage usage of biodegradable coagulants such as plant-based coagulants [86]. Electro-coagulation emerges as a compelling color removal option. Due to electro-flotation brought on by tiny H_2 bubbles created at the cathode, metal ions in electro-coagulation instantly adsorb OH^- ions generated by electrochemical reduction at the cathode and create a polymeric metal hydroxide to trap dyes,

resulting in a more effective decolorization efficiency. It may be possible to repurpose this cleaned wastewater in a dyeing procedure to create premium textile fabric [87].

II. AOPs

AOPs are emerging substitutes that can be utilized to produce hydroxyl radicals (HO·) which can eliminate dye and other refractory pollutants [88]. AOPs generally encompass a number of techniques, including Fenton reactions, photocatalysis, ozonation, and Fenton-like processes [89]. Unpaired electrons give HO· its high reactivity, and these radicals can aid in oxidizing organic materials that are difficult to remove. HO· is an extremely potent and nonselective oxidizing agent. The disadvantages of the homogeneous Fenton or Fenton-like process and catalytic ozonation can be effectively mitigated by the use of heterogeneous nanomaterial catalysts, such as iron-based catalysts (FeOCl, zero-valent iron, Fe_3O_4, FeOOH, and FeS_2) and iron-free catalysts (metal organic frameworks (MOFs) or MOF derivatives), which exhibit comparable degradation performance even under extreme conditions [90]. Among AOPs' benefits include quick breakdown of dye and effective with a variety of dyes. However, the high cost of reagents, pH-sensitive reactions (Fenton, for example, requires a pH of about 3), and the creation of residual sludge in some processes are drawbacks. Hence, there is an urgent need for identification, evaluation, and mitigation measures due to the possible environmental danger of harmful by-products produced during dye degradation by AOPs, such as phenols, aromatic amines, and their derivatives.

III. Photocatalysis

Without continuously administering potent oxidizing agents, photocatalysis creates valence band holes (h^+) and conduction band electrons (e^-) on the surface of semi-conductors under ultraviolet (UV) or visible light irradiation [91]. This starts the redox reaction with dissolved oxygen and H_2O to produce radicals (OH· and O_2·) for dye degradation. Commercial TiO_2 nanoparticles, such as rutile and anatase, have been employed extensively as potent photocatalysts under UV light because of their low biotoxicity, high efficiency, and physicochemical stability [92]. Because it necessitates additional chemical consumption or energy input for certain reactors, chemical remediation is economically unappealing and has a high operating cost. Unwanted hazardous byproducts can still form even though chemical remediation typically achieves a high decolorization efficiency with the input of chemicals or energy.

2.6.3 Overview of Commonly applied Biological Remediation Methods

Utilizing living organisms, mostly microorganisms like bacteria and fungi, bioremediation eliminates or neutralizes pollutants from contaminated settings, such soil or water. It makes use of these organisms' innate metabolic capacities to convert toxic chemicals into less toxic or non-toxic forms. The enzymes of bacteria, algae, yeast, or fungi can be used to bioremediate textile dyes. Microorganisms in charge of biodegradation may use a variety of methods, such as adsorption, biosorption, bioaccumulation, elimination or conversion of toxic waste molecules into harmless or even beneficial compounds. Biological remediation produces a little

amount of sludge for dye degradation and is more economical and environmentally benign than chemical or physical cleanup methods. However, bioremediation methods may need longer treatment periods, because they are susceptible to variations in pH, temperature, and nutrition availability [93].

I. Bacteria

Among these microorganisms, bacteria are generally more effective for dye degradation owing to their exponential proliferation rate and versatile biocatalytic effect on dyes. Particularly, bacteria exhibit a strong efficacy to degrade azo dyes. Decolorization of azo dyes is preferentially initiated by secreted azo reductases under anaerobic condition through azo bond cleavage along with the generation of azo-reductive intermediates (aromatic amines). However, aromatic amines have high mutagenicity and carcinogenicity, urging an additional degradation with oxidative enzymes (laccases or peroxidases) produced by aerobic bacteria for further mineralization during practical azo dye degradation. Compared with individual bacteria strains, bacteria consortia perform a more efficient dye degradation owing to their intensive metabolic activity induced by diverse secreted enzymes. However, some dyes are recalcitrant to bacterial degradation; incomplete mineralization may occur [94].

II. Algae

As photosynthetic microorganisms, algae capture CO_2 for their proliferation and growth, establishing a carbon-negative source. Therefore, algae-assisted bioremediation could have an important role in the mitigation of greenhouse gas emission, facilitating decarbonization. Algae have been shown to be effective at degrading dyes. Algae absorb azo dyes through extracellular polysaccharides and then produce azoreductase to transform the azo dyes into aromatic amines as nitrogen source for their photosynthesis. Additionally, O_2 produced by algae can be utilized by aerobic bacteria as electron acceptors and, thus, lead to mutually beneficial symbiosis between algae and bacteria. The formation of algae (*Chlorella vulgaris*)-bacteria consortia markedly enhances the degradation performance of Congo red dye, with 93% increase in decolorization rates via a synergistic effect of versatile enzymes produced by the consortia [95].

III. Yeast

Owing to their fast growth and tolerance to a harsh wastewater matrix (for example, high dye loading, low pH and high salinity), yeasts are promising candidates in remediation of dye-containing wastewater. Similar to bacteria, yeasts can produce azoreductases, laccase and peroxidase for dye degradation under the stress of dyes. Especially, certain types of yeasts have a strong tolerance to high salinity for dye degradation. For example, the *Galactomyces geotrichum* yeast strain yields a decolorization efficiency of >92% to acid scarlet GR dye in the presence of 40 g/L NaCl , demonstrating great potential in highly saline dye-containing wastewater treatment [96].

IV. Filamentous Fungi

Fungi are found in almost all types of ecosystems, including freshwater, marine, desert, tropical rain forest, and deep-sea sediment settings. One feature that distinguishes several fungal species from one another on a biochemical, physiological, and metabolic level is their capacity to metabolize or digest various harmful or persistent substances. The phenomena is known as Mycoremediation, a term coined by Paul Stamets, is one of the greatest ways to remove the contaminants from water and soil. Because of their innate ability to disintegrate, white-rot Fungi can naturally break down a variety of organic contaminants such as pesticides, heavy metals, pharmaceuticals, dye. If the natural ability of white-rot fungi can be directed towards dye containing wastewater treatment on larger scale, several Sustainable Development Goals (SDGs) could be supported [16]:

- SDG 6: White-rot fungus help to provide clean water by offering an efficient way to remove dyes from wastewater.
- SDG 12: Sustainable patterns of production and consumption are encouraged by the use of biological treatment techniques.
- SDG 14: Preserving marine habitats is aided by lowering the release of toxic dyes into aquatic settings.

2.7 White-Rot Fungi: pollutant degradation potential

White-rot fungi belong to the phylum Basidiomycota, which is further subdivided into the subphylum Agaricomycotina. Although some are found in Agaricales and other orders, white-rot fungi are mainly categorized in the phylum Basidiomycota, with many belonging to the order Polyporales. *Phanerochaete*, *Trametes*, *Pleurotus*, *Ganoderma*, and *Coriolus* are a few examples of WRF. They are able to fully mineralize lignin, a complex aromatic polymer found in plant cell walls. In contrast to brown rot fungi, which only break down cellulose and hemicellulose, WRF break down lignin and all other lignocellulosic biomass components, leaving behind a white residue, hence the term "white-rot." These fungi can degrade a wide range of resistant organic substances because they generate a special set of enzymes, such as laccase (Lacc), manganese peroxidase (MnP), and lignin peroxidase (LiP).

Beyond lignin, white-rot fungi have drawn notice for their remarkable capacity to break down a broad range of environmental contaminants. They can target xenobiotic substances with a variety of structural variations thanks to their non-specific oxidative enzymes. Many WRF are capable of breaking down long-lasting pesticides, including pentachlorophenol (PCP), atrazine, DDT, and lindane. Particularly, *Phanerochaete chrysosporium* and *Trametes versicolor* have demonstrated effectiveness in converting these substances into less harmful metabolites. They also have the ability to immobilize, change, or biosorb heavy metals like cadmium (Cd), lead (Pb), and chromium (Cr), lowering their mobility and toxicity. Fungal cell wall components and extracellular polymeric substances (EPS) frequently help with this. Antibiotics, anti-inflammatory drugs, and hormone disruptors such as diclofenac, ibuprofen, and 17β-estradiol can all be broken down by white-rot fungi. One important factor in the breakdown of these

compounds into less active forms is enzymatic biotransformation. White-rot fungus can break down a variety of xenobiotic substances, including dyes, polycyclic aromatic hydrocarbons (PAHs), and polychlorinated biphenyls (PCBs), because of their wide substrate selectivity. They are therefore prospective agents for the sustainable bioremediation [97,98].

Current research also shows involvement of *Trametes versicolor*, *Pleurotus ostreatus*, *Phanerochaete chrysosporium*, *Schizophyllum commune*, *Pleurotus sapidus*, and *Pleurotus florida* in dye degradation. There are three ways of fungal-mediated dye breakdown or removal processes: biosorption, bioaccumulation, and biodegradation. The main method of decolorization is dye adsorption onto the microbial cell surface [99]. While dead biomass mechanisms is based on physical and chemical removal processes, living fungal cells use metabolic activities to remove colored wastewaters [100,101]. The natural polysaccharide chitin and its derivative chitosan, which have a distinct molecular structure and a high affinity for numerous color classes, are found in the cell walls of dead fungal biomass [102]. Bioaccumulation is a metabolic and energy-dependent process in which pollutants are accumulated within the cytoplasm of actively growing cells [103,104]. Additionally, biodegradation is a metabolically reliant and energy-intensive process in which certain enzymes break down complex dye molecules into simpler ones. However, complete underlying mechanism of myco-remediation is not very well known [105]. WRF generates low-specificity intracellular and extracellular degradative enzymes, which can be used to degrade different colors, hazardous compounds, and remediate wastewater. Finding the right fungal species to remove particular pollutants and comprehending the mechanism are the basic keys of myco-remediation.

Although biotechnology has developed numerous methods and techniques to increase enzymatic activity, one of the most widely used strategies for carrying out enzymatic activity in various ways is the immobilization of enzymes. Enzyme immobilization through covalent bonding, adsorption, encapsulation, entrapment, and chemical crosslinking has been used to improve the activity, stability, and reusability of enzymes in a harsh environment in order to promote enzyme-assisted remediation. Specifically, silica, carbon, metals, and bioderived materials are examples of nano-supports that have been identified as suitable carriers for enzyme immobilization due to their large specific areas and rich functional group sites. MOFs, one of these nano-supports, offer a flexible and capable platform for the quick and easy immobilization of enzymes through adsorption, covalent binding, encapsulation, and entrapment. They also have a number of significant advantages as well as few disadvantages as shown in Table 3. Hence, there is scope for development of fungal cell immobilization rather than enzyme immobilization. Numerous natural or synthetic carriers can be tested to enhance dye degradation capacity of fungi. Agricultural or industrial byproducts can be utilized as support for fungal growth.

Table 3. Advantages & disadvantages of Enzyme immobilization techniques (Published in **Publication 2**)

Advantages	Disadvantages
Enhanced level of strength & stability	Expensive
Increased level of reusability, reactivity and efficacy	Complex process, chances of failure
Improved level of product stability	Limited implementation,
High enzyme substrate ratio	Support/carrier related limitations
Enhanced level of continuous operation	Inactivation caused by heat generated in the system
Less chances of contamination	Cross-linker requirement issues

The processes of adsorption and absorption are referred to as "sorption" processes. Absorption is the process through which a material from one state is integrated into another (for example, when liquids are absorbed by solids or gases are absorbed by liquids). The process by which ions and molecules physically adhere to or bond with the surface of another molecule is known as adsorption. Because of its high adsorption capacity, activated carbon is frequently employed as a sorbent in industrial sorption systems to remove colors from wastewater. However, its widespread use is restricted due to its high cost [106]. In an attempt to develop more economical and effective adsorbents, numerous approaches have been studied recently. It has been demonstrated that biosorption is an effective method for extracting color molecules from diluted aqueous solutions using inactive and dead biomass. When it comes to dye cleanup, the fungal mycelium's morphological advantage could be quite helpful. Many pollutants are absorbed or adsorbed onto it because of the hyphae structure's increased surface area. Since the sorption process on WRF biomass is a metabolism-independent technique of pollutant removal, it can be utilized to remove environmental toxins that are difficult to biodegrade. It has been demonstrated that sorbents are better than other treatment techniques in terms of their simplicity of design, convenience of use, flexibility, and insensitivity to harmful pollutants. Most significantly, no hazardous chemicals are produced as a result of the sorption process [107]. Different biosorption capabilities of living and dead mycelium are said to be caused by changing structure and functional groups on the active site of autoclaved or dead mycelium. The dead autoclaved biomass was able to extract less Brilliant Green dye (48.85 ± 8.25%) when using the *Pleurotus ostreatus* strain (BWPH) than the live mycelium under shaking conditions (95.00 ± 0.27%) [108]. Peckova et al. [109] found that using a different WRF to remove the monoazo dye Allura Red AC produced similar findings. They discovered that the best biosorbent was heat-modified dead biomass of *P. ostreatus* (118.3 ± 9.9mg/g). The interaction between the dye's functional group and the carboxyl lipid group present in the fungal cell wall has been observed to result in varying dye removal capabilities. Given the aforementioned information, using living biomass as a biosorbent would have the major benefit of being able to eliminate a greater number of pollutants. However, there are also advantages and disadvantages to consider when using biomass of any form. Because dead biomass avoids

toxicity-related problems, requires no maintenance, can be stored for long periods of time without losing its effectiveness, is more practical to regenerate, and can be used to address a wider range of environmental variables, it is the focus of most applications. Additionally, it is possible to treat and cut this biomass into the appropriate particle size. Using living biomass can also be advantageous since, as was already said, the cells are metabolically active, even though dead biomass offers all these advantages. Because bioaccumulation facilitates the initial biosorption process, this permits the contaminants to enter the cell and boosts process efficiency [110]. This scenario would involve a first, metabolism-independent stage of the pollutant binding to the cell surface (biosorption in the strict sense) followed by a second, metabolism-dependent step of the pollutant passing past the cell membrane and into the interior of the cell. At this stage, it is crucial to take into account the possibility that some pollutants could pass through the membrane by passive diffusion [111].

Various organic, inorganic, or biowaste supports have been tried thus far for biomass immobilization. These are comparatively cheap support materials, leftover goods, or waste from various industrial processes, agricultural waste, etc. The researchers selected sunflower seeds [112], loofa sponge [113], sugarcane bagasse [114] and nylon sponge. The capacity of the biosorbent to eliminate dyes (mg/g) has been the subject of numerous investigations to date. It shows the dye absorption capability in milligrams per gram of dried biosorbent. In addition to being a sustainable wastewater treatment technique, biosorption can be used to treat wastewater by using waste materials.

Inadequate understanding of the comprehensive mechanisms governing the breakdown of harmful textile dyes may limit the application of biological treatments. The emergence of the "omics" sciences has made it possible to use integrated, high-throughput methods that quickly yield a large amount of data about microorganism and their metabolism. This makes it feasible to comprehend biochemical systems and their dynamic evolution as well as to develop strategies that promote the efficient breakdown of xenobiotics. Genomics, transcriptomics, proteomics, and metabolomics are the primary omics approaches. A thorough understanding of the microbiological processes leading to more successful bioremediation at the field scale can be attained by employing these methods.

In omics research, there are two fundamental approaches to biological system analysis. The first is a thorough, unguided examination of samples that doesn't require any prior understanding of the genes, proteins, or metabolic pathways of the microbe under study. This method, known as the shotgun approach, examines a large number of molecules found in a sample, producing a vast amount of data that needs to be compared and correlated across samples. The second tactic, known as a targeted approach, focuses on doing research to pinpoint particular molecules using existing knowledge. Multiple genomes research are combined in meta omics to facilitate data integration and horizontal meta-analysis. Integrative multi-omics approaches are frequently necessary because it's probable that the data produced by a single-omics study isn't always enough to completely comprehend a complex process like microbial bioremediation. Transcriptomics study was carried out by Sun et al. [115] while *Irpex lacteus* CD2 degraded Direct Red 5B azo dye with lignin supplementation. Under DR5B and

lignin treatments, they discovered a wide range of peroxidases and oxidases, radical-producing enzymes, and genes that were up-regulated. Synergistic enzymes and radical-mediated oxidative processes are necessary for the breakdown of aromatic dyes, according to the transcriptomics analysis confirmed by specific protein over-expression experiments.

Detoxification is not usually the same as dye decolorization. Since the transformation products may be more hazardous than the parent substances, the color's removal cannot be immediately attributed to a decrease in toxicity. Azo dyes, that are transformed into aromatic amines which are frequently more poisonous than the original dye, are the greatest examples. The almost total decolorization of the non-toxic azo dye Acid orange 7 (AO7) to more hazardous aromatic amines such aniline, 1-amino-2-naphthol, naphthalene, and phenyldiazene was reported by Rawat et al. [116]. These intermediates produced toxicity at the molecular, cellular, and organismal levels, in contrast to AO7. Therefore, it is essential to evaluate the decrease in dye toxicity following decolorization in order to completely describe the ongoing process and its impacts. Direct toxicity testing, which include indicator organisms such bacteria, microalgae, invertebrates, plants, and fish, are employed for this purpose. Toxicological effects include growth suppression, decreased chlorophyll synthesis, elevated oxidative stress, and growth and reproductive abnormalities, depending on the indicator organism utilized. Additionally, different cell lines can be used to investigate the genotoxicity of dyes and metabolites that occur from their decolorization. Methods of toxicity assessment have been thoroughly examined by Danouche et al. [117] and Ceretta et al. [118].

As a concluding remark of literature review of White-rot fungal mediated dye degradation, it has been thoroughly investigated in solid-state fermentation, immobilized systems, and batch reactors. Fungal enzymes have also been separated and used directly to treat textile effluents enzymatically. Systems based on biofilters and bioreactors are increasingly being used for on-site industrial wastewater treatment. However, full-scale applications are hampered by slow degradation kinetics and enzyme instability in industrial settings. Performance may be impacted by sensitivity to environmental factors such as pH, temperature, and dye concentration. The expense of growing fungal biomass and producing enzymes continues to be a hurdle. Toxic co-contaminants that prevent fungal growth or enzyme activity are frequently found in real textile effluents. Future studies must concentrate on the following areas in order to overcome these obstacles: improving strain via metabolic and genetic engineering; immobilizing enzymes for increased stability; integrating with other treatment technologies (such as membrane filtration and advanced oxidation); and improving our understanding of enzyme-dye interactions through multi-omics and systems biology.

CHAPTER 3
RESEARCH STATEMENT

3.1 Research Gap

Based on an extensive literature survey and the growing demand for effective treatment of large volumes of industrial wastewater containing synthetic dyes, significant research gaps have been identified in this field. There is a critical need for decentralized, industry-specific wastewater treatment solutions that can address dye pollutants at the source-before they are mixed with other effluent streams or released into natural water bodies [119–122]. Developing compact, efficient, and rapid bioreactor systems tailored to different dye types requires a deeper understanding of the underlying removal mechanisms and comprehensive process optimization.

In this context, the present research identified the following key research gaps:

1. **Limited Mechanistic Understanding**: While fungal bioremediation is a promising field, the exact mechanisms (biosorption vs. biodegradation) employed by Basidiomycota fungi in removing colored aromatic compounds remain poorly elucidated. Most existing studies lack detailed mechanistic insight at molecular and biochemical levels.
2. **Scope for Optimization Studies**: The dye degradation capacity of each fungal species varies significantly depending on key physicochemical factors such as immobilization, pH, temperature, dye concentration, biomass type (live or dead), and light conditions. A systematic and integrated study of these parameters is essential to fully understand their influence and to optimize the process for maximum efficiency.
3. **Limited Integration of Multi-Omics**: A quite studies have utilized a systems biology approach (transcriptomics, proteomics, enzyme activity) to correlate gene/protein expression with dye removal performance in Basidiomycota, limiting our understanding of the involved metabolic pathways.
4. **Lack of Comprehensive Toxicity Assessment**: Existing works often overlook the ecotoxicological safety of the treated effluents, especially through validated models like *Daphnia magna* and *Lemna minor*, which are essential for evaluating environmental applicability.
5. **Demand of Decentralized Wastewater Treatment**: Though lab-scale studies are prevalent, translating the dye removal process into scalable, engineered systems such as bioreactors has received limited attention, hindering industrial application. Not a single study address the need and solution for decentralized Wastewater Treatment for synthetic dye containing wastewater.

This research aims to bridge existing knowledge gaps and contribute to the development of customized fungal-based bioremediation systems for sustainable wastewater management.

3.2 Research Hypothesis

Recent progress in fungal bioremediation has underscored the efficacy of White-Rot Fungi in eliminating synthetic dyes from industrial effluents. Nevertheless, existing literature fails to comprehensively clarify the underlying mechanisms, especially the comparative roles of biosorption and biodegradation in dye elimination. Although many studies indicate the involvement of ligninolytic enzymes, including laccase, manganese peroxidase, and lignin peroxidase, there remains a shortcoming of comprehensive multi-omics investigations that connect these enzymatic systems to gene expression and dye degradation. In silico tools, such as molecular docking, genome-scale metabolic modeling (GEMs), and machine learning**,** to predict fungal performance or enzyme-dye interaction has been rarely studied in this field [123].

The removal effectiveness of fungal systems is significantly influenced by physicochemical parameters such as pH, temperature, dye concentration, and the kind of biomass (living versus dead); nevertheless, comprehensive optimization methodologies and standard kinetics model are not very well described in the literature to attain an uniformity in research. Notwithstanding encouraging laboratory-scale results, the application of fungal-based dye removal in scalable and decentralized bioreactor systems has garnered minimal focus, and Life Cycle Assessment (LCA) and techno-economic feasibility studies are rare, despite their importance for industrial uptake [124]. The ecotoxicity of treated effluents is seldom assessed using standardized bioassays on the organisms belonging to different tropic levels like *Daphnia magna* or *Spirodela polyrhiza*.

The hypothesis of this study is derived from these gaps that WRF such as *T. versicolor* and *P. ostreatus* exhibit dye removal capabilities via a synergistic mechanism of biosorption and enzymatic biodegradation, which can be markedly improved by optimizing critical physicochemical parameters and effectively applied in compact, decentralized bioreactor systems designed for specific dye categories. Moreover, this treatment can produce effluents with minimal ecotoxicological impacts, rendering the method environmentally viable. Multi-omics studies may help to decipher the connection between enzyme profile and gene expression which may provide base for predictive modelling of interaction between fungal enzymes and different class of dyes.

3.3 Scope of Research

In light of the existing research gaps in the decolorization of wastewater containing synthetic dyes using white-rot fungi, three broad research scopes have been delineated as shown in Figure 2. These can be further refined to address specific objectives within the field. This study seeks to investigate and optimize the application of white-rot fungi for the remediation of dye-laden wastewater through the following key aspects:

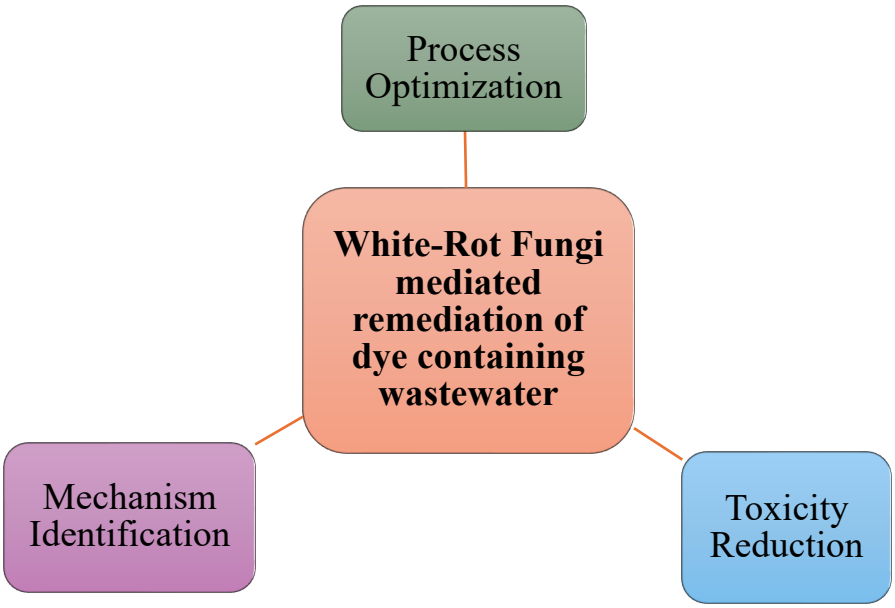

Figure 2. Schematic of Research Scope

3.3.1 Process Optimization

Process optimization is a critical component in enhancing the efficacy of white-rot fungi for dye removal and degradation. This involves the strategic selection of fungal species capable of degrading a broad spectrum of synthetic dyes with diverse chemical structures and functional groups. In addition to species selection, variations in biomass formulation play a significant role. These include the use of live versus dead fungal biomass, immobilized versus free biomass [125], and the identification of suitable immobilization carriers to enhance stability and reusability.

A major focus lies in the optimization of key operational parameters such as pH, temperature, initial dye concentration, biomass dosage, incubation time, and biomass reusability. Fine-tuning these parameters is essential for maximizing the bioremediation efficiency [126]. The complexity of interactions among these variables necessitates the application of advanced statistical and modelling tools. Plackett-Burman (PB) design matrix, Response Surface Methodology (RSM) and Central Composite Design (CCD) are particularly valuable for identifying optimal conditions and understanding the interactive effects between dependent and independent variables, thereby facilitating a data-driven approach to process optimization [127].

3.3.2 Mechanism Identification

The elucidation of biochemical and molecular mechanisms underlying dye degradation by white-rot fungi remains a critical yet underexplored area. Comprehensive understanding of the processes involved - namely biodegradation, biosorption, and bioaccumulation - is essential for advancing the application of these fungi in pollutant remediation. Current knowledge gaps necessitate in-depth investigation into the enzymatic and metabolic pathways responsible for dye transformation and mineralization [128].

Mechanistic insights can pave the way for targeted strategies involving genetically engineered fungal strains or enzymes, enabling more efficient degradation of specific classes of pollutants. To achieve this, the integration of multi-omics approaches - including genomics, transcriptomics, proteomics - are crucial. These approaches, in conjunction with detailed enzyme profiling (e.g., lignin peroxidase, manganese peroxidase, laccase), can reveal the expression patterns and functional roles of key enzymes in dye degradation [129]. Overall, the application of advanced molecular and systems biology tools is indispensable for unravelling the complex mechanisms of white-rot fungi-mediated dye remediation and enabling process optimization at the molecular level [130].

3.3.3 Toxicity Reduction

Effective dye wastewater treatment must go beyond mere decolorization to ensure the elimination of toxicological risks associated with dye residues and their degradation by-products. The ecological safety of treated effluents is a prerequisite for their reuse in industrial processes, agricultural irrigation, or safe discharge into natural water bodies. However, in many existing studies on biological dye degradation, toxicity assessment is often overlooked, resulting in incomplete evaluation of treatment efficacy [131].

This research scope emphasizes the comprehensive assessment of toxicity reduction following fungal treatment. Specifically, it aims to evaluate the residual toxicity of treated wastewater across various trophic levels—including primary producers and consumers. Comparative ecotoxicological assays will be conducted using both untreated (pure dye) and white-rot fungi-treated samples to determine the extent of detoxification. Such assessments are vital to verify that fungal remediation not only removes visible coloration but also neutralizes harmful effects, thereby ensuring environmental and public health safety. This holistic approach to wastewater evaluation supports sustainable reuse and aligns with environmental protection regulations [132].

3.4 Objectives of research

Based on the delineated research scope, specific objectives have been systematically formulated to address each aspect in a comprehensive and practically feasible manner (Figure 3).

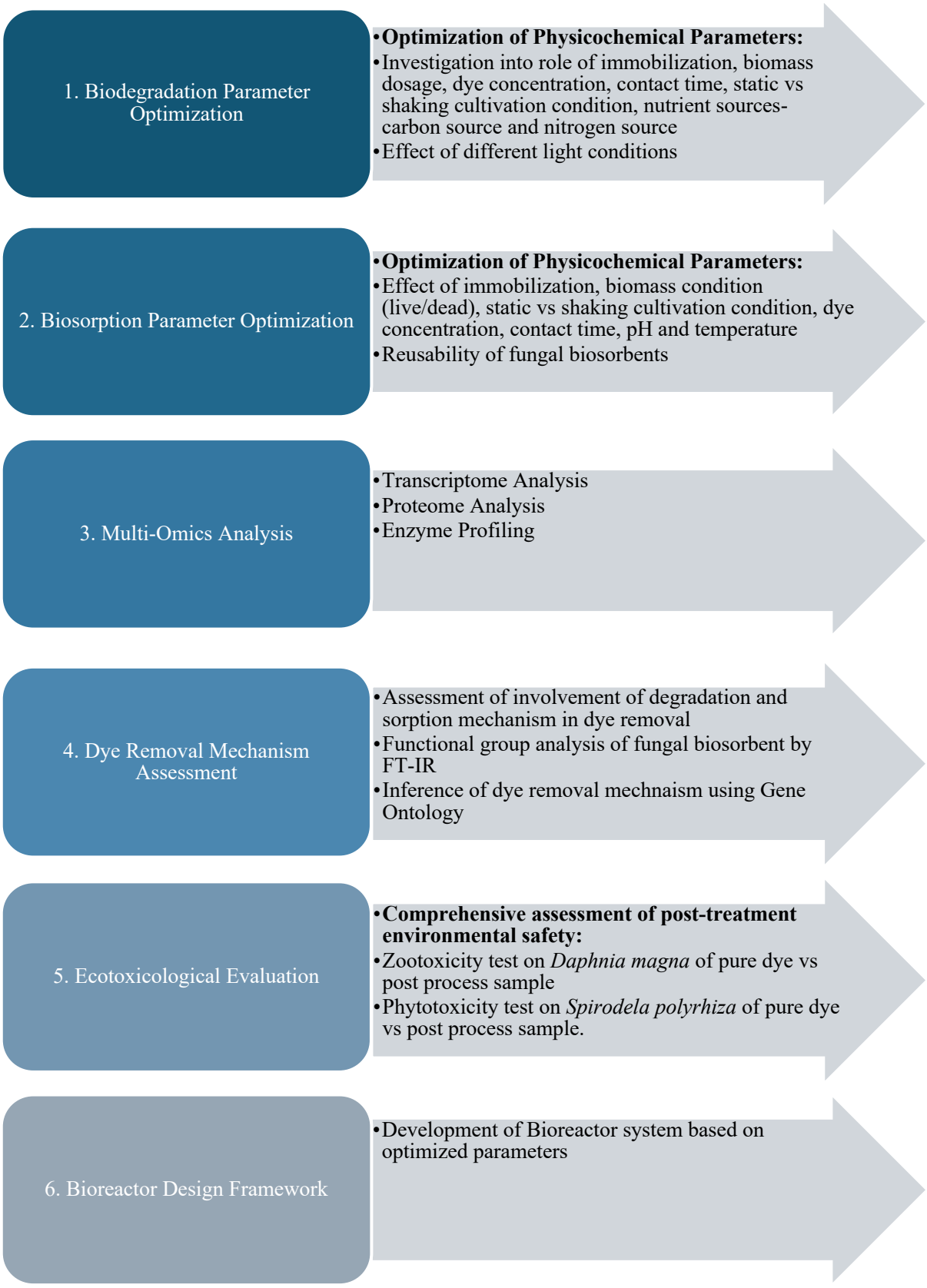

Figure 3. Schematic of Research Objectives

CHAPTER 4
MATERIALS AND METHODOLOGY

4.1 Test Substances -Synthetic Dyes

In this study, a range of synthetic dyes representing three major structural classes - azo, triphenylmethane, and anthraquinone - were selected for the fungal decolorization and biodegradation experiments. These included:

- Azo dyes: Congo Red (CR), Evans Blue (EB),
- Triphenylmethane dyes: Brilliant Green (BG), Crystal Violet (CV),
- Anthraquinone dyes: Remazol Brilliant Blue R (RBBR).

The selected dyes are well-known for their great stability and resilience to traditional wastewater treatment techniques, and they represent classes that are often used in the paper, leather, textile, and printing industries. The chemical complexity and structure of these dye classes vary, as do the types of chromophores (such as azo linkages, quinonoid groups, or triphenylmethane cores), environmental persistence, and toxicological characteristics, allowing for a comprehensive assessment of the fungal strains' degradation capabilities across chemically diverse pollutants [105,133]. The physicochemical parameters are detailed in Table 4, and the structures of the dyes are illustrated in Figure 4.

All dyes used in this study were of analytical grade and procured from certified suppliers. Stock solutions of each dye were prepared by dissolving the dye in deionized water to a final concentration of 1000 mg/L. These solutions were autoclaved at 121°C for 15 minutes to ensure sterility and prevent microbial contamination during storage. The sterilized stock solutions were stored in dark conditions at 4°C to maintain chemical stability and prevent photodegradation. Working solutions were freshly prepared by appropriate dilution of the stock with sterile deionized water to the desired concentrations, depending on the experimental design. All dilutions and experimental preparations were performed under aseptic conditions to avoid contamination and ensure reproducibility of results.

To quantify the concentration of dyes in the experimental samples, standard calibration curves were established for each dye used in the study. Standard solutions were prepared over a defined concentration range of 0-100 mg/L, depending on the specific dye's molar absorptivity and expected concentration in the samples. The absorbance of each standard solution was measured using a Hitachi U-1900 UV-Visible spectrophotometer at the dye's characteristic maximum absorption wavelength (λmax), previously determined through a wavelength scan from 200 to 1100 nm. A calibration curve was plotted by graphing absorbance against dye concentration, and the resulting curve demonstrated a linear relationship within the selected concentration range ($R^2 > 0.99$).

During the experimental analysis, the absorbance of the dye-containing samples was measured at the λmax using the Hitachi U-1900 UV-Vis spectrophotometer. The real-time concentration of dye in each sample was then determined by interpolating the measured absorbance values against the corresponding standard curve. All measurements were performed in triplicate to ensure accuracy and reproducibility.

Table 4. Physicochemical Properties of Dyes along with classification (Published in **Publication 1**)

Name of Dye	**Congo Red**	**Evans Blue**	**Brilliant Green**	**Crystal Violet**	**Remazol Brilliant Blue R**
Class	Azo	Azo	Triphenyl-methane	Triphenyl-methane	Anthra-quinone
Molecular formula	$C_{32}H_{22}N_6Na_2O_6S_2$	$C_{34}H_{24}N_6Na_4O_{14}S_4$	$C_{27}H_{34}N_2O_4S$	$C_{25}H_{30}N_3Cl$	$C_{22}H_{16}N_2Na_2O_{11}S_3$
Molecular weight (g/mol)	696.67	960.79	482.65	407.98	626.54
C.I.	CAS. 573-58-0	CAS: 314-13-6	C.I 42040; CAS Number: 633-03-4	C.I. 42555	61200
Absorbance maxima (nm)	492	598	623	584	596

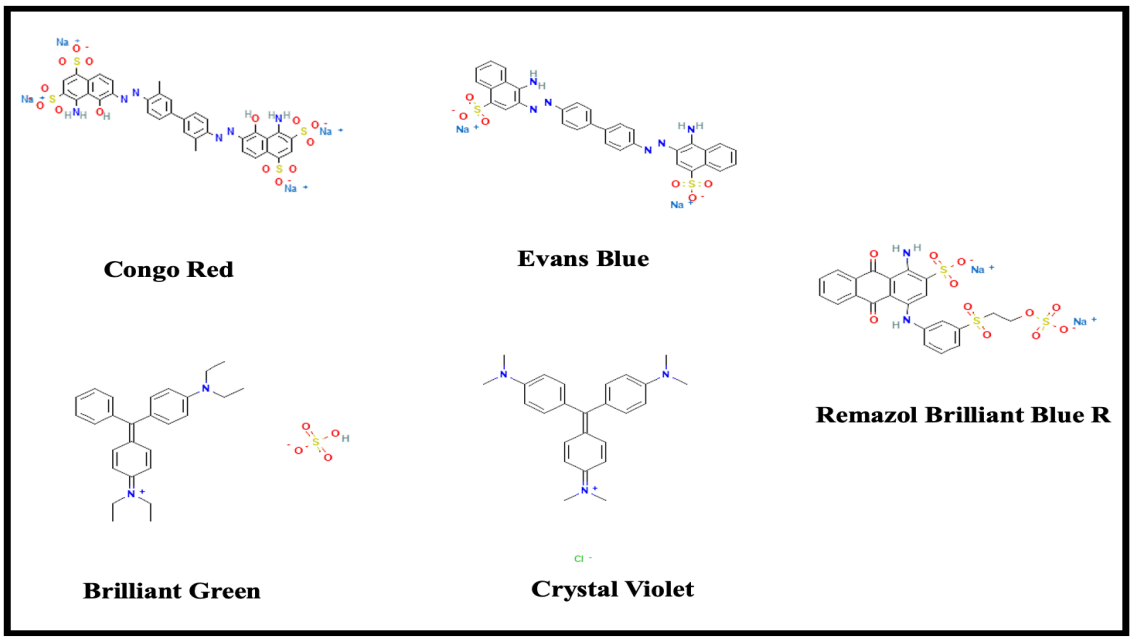

Figure 4. Molecular structure of Dyes

4.2 Selection of Fungal strain and Culture condition

The fungal strains employed in this study were selected for their potential capabilities in biodegradation and biosorption, particularly in the context of dye-containing wastewater treatment. Two pure cultures of White-Rot Fungi, namely *Pleurotus ostreatus* (strain BWPH) and *Trametes versicolor* (strain CB8), were utilized. These strains were obtained from the depository of Fungal Strain Collection of Environmental Biotechnology Department, Silesian University of Technology, 44-100 Gliwice, Poland. *Pleurotus ostreatus* (strain BWPH) was previously widely tested by Przystaś et al. [108,125,134] for decolorization of various dyes belonging to azo, anthraquinone and triphenylmethane dyes and it showed great potential for removal of various dyes. Both fungal strains were previously tested for cytostatic drugs removal by Jureczko et al. [107,135] and achieved fair percentage of degradation of drugs. Hence, both strains have been proven worthwhile for degradation of xenobiotics.

The isolation, identification, and characterization of these fungal species were previously described in detail by Jureczko et al. [136]. Both strains were preserved on Malt Extract Agar (MEA) plates and maintained at 4°C for long-term storage. Sub-culturing was performed periodically to ensure the viability and metabolic consistency of the fungal cultures. For experimental procedures, active fungal cultures were initiated by transferring 5 mm mycelial plugs from freshly grown MEA plates into a defined liquid organic medium designed to promote mycelial growth and enzymatic activity. The composition of the liquid organic medium or Regular Medium (RM) was as follows: glucose -5 g/L (as a carbon and energy source), peptone -1 g/L (as a nitrogen source), magnesium sulfate heptahydrate ($MgSO_4 \cdot 7H_2O$) -1 g/L, potassium dihydrogen phosphate (KH_2PO_4) -1 g/L. The pH of the medium was adjusted to 5.7 before sterilization. The medium was autoclaved at 121°C for 20 minutes to ensure sterility. Inoculated flasks were incubated under static conditions at 22 ± 2°C for optimal fungal

growth. All culture operations were conducted under aseptic conditions in a laminar airflow cabinet. Mycelial development was monitored visually throughout the experimental phases. The use of these standardized culture conditions ensured consistency in fungal performance, enzymatic activity, and dye removal efficiency during bioremediation trials.

4.3 Selection of carrier for immobilization

The immobilization of fungal biomass was employed to enhance the structural stability and reusability of the fungal cultures during bioremediation processes [137]. Immobilized systems offer several advantages, including improved tolerance to environmental fluctuations, enhanced pollutant degradation efficiency, and simplified biomass separation from the treated effluent [138–140].

The selection of suitable carriers for fungal immobilization was guided by multiple criteria:

- Ease of availability and cost-effectiveness,
- Minimal pre-processing requirements,
- Chemical inertness to the target pollutants,
- Environmental neutrality,
- Mechanical stability, and
- Ease of setup and separation from liquid media after treatment.

Based on these criteria, two support materials were selected for evaluation which can be seen in Figure 5:

- Support S1: Dishwasher-grade polypropylene,
- Support S2: Sponge - Commercial polyurethane.

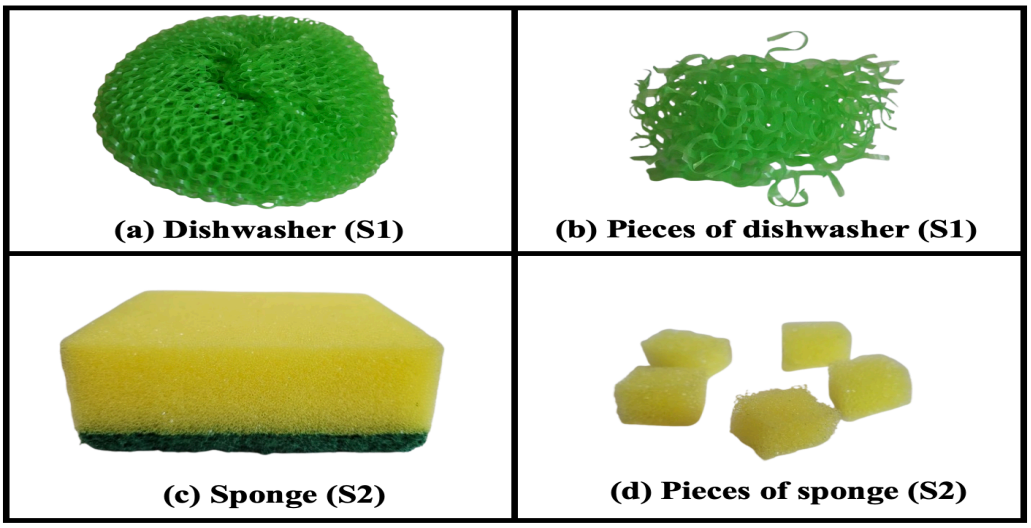

Figure 5. Carriers utilized for immobilization (a) Dishwasher- Polypropylene (S1) and (b) Pieces of dishwasher (S1) (c) Sponge- Polyurethane (S2) and (d) Pieces of sponge (S2) (Photo by R. Upadhyay)

4.4 Preparation of alive and dead Fungal Biomass and its immobilization

The cultivation and preparation of fungal biomass were carried out under four different conditions to obtain (i) free fungal biomass and (ii) self-immobilized fungal biomass and (iii) Immobilized fungal biomass on carrier (iv) dead-autoclaved fungal biomass. These preparations were used in subsequent biosorption and biodegradation experiments involving synthetic dyes.

The variations in fungal biomass type have been denoted based on immobilization type (dishwasher or sponge or not immobilized), biomass condition (alive or dead) and fungal strain (*T. versicolor* (strain CB8) or *P. ostreatus* (strain BWPH)) (Figure 6).

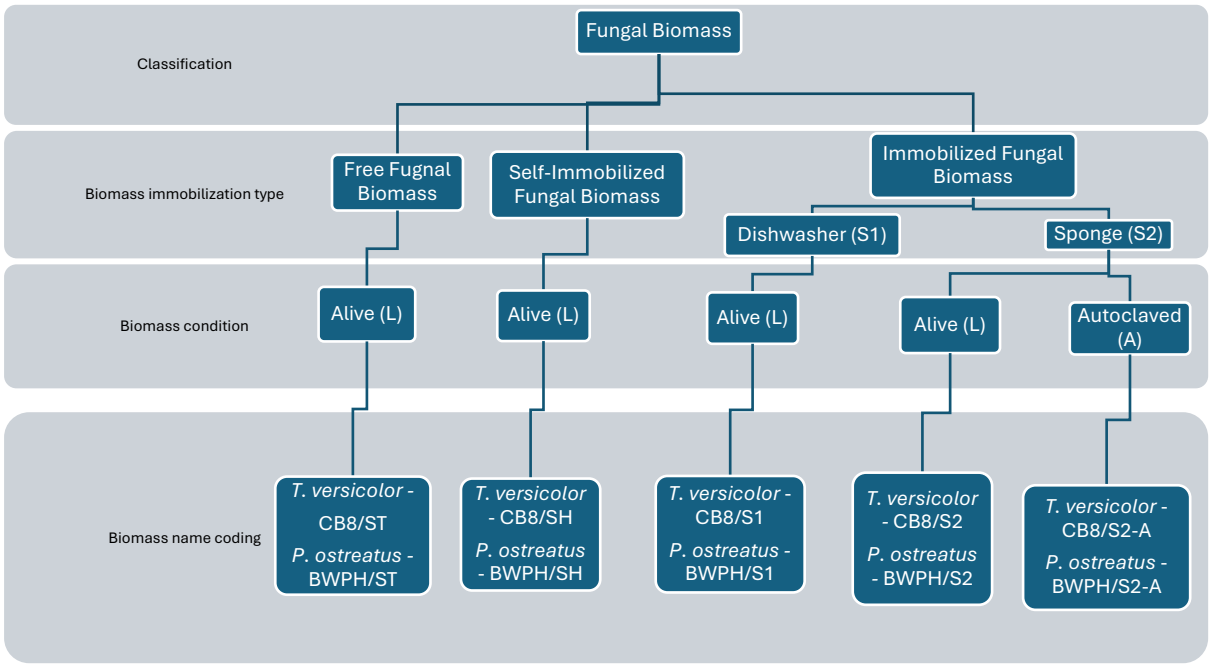

Figure 6. Schematic representation of Fungal biomass variations and their abbreviations

4.4.1 Cultivation of Free Fungal Biomass

Free fungal biomass was cultivated using an actively growing culture maintained on malt extract agar (MEA). Two mycelial plugs (5 mm in diameter) were aseptically expunged from the periphery of a 7-day-old colonies on MEA plate and inoculated into a 250 mL Erlenmeyer flask containing 100 mL of sterile liquid organic medium. The inoculated flasks were incubated under static conditions at 22 ± 2 °C for a period of seven days. This incubation regime facilitated the development of a uniform, mat-like mycelial biomass as depicted in Figure 7. Upon completion of the incubation period, the fungal biomass was either directly used in dye degradation experiments by adding dye solutions to the flask, or it was transferred aseptically to bag and homogenized using a BagMixer for 90 seconds. A measured aliquot of the homogenized biomass was then transferred to fresh experimental setups as required for further

analysis. For preparation of dead biomass, the seven day old alive biomass was autoclaved at 121°C for 20 minutes and used in subsequent analysis.

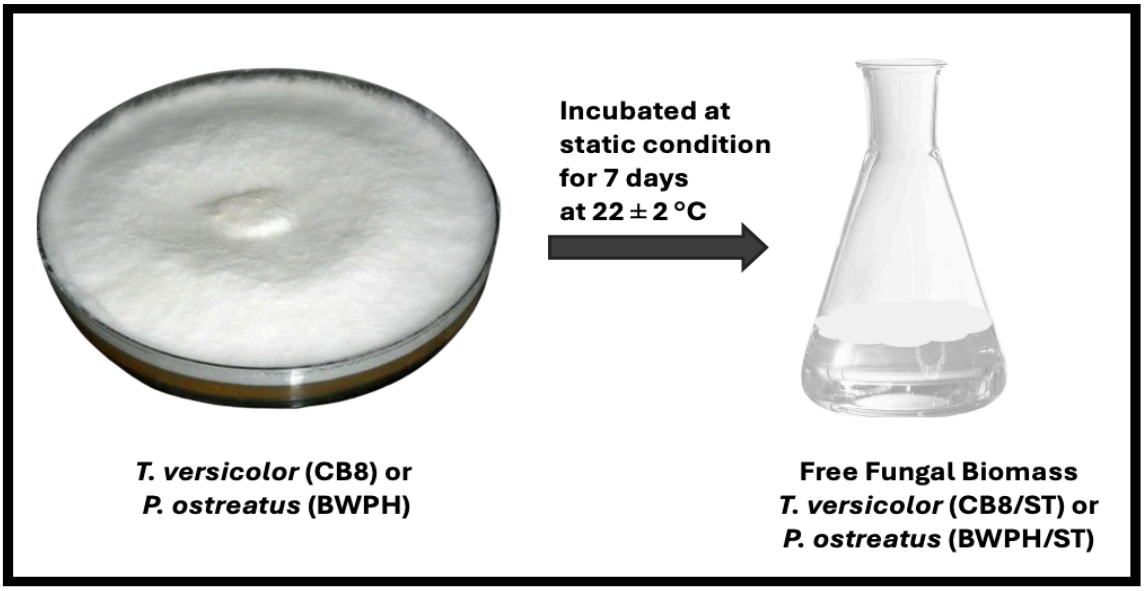

Figure 7. Schematic methodology of preparation of Free Fungal Biomass (Photo by R. Upadhyay)

4.4.2 Cultivation of Self-immobilized Fungal Biomass

Self-immobilized fungal biomass was prepared using the same inoculation protocol as described above in 4.4.1. However, these flasks were incubated under agitated conditions on a rotary shaker at 150 rpm at ambient temperature (22 ± 2 °C) for seven days. Continuous agitation promoted the formation of compact, spherical mycelial aggregates (mycelial pellets) as depicted in Figure 8. The size and morphology of which varied depending on the fungal strain and hydrodynamic shear forces [141]. These naturally formed spherical mycelial structures were referred to as self-immobilized fungal biomass.

For biosorption experiments, the mycelial pellets were harvested and transferred to sterile vials containing aqueous dye solutions under controlled experimental conditions. In the case of biodegradation experiments, the dye solution was directly added to the original culture flask containing the self-immobilized biomass, allowing in situ dye degradation to occur.

4.4.3 Cultivation of Carrier Immobilized Fungal Biomass

Both supports: dishwasher and sponge were cut into uniform cubes of approximately 1000 mm^3 to ensure consistent surface area for fungal attachment. For immobilization, 12 support pieces were placed in 250 mL Erlenmeyer flasks containing 100 mL of sterile liquid organic medium as depicted in Figure 9. The immobilization experiments were conducted using both fungal strains: *Trametes versicolor* (strain CB8) and *Pleurotus ostreatus* (strain BWPH). Fresh two fungal mycelial plugs of 5mm diameter were inoculated into the flasks and incubated under continuous shaking conditions (150 rpm) at 22 ± 2°C for seven days to promote colonization

of the carrier surface. Visual observation was used to confirm fungal colonization on the support surfaces prior to use in dye removal assays.

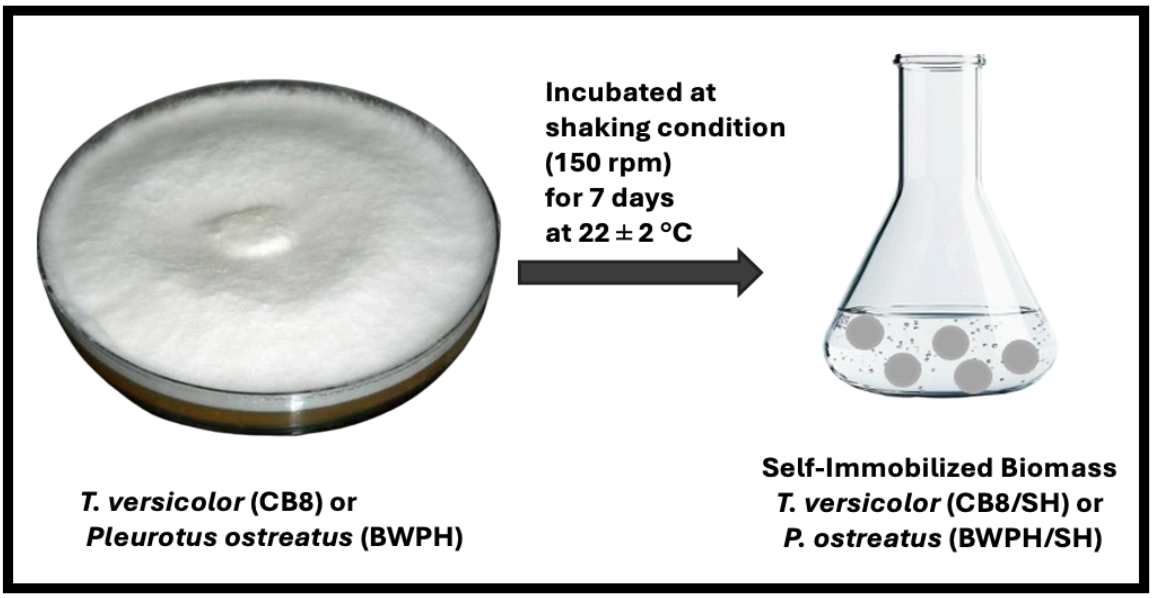

Figure 8. Schematic methodology of preparation of Self- Immobilized Fungal Biomass (Photo by R. Upadhyay)

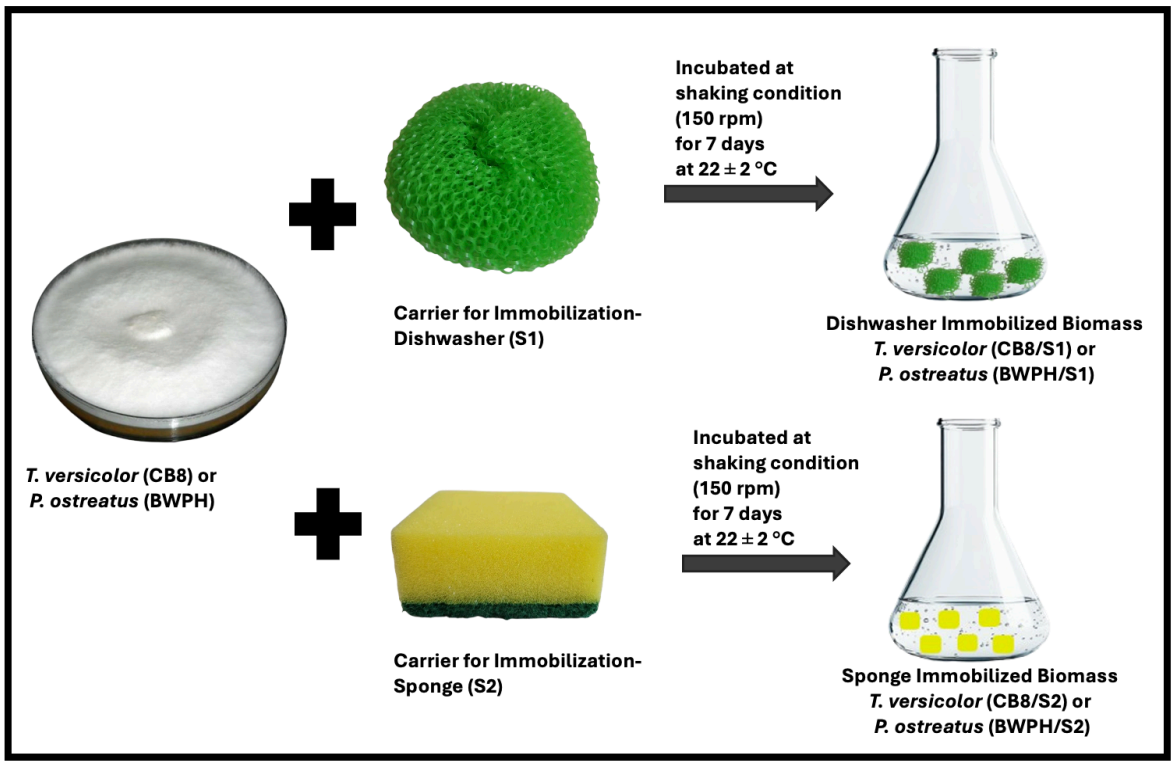

Figure 9. Schematic methodology for Carrier Immobilized Biomass preparation (Photo by R. Upadhyay)

4.4.4 Preparation of Dead-autoclaved Fungal Biomass

To prepare inactivated (dead) fungal biomass for comparative analysis in biosorption studies, actively growing fungal cultures were first cultivated under standard conditions as described in section 4.4.1, 4.4.2 and 4.4.3. After a 7-day incubation period, the fully developed live fungal biomass was subjected to thermal inactivation by autoclaving at 121°C under 15 psi pressure for 20 minutes using a laboratory autoclave. Following autoclaving, the biomass was allowed to cool to room temperature under sterile conditions and then harvested aseptically from the culture flasks. This process ensured complete denaturation of cellular components and enzymatic systems, effectively terminating all metabolic activity while preserving the structural integrity of the biomass required for adsorption studies [125,142].

4.5 Preparation of Control samples

To ensure the reliability and accuracy of the experimental results, both abiotic and biotic control systems were established and maintained throughout the study. These controls served to distinguish the effects of fungal activity, support materials, and external factors on dye decolorization and degradation.

4.5.1 Abiotic Controls

Abiotic controls were designed to evaluate non-biological factors that may contribute to dye removal, such as interaction with medium components or adsorption onto immobilization supports [107].

- **Abiotic Dye Control**: Each dye solution was added to 100 mL of sterile liquid organic medium (composition as described in Section 4.4), without the addition of fungal biomass. These flasks were incubated under the same conditions as experimental flasks to monitor any spontaneous degradation or abiotic interactions influencing dye stability.
- **Abiotic Immobilization Support Control**: To assess the potential adsorption of dyes onto the immobilization materials, 12 pieces (10 mm^3) of polypropylene dishwasher sponge (support S1) or polyester sponge (support S2) were added to 100 mL of sterile liquid organic medium, followed by the addition of dye. No fungal biomass was introduced. These flasks helped isolate any physical dye removal due to the support matrices alone.

4.5.2 Biotic Controls

Biotic controls were prepared to evaluate any changes in the culture medium resulting solely from fungal metabolism in the absence of dye, ensuring that observed effects in test samples were due to dye-fungus interactions and not medium modification alone.

Biotic Controls for Free and Immobilized Biomass: These were prepared following the same protocols outlined in Sections 4.4.1 (free fungal biomass), 4.4.2 (self-immobilized fungal biomass), and 4.4.3 (immobilized biomass on synthetic supports). However, no dye was added to these cultures. The flasks were incubated under identical conditions to their respective

experimental counterparts. These controls were used to monitor changes in the medium unrelated to dye presence.

4.5.3 Water Control

A sterile water control (autoclaved distilled water) was maintained under the same incubation conditions to monitor potential contamination during handling and experimental procedures. This served as a negative control to validate aseptic conditions throughout the experimental duration.

The variation in control samples has been denoted as shown in Figure 10.

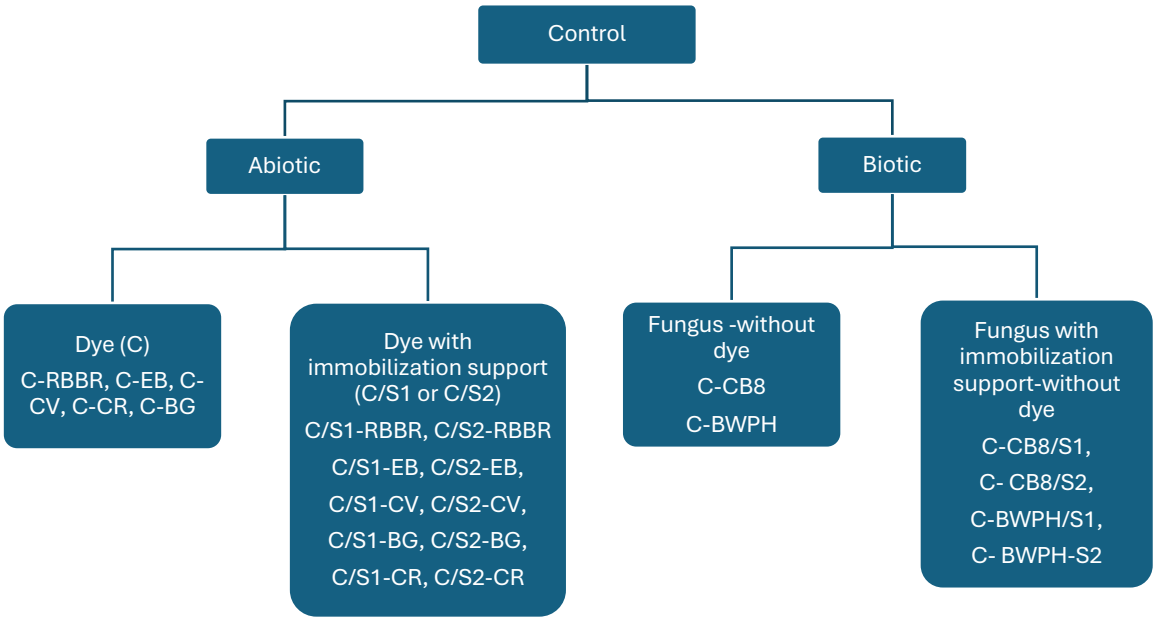

Figure 10. Schematic representation of Abiotic and Biotic control samples and their abbreviations

4.6 Preliminary assessment of dye decolorization

A preliminary investigation was conducted to evaluate the dye decolorization capabilities of selected fungal strains, *Trametes versicolor* (strain CB8) and *Pleurotus ostreatus* (strain BWPH) for dyes from different chemical classes. The research methodology related to CB8 strain dye decolorization efficiency has been mentioned in **Publication 1** [143]. Both free and immobilized forms of fungal biomass were tested. The immobilization was carried out using dishwasher and sponge materials, following the protocols detailed in Sections 4.4.1 and 4.4.3. Five synthetic dyes - BG, CV, CR, EB and RBBR - were selected for the assay. Initial dye concentrations ranged from 100 to 400 mg/L to assess the decolorization efficiency across a

gradient of initial dye concentrations. For each test, 2 mL of dye-containing medium was prepared at the desired concentration. A single piece of 7-day-old immobilized fungal biomass or 0.5 g homogenized free fungal biomass was introduced into each test sample as depicted in Figure 11. The samples were incubated statically at ambient room temperature (20°C ± 2°C) for 96 hours and it was observed visually on a regular basis. After 96 h incubation, the residual dye concentration in the samples was determined by measuring absorbance of decolorized medium using Hitachi U-1900 UV-VIS spectrophotometer using wavelength scan (200 -1100 nm) at scan speed of 200 nm/s. The maximum absorbance λmax for BG (623nm), CV (584nm), CR (492nm), EB (598nm), RBBR (596nm) dyes were determined by performing wavelength scan (200 - 1100 nm). Dye controls were included for each dye to ensure accurate comparison. Carriers without fungal immobilization were included in test to compare the physical efficiency of carrier material for dye sorption.

Based on the recorded absorbance, the concentration of dye in control samples and biomass containing samples were calculated by using standard curve. Appropriate dilution factors were applied where necessary. The dye decolorization percentage (DP%) was calculated using the below mentioned equation 1:

$$DP[\%] = \frac{C-S}{C} \times 100 \qquad \text{(Equation 1)}$$

Where, C is the current concentration of dye in a control sample with support or only medium (mg/L), and S is the current concentration of dye in samples with immobilized or free fungal biomass (mg/L).

To distinguish physical sorption from biodegradation, a desorption analysis was conducted following the modified procedure based on Sun et al. [144]. After 96 hours of incubation, the fungal biomass was separated from the culture medium. The pellets were gently washed with distilled water and then incubated in 2 mL of 70% (v/v) methanol solution for 24 hours under static conditions at room temperature (20 ± 2°C) to extract physically adsorbed dye. The absorbance of the methanol extract was measured at the corresponding λmax of each dye to determine the concentration of desorbed dye. The calculations for estimation of desorption were performed by slightly modifying equation used by Rybczyńska-Tkaczyk, Korniłłowicz-Kowalska [145].The percentage of dye desorbed (DS%) from each sample was calculated by using equation 2.

$$DS[\%] = \frac{Cs}{Cc} \times 100 \qquad \text{(Equation 2)}$$

where, DS[%] is desorption percentage, C_S is the desorb dye concentration in sample with fungal biomass (mg/L), C_C is the desorb dye concentration in control sample without biomass (mg/L).

(a)

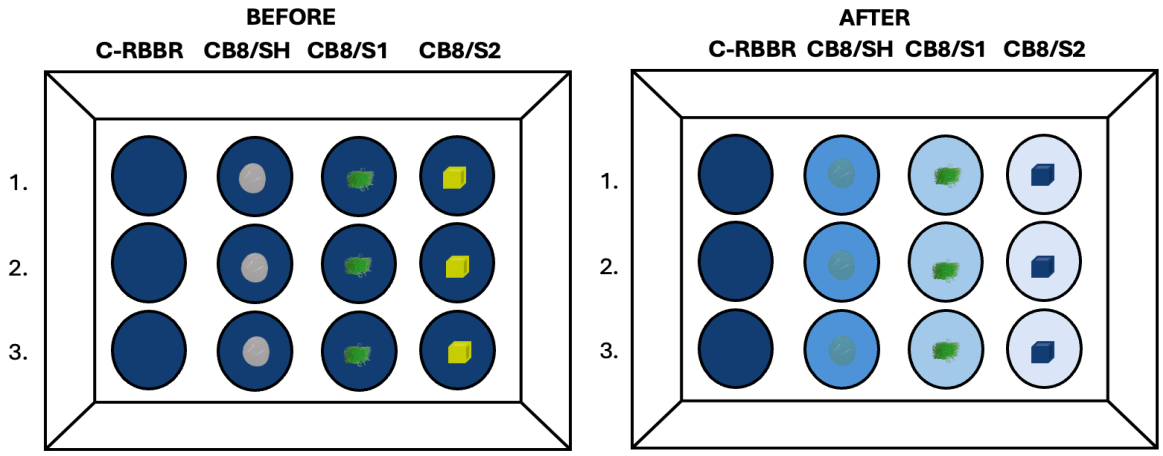

(b)

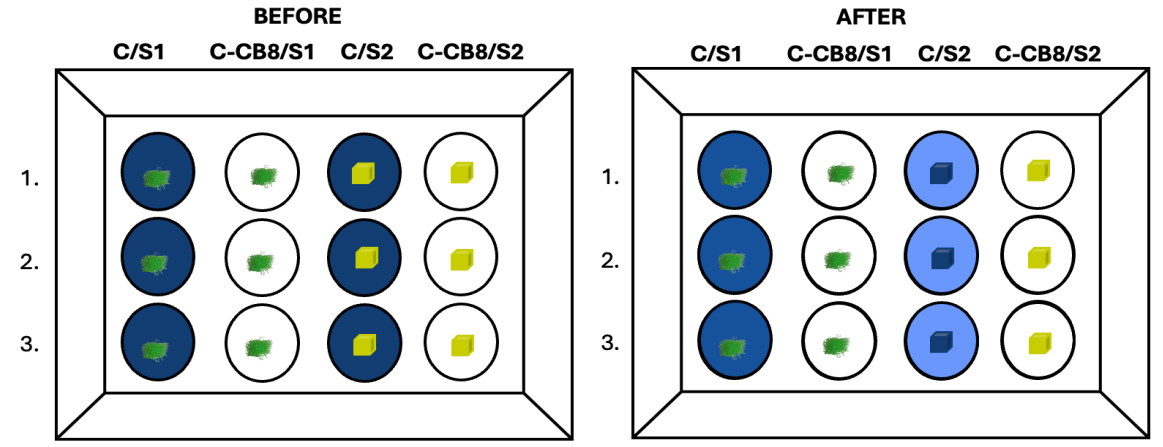

Figure 11. Schematic representation of Remazol Brilliant Blue R dye decolorization by (a) Self-immobilized and dishwasher immobilized and sponge immobilized biomass along with (b) their control samples (Photo by R. Upadhyay)

Based on the outcomes of the preliminary dye decolorization experiments, sponge was identified as the more suitable immobilization support compared to dishwasher, due to its superior performance in supporting fungal-mediated dye degradation. Consequently, all subsequent experiments employed sponge as the immobilization matrix, while the use of dishwasher material was discontinued.

Among the five dyes initially tested, three-RBBR, EB and CV were selected for further investigation. This selection was based on the high decolorization efficiency observed with both *T. versicolor* and *P. ostreatus* strains for these specific dyes, indicating their potential for effective bioremediation. To facilitate more detailed kinetic and mechanistic studies, the working volume of the decolorization system was scaled up from the 2 mL micro-assay used

in preliminary screening to a 100 mL batch system. This upscaling will allow to evaluate fungal strains' ability to treat large dye containing volume and optimize process.

4.7 Assessment of dye biodegradation efficiency at different parameters

4.7.1 Impact of fungal culture agitation on dye decolorization

It is important to investigate how physical growth conditions - specifically static versus shaking incubation - influence the fungal growth and their efficiency in decolorizing synthetic dyes. This experiment helps discern how fungal morphology, influenced by physical growth conditions, directly affects the efficiency of dye decolorization [146]. It provides insights into optimizing incubation setups for enhanced fungal bioremediation performance. Fungal strains *Trametes versicolor* (CB8) and *Pleurotus ostreatus* (BWPH) were used to evaluate the influence of physical conditions on growth and dye degradation potential. Each fungal strain was inoculated into 100 mL of liquid organic medium (Regular Medium) contained in 250 mL Erlenmeyer flasks**.** Two distinct incubation conditions were employed: In Static Condition, flasks were incubated at room temperature without agitation. Whereas in shaking Condition, flasks were incubated at room temperature on a rotary shaker at 150 rpm. All flasks were incubated for 7 days**,** and fungal growth patterns were visually monitored throughout. Under static conditions, the fungus grew as a mat on the surface and in submerged filamentous form. Under shaking conditions, the fungus formed discrete, compact mycelial pellets, indicating altered morphology due to increased aeration and shear forces. Following the growth period, a fixed concentration **(**250 mg/L**)** of one of the dyes - RBBR**,** EB, or CV - was added to each flask. Post dye addition, all flasks were incubated under static conditions for further monitoring. Samples were collected at 0, 24, 48, 72, and 96 h to evaluate dye degradation. Medium plus dye (no fungus) was incubated in same condition as control to assess abiotic degradation. While medium plus fungus (no dye) was incubated as control to confirm no background absorbance due to fungal metabolites. At each time point, the absorbance of the medium was measured at the dye's maximum absorbance wavelength using a UV-Visible spectrophotometer. Using dye-specific standard curves, the residual dye concentration in the medium was calculated and finally percentage of dye decolorization was computed.

To explore the influence of static and shaking growth conditions on enzyme production and activity as these conditions may simulate different oxygenation and nutrient distribution scenarios, which can significantly affect fungal metabolism and enzyme secretion. By comparing enzyme activity profiles under both conditions, the study aimed to capture not only the physical but also the biochemical responses of the fungi during dye degradation [147]. To investigate the role of ligninolytic enzymes during dye degradation, extracellular crude enzyme extracts were collected from fungal cultures at three time points: 0 hours (baseline), 24 hours, and 72 hours post-introduction of respective dyes: RBBR, EB or CV. These samples were analyzed to determine the activities of four key enzymes involved in the degradation of xenobiotic compounds: Laccase (Lacc)**,** Manganese Peroxidase (MnP), Manganese-Independent Peroxidase (MnIP), and Lignin Peroxidase (LiP). The enzyme assays were performed following the protocols described in Section 4.8. In parallel, control fungal cultures

(without dye) were maintained under the same static and shaking conditions to assess the baseline enzymatic activity in the absence of dye. This allowed for a comparative analysis to distinguish dye-induced enzymatic responses from natural metabolic processes.

4.7.2 Impact of Carbon source and agitation on dye decolorization

The selection of carbon source significantly impacts fungal metabolism, growth patterns, and enzyme secretion profiles, all of which directly affect dye decolorization potential. Understanding this relationship helps in optimizing conditions for maximum bioremediation efficiency [148]. To evaluate how different carbon sources influence the growth of both fungal strains - *T. versicolor* (CB8) and *P. ostreatus* (BWPH) - and its potential to decolorize RBBR, EB and CV dyes in liquid culture, three media types were prepared as shown in Figure 12.

The Glucose Medium (GM) contains additional amount of glucose, a simple sugar (monosaccharide) which can be readily utilized by most fungi as a primary carbon and energy source [149]. Its rapid uptake leads to quick fungal proliferation and may support high biomass production. Sucrose, present in Sucrose Medium (SM), is a disaccharide composed of glucose and fructose, it must be hydrolyzed before utilization. Its metabolism may trigger different regulatory pathways [150]. It can induce certain oxidative enzymes more effectively than glucose, possibly improving dye breakdown in some fungi. Regular Medium (RM) represents the baseline organic nutrient-rich medium used throughout the study. It supports balanced fungal growth and metabolic activity. It can be used as control to evaluate how glucose and sucrose influence degradation efficiency relative to the standard medium.

To prepare the inoculum, the fungal strain was cultivated in Regular Medium (RM) for a period of seven days to achieve optimal growth. The resulting homogenized mycelium of either CB8 or BWPH was then transferred into 250 mL Erlenmeyer flasks containing 100 mL of the designated media—RM, Glucose Medium (GM), or Sucrose Medium (SM). To evaluate both the influence of carbon source and incubation conditions, experiments were conducted under two different setups: one set of flasks was maintained under static conditions at room temperature, while another set was incubated on a shaker at 150 rpm, also at room temperature. Both sets were incubated for seven days. Fungal growth was observed visually throughout the incubation period. Following the growth phase, each culture was supplemented with dye (RBBR, EB or CV) at a fixed concentration of 250 mg/L to assess decolorization performance. Absorbance readings were taken at the dye's maximum absorbance wavelength using a spectrophotometer at 0, 24, 48, 72, and 96 hours. The percentage of dye decolorization was then determined using a standard calculation formula (Equation 1).

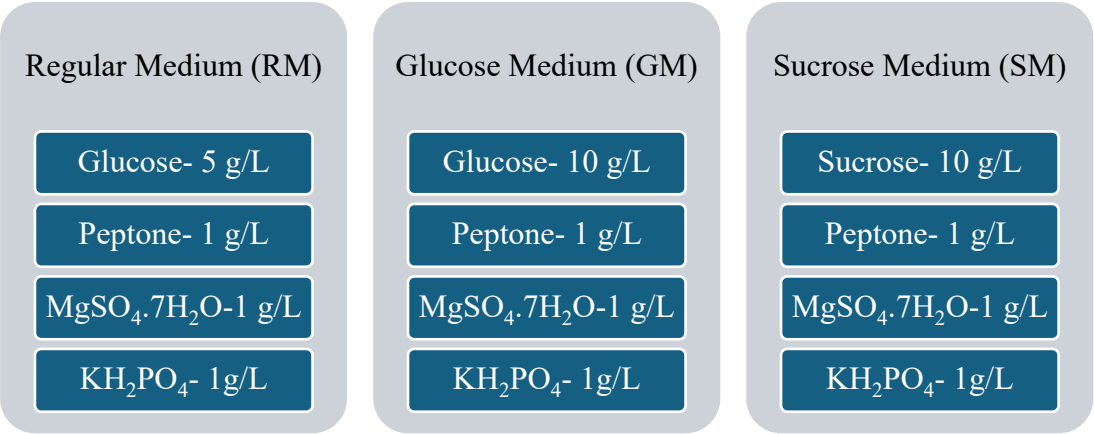

Figure 12. Medium composition - Modification in carbon source

4.7.3 Impact of Nitrogen source and agitation on dye decolorization

Likewise, the carbon source, the selection of nitrogen source significantly impacts fungal metabolism, growth patterns, and enzyme secretion profiles, all of which directly affect dye decolorization potential [151,152]. Understanding this relationship helps in optimizing conditions for maximum bioremediation efficiency. To evaluate how different nitrogen sources influence the growth of both the fungal strains and its potential to decolorize RBBR, EB and CV dyes in liquid culture, two media types were prepared as shown in Figure 13.

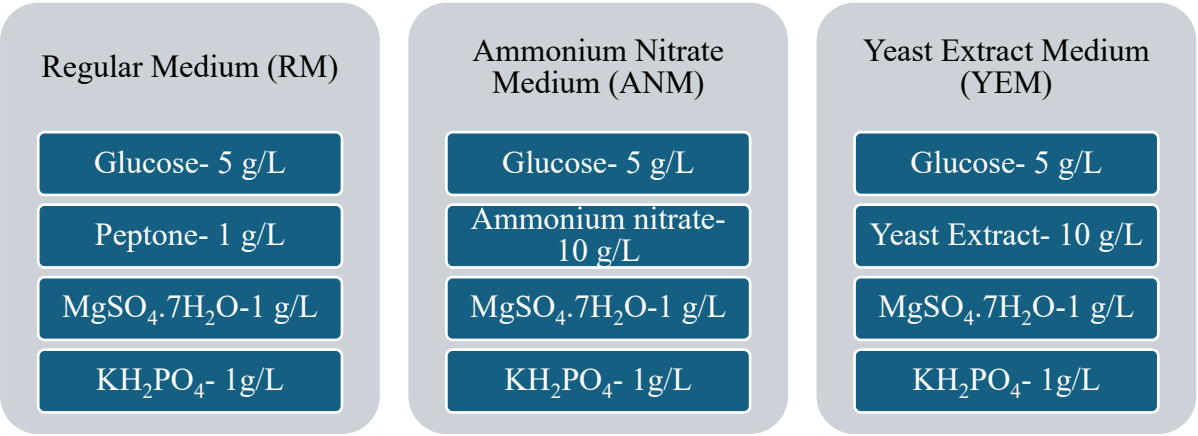

Figure 13. Medium composition - Modification in nitrogen source

The regular medium contains peptone, which is organic nitrogen source, a mixture of peptides and amino acids. It supports robust fungal growth and enzyme synthesis which makes it ideal for general metabolic activity [153]. Balanced nutrient profile of RM may facilitate moderate dye decolorization and consistent biomass production. While in Ammonium Nitrate medium (ANM), the peptone was replaced with ammonium nitrate - an inorganic nitrogen source. It provides readily available nitrogen ions; often induces stress-responsive pathways. It can potentially enhance oxidative enzyme (like laccase or peroxidase) production, leading to improved dye degradation in some fungi. However, excessive inorganic nitrogen may also

suppress growth. Yeast Extract Medium (YEM) contains rich organic nitrogen source which may enhances fungal biomass and enzyme secretion due to its complex nutritional content. It often promotes higher dye decolorization efficiency by stimulating enzyme-rich metabolic states.

To prepare the inoculum, the fungal strain was cultivated in Regular Medium (RM) for a period of seven days to achieve optimal growth. The resulting homogenized mycelium of either CB8 or BWPH was then transferred into 250 mL Erlenmeyer flasks containing 100 mL of the designated media - RM, Ammonium Nitrate Medium (ANM), or Yeast Extract Medium (YEM). To evaluate both the influence of nitrogen source and incubation conditions, experiments were conducted under two different setups: one set of flasks was maintained under static conditions at room temperature, while another set was incubated on a shaker at 150 rpm, also at room temperature. Both sets were incubated for seven days. Fungal growth was observed visually throughout the incubation period. Following the growth phase, each culture was supplemented with dye (RBBR, EB or CV) at a fixed concentration of 250 mg/L to assess decolorization performance. Absorbance readings were taken at the dye's maximum absorbance wavelength using a spectrophotometer at 0, 24, 48, 72, and 96 hours. The percentage of dye decolorization was then determined using a standard calculation formula.

Among the tested carbon and nitrogen sources for media preparations, the regular medium (RM) supported the highest fungal biomass production. Furthermore, shaking conditions resulted in superior dye decolorization efficiency compared to static cultures. The enzyme activity assays corroborated these findings, indicating enhanced production of extracellular enzymes under shaking conditions in RM. These enzymes are considered pivotal for effective dye degradation. Therefore, for all subsequent experiments, RM was selected as the growth medium, and shaking conditions were adopted as the standard cultivation method.

4.7.4 Impact of Immobilization on dye decolorization

The influence of sponge-immobilized fungal biomass (CB8/S2 and BWPH/S2) on dye degradation efficiency was evaluated. Fungal biomass was prepared as described in the previous section 4.4.3. Following incubation, individual flasks were supplemented with RBBR, EB, and CV dyes at a final concentration of 250 mg/L. Dye degradation was assessed spectrophotometrically at the respective absorbance maxima of each dye at intervals of 0, 24, 48, 72, and 96 h. The percentage of dye decolorization was calculated using the equation 1.

To choose optimal dye decolorizing nutrient condition, a three-factor Analysis of Variance (ANOVA) was performed to evaluate the effects of carbon source, nitrogen source, and fungal species on the dye removal efficiency as response variable. Each factor was treated as an independent variable, and experiments were conducted in a factorial design. The total variation in the data was partitioned into components due to the main effects of each factor and residual (error) variation. For each factor, the sum of squares (SS), degrees of freedom (df), and mean square (MS) were calculated. The F value was obtained by dividing the MS of each factor by the residual MS, and p-values were used to assess statistical significance. This analysis allowed

determination of which nutrient factor and fungal species had significant influence on the response. After performing ANOVA, Tukey's post hoc test was conducted to perform pairwise comparisons of mean dye decolorization percentages across all tested conditions, including agitation, immobilization, nutrient medium composition, and fungal biomass type. The objective of this analysis was to identify statistically significant differences in dye decolorization efficiency among treatments and to determine the optimal experimental conditions for subsequent experiments and molecular-level analyses.

4.7.5 Evaluation of Dye mixture decolorization efficiency

In order to ensure that the evaluation was limited to the fungal capacity to degrade mixed dyes and not to individual environmental parameters, all experiments were conducted under previously optimized physicochemical conditions (temperature, pH, agitation, and nutrient content). Evans Blue (EB), Crystal Violet (CV), and Remazol Brilliant Blue R (RBBR) were used to prepare a ternary synthetic dye mixture. To reach a final combined concentration of 250 mg/L in the reaction medium, each dye was added in an equal ratio (1:1:1). To prevent deterioration or changes in absorbance properties during storage, the dye mixture was made freshly before experiment. A UV-visible wavelength scan of the dye mixture was carried out to determine the absorption maxima for dye mixture. The Hitachi U-1900 UV-VIS spectrophotometer was used to scan the dye solution at a speed of 200 nm/s utilizing a wavelength scan of 200-1100 nm. The highest absorbance was recorded at 590 nm.

Decolorization tests were conducted in 250 mL Erlenmeyer flasks using 100 mL of Regular Medium (RM). Following sterilization and cooling, fungal biomass were prepared as described in sections 4.4.2 and 4.4.3 and allowed to grow for seven days. After incubation, dye mixture was added aseptically to reach a final concentration of 250 mg/L. Over the course of the 96-hour treatment period, the dye mixture's decolorization was observed. At 0, 24, 48, 72, and 96 hours, 1 mL of the supernatant was extracted and used for spectrophotometric analysis. The previously described standard dye removal equation 1 was used to determine the percentage of decolorization.

4.8 Evaluation of Enzymatic Activity

The study of enzyme activity patterns under non-immobilized, self-immobilized, and carrier-immobilized circumstances was performed to clarify the impact of physical and biochemical parameters of fungal systems during dye degradation. These growth tactics were chosen to replicate different oxygenation levels and nutrient distribution patterns, which are recognized to substantially affect fungal metabolism and extracellular enzyme production.

To assess enzymatic reactions in the dye biodegradation process, fungal biomass was cultured according to the protocols outlined in Sections 4.4.1, 4.4.2, and 4.4.3 for free fungal biomass, self-immobilized, and carrier-immobilized conditions, respectively. Extracellular crude enzyme extracts were collected from 7-day-old fungal cultures at specified time intervals after dye addition: 0 h (day 7), 24 h (day 8), 48 h (day 9), 72 h (day 10), and 96 h (day 11). The

cultures were subjected to the appropriate dyes-Remazol Brilliant Blue R (RBBR), Evans Blue (EB), or Crystal Violet (CV). The daily timeline indicates the age of the fungal culture, whereas the hourly timeline reflects the duration after dye supplementation.

The extra cellular crude samples were examined to assess the activity of three principal extracellular ligninolytic enzymes implicated in the breakdown of xenobiotic compounds: laccase (Lacc), manganese peroxidase (MnP), and lignin peroxidase (LiP). Enzyme assays were conducted in accordance with the methods outlined in the following sections. Enzymatic activities were measured spectrophotometrically with a Hitachi U-1900 spectrophotometer at 25 °C. All measurements were conducted in triplicate to guarantee reproducibility and precision. Simultaneously, fungal cultures devoid of dye supplementation were incubated under the same experimental conditions to ascertain baseline enzymatic activity. This method facilitated a comparative evaluation of dye-induced enzymatic reactions in relation to intrinsic fungal metabolic activity.

4.8.1 Laccase

Laccase plays a crucial role in the biodegradation of synthetic dyes by white-rot fungi due to its broad substrate specificity and strong oxidative potential [154,155]. Its ability to act on a wide range of aromatic substrates makes it particularly significant in the detoxification and decolorization of industrial dye effluents. Laccase activity was measured based on the oxidation of 2,6-dimethoxyphenol (DMP), following the method described by de Jong et al. [156] and Jureczko et al. [135] with slight modifications. The reaction mixture contained 1.17 mM DMP in 58.8 mM sodium malonate buffer (pH 4.5), in a total volume of 850 µL. The change in absorbance was monitored at 468 nm (λ=468 nm). The extinction coefficient used for the oxidized DMP product was 49,600 M^{-1} cm^{-1}.

4.8.2 Manganese Peroxidase

Manganese Peroxidase (MnP) is one of the key ligninolytic enzymes secreted by white-rot fungi. MnP catalyzes the oxidation of Mn^{2+} to Mn^{3+} in the presence of hydrogen peroxide (H_2O_2) [157]. The Mn^{3+} formed acts as a diffusible oxidizer capable of breaking down a wide range of phenolic and non-phenolic dye structures. To evaluate the activity of MnP, extracellular crude enzyme extracts were obtained at previously mentioned timepoints from fungal cultures grown under dye-containing conditions. The MnP activity was determined by monitoring the oxidation of 1 mM 2,6-dimethoxyphenol (DMP) in the presence of 1 mM $MnSO_4$ and 0.4 mM H_2O_2, using 50 mM sodium malonate buffer (pH 4.5), as described by de Jong et al. [156] and Moreira et al. [158]. The total reaction volume was 1 mL, and absorbance was measured at 468 nm. The extinction coefficient for the oxidized DMP product was 49,600 M^{-1} cm^{-1}. To assess Manganese independent Peroxidases (MnIP) activity, a parallel reaction was conducted under the same conditions, but with 1 mM EDTA replacing $MnSO_4$ to chelate Mn^{2+} and eliminate MnP activity. The MnIP value was taken as the activity measured in this EDTA-containing assay. The net MnP activity was calculated by subtracting the MnIP activity from the total peroxidase activity measured in the $MnSO_4$-containing reaction.

4.8.3 Lignin Peroxidase

Lignin Peroxidase (LiP) is a key extracellular heme-containing enzyme, catalyzes the oxidative cleavage of non-phenolic aromatic substrates by utilizing hydrogen peroxide (H_2O_2) as an electron acceptor. Its high redox potential enables it to break down stable aromatic rings and chromophores present in various textile dyes, thereby contributing significantly to fungal dye decolorization mechanisms. To quantify LiP activity during dye degradation, the oxidation of veratryl alcohol to veratraldehyde was monitored, as per the method described by de Jong et al. [156] and Moreira et al. [158], with appropriate modifications. The reaction mixture consisted of 50 mM sodium tartrate buffer (pH 3.0), 2 mM veratryl alcohol (substrate) and 0.4 mM hydrogen peroxide (H_2O_2) (oxidizing agent) in a total reaction volume of 1 mL. The enzymatic oxidation of veratryl alcohol was initiated by the addition of H_2O_2 and monitored spectrophotometrically by measuring the increase in absorbance at 310 nm, which corresponds to the formation of veratraldehyde. The molar extinction coefficient used for the calculation of enzymatic activity was 9,300 M^{-1} cm^{-1}.

Enzyme activities were calculated using the following equation 3, with the unit definition of l μmol/min for product formation.

$$Activity = \frac{\Delta A \cdot DF \cdot 10^6}{\Delta t \cdot \varepsilon \cdot d} \qquad \text{(Equation 3)}$$

Where,

- $\Delta\mathbf{A}$ = change in absorbance,
- **DF** = dilution factor ($DF = V_t/V_s$),
- $\mathbf{V_t}$ = total reaction volume (mL),
- $\mathbf{V_s}$ = sample volume (mL),
- **d** = path length of cuvette (cm),
- $\Delta\mathbf{t}$ = reaction time (min),
- $\boldsymbol{\varepsilon}$ = molar extinction coefficient (M^{-1} cm^{-1}).

4.9 Transcriptome Analysis of CB8 strain

4.9.1 Fungal Cultivation and Dye Treatment

Based on preliminary dye decolorization experiments, *Trametes versicolor* strain CB8 was identified as the most effective isolate for the degradation of Remazol Brilliant Blue R (RBBR) and Evans Blue (EB). This strain was, therefore, selected for detailed transcriptomic profiling to investigate differential gene expression in response to dye exposure.

CB8 biomass was prepared as mentioned in section 4.4.2 and incubated for 7 days. Post-incubation, one flask was maintained as an untreated control, while the remaining flasks were each supplemented with one of the dyes (RBBR or EB) to a final concentration of 250 mg/L. Upon dye addition, the fungus may initiated the secretion of oxidative enzymes -namely laccase (Lacc), manganese peroxidase (MnP), and lignin peroxidase (LiP) - as part of its

biodegradation response. After 24 hours of exposure, the culture media were discarded, and the fungal pellets were collected by filtration and subsequently washed thoroughly with deionized water to remove residual dye and medium components. The washed fungal biomass was subjected to centrifugation to obtain concentrated mycelial pellets. These pellets were immediately processed for total RNA extraction. The RNA extraction and subsequent analysis was performed in triplicates for each sample. It was labelled respectively as 1CB8CONT, 2CB8CONT, 3CB8CONT, 4CB8RBBR, 5CB8RBR, 6CB8RBBR, 7CB8EB, 8CB8EB AND 9CB8EB. Due to limitation of funding, CB8/CV and samples from other strains could not send for transcriptomic analysis. We choose best decolorizing conditions to perform differential gene expression (DEGs) analysis.

The transcriptomic analysis was systematically divided into three key stages: RNA extraction and quantitation, RNA sequencing, and Data analysis. The assessment of the metabolic condition of bioremediating fungi via mRNA analysis can yield prompt insights into the intricate bioremediation processes [159,160]. Transcriptome profiling can also result in the identification of novel genes whose roles are unknown and whose involvement in the bioremediation was previously unexpected, given our incomplete understanding of the full genomic picture of bioremediation [120].

4.9.2 RNA Extraction and quantitation

The Qiagene RNeasy Plant Mini kit has been utilized for RNA extraction. The kit has been purchased from Qiagen polska Sp. z o.o., Wrocław, Poland. This kit is suitable for purification of total RNA from plant cells and tissues and filamentous fungi. It contains RNeasy mini spin columns, QIAshredder spin columns, collection tubes (1.5 ml), collection tubes (2 ml), Buffer RLT, Buffer RLC, Buffer RW1, Buffer RPE (concentrate) and RNAse-Free Water.

The RNeasy Plant Mini Kit provides two options for lysis buffers: Buffer RLT (containing guanidine thiocyanate) and Buffer RLC (containing guanidine hydrochloride). Due to reports suggesting that guanidine thiocyanate in Buffer RLT may cause the solidification of filamentous fungal mycelia—thus hindering RNA extraction-Buffer RLC was selected for this protocol. Prior to use, 10 µL of β-mercaptoethanol (β-ME) was added per 1 mL of Buffer RLC. Buffer RPE, provided as a concentrate, was prepared by adding four volumes of 96-100% ethanol to make a working solution. All experimental steps were carried out in a fume hood with appropriate safety precautions.

Fungal mycelial pellets were immediately processed after collection. Approximately 100 mg of wet mycelium was weighed and transferred to mortar. Liquid nitrogen was added, and the tissue was ground thoroughly using a pestle. The powdered tissue was quickly transferred to a 2 mL RNase-free microcentrifuge tube pre-cooled with liquid nitrogen. To the powdered tissue, 450 µL of Buffer RLC was added, and the sample was vortexed vigorously to ensure complete lysis. The homogenate was then applied to a QIAshredder spin column and centrifuged at maximum speed for 2 minutes. The resulting flow-through, containing the clarified lysate, was carefully transferred to a fresh RNase-free tube, avoiding any disturbance of the pellet. 0.5

volume of 96-100% ethanol was added to the lysate, mixed thoroughly by pipetting, and the entire volume was loaded onto an RNeasy spin column placed in a 2 mL collection tube. The column was centrifuged at 10,000 rpm for 15 seconds. The flow-through was discarded. To wash the spin column membrane, 700 µL of Buffer RW1 was added and centrifuged at 10,000 rpm for 15 seconds. The flow-through was discarded, and 500 µL of Buffer RPE was added, followed by centrifugation at 10,000 rpm for 15 seconds. A second wash with 500 µL of Buffer RPE was performed, this time centrifuging for 2 minutes at 10,000 rpm to ensure complete removal of ethanol from the membrane. The RNeasy spin column was then placed in a new 2 mL collection tube and centrifuged at full speed for 1 minute to remove any residual Buffer RPE. For RNA elution, the column was transferred to a clean 1.5 mL microcentrifuge tube, and 30 µL of RNase-free water was applied directly to the membrane. The column was centrifuged at 10,000 rpm for 1 minute. The eluted RNA was immediately transferred to a mini cooler and used for RNA quantification.

A volume of 2 µL from each extracted RNA sample was used for quantification using a NanoDrop spectrophotometer. The nucleic acid concentration (ng/µL), along with the absorbance ratios A260/A280 and A260/A230, were recorded to assess RNA purity and integrity. Samples exhibiting an A260/A280 ratio greater than 1.8 and an A260/A230 ratio above 1.2 were considered acceptable for sequencing. RNA samples not meeting these quality criteria were discarded, and RNA extraction was repeated until both high purity and sufficient concentration were achieved.

The RNA extraction experiments were carried out at Biotechnology Center, Faculty of Automation, Electronics and Computer Science, Department of Systems Engineering and Biology, Silesian University of Technology, Krzywoustego 8, 44-100 Gliwice under supervision of dr hab. Prof. Magdalena Skonieczna.

4.9.3 RNA Sequencing Library Preparation and Processing

The isolated total RNA samples were transported to Macrogen (Netherlands) for sequencing and further analysis. The following steps, as provided by Macrogen, were employed in the RNA library preparation and sequencing process:

Total RNA samples were treated with DNase to eliminate any residual genomic DNA contamination, ensuring the purity of RNA for downstream applications. Depending on the RNA type, appropriate purification methods were selected. For messenger RNA (mRNA) containing poly-A tails, mRNA purification kits were used. For non-coding RNAs such as long intergenic non-coding RNAs (lincRNAs) was removed using a Ribo-Zero RNA removal kit to enrich the RNA species of interest. The purified RNA was randomly fragmented to generate short RNA fragments, suitable for short-read sequencing platforms. The fragmented RNA was reverse transcribed into complementary DNA (cDNA) using reverse transcriptase enzymes. Sequencing adapters were ligated to both ends of the cDNA fragments to facilitate sequencing and amplification. The adapter-ligated cDNA fragments were amplified by PCR. Fragments with insert sizes ranging between 200 and 400 base pairs were selected for sequencing. For

paired-end sequencing, both ends of the cDNA fragments were sequenced according to the desired read length.

4.9.4 RNA-Sequencing Data Analysis

The quality of the raw sequencing reads was first assessed to ensure data integrity. Key parameters such as overall read quality, total number of bases, total reads, GC content, and other basic statistics were calculated. To minimize biases during downstream analyses, low-quality reads, adapter sequences, contaminant DNA, and PCR duplicates were identified and removed. The resulting high-quality trimmed reads were then aligned to the reference genome using HISAT2, a splice-aware aligner. Transcript assembly was carried out using StringTie based on the aligned reads. Gene expression levels were quantified in terms of read counts and normalized values, considering transcript length and sequencing depth. These normalization metrics were expressed as FPKM (Fragments Per Kilobase of transcript per Million mapped reads), RPKM (Reads Per Kilobase of transcript per Million mapped reads), and TPM (Transcripts Per Kilobase Million). Differential expression analysis was then performed to identify genes or transcripts that were significantly differentially expressed across experimental conditions with an absolute fold change ≥2 (|FC| ≥2) and nbinomWaldTest raw p-value <0.05. A two-way hierarchical clustering heatmap was generated from Z-score-scaled, log2-normalized expression values of differentially expressed genes (DEGs) identified in CB8CONT and CB8RBBR/ CB8EB conditions, including their replicates, for enhanced organization of genes and samples into related groups. Z-score transformation standardizes gene expression among samples, enabling direct comparison of relative upregulation and downregulation regardless of baseline expression levels.

For Gene Ontology (GO) and KEGG (Kyoto Encyclopedia of Genes and Genomes Orthology) pathway analyses, differentially expressed genes (DEGs) with an absolute fold change ≥2 (|FC| ≥2) and nbinomWaldTest raw p-value <0.05 were selected. Corresponding protein IDs for the comparisons CB8RBBR vs CB8CONT and CB8EB vs CB8CONT were extracted from the NCBI database and uploaded to the NCBI BatchEntrez portal to retrieve protein sequences in FASTA format, resulting in 1106 and 1830 differentially expressed protein sequences, respectively. These FASTA files were uploaded to the useGalaxy.eu web platform, where functional annotation was performed using eggNOG-mapper based on functional orthologs. The analysis generated outputs including seed orthologs, GO annotations, Clusters of Orthologous Groups (COG) functional classes, and Kyoto Encyclopedia of Genes and Genomes Orthology (KEGG-KO) assignments for DEGs of *Trametes versicolor* (CB8) under Remazol Brilliant Blue R (RBBR) and Evans Blue (EB) dye-degrading conditions compared to control cultures. GO terms and descriptions were referenced using UniProt and the Mouse Genome Informatics Gene Ontology resource. Subsequently, the most significantly up- and down-regulated DEGs were selected for detailed GO enrichment analysis and categorized into Molecular Function (MF), Biological Process (BP), and Cellular Component (CC) based on the most appropriate GO accession numbers.

4.10 Proteome Analysis of CB8 strain

4.10.1 Fungal cultivation and dye treatment

Based on preliminary dye decolorization experiments, *Trametes versicolor* strain CB8 was identified as the most effective isolate for the degradation of Remazol Brilliant Blue R (RBBR), Evans Blue (EB), and Crystal Violet (CV). This strain was, therefore, selected for detailed proteomic profiling to investigate differential protein expression in response to dye exposure.

Homogeneous fungal mycelia of *T. versicolor* CB8 were inoculated into 250 mL Erlenmeyer flasks, each containing 100 mL of sterile liquid organic growth medium. The cultures were incubated under continuous shaking at 150 rpm at room temperature for a period of seven days to ensure adequate biomass accumulation. Post-incubation, one flask was maintained as an untreated control, while the remaining flasks were each supplemented with one of the dyes (RBBR, EB, or CV) to a final concentration of 250 mg/L. Upon dye addition, the fungus may initiated the secretion of oxidative enzymes and many different proteins-namely laccase (Lacc), manganese peroxidase (MnP), and lignin peroxidase (LiP)-as part of its biodegradation response. After 48 h of exposure of dye, the fungal culture was subjected to separation of biomass and extracellular liquid. The entire culture medium was passed through filter paper to remove the fungal biomass. The filtrate obtained, referred to as the crude culture extract or extracellular liquid, was collected in sterile 50 ml centrifuge tubes and was subjected to overnight freezing at -20 °C to facilitate protein precipitation.

The proteomic analysis was systematically divided into three key stages: (1) Protein extraction & quantification, (2) Liquid Chromatography- Mass Spectrometry (LC-MS), and (3) Data analysis.

4.10.2 Protein Extraction & Quantification

The frozen extracellular liquid samples were allowed to thaw at room temperature on the following day. Once thawed, the samples were centrifuged at 8000 rpm for 20 minutes at 4 °C using a refrigerated centrifuge. This step was employed to remove any remaining insoluble particles and aggregates. The resulting supernatant, containing the soluble extracellular proteins, was carefully decanted into a fresh, sterile centrifuge tube to avoid disturbing the pellet. The supernatant was then subjected to ultrafiltration for protein fractionation.

Ultrafiltration was performed using VIVASPIN TURBO ultrafiltration units equipped with a 10 kDa molecular weight cut-off (MWCO) membrane. The selected MWCO allowed for the retention of proteins larger than 10 kDa while permitting smaller molecules to pass through. The ultrafiltration tubes were centrifuged at 4000 x g for 20 minutes at 4 °C in a refrigerated centrifuge.

Following centrifugation, the low-molecular-weight filtrate that passed through the membrane and collected in the bottom compartment was discarded. A small volume of the sample

remained above the membrane. Additional portions of the original filtrate were incrementally added to the upper chamber, and the centrifugation process was repeated. This step was cycled multiple times until the entire 100 mL volume of filtrate had been processed and the retained fraction in the upper chamber appeared free of dye, indicating successful removal of low-molecular-weight contaminants. This iterative ultrafiltration process allowed for the concentration and partial purification of the protein content, which was retained above the MWCO membrane in the upper reservoir.

Protein concentration in the extracted samples was determined using a colorimetric method based on a standard curve prepared with bovine serum albumin (BSA). A BSA stock solution with a concentration of 20 μg/mL was used as the protein standard. Serial dilutions of the BSA solution were prepared to generate a calibration curve covering a range of known concentrations. The absorbance of these standards was measured spectrophotometrically at the 595 nm for the Bradford assay. The use of albumin as a standard allows for consistent and reliable quantification of protein content in unknown samples, as albumin is a well-characterized, water-soluble protein with properties similar to many proteins present in biological extracts. This quantification was critical for subsequent normalization and comparison of protein expression among different treatment groups.

The absorbance values of protein extracts from experimental fungal samples - CB8/CONT, CB8/RBBR, CB8/EB, and CB8/CV - were recorded under the same conditions. The concentration of proteins in these samples was calculated by comparing their absorbance to the standard curve generated from the BSA standards.

The protein extraction experiments were carried out at Maria Curie-Skłodowska University, Faculty of Biology and Biotechnology, Institute of Biological Sciences, Akademicka 19, 20-033 Lublin during one month internship under supervision of dr hab. Prof. Grzegorz Janusz. The protein samples were lyophilized and sent to Institute of Biochemistry and Biophysics, Polish Academy of Sciences (PAS), Warsaw for further analysis.

4.10.3 Liquid Chromatography- Mass Spectrometry

Mass spectrometry experiments were performed at the Mass Spectrometry Laboratory at the Institute of Biochemistry and Biophysics PAS. The submitted samples were suspended in dissolution buffer (100mM NH_4HCO_3). The cysteines were reduced by 1 hour incubation with 5 mM tris(2-carboxyethyl) phosphine (TCEP) at 60 ^oC followed by 10 min. incubation at a room temperature with 20 mM methyl methanethiosulfonate (MMTS). Digestion was performed at 37°C overnight with 1 μg of trypsin (Promega). After digestion, pH was reduced by adding 5%TFA. 30 μl of each sample was introduced into LC-MS system comprised of Evosep One (Evosep Biosystems) directly coupled to an Orbitrap Exploris 480 mass spectrometer (Thermo Fisher Scientific). Obtained raw spectra were pre-processed with Mascot Distiller (version 2.8, Matrixscience) and searched against database comprising of *Trametes versicolor* protein sequences deposited in NCBI (version 20231124, 42,745 sequences) supplemented with popular MS contaminants (Crap, 115 sequences) using Mascot

search engine (version 2.8, Matrixscience). Search parameters were as follows: enzyme - Trypsin, max missed cleavages - 1, instrument - HCD (Higher-energy Collisional Dissociation), fixed modifications - Methylthio (C) , variable modifications - Oxidation (M). Data were recalibrated offline, with typical resulting parent mass window around 5 ppm and fragment mass window of 0.01 Da. FDR (False Discovery Rate) was kept under 1%.

4.10.4 Proteomic Data Analysis

Raw mass spectrometry data generated at the Mass Spectrometry Laboratory were processed using MaxQuant software (version 2.7.5.0). For each comparison pair-CB8RBBR vs. CB8CONT, CB8EB vs. CB8CONT, and CB8CV vs. CB8CONT-group-wise raw data files were uploaded into MaxQuant. Protein identification was performed against the *Trametes versicolor* reference proteome (Taxon ID: 5325), downloaded from UniProt in FASTA format. The database included common contaminant proteins obtained from the cRAP (Common Repository of Adventitious Proteins) database and was used as the reference for global search parameters. Database search parameters were defined as follows: Trypsin was specified as the proteolytic enzyme, with a maximum of one missed cleavage allowed. The minimum peptide length was set to 7 amino acids, and the peptide-spectrum match (PSM) false discovery rate (FDR) was fixed at 0.01. Data acquisition was specified as higher-energy collisional dissociation (HCD). Methylthio (C) was set as a fixed modification, while oxidation (M) was included as a variable modification. Label-free quantification (LFQ) was disabled (LFQ = FALSE) due to the absence of biological replicates.

Owing to limited funding, only a single sample from each experimental group was analyzed, without biological replicates. Consequently, this study was designed as an exploratory proteomics analysis aimed at identifying trends in differential protein expression under dye-degrading conditions relative to control samples. As a result, statistical significance testing was not applied. Protein identification and quantification outputs were extracted from the proteinGroups.txt files generated by MaxQuant for each comparison. Downstream data processing was carried out using Perseus software (version 2.1.6.0). Reverse hits, potential contaminants, and proteins identified only by site were excluded to generate high-confidence protein datasets. Protein intensity values were $\log_2$-transformed, and $\log_2$ fold change ($\log_2$FC) was calculated as the difference between treatment and control conditions. Proteins with zero intensity values were excluded from further analysis. In the absence of biological replicates, no p-value-based filtering was performed. Proteins exhibiting a $\log_2$ fold change ≥ 0.3 were considered differentially abundant. Data visualization, including scatter plots, was performed using R software (version 4.5.0).

For Gene Ontology (GO) and KEGG pathway analyses, differentially expressed proteins (DEPs) with log2fold change ≥ 0.3 were selected. Similar methodology to transcriptomic analysis was applied here as protein IDs for the comparisons CB8RBBR vs CB8CONT, CB8EB vs CB8CONT and CB8CV vs CB8CONT were uploaded to UniProt portal to retrieve protein sequences in FASTA format. These FASTA files were uploaded to the useGalaxy.eu web platform, where functional annotation was performed using eggNOG-mapper based on

functional orthologs. The analysis generated outputs including seed orthologs, GO annotations, Clusters of Orthologous Groups (COG) functional classes, and Kyoto Encyclopedia of Genes and Genomes Orthology (KEGG-KO) assignments for DEPs of *Trametes versicolor* (CB8) under Remazol Brilliant Blue R (RBBR), Evans Blue (EB) and Crystal Violet (CV) dye-degrading conditions compared to control cultures. GO terms and descriptions were referenced using UniProt. Subsequently, the most significantly up- and down-regulated DEPs were selected for detailed GO enrichment analysis and categorized into Molecular Function (MF), Biological Process (BP), and Cellular Component (CC) based on the most appropriate GO accession numbers.

4.11 Ecotoxicological evaluation of dye and post-treated samples

4.11.1 Assessment of Zootoxicity

The zootoxicity test was performed to evaluate the toxicity of pure dye and fungal treated dye containing sample. The DAPHTOXKIT F ^{TM} MAGNA was ordered from the TIGRET Sp. z o.o., Warsaw, Poland. The kit contains all the materials, including the test species *Daphnia magna* in the form of "dormant eggs (ephippia)", to perform acute toxicity tests according to internationally accepted Standard Methods OECD 211 (2012) and ISO 6341 (2012).

The zoo toxicity tests were performed in accordance with protocol provided with kit. Standard Freshwater (ISO formula according to ISO 6341) was prepared by filling a 2 liter volumetric flask with approximately one liter deionized water and 4 vials of concentrated salt solutions were added in the sequence 1 to 4 (provided with kit). Remaining deionized water was added up to the 2000 ml mark and shaken to homogenize the medium. The standard freshwater was aerated for 2 days before beginning of experiments and later utilized as hatching and dilution medium.

Hatching of the ephippia was initiated 3 days prior to the start of the toxicity test. The contents of one vial of ephippia was poured into the microsieve and rinsed thoroughly with tap water to eliminate all traces of the storage medium. Then ephippia was transferred into the hatching petri dish containing 15 ml pre-aerated Standard Freshwater, covered with lid and incubated for 3 days, at 20-22°C, under continuous illumination of min. 6000 lux. It is very important to pre-feed neonates prior to the test in order to avoid "Starvation to death" of the weakest individuals which may result in false mortality count. In order to avoid this problem, Spirulina powder was mixed with standard freshwater and then the homogenized solution was fed to neonates 2 hours prior to collection for toxicity test.

The dilutions of pure dye and post process samples were prepared in geometric series of 2. The collected post process sample was considered as 100% and then diluted to 50%, 25%, 12.5%, 6.25% using standard fresh water. Similarly pure dye control medium was considered as 100% and then diluted in same manner as samples.

The bioassays multiwell test plates had 30 test wells. Each plate was provided with 4 wells for the controls and 4 wells (A,B,C,D) for each toxicant concentration. Additionally, the plates were provided on the left side with a column of "rinsing wells" to prevent dilution of the

toxicant during the transfer of the neonates from the hatching petri dish to the test wells. The wells were labelled vertically as rows X (for the controls) and C1 (highest concentration), C2, C3, C4 and C5 (lowest concentration) for the toxicant dilutions. Each well of the test plates was filled with 10 ml toxicant solution or standard freshwater in the control column. 20 (actively swimming) neonates were transferred with a micropipette into each rinsing cup and then exactly 5 neonates were transferred from the rinsing wells into each of the 4 wells of each column. This transfer was performed in the order of increasing test concentrations (C5 to C1). Multiwell plate was covered with Parafilm strip and incubated in darkness at 20°C. After 24h and 48h incubation, the test plate was kept on transparent stage of the light table and determined the number of dead and immobilized test organisms. Based on the recorded data, concentration vs mortality% graph was plotted and 50% Effective Concentration (EC_{50}) value was determined. In order to classify the toxic substances, this value was converted into toxicity units according to the equation 4 and were classified to appropriate toxicity group as per Persoone Toxicity classes [161] as seen in Table 5.

$$TUa = 100/EC_{50} \qquad \text{(Equation 4)}$$

Table 5. Persoone Toxicity Classes (Published in **Publication 4**) [161]

TUa	**Class**	**Toxicity**
<0.4	Class I	no acute toxicity
0.4 <TU <1	Class II	low acute toxicity
1 <TU <10	Class III	acute toxicity
10 <TU <100	Class IV	high acute toxicity
TU> 100	Class V	very high acute toxicity

4.11.2 Assessment of Phytotoxicity

For assessment of toxic effect of pure dye and fungal treated dye containing samples at the producer level of ecosystem, the growth inhibition microbiotest was conducted with *Spirodela polyrhiza*, an aquatic freshwater duckweed. SPIRODELA DUCKWEED TOXKIT was ordered from TIGRET Sp. z o.o., Warsaw, Poland.

The test was performed as per standard protocol given with kit. The Steinberg growth medium prescribed by ISO for Lemna toxicity tests (ISO 20079) has been selected for the Spirodela microbiotest. This medium was prepared by transferring 10 ml of concentrated solutions from the vials A, B and C and 0.5 ml from vials D and E in 300 ml deionized water in a 500 ml liter volumetric flask. The flask is then filled to the mark with pure water. The contents of a tube with turions were poured in the microsieve and rinsed with deionized water to remove the storage medium. The microsieve was turned upside down above a petri dish containing 10 ml Steinberg medium, and another 10 ml Steinberg medium was then poured over the sieve to transfer the turions into the Petri dish. The Petri dish was then filled by adding 10 ml Steinberg

medium. The covered Petri dish was incubated for 3 days at 25 °C with continuous illumination at 6 000 lux.

The control with pure dye and post process samples were considered as 100% and then diluted to 50%, 25%, 12.5%, 6.25% according to standard methods. 1 ml Steinberg growth medium was put into the 8 cups of the control row, and 1 ml toxicant solution into each cup of the corresponding rows for the 5 toxicant concentrations, starting in sequence from the row under the control row (row B at the top of the test plate) towards the row with the highest test concentration (row F, at the bottom of the test plate). One germinated turion was transferred into each test cups with the aid of a spatula. A photo of the multiwell plate was taken with a digital camera (at t= 0h) and transferred to a computer file. The covered test plates were incubated for 3 days at 25 °C and with (continuous) 6 000 lux illumination, after which a digital picture of the multiwell was taken again (at t=72h) after removal of the lid.

The area of the first fronds was measured 2 times as the initial (small) frond of the germinated turions (t= 0h) and the area of the (grown) first fronds of the germinated turions (t= 72h). The photos of the multiwells were processed with an image analysis program- Image J. The mean area of the "Initial" fronds was calculated in each row (= I), as well as the mean area of the "Final" fronds (= F). These mean data were scored on the Data Treatment Sheet. Subtracting I from F gives "the growth" of the duckweeds in each row of the test plate. The percentage growth inhibition was calculated in each test concentration and 72h EC_{50} was computed by Probit analysis and converted into Toxicity Unit using equation 4.

4.12 Evaluation of different light intensities on dye degradation

The effect of different light conditions-white, red, blue, and green-on the degradation of two synthetic dyes (Remazol Brilliant Blue R [RBBR] and Evans Blue [EB] by white-rot fungi (WRF) was evaluated. Two fungal strains were used: *Trametes versicolor* (CB8) and *Pleurotus ostreatus* (BWPH). The initial concentration of each dye was set at 250 mg/L. Fungal mycelia were initially cultured in 100 mL of liquid organic medium contained in 250 mL Erlenmeyer flasks. The medium composition was as follows: glucose (5 g/L), peptone (1 g/L), $MgSO_4 \cdot 7H_2O$ (1 g/L), and KH_2PO_4 (1 g/L), adjusted to pH 5.7. Cultures were incubated at 20 ± 2 °C for 7 days. Following incubation, the mycelial biomass was harvested and homogenized using a disperser homogenizer (T18 basic ULTRA-TURRAX, IKA, Staufen, Germany) to prepare fungal suspensions for inoculation.

Two treatment sets were designed to assess the effect of light on dye degradation:

- Treatment 1 (Pre-grown Mycelia): Fungal suspensions were incubated under different light conditions for 7 days to allow mycelial growth. After this period, dye was added to the culture flasks, and decolorization was measured after 24 h and 72 h.
- Treatment 2 (Simultaneous Inoculation): Fungal inoculum and dye were added to the flasks simultaneously on day 1. Decolorization was assessed after 48 h and 120 h.

All treatments were performed under continuous light exposure (20 lux) using LED illumination cassettes (KT 115, Binder, Germany). The following light spectra were applied: White light (color temperature 4000-4750 K), Green light (wavelength 510-520 nm), Blue light (wavelength 465-470 nm), Red light (wavelength 620-625 nm). A dark condition was included as a control. Absorbance spectra of the dye-containing solutions were recorded in the range of 300-800 nm using a UV-Vis spectrophotometer to monitor decolorization. Previously mentioned equation 1 was used for calculation of dye decolorization percentage.

The effect of different light intensities on dye degradation experiments were carried out at Maria Curie-Skłodowska University, Faculty of Biology and Biotechnology, Institute of Biological Sciences, Akademicka 19, 20-033 Lublin during one month internship under supervision of dr hab. Prof. Grzegorz Janusz.

4.13 Evaluation of triphenylmethane dye decolorization by biosorption

This set of experiments was designed to quantify the contribution of fungal biomass (surface adsorption, absorption and intracellular accumulation) to dye removal independently of extracellular enzymatic biodegradation. The research methodology connected to biosorption of dyes have been published in **Publication 3**.

4.13.1 Preparation of Self-Immobilized and Sponge Immobilized Fungal Biosorbents

Self-immobilized and Sponge Immobilized biosorbents were prepared as mentioned in section 4.4.2 and 4.4.3 respectively. To remove the contribution of secreted extracellular enzymes and metabolic transformation, growth medium was decanted after 7 d of shaking culture and biomass washed twice with deionized water and used as biosorbents (BS) (Figure.14 and 15). Both live (L) (metabolically active) and dead (A) (autoclaved) biosorbents were tested for biosorption of dyes. To prepare dead fungal biosorbents, 7 d grown biomass of CB8/S2 was autoclaved at 121 °C for 20 min. Rest the procedure was same as mentioned previously. Biotic and abiotic controls were prepared as mentioned in previous section 4.5. As a variant of fungal biomass, fungi was grown in static conditions for 7 days, homogenized using Bagmixer and 0.5 g wet biomass taken for dye sorption.

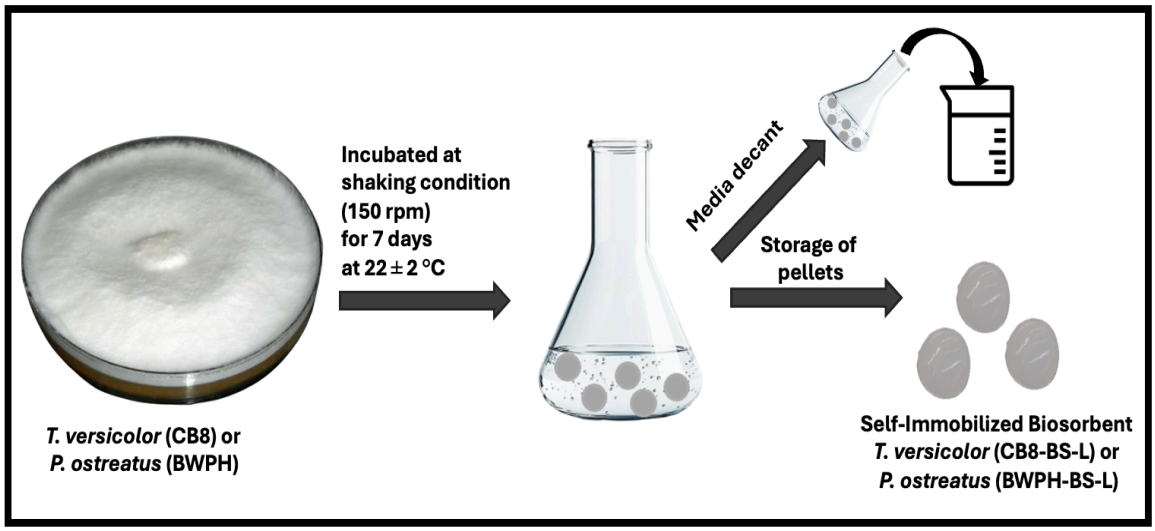

Figure 14. Schematic methodology for preparation of Self Immobilized Fungal Biosorbents (Photo by R. Upadhyay)

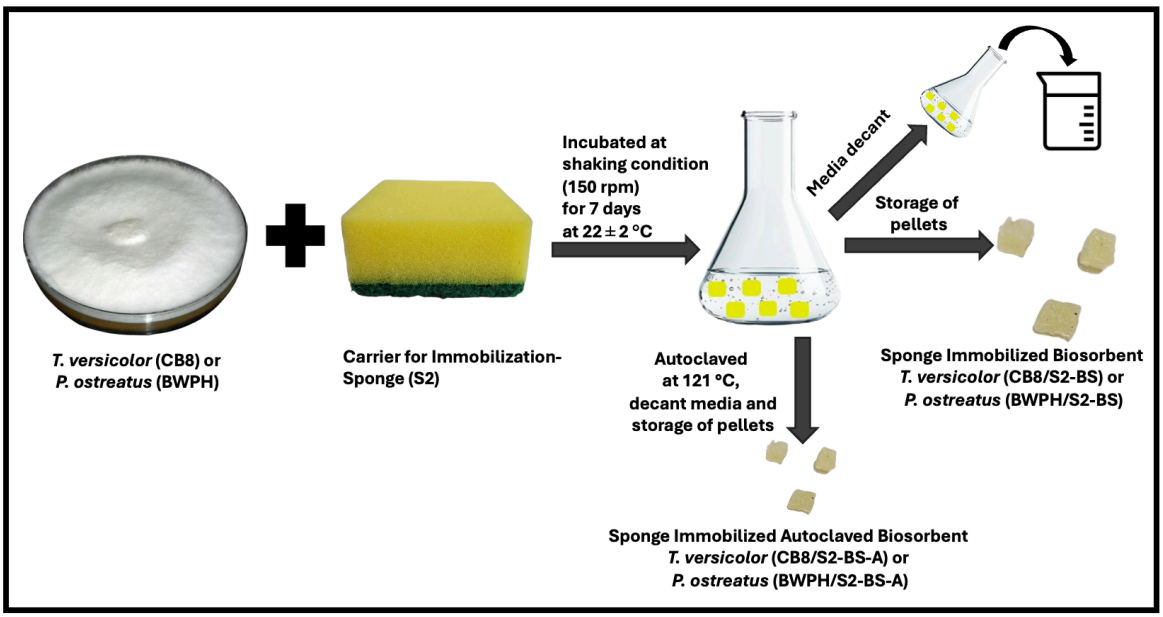

Figure 15. Schematic methodology for preparation of Sponge Immobilized Fungal Biosorbents (Photo by R. Upadhyay)

4.13.2 Biosorption Assay

Each biosorbent variation was evaluated for its efficacy in removing the triarylmethane dyes BG and CV. Each vial contained 0.5 g of either wet live biomass or autoclaved dead biomass of free-fungal biomass pellets (CB8-BS and BWPH-BS), or a single piece (uniform cubes of approximately 10 mm^3) of immobilized sponge fungal pellets (CB8/S2-BS and BWPH/S2-BS), mixed to 10 mL of dye solution at a concentration of 200 mg/L as seen in Figure 16. The dye solutions exhibited their inherent pH levels, measuring 4.36 for BG and 4.35 for CV. The incubation occurred for 24 hours at 22 °C. The absorbance of the cell-free supernatant was quantified using a Hitachi U-1900 UV-VIS spectrophotometer (Hitachi High-Tech Analysis

Corporation, Tokyo, Japan) at 0, 1, 2, 4, 6, and 24 hours, while the dye removal via sorption was assessed by indirectly measuring the pollutant concentration in the solution. The quantities of dyes in the samples were ascertained by measuring the absorbance of BG dye at 623 nm and CV at 584 nm. All experiments were performed in a minimum of three experimental duplicates. This experiment facilitated an evaluation of the impact of contact duration and biomass type. Simultaneously, the dry matter content was assessed during a 7-day drying period at 35 °C until a consistent weight was achieved. These values were used to determine the removal of dye per gram of dry matter of the mycelium. Following the adjustment for the loss observed in the abiotic sample (control), the quantity of dye adsorbed was determined. The same equation 1 was employed to calculate the overall percentage of dye decolorization via the sorption process:

The maximum amount of dye adsorption at measurement points was determined using the following equation:

$$q_t = (c_i - c_t)\frac{V}{M} \qquad \text{(Equation 5)}$$

Where, Ci is the initial dye concentration and Ct is the concentration at time t (mg/L), V is the solution volume (L), and M is the mass of fungi biomass used (g).

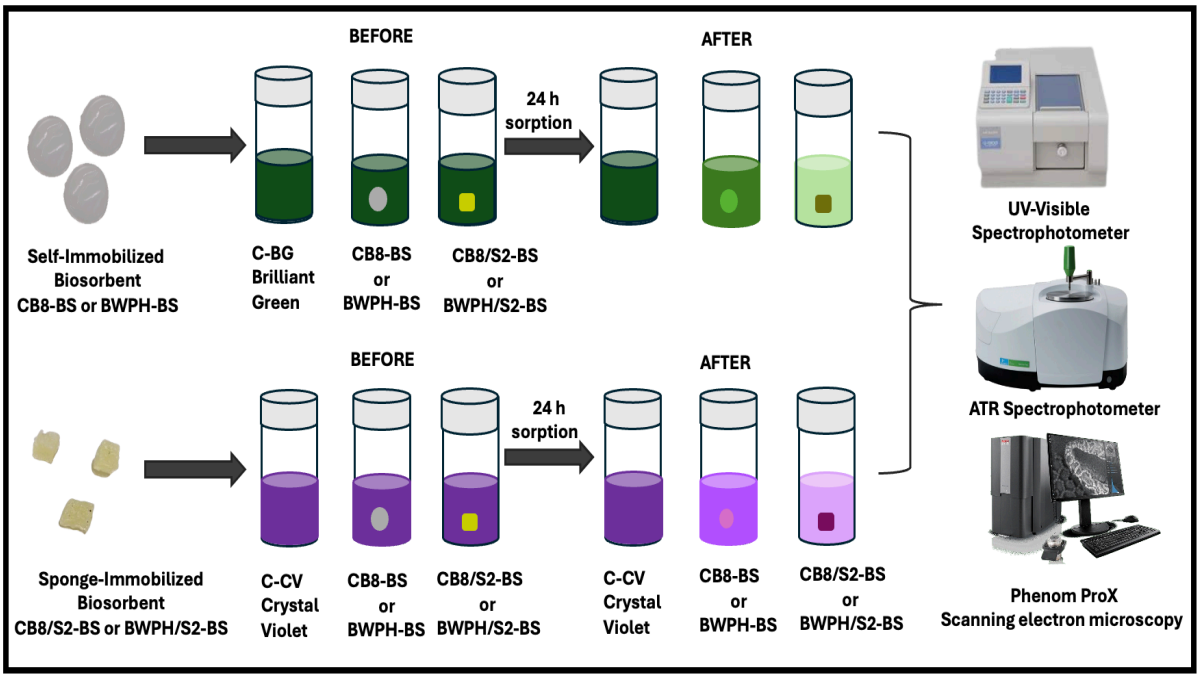

Figure 16. Schematic methodology of Brilliant Green and Crystal Violet biosorption by Self- and Sponge-Immobilized Fungal Biosorbents (Photo by R. Upadhyay) (Published in **Publication 3**)

A Welch's t-test for two independent samples, assuming unequal variances, was performed using Microsoft Excel (Microsoft Corp., Redmond, WA, USA) to evaluate differences in dye removal efficiency between the immobilization methods. The investigation compared sponge-immobilized biomass with self-immobilized biomass for each fungal species and biosorbent

variant, including both living and deceased biomass. A one-tailed test was performed based on a preceding premise that sponge-immobilized biomass will exhibit greater dye removal efficiency than self-immobilized biomass. Statistical significance was assessed at $p = 0.05$.

4.13.3 Characterization of Fungal biosorbents

All kinds of biomass were incubated for 24 hours in both dye solutions at a concentration of 250 mg/L, collected via filtration, and dried at 37 °C until a consistent weight was achieved. The desiccated biomass of CB8 and BWPH with or without dye was transformed into powder using a mortar and pestle. The samples with immobilized sponges were allowed to dry in its natural form and then cut into thin slice at time of measurements. The characterisation of the adsorbent was conducted using FT-IR Attenuated Total Reflectance (ATR) spectroscopy with a Perkin Elmer Spectrum Two FTIR spectrometer equipped with a UATR diamond attachment, over a spectral range of 650-3700 cm^{-1}. A Phenom ProX scanning electron microscope with an EDS analyzer (Phenom ProX, Thermo Fisher Scientific, Waltham, MA 02451, USA) operating at 10-15 kV in backscattered electron (BSE) mode was employed for the morphological evaluation of biosorbents.

4.14 Evaluation of dye decolorization by Biosorption at different parameters

4.14.1 Effect of initial dye concentration and contact time

The effect of initial dye concentration on the biosorption efficiency of live biosorbents (BS-L) of CB8-BS-L, BWPH-BS-L, CB8/S2-BS-L, BWPH/S2-BS-L was checked. Appropriate concentration of both dye - 100, 200, 300, 400 mg/L was reached by preparing dilution of Stock Solution (1000 mg/L) using deionized water. For determining the effective contact time for dye removal, the absorbance of the cell-free supernatant was measured at following time points: 0, 1, 2, 4, 6 and 24 h. Principal component analysis (PCA) was performed to evaluate the combined effect of initial dye concentration and contact time on dye sorption.

4.14.2 Effect of pH and temperature

To optimize biosorption, we employed statistical methods to determine the best values of temperature and pH, two critical elements that significantly affect the testing process. We employed Central Composite Design (CCD) in conjunction with response surface methodology (RSM) to derive a mathematical relationship that elucidates the influence of independent parameters and their interacting effects on the response, which was represented by a polynomial quadratic equation, as illustrated in Equation 6.

$$\text{Effect} = a \cdot \mathbf{pH} + b \cdot \mathbf{T} + c \cdot \mathbf{pH}^2 + d \cdot \mathbf{T}^2 + e \cdot \mathbf{pH} \cdot \mathbf{T} + f \qquad \text{(Equation 6)}$$

where T is temperature and a, b, c, d, e, f are coefficients.

Given that we conducted a two-factor analysis (k=2), our Central Composite Design (CCD) comprised nine experimental setups: one central point and eight "star points," which include factorial points (k^2) and axial points ($2 \cdot k$). The former, in conjunction with the center point, is necessary for the first-order regression coefficients, whereas the latter facilitates the estimation of the second-order model. The distance from the center to each "star point" is uniform and

measures α=√2, yielding a spherical, rotational configuration. Figure 17 illustrates the graphical depiction of CCD. To enhance the precision of the experiment, the center point was replicated four times, resulting in a total of 12 experimental sets [107,162,163]. In our investigation, the temperature range was determined to be between 15 °C and 55 °C, while pH was assessed from 2 to 10. The CCD experimental plan, incorporating both coded and natural data, is presented in Table 6. We employed Design Expert (Stat-Ease) software to compute the coefficients of the second-order polynomial equation by regression analysis during results evaluation. The derived mathematical model was evaluated by analysis of variance - ANOVA.

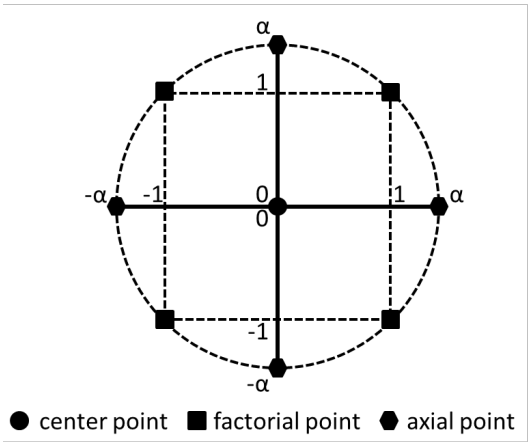

Figure 17. Graphical representation of a Central Composite Design for two factors, consisting of one center point and four points each for both factorial and axial designs (Published in **Publication 3- Supplementary material**)

Table 6. Central Composite Design experimental plan with coded values and natural values of temperature (°C) and pH; α≈1.41 (Published in **Publication 3**)

Experiment number	Coded values	Natural values	
		Temp. (°C)	pH
1	0/0	35	6
2	-α/0	15	6
3	−1/−1	20.85	3.2
4	0/0	35	6
5	1/1	49.15	8.8
6	0/0	35	6
7	0/α	35	10
8	0/0	35	6
9	0/−α	35	2
10	1/−1	49.15	3.2
11	α/0	55	6
12	−1/1	20.85	8.8

4.14.3 Evaluation of Reusability of Fungal biosorbent

To enhance the sustainability of this technique, the efficacy of the fungal pellets was evaluated for reusability. Both dyes were incubated with CB8/S2 and BWPH/S2 for six hours, and the elimination of the dyes was quantified. To desorb the dye, one set was incubated overnight (about 8 hours) with 5 mL of a 70% methanol solution [164], whereas the second set underwent no treatment. The subsequent day, the dye was reintroduced to evaluate its capacity for reabsorption by the medium.

4.15 Bioreactor Study

Previous bench-scale investigations indicated that self-immobilized and sponge-immobilized *T. versicolor* (CB8/SH and CB8/S2) demonstrated the most superior and rapid RBBR elimination efficacy under optimal conditions. Consequently, this biomass configurations were chosen for the bioreactor tests. A bioreactor-based decolorization research of CB8 strain was performed under optimal circumstances, incorporating four consecutive dye-addition cycles.
Each bioreactor held 0.2 L of Regular Medium (RM) and was fitted with two sterile probes: one for sampling and another for administering consecutive doses of dye as seen in Figure 18. Both the inlet and sample lines were equipped with 0.45 μm filters to reduce contamination. The RM-filled bioreactors were autoclaved at 121 °C for 30 minutes before inoculation. To prepare immobilized biomass, 24 sponge cubes (each measuring 1000 mm^3) were incorporated into the RM and subjected to autoclaving. Independently, 7 day old CB8 mycelium cultivated on RM was homogenized utilizing a BagMixer® 400 P stomacher, and 1 mL of the homogenized solution was introduced into each reactor. All reactors were incubated for seven days at 22 °C, agitated at 150 rpm, facilitating the development of both self-immobilized and sponge-immobilized fungal biomass.

Two abiotic controls were concurrently established:
1. RM devoid of fungus inoculum.
2. RM including 24 autoclaved sponge fragments devoid of fungal inoculum.

Following the 7-day growth period, two fungal reactors and the abiotic controls were each introduced with 125 mg/L of sterile RBBR dye to commence the first dye-addition cycle. No supplementary nutrients or aeration were provided throughout the decolorization procedure. Decolourisation tests were carried out for 4 cycles of 5 days each. Subsequent to the fourth cycle, the total dye introduced to each reactor amounted to 500 mg/L. Samples of 1 mL were extracted from each reactor within one hour of each dye addition, to ascertain the overall dye concentration present immediately following introduction. After 48 hours of each cycle, to assess fungal decolorization efficacy, samples were collected. The RBBR dye concentration was measured using UV-Vis spectrophotometry at 596 nm utilizing an HITACHI U-1900 spectrophotometer. The percentage of dye removal for each cycle was computed in relation to the respective abiotic control utilizing standard decolorization equation 1.

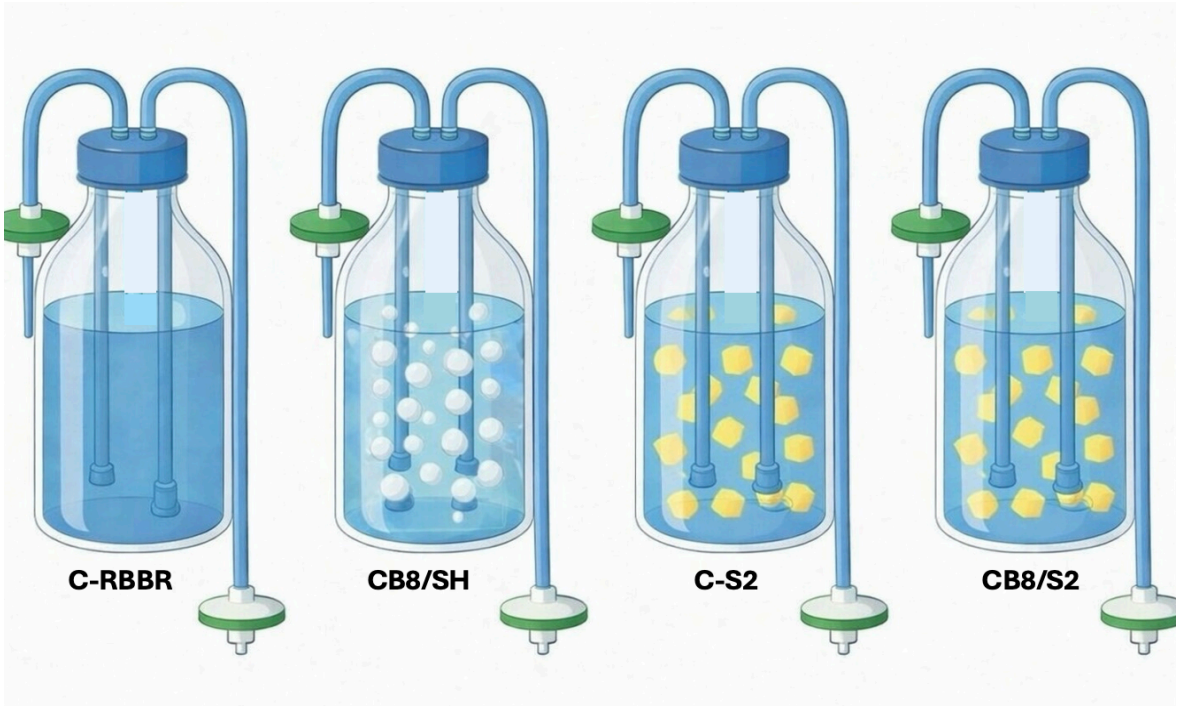

Figure 18. Design of Bioreactor (Photo by R. Upadhyay)

4.16 Statistical Methods and Software Used for Data Analysis

All experiments were performed in triplicate, and the findings are presented as mean ± standard deviation unless specified otherwise. Statistical analyses and graphical visualizations were conducted utilizing specialized software programs to guarantee precise interpretation and reproducibility of outcomes.

Microsoft Excel (version 16.105, Microsoft Corporation, USA) was utilized for initial data processing, computation of dye degradation efficiency, enzyme activity assays, and general quantitative analysis. Toxicity assessment data were evaluated by probit analysis to ascertain dose-response relationships and toxicity EC_{50} values.

Response Surface Methodology (RSM) and Central Composite Design (CCD) were utilized to assess the interactive impacts of process factors on dye removal efficacy. The analyses, encompassing model fitting, regression analysis, analysis of variance (ANOVA), and optimization, were conducted utilizing Design-Expert software (Stat-Ease free trial version Inc., USA). The efficacy of the constructed models was evaluated using statistical metrics including the coefficient of determination (R^2), adjusted R^2, predicted R^2, and lack-of-fit tests.

Inferential statistical analyses, comprising one-tailed t-tests, one-way ANOVA, two-way ANOVA and post hoc Tukey's honestly significant difference (HSD) tests, were conducted to ascertain statistically significant differences among experimental groups. A confidence level of 95% ($p < 0.05$) was deemed statistically significant. Principal Component Analysis (PCA) was utilized to investigate multivariate correlations and patterns among experimental variables. The R studio (4.5.0. version) was utilized for sophisticated statistical analysis, principal

component analysis, heatmaps generation and high-quality data visualization. Graphical outputs were produced utilizing suitable R packages to guarantee clarity and reproducibility.

The Fourier Transform Infrared (FT-IR) spectra were analyzed and displayed with OriginPro Learning Edition software (OriginLab Corporation, USA) to examine the alterations in functional groups related to dye biosorption and degradation. UV-Visible spectral analysis, including wavelength scanning and peak absorbance measurements, was conducted utilizing a Hitachi UV-Visible 1900 spectrum (version 4.2), and the spectra were employed to observe dye decolorization and degradation behaviour.

Proteomic data analysis using MaxQuant (version 2.7.5.0) for protein identification and quantification, followed by downstream statistical analysis and visualization with Perseus software(version 2.1.6.0). The functional annotation and Gene Ontology (GO) classification of the discovered proteins were conducted utilizing the eggNOG-mapper tool.

Artificial intelligence tools were used in a limited and supportive role for figure preparation and for writing R code used to generate selected graphs; all analyses and interpretations were conducted by the author.

CHAPTER 5
RESULT AND DISCUSSION

The biological elimination of synthetic dye in wastewater treatment relies on the biosorption and biodegradation capabilities of the selected organism. The primary research was conducted to check the decolorization efficiency of five structurally distinct dyes using the white-rot fungus *Trametes versicolor* (strain CB8) and *Pleurotus ostreatus* (strain BWPH). The efficacy of free fungal biomass and immobilized fungus on solid supports in removing dye was assessed across various initial dye concentrations. The results of preliminary research were partly published in **Publication 1**. The research data presented in that publication are connected to CB8 strain decolorization efficiency.

5.1 Assessment of Fungal Growth

For adsorption and biodegradation of different pollutants, fungus biomass is utilized as a sorbent and/or an enzyme producer. The specific structure of the dye, the strain employed in the decolorization procedure, the method of applying biomass, and the chemical makeup of the dye effluents all affect how well a dye is removed. The mycelium may be more vulnerable to adverse environmental circumstances, which is a drawback of using fungal free-cell technique; immobilizing biomass on different carriers could be a powerful substitute as it preserves the production of several enzymes and increases fungal activity while preserving biomass and increases fungal strains' resilience to environmental stress at levels greater than those obtained from mycelial pellet or free fungal suspension forms [165]. Immobilization, however, not always promotes improved fungal growth and, thus, dye decolorization effectiveness. According to Przystaś et al.[125], six distinct solid supports were examined. Due to the significant growth in fungal biomass, only two supports were chosen for fungal immobilization and rest were discontinued. To get the optimum dye decolorization efficiency, it is therefore essential to experiment with various immobilization matrices and maximize their development.

The evaluation of development of immobilized fungal biomass on two distinct solid supports, as well as free fungal biomass, was conducted through visual observation, as detailed in Table 7. The most intensive and uniform development of CB8 and BWPH was noted on sponge. Each sponge piece was uniformly coated in comparison to the another support (dishwasher) when cultivated under constant shaking conditions. The primary issue pertained to the dishwasher, as merely 30% to 40% of the pieces were colonized by fungi. The residual fragments were not effectively colonized by fungus and hence were dissipated. Consequently, an increased quantity of dishwashers was required to conduct the dye degradation experiment. While each sponge piece was covered by fungi hence, there was no such kind of issue noted.

Under shaking circumstances, self-immobilized fungal biomass resulted in the formation of mycelium pellets. CB8/SH strain produced quite bigger pellets (1 cm diameter) as compared to BWPH/SH strain (0.5 cm diameter). It was homogenized with a Bagmixer prior to its

incorporation with the dye solution. The mycelium pellets with an increased surface area may enhance dye sorption by fungi, as sorption occurs during the initial phase of dye degradation and may impact the final elimination, including enzymatic degradation. Control samples with suitable supports were also incubated under similar conditions. It exhibited no growth. The dry weights of CB8/SH, CB8/S1, and CB8/S2 biomass were 0.011 ± 0.003 g, 0.019 ± 0.005 g, and 0.022 ± 0.006 g, respectively. Whereas dry weights of BWPH/SH, BWPH/S1, and BWPH/S2 biomass were 0.012 ± 0.004, 0.018 ± 0.003, and 0.024 ± 0.005 respectively.

Table 7. Growth Analysis of Immobilized and Self-immobilized Fungal Biomass after 7 days (Growth condition: 150 rpm, pH 5.7, temperature 20±2°C) (Partially published in **Publication 1**) [143]

Culture Condition	Dishwasher (S1)	Sponge (S2)	No Support
T. versicolor (CB8)	+ +	+ + +	+ + +
P. ostreatus (BWPH)	+ +	+ + +	+ + +
Control (Medium)	-	-	-

(Note: -, lack of growth (0%); + +, medium growth (50-70%); + + +, intensive growth (70-100%))

5.2 Dye removal capacity of Carriers

The bar graph (Figure 19) illustrates the dye removal efficiency (%) of two distinct support materials: C/S1 (polypropylene dishwasher) and C/S2 (polyurethane sponge) across different initial dye concentrations (100-400 mg/L). The evaluated dyes comprise EB (Evans Blue), CR (Congo Red), BG (Brilliant Green), CV (Crystal Violet), and RBBR (Remazol Brilliant Blue R). Overall, C/S2 demonstrates significantly greater dye removal effectiveness than C/S1 across all dyes and concentrations due to the compositional differences between the two materials.

For C/S1, dye removal was minimal across all dyes, varying from 0% to 20%. Marginal increases are noted with elevated dye concentrations; however, the total removal efficacy remains inadequate. The hydrophobic characteristics of the polypropylene dishwasher likely restrict dye sorption efficacy. Therefore, the dishwasher is significantly reliant on fungal colonization/adsorption to enhance dye sorption ability [166] which will be discussed in section 5.3. C/S2 demonstrates markedly superior dye removal, contingent upon dye type and concentration. The maximum removal is observed for CR, CV, and RBBR, exceeding 50% at specific doses. EB and BG demonstrate moderate elimination. This improved performance results from the high porosity, hydrophilicity, and increased surface area of the polyurethane substance. Enhanced mass transfer and dye diffusion occurred within the matrix. It is important to check whether combination of sponge and fungal species increases natural dye sorption capacity of sponge material or not. Dye removal for both carriers typically escalates with concentration until reaching a threshold of 300 mg/L, beyond which it may marginally stabilize at 400 mg/L, presumably due to the saturation of active binding sites. The tendency is more

pronounced in C/S2, indicating that the immobilized biomass retains efficacy throughout a wider concentration spectrum.

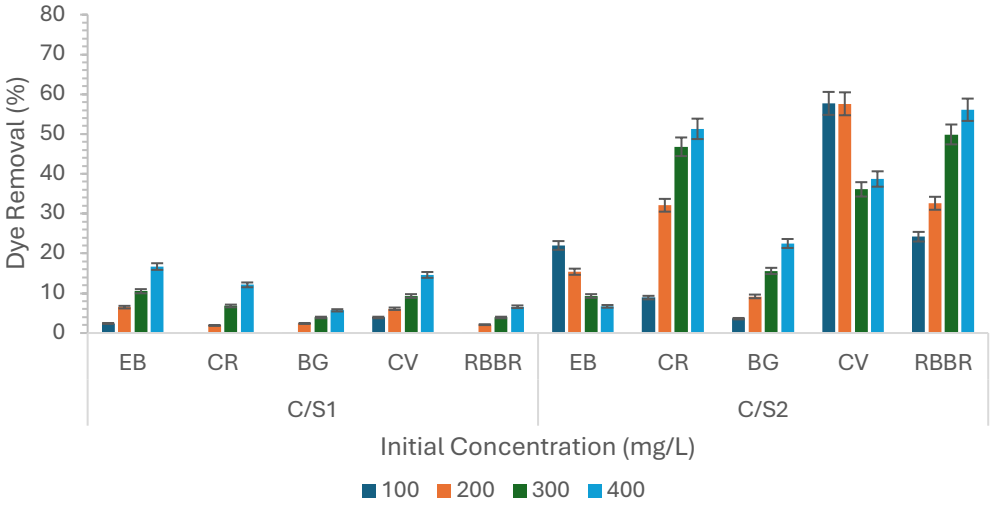

Figure 19. Dye removal capacity of carriers- dishwasher (C/S1) and sponge (C/S2)

5.3 Preliminary assessment of dye decolorization

To assess the white-rot fungus capacity to degrade dyes having different chromophore groups, we had chosen self-immobilized and carrier immobilized biomass of CB8 and BWPH strain. CB8 strain was immobilized on dishwasher and sponge. Their decolorization potential have been already published in **Publication 1**. As a conclusion of **Publication 1**, the self-immobilized and sponge immobilized CB8 biomass was very much efficient for dye decolorization as compared to dishwasher immobilized biomass. And as mentioned previously that only 30-40% of dishwashers were colonized by fungi. Hence, for BWPH strain, only self-immobilized and sponge immobilized biomass was chosen for further studies.

Evans Blue, Crystal Violet, and RBBR were specifically eliminated with superior effectiveness (more than 90%) at all starting dye concentrations by the isolated *T. versicolor* CB8 strain, whereas BWPH/S2 was able to decolorize more than 80%, which demonstrated considerable potential for decolorization of all tested dyes to varying degrees. Both in self-immobilized and carrier immobilized form, the CB8 strain and BWPH strain demonstrated excellent dye decolorization efficiency.

5.3.1 Evans Blue decolorization

At varying starting dye concentrations (100-400 mg/L), the decolorization effectiveness of Evans Blue dye was assessed using free and immobilized fungal biomasses of *T. versicolor* (CB8) and *P. ostreatus* (BWPH). With discernible variations between free and immobilized forms, the data show consistently strong dye removal by all fungal systems. In comparison of dyes belonging to the Azo group, the CB8 strain and BWPH strain were able to remove Evans Blue dye to a greater extent than Congo Red dye.

Across all examined concentrations, the self-immobilized fungal biomass of CB8/SH demonstrated very good decolorization effectiveness (97-98%) as seen in Figure 20. The fungus's ability to eliminate Evans Blue is demonstrated by the performance's relative stability, which may be attributed to its potent oxidative enzyme system (laccase, manganese peroxidase, and lignin peroxidase). The efficacy of CB8 immobilization on dishwasher and sponge remained consistently high throughout concentrations (95-97%). This implies that the fungus was able to tolerate dye stress at higher concentrations because immobilization did not impair metabolic activity and might have provided mechanical stability. The best overall performance was demonstrated by CB8/S2, which peaked at 98.8% at 400 mg/L and had greater than 96% removal across all concentrations. The improved performance suggests that sponge offers a favourable milieu that maintains enzyme activity and improves dye-fungus contact.

The efficiencies of BWPH/SH biomass ranged from 94% at 100 mg/L to 82% at 400 mg/L, which is somewhat lower than that of CB8/SH. The decrease at higher concentrations points to a potential vulnerability to enzyme inhibition or dye toxicity. Compared to self-immobilized biomass, immobilization on sponge increased stability and efficiency. Decolorization outperformed the free form, particularly at lower concentrations, with ranges of 99% at 100 mg/L to 89% at 400 mg/L. This suggests that immobility lessens the inhibitory effects of a large dye load to some extent. When compared to *P. ostreatus*, *T. versicolor* (CB8, particularly CB8/S2) showed better efficiency.

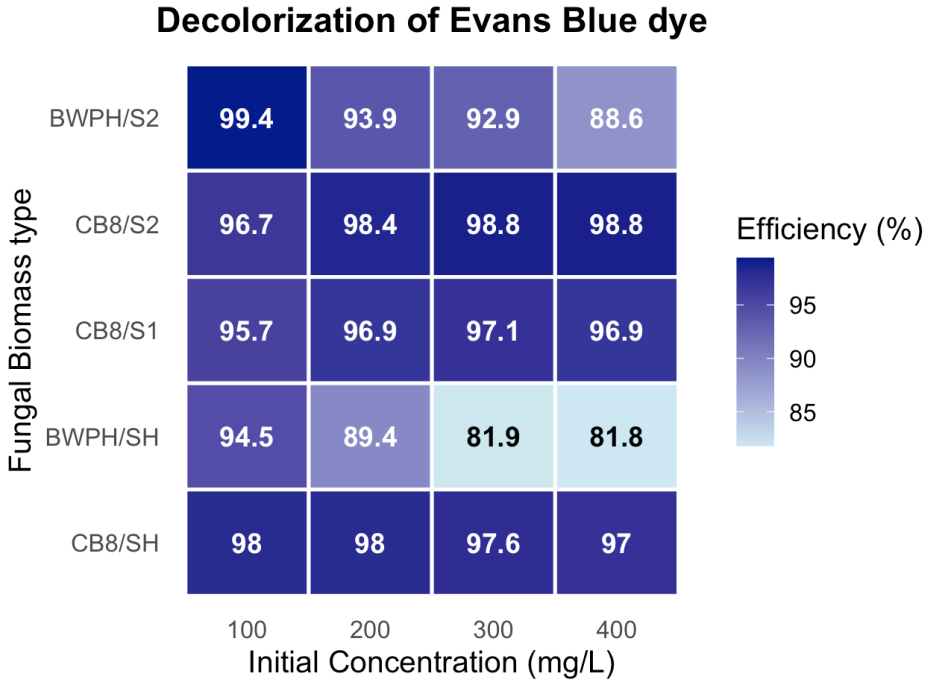

Figure 20. Decolorization of Evans Blue dye by Self-immobilized and Carrier immobilized biomass of *Trametes versicolor* (CB8/SH, CB8/S1,CB8/S2) and *Pleurotus ostreatus* (BWPH/SH, BWPH/S2)
(conditions:C_0= 100-400 mg/L, biomass dose of self-immobilized biomass= 0.5 g wet/ 2 mL, biomass dose of carrier-immobilized biomass= 1 piece/ 2 mL, T= 22.5 ± 2 °C, t= 96 h)

5.3.2 Congo Red decolorization

Compared to fungi immobilized on solid supports, the self-immobilized CB8 fungal biomass was more suited to decolorize Congo Red dye. As previously stated, only sponge was more effective in removing Congo Red; nevertheless, the sponge's decolorization efficacy decreased when it was covered with CB8 strain. The percentage of dye decolorization increased by CB8/SH to 91.05% when the initial CR dye concentration increased as seen in Figure 21. Our results are consistent with the earlier study [167], which found that the WRF fungus could eliminate the CR dye more at 400 mg/L as opposed to lesser concentrations like 100 and 200 mg/L after 30 hours of incubation. Chakraborty and Basak et al. tested the removal efficiency of CR dye over a wide pH range (3-7) and found that the best decolorization efficiency (89%) occurred at a comparatively higher pH (8). They attributed this to the concentration of [H+] ions, indicating that pH plays a significant role in pollutant removal [167,168].

In opposite to CB8/SH, the BWPH/SH removed higher amount of dye (49.9%) at 100 mg/L and lower amount (11.7%) at 400 mg/L. The dye toxicity affected more to BWPH/SH strain at higher concentrations. Immobilization on sponge proven to be effective for *P. ostreatus* strain (BWPH/S2) as it could lead to 85.3% Congo red dye decolorization at lower concentrations. The study of the Congo Red dye's UV-Vis spectrum revealed two extended peaks: one at 495 nm, which was related to the dye molecule's large conjugated system and azo double bond, and another at 330 nm, which may have been caused by the interaction of aromatic hydrocarbon or polycyclic aromatic hydrocarbon groups with other chromophores [169].

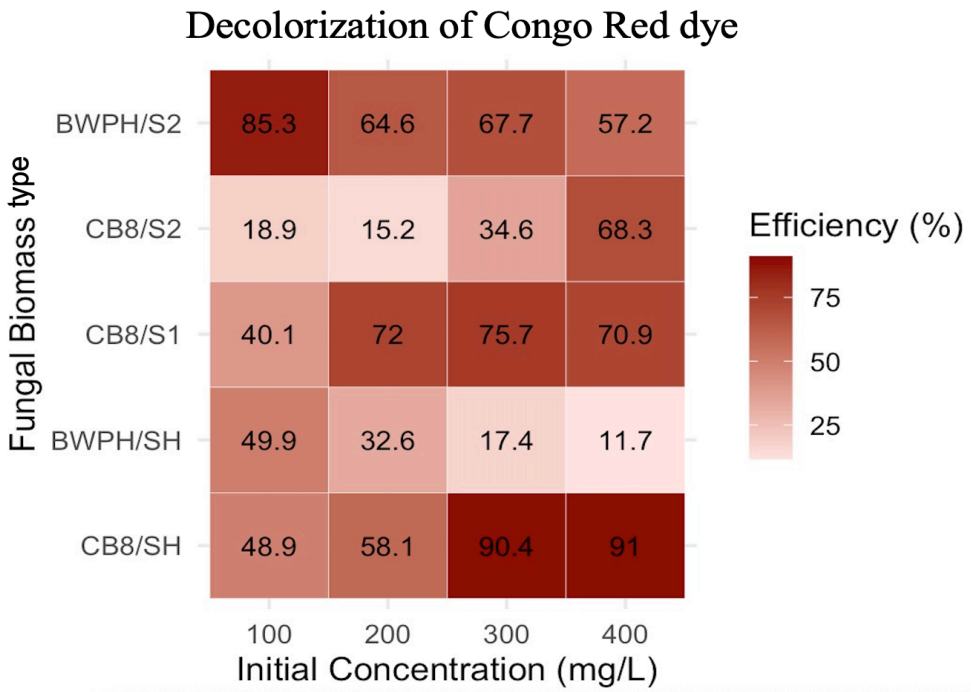

Figure 21. Decolorization of Congo Red dye by Self-immobilized and Carrier immobilized biomass of *Trametes versicolor* (CB8/SH, CB8/S1,CB8/S2) and *Pleurotus ostreatus* (BWPH/SH, BWPH/S2)
(conditions:C_0= 100-400 mg/L, biomass dose of self-immobilized biomass= 0.5 g wet/ 2 mL, biomass dose of carrier-immobilized biomass= 1 piece/ 2 mL, T= 22.5 ± 2 °C, t= 96 h)

5.3.3 Brilliant Green decolorization

When *T. versicolor* fungus were immobilized on sponge (CB8/S2), Brilliant Green dye (triphenylmethane group) demonstrated the best clearance (97%) across the whole dye concentration range. The trend for CB8/SH biomass and CB8 immobilized on support 1 was significantly different. Figure 22 makes it evident that the BG dye was more effectively eliminated at the lowest tested concentrations (88% by CB8/SH and 85.2% by CB8/S1, respectively) and highest concentrations (97.5% by CB8/SH and 98.1% by CB8/S1, respectively), with less effectiveness at intermediate concentrations. At varying concentrations, immobilized biomass on the dishwasher and CB8 produced a similar pattern for dye decolorization.

BWPH/SH was more effective and more consistent at all concentrations of brilliant green dye. It removed dye in a range of 92.4%-97.1%. Whereas the immobilization of fungal biomass on sponge (BWPH/S2) lead to decrease in brilliant green dye decolorization efficiency, which ranged from 45.7% to 91.7%. However, sponge provided protection at higher dye concentrations and resulted in more dye removal even at high concentrations. The UV-Vis absorbance spectral profile showed that the BG dye had mineralized since, upon deterioration, the absorbance peak at 623 nm completely vanished and no new peak appeared. When BG dye was broken down in a recirculating packed bed bioreactor, comparable outcomes were seen. As noted by Kumar et al. [170] in relation to the control BG dye, samples obtained on days 4, 8, and 16 displayed diminishing absorbance at 630 nm, and on day 20, it was extremely low.

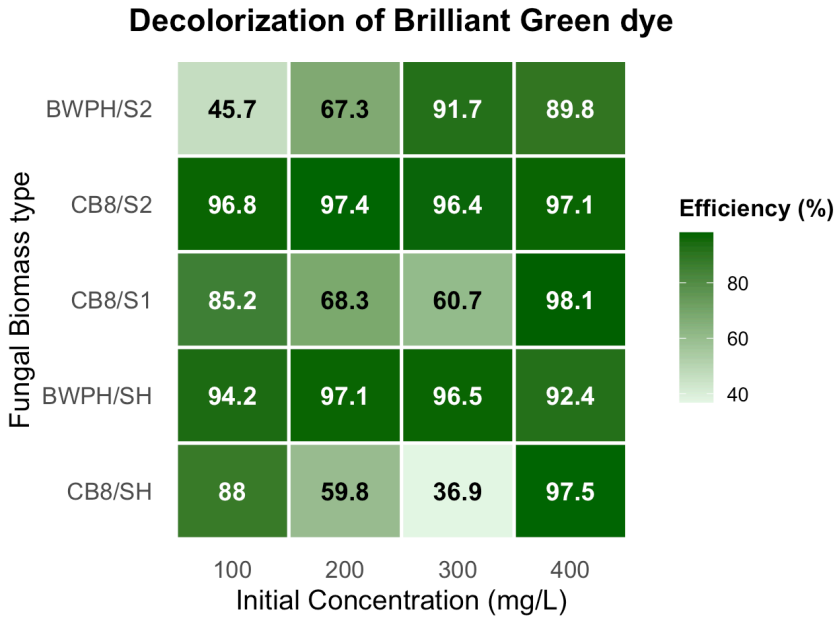

Figure 22. Decolorization of Brilliant Green dye by Self-immobilized and Carrier immobilized biomass of *Trametes versicolor* (CB8/SH, CB8/S1,CB8/S2) and *Pleurotus ostreatus* (BWPH/SH, BWPH/S2)
(conditions:C_0= 100-400 mg/L, biomass dose of self-immobilized biomass= 0.5 g wet/ 2 mL, biomass dose of carrier-immobilized biomass= 1 piece/ 2 mL, T= 22.5 ± 2 °C, t= 96 h)

5.3.4 Crystal Violet decolorization

This graph shows how well different fungal biomass preparations decolorize Crystal Violet dye at varying dye concentrations. In every combination examined, Crystal Violet, another dye from this triphenyl group, was effectively eliminated as seen in Figure 23. The best of these was the fungal-support 2 combination, which produced the most color removal (97.36%) at the maximum dose (400 mg/L). In contrast to the brilliant green dye, the outcomes are overwhelmingly favourable in this case.

All evaluated concentrations (100-400 mg/L) show very good efficiency (over 90%) in the majority of immobilized systems. This implies that these fungi are quite adapted at decolorizing Crystal Violet dye, especially when supported by a matrix. The performance of *T. versicolor* (CB8/SH) is consistent and good. At 400 mg/L, it significantly improves to 96% from its initial level of 93.2%. This suggests that this fungus is highly resistant to Crystal Violet, even when it is free. As mentioned previously that CB8/S2 ability was the most notable. In addition to being highly consistent and reliable, its efficiency actually increased from 94.6% to a peak of 98% at 300 mg/L. This implies that even in stressful situations, the sponge offers the perfect conditions for the fungus to grow and break down the dye. CB8/S1 also performed exceptionally well and consistently, exhibiting 88.7-94.7% efficiency at all concentrations.

P. ostreatus (BWPH/SH) exhibited notable vulnerability to crystal violet dye. At 300 mg/L, its efficiency falls precipitously from 90.6% to 62.8%. This demonstrates that the dye inhibits BWPH free cells at medium-high concentrations. On a positive note, immobilization helped to improve the performance of the more sensitive BWPH/SH strain and further stabilizes the already strong performance of CB8/SH. It successfully protects the fungi from the dye's harmful effects. The type of dye used has a significant impact on the fungus's performance. The fungal biomass had trouble with brilliant green dye removal, but they were quite good with Crystal Violet. This emphasizes how crucial it is to match the appropriate biological agent with the particular contaminant.

We used Crystal Violet at its native pH, and it produced two comparatively little peaks at 299 and 246 nm along with its maximum absorbance at 585 nm. In contrast to CB8/SH and dishwasher immobilized CB8, which displayed two peaks (at 567 and 220 nm) at the same time interval, sponge immobilized CB8 biomass only displayed one peak (at 567 nm) following dye degradation, according to the UV-Vis spectrum analysis. Following the decolorization procedure, the dyes' color remained unchanged. According to Asgher et al. [171], in neutral conditions (pH 7), Crystal Violet dye has a main absorption peak at 584 nm and three lesser peaks at 210, 245, and 295 nm. However, in strongly acidic conditions, this peak shifts to 420 nm. The N-demethylation route in *Aspergillus* species for triphenylmethane groups containing methyl violet dye was documented in few studies [172].

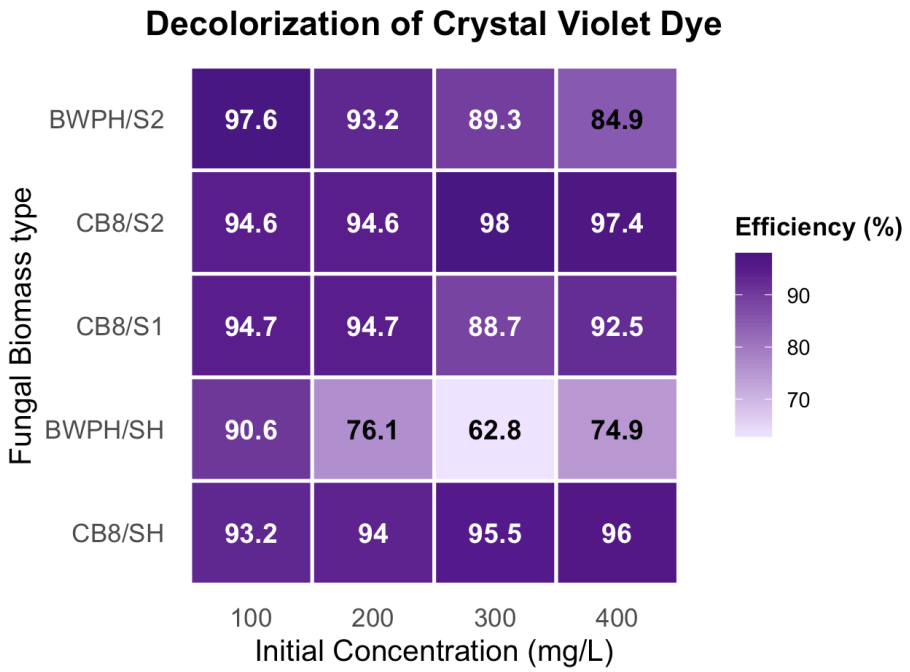

Figure 23. Decolorization of Crystal Violet dye by Self-immobilized and Carrier immobilized biomass of *Trametes versicolor* (CB8/SH, CB8/S1,CB8/S2) and *Pleurotus ostreatus* (BWPH/SH, BWPH/S2)
(conditions:C_0= 100-400 mg/L, biomass dose of sself-immobilized biomass= 0.5 g wet/ 2 mL, biomass dose of carrier-immobilized biomass= 1 piece/ 2 mL, T= 22.5 ± 2 °C, t= 96 h)

5.3.5 Remazol Brilliant Blue R decolorization

The Figure 24 shows that the fungus species, their immobilized state, and the structure of the particular dye interact in a complex way to determine the decolorization efficiency. Both free cells have exceptionally high intrinsic efficiency for RBBR. Although immobilization still has advantages for certain systems, its effects are not as widespread as those of Crystal Violet. The decolorization efficiency of BWPH/SH is exceptional, however it is adversely associated with concentration. At 100 mg/L, it begins at the highest efficiency for RBBR, an astounding 97.8%. But at 400 mg/L, its effectiveness progressively drops to 85.4%. This implies that whereas free BWPH cells are highly effective at breaking down RBBR at lower concentrations, their ability to do so is somewhat reduced as the dye concentration rises. However, this efficiency is not so lower among other research.

The performance of CB8/SH is excellent and very stable. From 200 mg/L onward, it rises to a relatively consistent 96-97% after starting strong at 91.6%. This shows that even at high concentrations, free cells of CB8/SH are not only very effective but also exceedingly resistant to the harmful effects of RBBR. RBBR decolorization is affected by immobilization in a species-dependent manner: Immobilized CB8/S1 showed upward trend from 95.1% to 97.6%, the efficiency of this system is ideal and independent of concentration. At nearly all concentrations, performance of CB8/S2 was very good and stable (89.8% - 93.7%), although noticeably lower than its free-cell counterpart. Immobilized BWPH/S2 has a significantly positive connection with concentration. It rises to 97.5% at 400 mg/L from a comparatively

low starting point of 52.2% at 100 mg/L. Its free-cell variant is the exact opposite of this. This implies that BWPH's activity is first slowed down by immobilization on sponge, but that it is eventually protected and able to remove most hazardous dye concentrations.

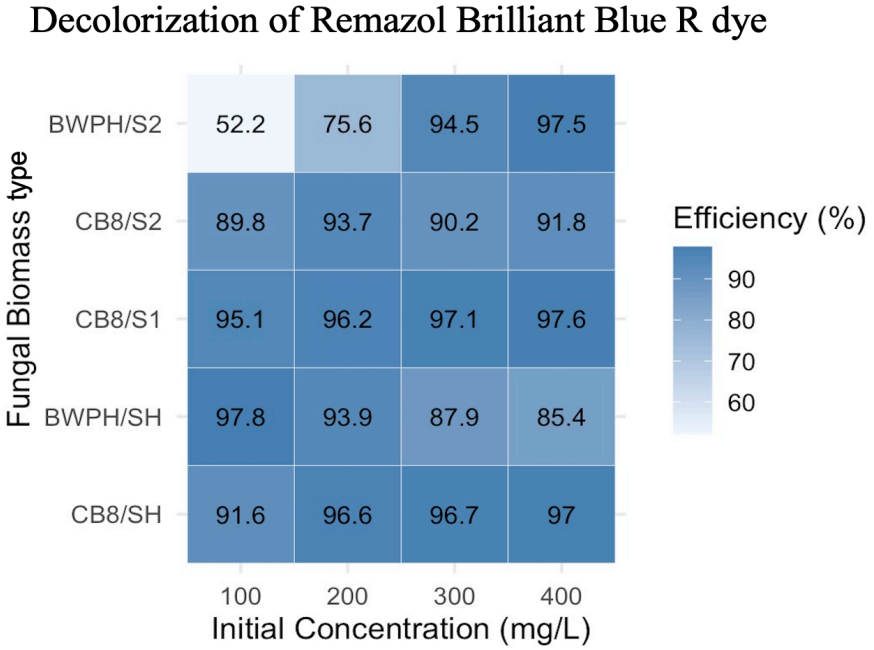

Figure 24. Decolorization of Remazol Brilliant Blue R dye by Self-immobilized and Carrier immobilized biomass of *Trametes versicolor* (CB8/SH, CB8/S1,CB8/S2) and *Pleurotus ostreatus* (BWPH/SH, BWPH/S2)
(conditions:C_0= 100-400 mg/L, biomass dose of self-immobilized biomass= 0.5 g wet/ 2 mL, biomass dose of carrier-immobilized biomass= 1 piece/ 2 mL, T= 22.5 ± 2 °C, t= 96 h)

The disparity in dye removal efficacy between the two strains is attributable to differing dye characteristics, such as chemical structure, molecular weight, and concentration, alongside the distinct enzymatic activity of the fungal strains, particularly laccase, and the process's dependence on enzymatic degradation as opposed to biosorption [173]. The efficacy of this enzymatic degradation is dependent upon the enzyme's affinity for the chemical structure of a particular dye. Dyes characterized by simpler structures and lower molecular weights, such as crystal violet or brilliant green, are eliminated more effectively than those with intricate structures, such as congo red, which is inadequately removed by certain strains [174]. The initial dye concentration can profoundly influence removal efficiency; below a specific threshold, enzymes may not activate effectively, while excessively high concentrations can be detrimental to the fungus, impeding its growth and dye degradation capabilities, or obstructing the enzyme's active site [175].

In conclusion, it was essential to identify which dyes were most effectively removed by both fungal strains in self-immobilized and carrier-immobilized forms to continue research on specific dyes. It was observed that RBBR, EB, and CV were efficiently eliminated by both strains throughout varying fungal biomass types. Consequently, more research on the optimization of the biodegradation process was conducted by optimizing nutrient supplies,

measuring enzyme activity, and assessing toxicity in relation to EB, CV and RBBR dyes as a representative dyes from each class of azo, triarylmethane and anthraquinone respectively.

5.3.6 Comparative analysis of dye desorption

The aim of the performance of desorption studies was to check the proportion of dye sorption during the decolorization process as the mentioned previously that there are mainly three ways for dye decolorization by fungi: biosorption, bioaccumulation and biodegradation. In addition to assessing the sorption process's involvement in the dye's decolorization, the desorption tests helped to clarify the recycling and reusability of the used immobilized fungal system [176] as it clarifies the proportion of loosely bound dye during physisorption. Mycelium pellets can be recycled up to four or five times if the right desorbing agent is employed for dye desorption. This agent should desorb dye without destroying the biomass's structural integrity and functional groups. It should be applied after each successive cycle. Following five cycles of sorption and desorption, the brown macroalga *Nizamuddinia zanardinii*'s Methylene Blue dye sorption efficiency dropped from 96.99% ± 0.90% to 48.16% ± 1.98%, while the dye desorption efficiency dropped from 68.70% ± 2.03% to 46.83% ± 1.49% [176,177]. The stability of the sorption process following decolorization has been examined using a variety of physical and chemical tests, including autoclaving, the addition of 1 M HCl, or 1 M NaOH [167]. A reasonably priced eluent can be used in the ion exchange reaction to accomplish desorption [178]. Ethanol and methanol are two of the most popular. It also provides information on how the functional groups of the dye interact with the ionic charge that is present on the fungal mycelium's cell surface.

Following incubation with a dye-containing solution, the fungal hyphae were pigmented darkly. It demonstrated how strongly the sorption process contributes to the fungal decolorization of the dye. Both fungal strains desorption were evaluated with all different biomass compositions and dyes. While evaluating the only carriers' desorption percentage, it was very low desorption observed for C/S1 as polypropylene dishwasher does not have tendency to absorb-desorb dye due to its hydrophobic nature. Still desorption percentage ranges from 2-14% for C/S1 which is connected with release of dye which were just physically trapped in the void spaces of dishwasher. Another solid support's porous surface, like that of a sponge (C/S2),shown high sorption-desorption potential. As seen from Figure 25(a) and (b), the desorption of EB and CR dyes increased with elevated initial dye concentrations whereas slight reverse trend was observed for BG and RBBR (Figure 25 (c) and (e)). CV shown more or less similar desorption at all teste concentrations. Depending on the functional groups interaction between dye and sponge, it resulted in different desorption trend.

The highest desorption efficiency was seen with Evans Blue (Figure 25 (a)) and Crystal Violet (Figure 25 (d)) dyes. Free fungal biomass of both strains exhibited significantly more dye desorption than immobilized biomass (Figs. 25 (a) and (d)). The desorption of EB dye increased with as the initial dye concentration increases. The desorption of CV dye was significantly elevated, suggesting a greater extent of irreversible dye binding. Hence, there may be a potential reaction between the fungal enzyme and the dye molecule that significantly

resulted in biochemical decolorization of colored medium. This was also reported earlier by Przystaś et al. [125]. The quantity of positively charged groups on the biomass surface escalates in acidic conditions. The desorption efficiency of Methylene Blue dye was enhanced due to electrostatic repulsion between positively charged sites in biomass and the cationic dye [179].

The biosorption process occurs due to the contact between the cell wall and the dye molecule. Various types of metabolism and pollutant sorption reactions are accountable. The biosorption of pollutants by WRF is attributed to extracellular accumulation of pollutants, intracellular accumulation, physical sorption, ion exchange, and cell surface sorption. Following the introduction of 70% methanol, the physically adsorbed dye was extracted from the hyphae and solid substrates enveloped by mycelium. In comparison, the maximum desorption was attained by free CB8 and BWPH hyphae, especially at elevated starting dye concentrations. However, when the fungus were cultivated on solid substrates, there was a diminished physical desorption of dye, with a greater elimination achieved by chemical or biochemical processes. The fungi adhered to the sponge exhibited highly permanent sorption, since the dye was not removed from the mycelium. It was least desorption in comparison to only carrier and only fungal biomass. The utilization of supports for the immobilization of fungal biomass facilitated a stable interaction between fungal hyphae and dye. The corrugated parallel bundle model (CPBM) has been employed by Biria et al. to analyse the efficacy of immobilized cells and supports that assertion that cell immobilization can enhance the operational lifespan of the system [180]. This experiment was beneficial for examining the sorption mechanism of dye molecules at various concentrations. Adsorption models are accessible for examining the sorption mechanism and dynamics of dye removal. This study offers new insights and distinctions on the potential roles of physisorption and chemisorption in the overall dye removal mechanism. The conducted analysis identifies the *T. versicolor* strain CB8 as a potent option for aqueous solution removal. This is a sustainable method for the extraction of dyes from various classes in elevated concentrations. The supports utilized for the immobilization of fungal biomass enhance the stability of the dye-cell wall-support complex, which is advantageous for disposal. The intricate enzymatic system of white-rot fungus and their morphology are pivotal in many pollution removal processes from the environment; however, additional research is necessary to investigate the molecular mechanisms behind WRF-mediated bioremediation [181].

Congo Red is an anionic azo dye, also referred to as Direct Red 28. The CR dye exhibited an elevation in the desorption proportion (59.34% and 37.3% respectively for CB8/SH and BWPH/SH) at elevated starting dye concentrations (300 and 400 mg/L) (Fig. 25 (b)). This tendency contrasts with Brilliant Green (triphenylmethane) (Fig. 25 (c)). The interaction between the fungal cell wall and the dye is contingent upon the dye's structure and the characteristics of the solid support used for immobilization [108,125]. Increased anion exchange may occur at elevated dye concentrations, leading to enhanced desorption of dye into the medium. It highlighted the necessity to experiment with various solid supports for the immobilization of fungal biomass to enhance the decolorization process, as well as to refine the selection and volume of different eluents to achieve optimal desorption rates.

The desorption order in Brilliant Green dye was shown to be CB8/SH > BWPH/SH>CB8 with support 1 > BWPH with support 2 >CB8 with support 2 (Fig. 25 c). It is connected to the dye's stable chemisorption on fungus that include sponges. In samples containing free CB8 biomass, the percentage of desorption was higher (about 46%) at lower starting dye concentrations (100 and 200 mg/L), but the percentage of desorption declined as the dye concentration climbed (400 mg/L). When the BG dye was sorbed on fungal biomass, CB8/SH displayed a higher likelihood of irreversible binding. Regardless of the variation in the initial dye concentration, a low percentage of desorption range (0.36%-0.72%) was observed when biomass was immobilized on sponge (Fig. 25 c). Additionally, it implies that enzymatic degradation in the immobilized fungal system is stable. The other scientists noticed that as the ethanol content rose from 0% to 80%, so did the desorption of the basic dye rhodamine B. At the maximum ethanol concentration, its desorption efficiency was 99.7% [182].

In samples containing anthraquinone dye (RBBR) (Fig. 25 (e)), the observed percentage of sorption ranged from 6.55% to 11.09% for fungi immobilized on the dishwasher (CB8/S1). This combination exhibited the greatest decolorization through a biochemical reaction. The sequence of desorption for RBBR dye was documented as: fungus> fungi with support 2> fungus possessing Support 1 for CB8 strain and fungus> fungi with support 2 for BWPH strain (Figure 25 (e)). In the executed experiment, we have noted that in free fungal biomass, the desorption percentage escalated with the augmentation in dye concentration. This signifies that sorption increased with elevated dye concentration. It discovered that the Loofa sponge immobilized *Phanerochaete chryosporium* exhibits a dye removal and biosorption capability of 18.60% more in relative to unbound biomass [44]. When the biomass was confined within the dishwasher, the primary elimination of the dye was noted through biochemical analysis. route. Chemisorption leads to irreversible binding of dye molecules to fungus, which exhibit reduced desorption upon inclusion of methanol. In the research conducted by Namasivayam et al. on sorption, the desorption ratio was evaluated at various pH levels. They have also noted that chemisorption has significantly contributed to the elimination of Brilliant Blue as the maximal desorption of the dye was merely 32% at the specified pH range: 4-10 [176].

As a concluding remark for the work elucidates the mechanism of dye removal, highlighting the significance of the sorption process and biochemical decolorization in the decolorization of the recalcitrant compound. The favourable desorption capability of methanol provided the primary understanding about involvement of sorption during decolorization process and indicated the opportunity for the reutilization of fungal biomass throughout multiple cycles of decolorization. It also provides an increased likelihood of safe disposal of biomass following its use in the treatment of aqueous dye solutions. This work also highlights the necessity of establishing effective methodologies for investigating the physical sorption of dye by fungal mycelium. Further research is necessary to optimize various physicochemical parameters for enhanced dye decolorization effectiveness and to examine the metabolites produced.

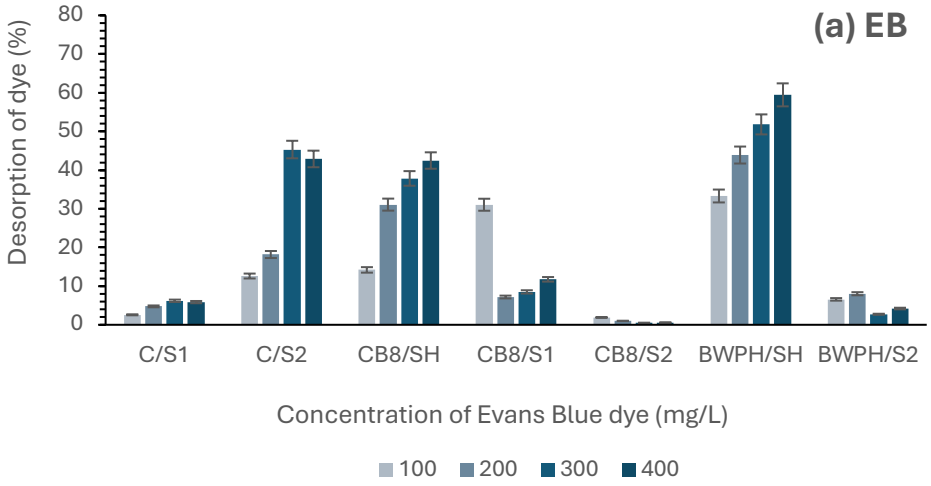
(a) EB
Desorption of dye (%)
80
70
60
50
40
30
20
10
0
C/S1
C/S2
CB8/SH
CB8/S1
CB8/S2
BWPH/SH
BWPH/S2
Concentration of Evans Blue dye (mg/L)
100
200
300
400

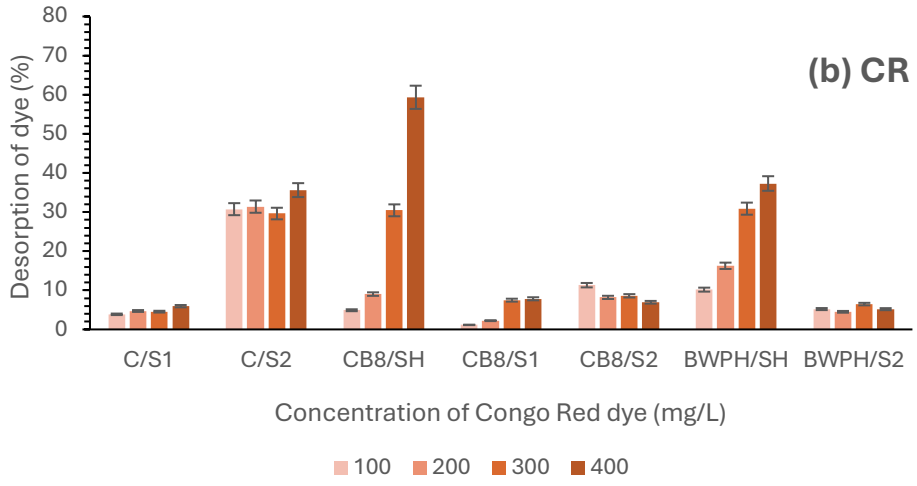
(b) CR
Desorption of dye (%)
80
70
60
50
40
30
20
10
0
C/S1
C/S2
CB8/SH
CB8/S1
CB8/S2
BWPH/SH
BWPH/S2
Concentration of Congo Red dye (mg/L)
100
200
300
400

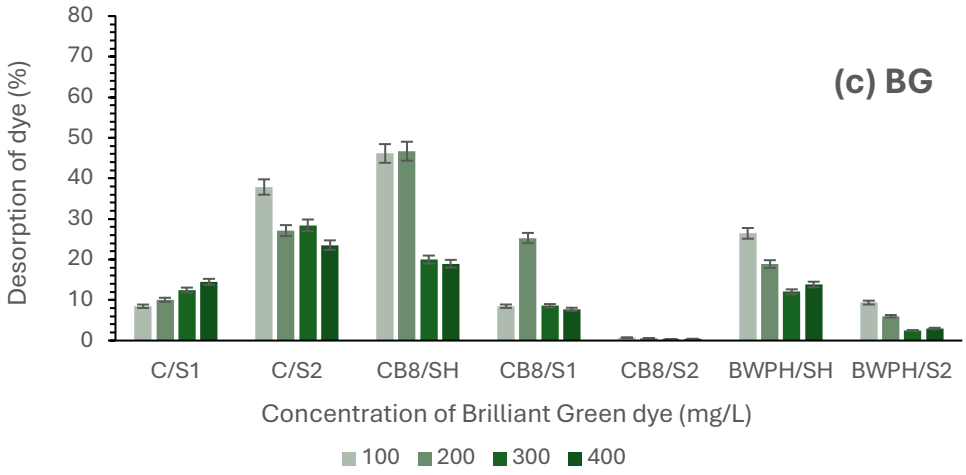
(c) BG
Desorption of dye (%)
80
70
60
50
40
30
20
10
0
C/S1
C/S2
CB8/SH
CB8/S1
CB8/S2
BWPH/SH
BWPH/S2
Concentration of Brilliant Green dye (mg/L)
100
200
300
400

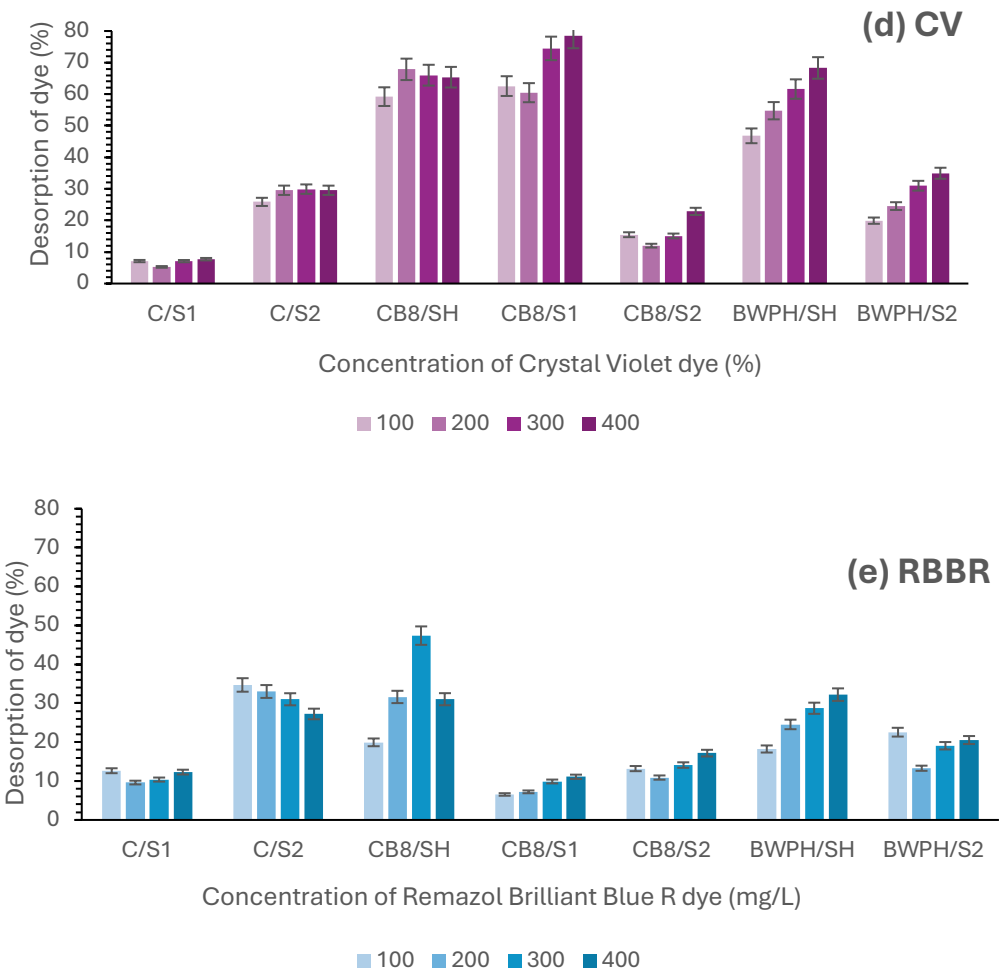

Figure 25. Analysis of desorption (DS%) of (a) Evans Blue, (b) Congo Red, (c) Brilliant Green, (d) Crystal Violet and (e) Remazol Brilliant Blue R dye by carriers, self-immobilized and carrier immobilized CB8 and BWPH fungal biomass with respect to initial concentration of dye (Desorbing agent-70% methanol, static condition, T=20°C ± 2°C, t=24 h)

5.4 Assessment of dye biodegradation efficiency at different parameters

The principal elements affecting fungal dye degradation encompass several physicochemical parameters, media composition, and microbial and environmental influences, as seen in the Figure 26. In this series of studies, we aimed to optimize the dye degradation process as a primary objective of the thesis research work. We transitioned from the micro-assay method used in previous tests to a 100 ml system to assess the dye degradation efficiency of fungus with bigger volumes.

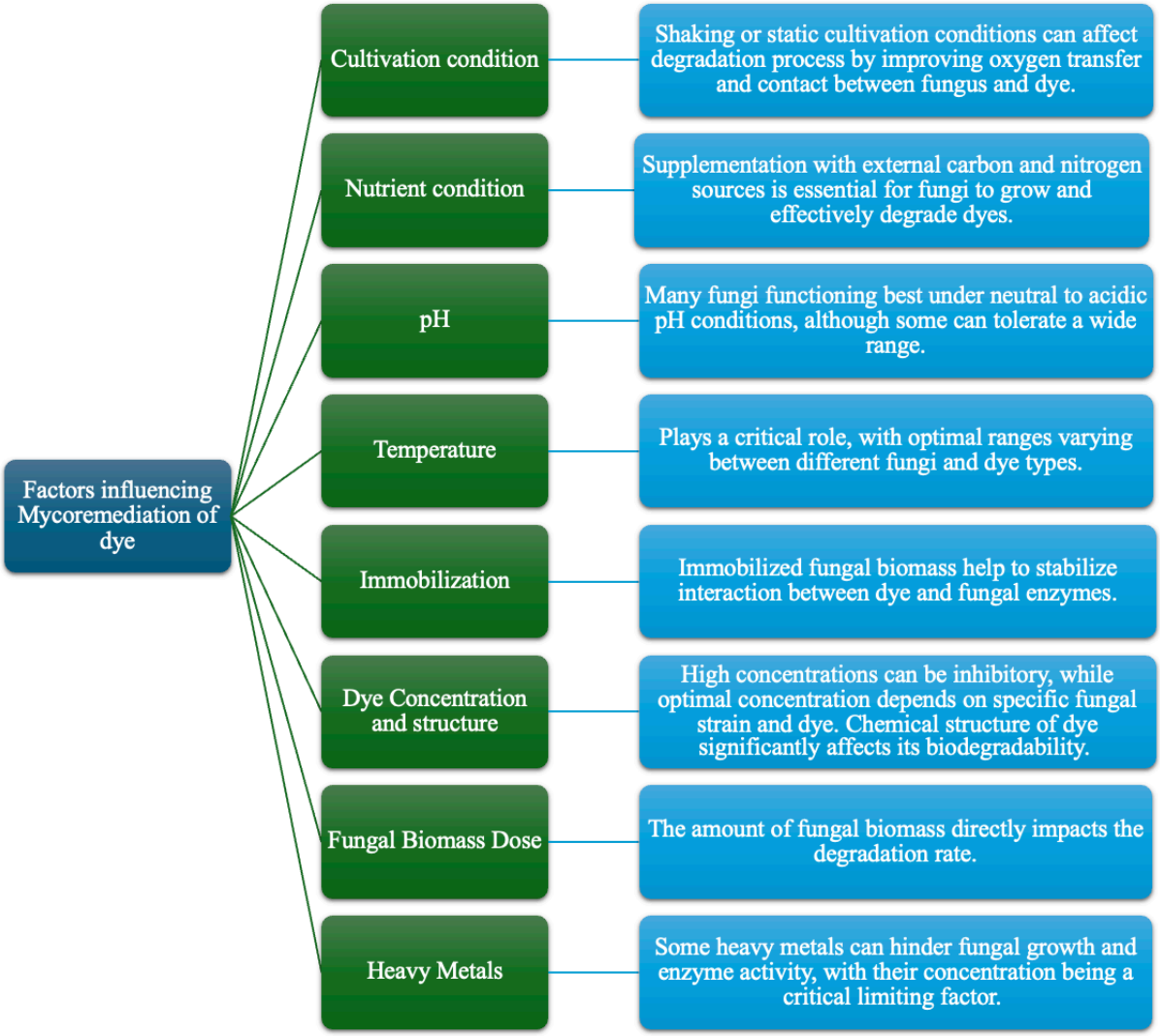

Figure 26. Schematic for factors influencing dye decolorization by White-Rot Fungi

5.4.1 Impact of fungal culture agitation on dye decolorization

Figures 27 (a), (b), and (c) depict the comparative decolorization efficiencies of *T. versicolor* (CB8) and *P. ostreatus* (BWPH) for Remazol Brilliant Blue R (RBBR), Evans Blue, and Crystal Violet dyes under static (ST) and shaking (SH) conditions. A distinct disparity in dye removal behaviour was noted between the two fungal species and among the three dye types. *T. versicolor* (CB8) shown markedly superior decolorization efficacy for the anthraquinone dye RBBR compared to *P. ostreatus* (BWPH). Under static conditions, CB8 attained considerable removal over 96 hours, but BWPH exhibited very less decolorization. Under shaking circumstances, dye removal by CB8 significantly enhanced, surpassing 90% within 24 hours. The significant improvement observed during agitation suggests that agitation is essential for enhancing oxygen and nutrient transfer, thus promoting the synthesis of ligninolytic enzymes including laccase and lignin peroxidase, which are pivotal for the oxidative breakdown of anthraquinone dyes. Conversely, whereas *P. ostreatus* exhibited enhanced RBBR decolorization under agitation, its efficacy was significantly lower to that of

T. versicolor, indicating a somewhat diminished ligninolytic enzyme activity or a slower metabolic reaction to this dye.

A contrasting tendency was noted for the azo dye Evans Blue. Both fungal strains demonstrated the ability to effectively decolorize this dye under static and agitated conditions. *T. versicolor* accomplished nearly total elimination (exceeding 90%) within 24 hours, whereas *P. ostreatus* exhibited a significant rise in decolorization over time (up to 90%). The limited difference between static and shaking treatments in Evans Blue removal suggests that biosorption and enzymatic mechanisms involved in azo dye degradation by these fungi are less dependent on aeration compared to the oxidative degradation of anthraquinone dyes. This observation aligns with previous findings that white-rot fungi can effectively decolorize azo dyes through combined mechanisms of adsorption onto the mycelial biomass and enzymatic cleavage of the azo bond [183,184].

Under static conditions, CB8 demonstrated superior CV dye decolorization effectiveness relative to BWPH at identical time intervals (Fig. 27(c)). Under shaking circumstances, both fungal strains exhibited significantly improved decolorization, achieving 90% within 72 hours. Presumably aeration via agitation supplies adequate dissolved oxygen essential for the production and function of ligninolytic enzymes, including laccase, manganese peroxidase (MnP), and lignin peroxidase (LiP), which facilitate the oxidative degradation of intricate aromatic dye compounds. In static cultures, restricted oxygen transport and localized nutrient gradients frequently hinder enzyme production and result in diminished degradation kinetics. Comparable patterns have been documented in research indicating that shaking circumstances markedly enhanced enzyme activity and dye decolorization effectiveness in white-rot fungus [133,185]. At extended incubation periods (72-96 h), both species under agitation conditions attained nearly total decolorization (>90%), indicating that enzyme-mediated biodegradation emerged as the predominant process over time. Dye removal presumably happened initially through biosorption onto fungal cell walls, aided by functional groups including carboxyl, amino, and hydroxyl moieties in fungal biomass. However, with prolonged incubation and increased enzyme production, biodegradation progressively replaced biosorption as the principal removal pathway. This two-step mechanism-rapid adsorption followed by enzymatic oxidation has been reported in white-rot fungal systems addressing triphenylmethane, anthraquinone and azo dyes degradation [186,187]. The superior decolorization capability of *T. versicolor* relative to *P. ostreatus* under static conditions signifies interspecies differences in enzyme synthesis and dye-binding properties. *T. versicolor* is recognized for its production of a varied ligninolytic enzyme system, comprising LiP, MnP, and several isoforms of laccase [188], which facilitates the efficient degradation of triphenylmethane dyes like crystal violet. Conversely, *P. ostreatus* primarily utilizes laccase as its principal oxidative enzyme, which frequently necessitates extended incubation periods or increased oxygen availability for optimal efficacy [189]. Thus, the superior performance of CB8 in static conditions can be attributed to its extensive enzymatic repertoire and accelerated onset of oxidative metabolism.

The current findings demonstrate that *T. versicolor* (CB8) exhibits superior efficacy in the biodegradation of complex anthraquinone dyes, such as RBBR, especially under shaking

conditions that enhance enzyme activity. In contrast, both *T. versicolor* and *P. ostreatus* are proficient in the removal of simpler azo dyes, including Evans Blue. These findings underscore the necessity of choosing suitable fungal species and optimising growth conditions based on dye structure for effective bioremediation of dye-laden wastewater.

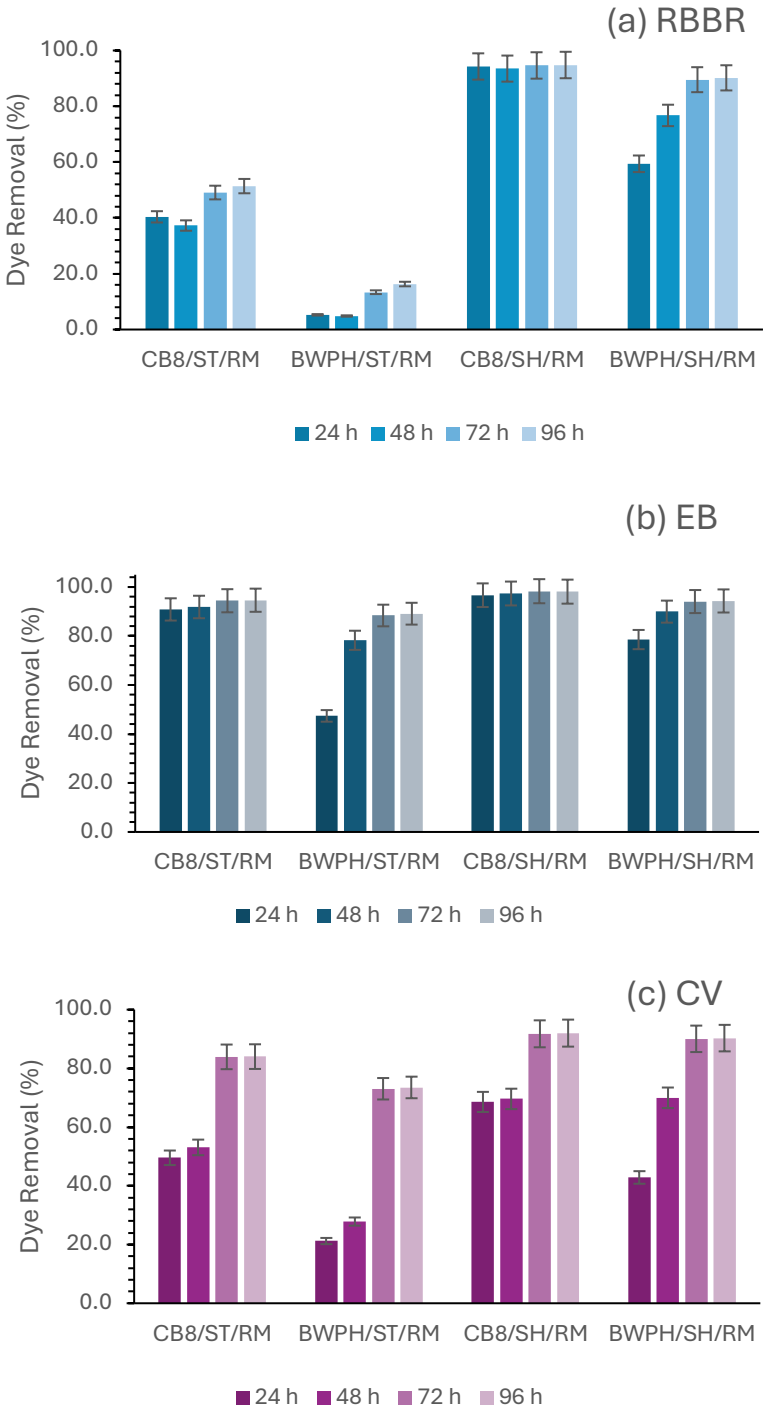

Figure 27. Evaluation of static (ST) and shaking (SH) growth condition for decolorization of (a) Remazol Brilliant Blue R (b) Evans Blue and (c) Crystal Violet dye by *T. versicolor* (CB8) and *P. ostreatus* (BWPH) fungal biomass grown in regular medium (RM)

5.4.2 Impact of Carbon source and agitation on dye decolorization

The impact of carbon supplementation on dye decolorization efficiency was examined by utilizing sucrose (SM) as the principal carbon source, in conjunction with other vital nutrients, to facilitate the growth of *T. versicolor* (CB8) and *P. ostreatus* (BWPH). The fungal biomass derived from static (ST) and shaking (SH) growing conditions was utilized for the decolorization of three synthetic dyes - Remazol Brilliant Blue R (RBBR), Evans Blue (EB), and Crystal Violet (CV) - over a period of 24 to 96 hours. Figures 28 (a), (b), and (c) demonstrate a significant influence of both fungal species and growth conditions on decolorization efficacy.

The maximum decolorization of RBBR was recorded with CB8 cultivated under shaking conditions, attaining 93% elimination in 24 hours. Conversely, the same fungus cultivated under static circumstances attained merely 45.6% decolorization after 96 hours. *P. ostreatus* exhibited minimal decolorization in both situations, achieving only 21.4% under shaking and 18.3% during static growth. This inequality demonstrates that aeration and agitation during the growth phase (shaking condition) significantly augmented the dye-degrading capacity of both fungi, especially *T. versicolor*. The use of sucrose as the only carbon source did not provide greater RBBR decolorization compared to the regular medium (RM), which utilized a lesser quantity of glucose as the carbon source (Figure. 27 (a)). Nevertheless, it proved to be less effective with BWPH in shaking conditions.

Both fungi demonstrated substantial decolorization of the diazo dye Evans Blue, with *T. versicolor* surpassing *P. ostreatus* once more. The highest removal rate of 88.6% was attained in the CB8/SH/SM system, whereas BWPH under agitation conditions obtained 68.5% decolorization after 96 hours (BWPH/SH/SM). Under static conditions, the decolorization percentages were slightly lower - 79.6% for CB8/ST/SM and 74.9% for BWPH/ST/SM. The greater decolorization of Evans Blue compared to RBBR by both fungi may result from the dye's more simpler azo structure, which is more amenable to enzymatic breakage by oxidative enzymes. The findings further validate that agitation of culture conditions amplifies the expression and functionality of extracellular oxidoreductases, hence expediting electron transport and the degradation of dye molecules.

The decolorization of the triphenylmethane dye Crystal Violet was relatively slower than that of RBBR and EB, however exhibited a comparable pattern in both fungi. *T. versicolor* cultivated under shaking conditions attained 81.7% decolorization after 96 hours, whereas the static culture exhibited 78.0% elimination. *P. ostreatus* exhibited reduced efficiency, achieving 68.2% under shaking circumstances and 49.9% under static conditions. Crystal Violet is recognized for its recalcitrance attributed to its intricate aromatic structure and persistent carbon-nitrogen bonds. The enhanced performance under shaking conditions reiterates the significance of oxygen transfer and enzyme stimulation in augmenting fungal degradation capacity. Similar to RBBR, in case of SM did not attain greater level in the decolorization of EB and CV dyes. The disparity in the accessibility of carbon sources and the carbon-to-nitrogen ratio may influence the dye decolorization efficacy of fungi. The comparatively elevated

elimination by *T. versicolor* under both conditions indicates strong enzyme activity even in poorly aerated environments.

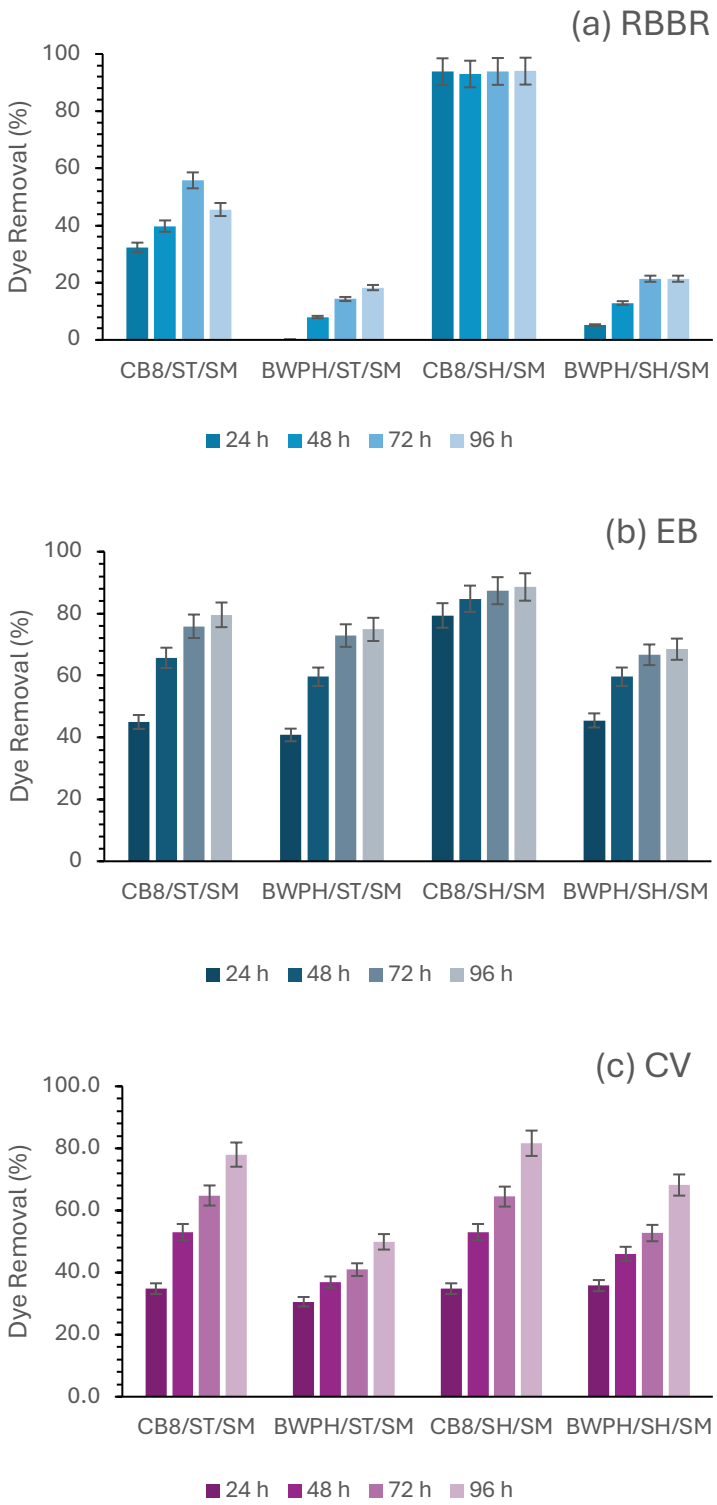

Figure 28. Evaluation of Sucrose medium (SM) for decolorization of (a) Remazol Brilliant Blue R (b) Evans Blue and (c) Crystal Violet dye by *T.versicolor* (CB8) and *P.ostreatus* (BWPH) biomass grown at static (ST) and shaking (SH) growth condition

The aim of further research was to assess the impact of glucose concentration on dye degradation efficiency since the glucose-containing regular medium (RM) performed better in dye decolorization efficiency than the sucrose medium (SM). While regular medium (RM) has a typical glucose concentration of 5 g/L, the performance of *T. versicolor* (CB8) and *P. ostreatus* (BWPH) was examined in media with 10 g/L glucose as the carbon source along with other nutrients. Before conducting dye decolorization tests using Remazol Brilliant Blue R (RBBR), Evans Blue (EB), and Crystal Violet (CV) over a 96-hour period, fungi were grown in both static (ST) and shaking (SH) conditions.

A slight improvement in decolorization efficiency was noted when the glucose concentration (GM) was doubled, particularly for the BWPH strain under static conditions (Figure 29(a)). The maximal decolorization values in shaking-grown cultures, however, were marginally lower than in RM (93.5% for CB8/SH/GM and 74.8% for BWPH/SH/GM). Catabolite repression, which occurs when an excess of an easily metabolizable carbon source (like glucose) inhibits the synthesis of ligninolytic enzymes like laccase, manganese peroxidase (MnP), and lignin peroxidase (LiP), is most likely the cause of this decrease in dye degradation at higher glucose concentrations. However, the occurrence of carbon catabolite repression (CCR) in white-rot fungi is poorly understood [190]. The examination of glucose-induced CCR in wood-decaying fungi is confined to a restricted number of transcripts and enzymatic functions. In specific *Polyporales* species of white-rot fungi, the activities of cellulase and xylanase were markedly diminished upon the addition of glucose to the cultures [191]. Anthraquinone dyes like RBBR are broken down oxidatively by these enzymes. In contrast, moderate glucose levels in RM provided sufficient metabolic energy without significantly repressing enzyme synthesis, leading to higher decolorization efficiency.

For Evans Blue results showed a similar trend (Fig. 29 (b)), with decolorization efficacy sharply declining as glucose concentration increased. In the RM system, *T. versicolor* (CB8/SH/RM) attained nearly complete decolorization (98.1% after 96 hours), closely followed by *P. ostreatus* (BWPH/SH/RM) with 94.3%, as shown in the preceding Figure 27 (b). CB8 eliminated 94.6% while BWPH achieved 89.1% in static conditions. However, both fungus demonstrated moderate decreases in dye removal in the glucose-enriched GM media. Decolorization efficiency was 90.7% (CB8/SH/GM) for *T. versicolor* and 87.2% (BWPH/SH/GM) for *P. ostreatus*. Efficiency was lower under static conditions. These results confirm that enzyme activity is favoured by optimal glucose levels rather than high ones. Although glucose promotes fungal growth and energy consumption, regulatory mechanisms that prioritize primary metabolism over secondary enzyme synthesis may cause an excessive quantity of glucose to inhibit the formation of oxidative enzymes. Furthermore, decolorization was significantly enhanced by shaking conditions, suggesting the significance of oxygen availability and aeration for the production of oxidative enzymes involved in the degradation of azo dye complexes such as Evans Blue.

When both fungi were cultivated in GM medium, their effectiveness in decolorizing CV dye was lower than that on RM medium. The maximum decolorization for *P. ostreatus* was 60.1% (BWPH/ST/GM) and 78.3% (BWPH/SH/GM), whereas the removal for *T. versicolor* was

83.4% (CB8/SH/GM) and 66.1% (CB8/ST/GM) as seen in Figure 29 (c). The pattern was similar to that seen for other dyes: slower degradation rates were caused by partial inhibition of dye-degrading enzyme production at higher glucose concentrations. However, compared to EB and RBBR, crystal violet was more degraded despite having a recalcitrant structure. It's interesting to note that shaking-grown cultures maintained a significant capacity for decolorization even when glucose levels were suppressed. This suggests that oxygen transfer and mechanical agitation partially offset glucose-induced suppression by preserving active fungal metabolism and enzyme secretion [192]. In every treatment, *T. versicolor* demonstrated higher decolorization performance, suggesting a more effective ligninolytic system and greater flexibility in response to changing carbon contents [193]. Though it was still less effective than *T. versicolor* overall, *P. ostreatus* also showed a significant ability for dye degradation, especially for Evans Blue when shaken.

It was evident from the impact of carbon sources on dye decolorization efficiency that the dye decolorization capacity of white-rot fungi is greatly influenced by both glucose content and growing circumstances. Under shaking conditions, the best dye degradation took place in regular glucose medium (RM), where there was enough carbon available to support growth without showing CCR. The ligninolytic enzymes of white-rot fungi are mostly synthesized during the activation of secondary metabolism, which expresses under restrictive conditions, including the availability and concentration of accessible carbon and/or nitrogen sources [194]. The ligninolytic isoenzymes encoded by a gene family frequently display variations in differential expression, catalytic characteristics, regulatory mechanisms, and cellular localization [195]. Moreover, an examination of the promoters of ligninolytic enzyme-encoding genes in the *P. ostreatus* genome has identified many potential response elements. The elements comprise carbon catabolite repressor binding elements (CRE), nitrogen response elements (Nit2), xenobiotic-response elements (XRE), metal-response elements (MRE), and heat-shock elements (HSE), among others, which may regulate gene expression in response to environmental factors, including carbon and nitrogen sources, xenobiotics, temperature, and pH [196]. It has been reported that carbon catabolite repression (CCR), along with many signalling pathways, is essential for the utilization of diverse carbon sources by *P. ostreatus* and other Basidiomycota fungi [197]. The metabolic prioritization of primary growth processes over secondary oxidative enzyme production in excess glucose (GM) reduced the efficiency of decolorization. These results validate the importance of controlled carbon supply and sufficient aeration in optimizing the effectiveness of fungal dye degradation in bioremediation systems. Therefore, to maximize the bioremediation efficacy of white-rot fungi in treating wastewater that contains dyes, it is crucial to optimize both the carbon source and the growth conditions.

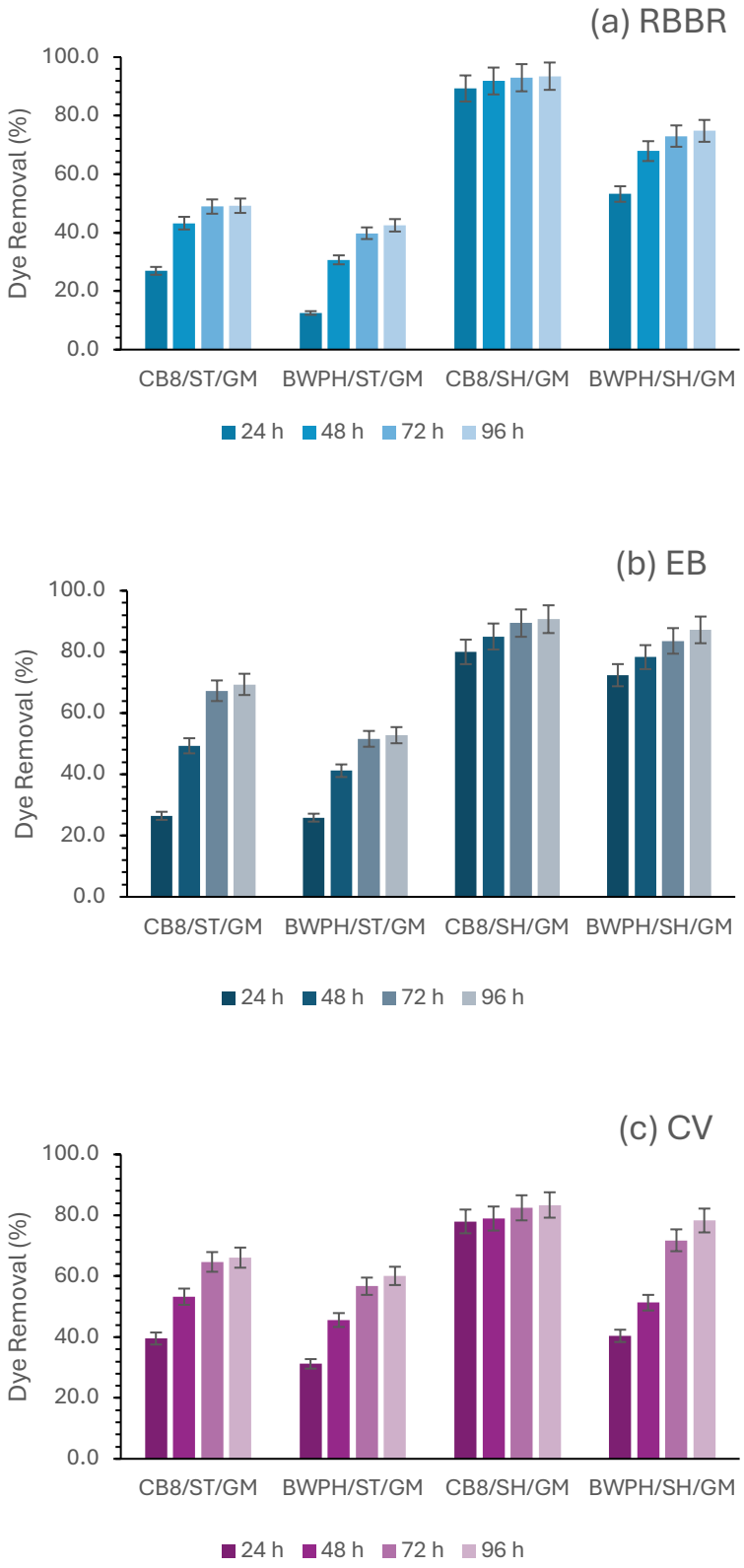

Figure 29. Evaluation of Glucose medium (GM) for decolorization of (a) Remazol Brilliant Blue R (b) Evans Blue and (c) Crystal Violet dye by *T.versicolor* (CB8) and *P.ostreatus* (BWPH) biomass grown at static (ST) and shaking (SH) growth condition

5.4.3 Impact of Nitrogen source and agitation on dye decolorization

Nitrogen availability is a significant regulatory component in fungal metabolism, especially for ligninolytic enzyme synthesis, which subsequently influences the decolorization of RBBR, Evans Blue, and Crystal Violet dyes. This series of experiments investigated three nitrogen regimes: YEM (Yeast Extract Medium) with abundant organic nitrogen (10 g/L); ANM (Ammonium Nitrate Medium) with inorganic nitrogen (10 g/L NH_4NO_3); and RM (Regular Medium) with low nitrogen content (1 g/L peptone). All three mediums were provided with a consistent quantity of additional basal nutrients. The trends illustrated in Figures 30 (a), (b), and (c) are strongly supported by existing literature on ligninolytic fungi as across all dyes, indicating that a moderate concentration of nitrogen consistently yields the highest decolorization efficiencies across all dyes, whereas nitrogen-rich conditions, particularly those involving inorganic nitrogen, significantly inhibit dye removal. This pattern closely corresponds with documented regulatory mechanisms governing ligninolytic enzyme synthesis in white-rot fungus [198–200].

For RBBR, decolorization was comparatively less in YEM and ANM medium (Figure 30 (a)). In YEM, elimination varied from 13% to 26%, while ANM exhibited even greater inefficacy, suggesting significant suppression under conditions of abundant nitrogen availability. In RM samples, RBBR decolorization significantly enhanced, surpassing 90% under most conditions and maintaining a high level throughout the incubation period. This strong induction of RBBR degradation under nitrogen-limited conditions is consistent with numerous studies showing that ligninolytic enzyme production in fungi such as *Phanerochaete chrysosporium*, *Pleurotus ostreatus*, and *Trametes versicolor* is triggered when limited amount of peptone is utilized as nitrogen source [199–201]. Tien and Kirk initially reported that the synthesis of lignin peroxidase in *P. chrysosporium* was nearly completely inhibited under elevated nitrogen levels [202]. Subsequent research validated that nitrogen limitation not only amplifies enzyme activity but also improves the breakdown of recalcitrant dyes, particularly those having anthraquinone structures [203]. Our results distinctly reflect this traditional pattern, suggesting that the fungal strain employed adheres to the conventional nitrogen-regulated ligninolytic pathway.

A comparably robust nitrogen-dependent reaction was noted for Evans Blue, an azo dye. Decolorization under YEM was low to moderate; whereas ANM exhibited superior performance for this dye compared to RBBR, the results were much lower than those attained for peptone as nitrogen source. Evans Blue decolorization in RM achieved 94 - 98% in the majority of treatments, a significantly higher level than any nitrogen-rich media. *Phanerochaete chrysosporium*, commence the destruction of azo dyes through extracellular, non-specific oxidative enzymes including laccases, manganese peroxidases (MnP), and lignin peroxidases (LiP). The generated by-products are predominantly less toxic in this instance. Whereas bacterial consortia generally initiate with the reductive breaking of the azo bond under anaerobic or microaerophilic conditions, mostly facilitated by azoreductase enzymes. This reduction process yields colorless yet frequently poisonous aromatic amines. In both cases, the final outcomes are different. Hence, the fungal degradation proven better for azo dye

degradation in comparison to other microbial degradation strategies [204]. Our findings align closely with previous findings that Evans Blue exhibited the most significant enhancement under nitrogen constraint, indicating a robust induction of the fungi's oxygen-dependent enzyme systems [205].

Crystal Violet, a triphenylmethane dye, exhibited a somewhat distinct although still nitrogen-dependent pattern. YEM facilitated moderate decolorization, with percentages increasing from approximately 28% to 61% over time. Under ANM medium, decolorization was markedly low (1-10%), suggesting that inorganic nitrogen imposed the most significant restriction on the enzymes or pathways necessary for CV breakdown. The RM medium consistently yielded the highest levels of decolorization, achieving 90% or greater in the majority of treatments. Triphenylmethane dyes typically necessitate robust oxidative intervention, and multiple studies indicate a considerable correlation between their breakdown and laccase activity [206]. Research on *T. versicolor* and *P. ostreatus* consistently indicates that laccase and MnP synthesis should be significantly elevated in nitrogen-deficient conditions which is supported by evidence in later section 5.5 of enzyme activity. The significant enhancement in CV decolorization noted in RM aligns precisely with the established nitrogen-dependent control of these enzymes. Other scientists, notably Verma et al. [207], have observed that inorganic nitrogen salts significantly impede laccase development, elucidating the markedly low decolorization values in ANM.

As a concluding remark for effect of nitrogen source on dye degradation, unequivocally indicates that nitrogen limitation is the ideal condition for optimizing decolorization across a variety of structurally different dyes. Organic nitrogen sources, such as yeast extract, facilitated moderate enzyme expression and intermediate dye elimination, but inorganic nitrogen consistently yielded the lowest values, indicating significant inhibition of ligninolytic metabolism. These patterns align with the conventional concept in fungal physiology, wherein nitrogen sufficiency promotes main metabolic activities while inhibiting secondary metabolism, such as lignin modification and dye degradation. Conversely, when nitrogen is limited, fungi transition to secondary metabolic pathways, significantly enhancing the production of extracellular oxidative enzymes that degrade complex aromatic molecules [208,209].

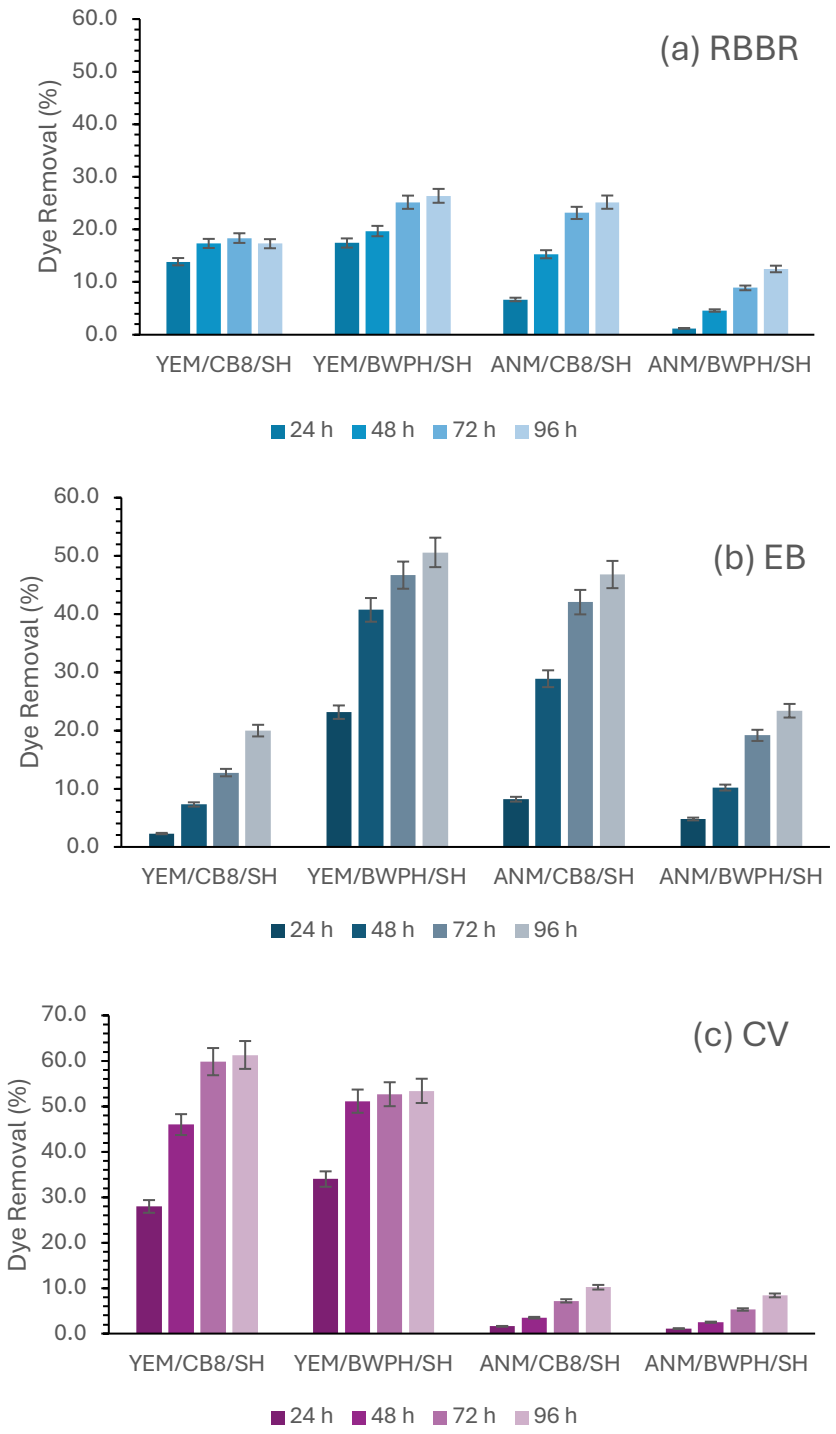

Figure 30. Evaluation of Yeast Extract medium (YEM) and Ammonium nitrate medium (ANM) for decolorization of (a) Remazol Brilliant Blue R (b) Evans Blue and (c) Crystal Violet dye by *T.versicolor* (CB8) and *P.ostreatus* (BWPH) biomass grown at shaking (SH) growth condition

5.4.4 Impact of Immobilization on dye decolorization

The observation of prior experiments stated that shaking conditions demonstrated superiority over static growth conditions (Figure 27), attributed to enhanced oxygen availability.

Furthermore, RM was established as optimal medium for enzyme production and dye removal efficiency. Consequently, we investigated the degradation of Remazol Brilliant Blue R (RBBR), Evans Blue, and Crystal Violet by *T. versicolor* (CB8) and *P. ostreatus* (BWPH) under sponge immobilized conditions.

The immobilization of both fungi onto sponge carriers (S2) resulted in an enhanced degrading efficiency, exceeding that of both static and shaken non-immobilized cultures (Figure 31). Immobilized *T. versicolor* accomplished nearly total elimination of all dyes, attaining 97- 99% degradation of RBBR and Evans Blue after 96 hours, and approximately 90% for Crystal Violet. Immobilized *P. ostreatus* shown significant enhancement relative to its free-cell cultures, attaining over 89% removal of RBBR, 89% removal of Evans Blue, and over 83% removal of Crystal Violet. Other researchers have also emphasizes the advantages of immobilized cultures, demonstrating that the immobilization of white-rot fungi on substrates such as polyurethane foam, loofa sponge, or alginate beads [210–213] results in enhanced and more consistent enzyme production, safeguards the biomass against shear stress and toxic dye intermediates, and facilitates the formation of dense fungal biofilms within the carrier's pores. These microenvironments facilitate sustained metabolic activity, augment oxidative enzyme production, and frequently provide extra adsorption capacity, resulting in expedited dye breakdown.

The consistently superior performance of CB8 relative to BWPH under all conditions also indicates recognized physiological disparities between the two fungi. *T. versicolor* is acknowledged as one of the most effective ligninolytic fungi, proficient in generating substantial quantities of laccase and peroxidases in nutrient-deficient and stress-inducing conditions, such as those found in dye-laden media [214–216]. The capacity to decompose structurally varied dyes - anthraquinone, azo, and triphenylmethane - has been thoroughly recorded. The comparison of non-immobilized static, non-immobilized shaking, and sponge-immobilized cultures unequivocally indicates that immobilization is the most efficacious approach for optimizing dye degradation. Agitation significantly improves degrading efficiency relative to static systems; yet, immobilization offers the most steady and prolonged activity for both fungi. The results collectively demonstrate that immobilization on sponge carriers is an effective method for enhancing the biodegradation of synthetic dyes in wastewater treatment, particularly with the use of robust ligninolytic strains like *T. versicolor*.

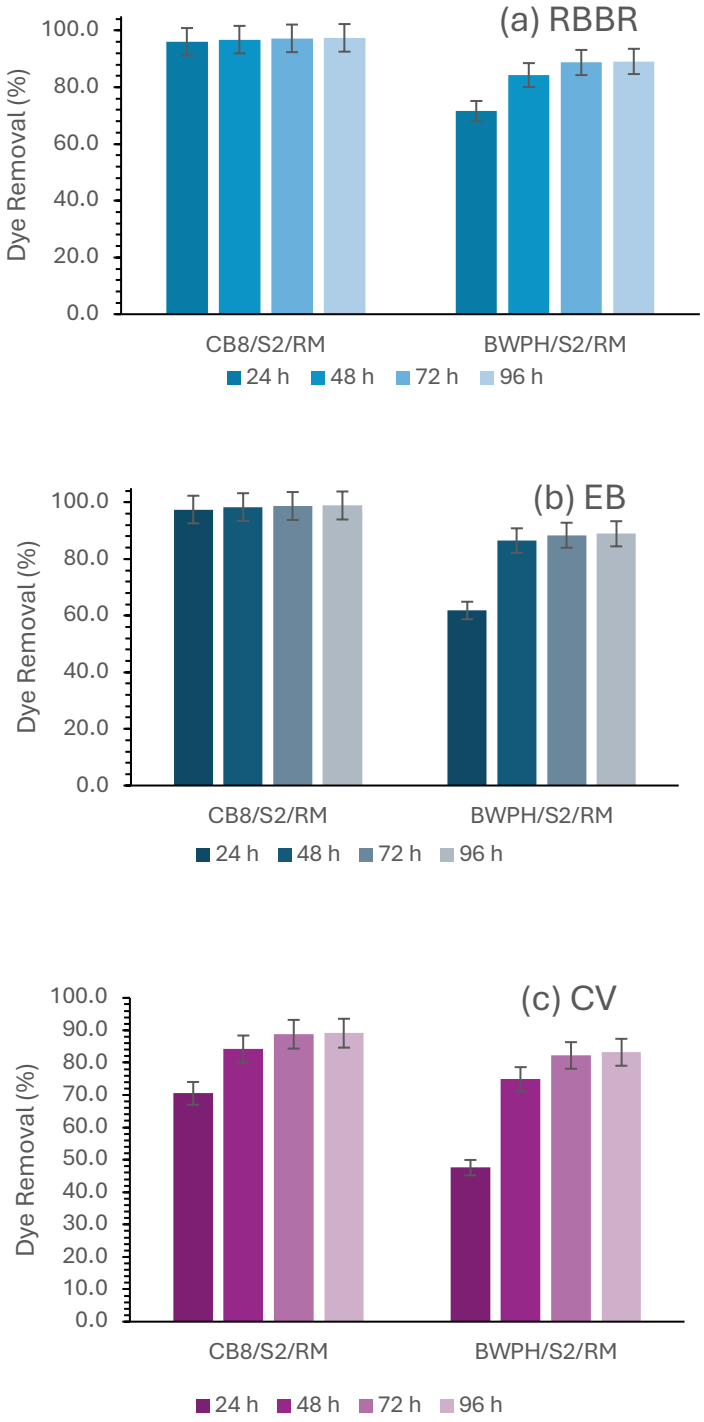

Figure 31. Evaluation of decolorization of (a) Remazol Brilliant Blue R (b) Evans Blue and (c) Crystal Violet dye by sponge immobilized *T. versicolor* (CB8) and *P. ostreatus* (BWPH) biomass grown in regular medium (RM)

To conclude the result, a three-factor Analysis of Variance (ANOVA) was conducted to determine the best nutrient conditions for dye decolorization, assessing the impacts of carbon source, nitrogen source, and fungal species on dye removal efficiency as the response variable. Each factor was considered an independent variable, and tests were executed using a factorial

design. The ANOVA results demonstrate that all three factors (carbon source, nitrogen source, and fungal species) had statistically significant effects on the response variable (Appendices Table A1). The carbon source showed a significant effect ($F = 4.81$, $p = 0.0125$). This indicates that different carbon sources caused measurable differences in the response, although the magnitude of this effect was relatively smaller compared to other factors. The nitrogen source exhibited a highly significant effect ($F = 226.64$, $p < 0.001$). The very large sum of squares and F value suggest that nitrogen source was the most influential factor in the experiment, contributing substantially to the observed variation in the response variable. The fungal species also had a highly significant effect ($F = 18.85$, $p < 0.001$). This result confirms that the choice of fungus plays an important role in determining the experimental outcome. The residual variation (SS = 2791, MS = 58) represents unexplained variability due to experimental error or other uncontrolled factors. The relatively low residual mean square compared to the treatment mean squares indicates a good model fit and reliable experimental data.

The ANOVA analysis confirms that nitrogen source is the dominant factor affecting the response variable, followed by fungal species, while carbon source has a smaller but still significant influence. These findings highlight the importance of nutrient composition and microbial selection in optimizing the studied process.

Following the ANOVA, Tukey's post hoc test was executed to facilitate pairwise comparisons of mean dye decolorization percentages across all experimental conditions, encompassing agitation, immobilization, nutritional medium composition, and fungal biomass type. The aim of this test was to discover statistically significant changes in RBBR, EB and CV dye decolorization efficiency between treatments and to ascertain the appropriate experimental settings for future studies and molecular-level investigations. Tukey's HSD analysis was employed to identify statistically significant differences among treatments, with treatments denoted by the same letter indicating no significant difference ($p < 0.05$).

Figure A1(a) (Appendices) illustrates the decolorization efficiency of RBBR by CB8 and BWPH under diverse growth circumstances, mediums, and biomass types. Post hoc analysis showed that *T. versicolor* with sponge-immobilized biomass in regular medium (CB8/S2/RM) achieved the highest RBBR decolorization (~98%), significantly outperforming all other treatments. Other *T. versicolor* combinations, including CB8/SH/RM, CB8/SH/SM, and CB8/SH/GM, also achieved high removal (~92-95%) with no significant differences among them. BWPH/SH/RM and BWPH/S2/RM treatments also performed well (~90%) in regular medium, and the lowest decolorization occurred in ammonium nitrate or yeast extract media for both fungi. Sponge immobilization enhanced dye removal relative to free biomass, and agitation improved *P. ostreatus* performance, while *T. versicolor* remained effective under both static and shaking conditions. Overall, the results highlight that fungal species, biomass immobilization, and medium composition critically influence RBBR bioremediation efficiency.

The decolorization of Evans blue dye was markedly affected by fungal species, growing conditions, immobilization strategies, and growth media, as demonstrated by the post hoc

treatment groupings in Figure A1(b) (Appendices). The greatest decolorization efficiencies were attained with CB8 cultivated on regular medium (RM), especially under sponge-immobilized (S2) and shaking (SH) conditions, with CB8/S2/RM and CB8/SH/RM (98.4-97.6%) constituting the leading statistical group ("a"), signifying no substantial difference between them and designating these as the optimal conditions. The static cultivation of CB8 on RM medium exhibited a little decreased performance (92.9%) however remained statistically equivalent ("ab"). Conversely, BWPH typically had diminished efficiency, while agitation and RM still facilitated moderate decolorization (75.8-89.2%). The substitution of carbon sources (glucose or sucrose media) resulted in a significant reduction in dye removal for both fungi, evidenced by lower mean values and distinct post hoc groupings ("abc" to "efg"). In contrast, nitrogen-rich media (yeast extract and ammonium nitrate) exhibited the least effective performance, corresponding to the lowest statistical groupings ("gh" to "h"). The post hoc analysis indicates that treatments with identical letters are not significantly different ($p < 0.05$) and definitively identifies CB8 cultivated on standard medium under immobilized or shaking conditions as the statistically superior and optimal system for Evans blue dye decolorization.

Likewise, when Tukey's post hoc test was performed to check the influential factor for crystal violet dye degradation, the immobilized CB8 fungus in RM medium proven to be best optimized conditions with the leading statistical group ("a") for CV (Figure A1(c) - Appendices). Self-immobilized CB8 biomass (CB8/SH) remained statistically equivalent ("ab") in RM, GM and SM medium. It corelates with ANOVA result that nitrogen source is more influential than carbon source as ANM/CB8/SH AND YEM/CB8/SH follows into different group ("fg" and "ghi"). *P.ostreatus* strain gave highest decolorization percentage in BWPH/SH/RM and BWPH/S2/RM condition with statistically near groups ("ab" and "b" respectively). Definitively identifies CB8 cultivated on standard medium under immobilized or shaking conditions as the statistically superior and optimal system for Crystal violet dye decolorization ($p < 0.05$).

5.4.5 Evaluation of Dye mixture decolorization efficiency

The decolorization of the ternary dye combination consisting of RBBR, Evans Blue, and Crystal Violet by *T. versicolor* (CB8) and *P. ostreatus* (BWPH), including their sponge-immobilized variants, exhibited distinct variations in degradation efficiency among strains and treatment periods as seen in Figure 32. In the case of CB8, the self-immobilized biomass demonstrated swift initial dye removal, attaining 53.5% decolorization within the first 24 hours, signifying a robust early enzymatic reaction and effective interaction with the dye molecules. Decolorization progressively increased, attaining 70.1% during 72 hours and culminating at 72.9% at 96 hours. The sponge-immobilized variant of the same strain (CB8/S2) originally exhibited superior performance, achieving 63.8% decolorization within 24 hours. Despite a reduction to 57.4% at 48 hours, the culture gradually stabilized and restored its efficacy, ultimately attaining the greatest decolorization rate of 77.9% among all treatments by 96 hours. This recovery indicates that during an initial acclimatization phase on the sponge matrix, the

fungus achieved persistent growth and maintained the release of ligninolytic enzymes proficient in degrading complicated chromophoric structures within the dye mixture.

For *P. ostreatus* (BWPH), the self-immobilized biomass had a relatively delayed initial response than CB8, achieving 45% decolorization in 24 hours. A significant enhancement was noted after 48 hours, with decolorization achieving 64%, and the progression persisted consistently to 72.7% at 96 hours. This pattern indicates a delayed yet strong activation of oxidative enzymes, potentially linked to the species' inherent control of peroxidases and laccases in reaction to intricate dye complexes. Conversely, the sponge-immobilized variant of *P. ostreatus* (BWPH/S2) samples exhibited significantly inferior performance, with merely 13.7% decolorization at 24 hours and a peak of 55.3% at 96 hours. This diminished effectiveness indicates that immobilization may have limited BWPH fungal growth, the flow of dye molecules and nutrients within the sponge matrix, leading to decreased enzymatic activity and less efficient dye breakdown.

In the wider context of dye bioremediation, these findings underscore the strain-specific reactions of white-rot fungi to immobilization and complicated dye mixtures. The enhanced efficacy of CB8, especially CB8/S2, compared to BWPH suggests that *T. versicolor* has a more efficient or higher-capacity ligninolytic enzyme system adapted at the concurrent breakdown of structurally varied dyes. Conversely, the enhanced late-stage performance of BWPH indicates that, once stimulated, its enzyme system is comparably effective but exhibits a delayed activation. The relatively lower performance of BWPH/S2 indicates that immobilization does not universally improve decolorization and may, contingent upon fungal morphology or physiological traits, hinder mass transfer or growth dynamics. The findings endorse the efficacy of *T. versicolor*, particularly in its immobilized state, as a viable option for treating mixed-dye wastewater, while underscoring the necessity of choosing suitable immobilization techniques specific to each fungal strain.

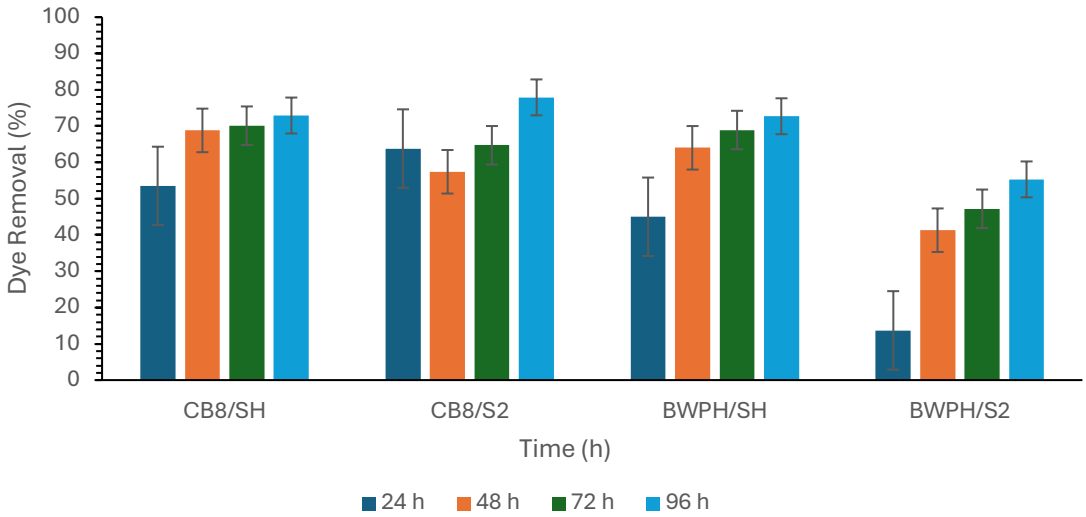

Figure 32. Evaluation of decolorization of dye mixture composed of Remazol Brilliant Blue R, Evans Blue and Crystal Violet dye (1:1:1) by self-immobilized and sponge immobilized *T.versicolor* (CB8/SH, CB8/S2) and *P.ostreatus* (BWPH/SH, BWPH/S2) biomass

5.5 Evaluation of Enzymatic Activity

5.5.1 Laccase

The incorporation of RBBR, Evans Blue, and Crystal Violet elicited a distinct induction of laccase activity in both *T. versicolor* (CB8) and *P. ostreatus* (BWPH), with the extent of enzyme production differing based on the dye, fungal species, and growth conditions as mentioned in section 4.8. In all treatments, laccase activity in dye-amended cultures shows clear changes than in the equivalent controls, suggesting that the dyes functioned as oxidative inducers of the ligninolytic system. Dyes were added on 7th day after growth of fungal culture enzyme activity were measured right after dye introduction and then after 24 h (8th day), 48 h (9th day), 72 h (10th day) and 96 h (11th day). While the control cultures exhibited a gradual increase in activity over the eleven days incubation period, indicative of natural growth-associated laccase secretion. The enhancements in the dye-treated cultures were significantly more pronounced in some culture conditions, thereby affirming the stimulatory impact of these xenobiotic aromatic compounds.

Growth conditions and fungus species clearly influenced laccase activity in CB8 strain in response to RBBR treatment (Figure 33 a). While BWPH strain exhibited a similar pattern but with lower absolute values, immobilized cultures of *T. versicolor* (CB8/S2) generated the highest enzyme levels, much surpassing those of shaking and static cultures. The oxygen-rich and mechanically stable environment provided by immobilization is reflected in this growth-condition hierarchy, which has been shown in earlier research in order to improve ligninolytic metabolism and promote secondary enzyme secretion. According to findings that these dyes upregulate oxidative enzymes through stress-mediated transcriptional activation, RBBR, an anthraquinone dye that mimics lignin-derived aromatics, acted as a potent inducer of laccase expression in both fungi. A positive relation between enzyme activity and decolorization effectiveness was confirmed by the decolorization percentage of RBBR dye as clearly seen in Figure 27(a) and 31(a). Static cultures showed noticeably slower removal (≈50% by 96 h), but immobilized CB8 cultures achieved >96% RBBR removal within 72-96 h, followed by CB8/SH with ~94-95% removal in the same period (section 5.4.1 and 5.4.4). BWPH exhibited the same growth-condition trend but with lower overall efficiency, underscoring species-level enzymatic variability. Together, these results highlight that elevated laccase production, particularly under immobilized conditions, was the primary determinant of RBBR decolorization capacity.

EB-induced enzyme levels in CB8/S2 and CB8/SH were significantly higher than those in static cultures, highlighting the advantage of improved aeration and mass transfer in enhancing oxidative enzyme synthesis as mentioned before (Figure 33(b)). Evans Blue exposure elicited substantial laccase production in both fungi, particularly in immobilized and shaking cultures of *T. versicolor*, reflecting literature that azo dyes act as potent oxidative-stress inducers stimulating ligninolytic pathways. Although this enzyme activity was not higher than in control samples with fungal biomass. Compared to *T. versicolor*, *P. ostreatus* displayed a similar reaction pattern, albeit with less enzyme intensity. The high breakdown efficiency seen in all EB treatments was strongly correlated with these enzymatic tendencies. As previously

mentioned in section 5.4.1 and 5.4.4 that within 72-96 hours, immobilized CB8 cultures removed 97-99% of the EB, with shaking cultures coming in second at >98% clearance (Figure 27(b) and 31(b)). Because of its structural vulnerability to enzymatic cleavage, EB is more easily oxidized than RBBR or CV, as seen by the >94% elimination that even static CB8 cultures achieved by 96 hours. BWPH showed similar patterns, with immobilized and shaking cultures exhibiting ~86-94% clearance, suggesting once more that the primary factors influencing degradation efficacy were growth mode and enzyme levels. EB is classified as a dye that is particularly susceptible to fungal biodegradation because of its strong inducibility and high enzyme-response coupling.

Because of its structural complexity as a triphenylmethane dye, it induced ligninolytic pathways across all fungal biomass variations as seen in Figure 33(c). *T. versicolor* immobilized and shaken cultures continued to generate significantly more enzyme than static cultures, demonstrating that growing conditions were still a critical factor in oxidative enzyme synthesis. The same pattern was seen in *P. ostreatus*, although overall enzyme yields were lower, which is consistent with species-level variations in baseline laccase production. Moderate but considerable dye removal was observed in the corresponding degradation data, which closely matched patterns of enzyme production. As previously seen in Figure 31 (c) and 27(c) respectively that by 96 hours, immobilized CB8 had removed around 88-89% of the CV, whereas shaking cultures had removed about 92% (section 5.4.1 and 5.4.4). This suggests that the recalcitrance of CV was overcome by increased laccase production in these circumstances. At 96 hours, static cultures only achieved ~84% removal for CB8 and ~73% removal for BWPH, indicating the combined impact of low enzyme levels and dye resistance. The substantial correlation between decolorization efficiency and enzyme patterns (Figure 27(c), 31(c) and Figure 33(c)) highlights the fact that laccase availability continues to be the primary factor controlling degradation performance, even for structurally resistant dyes like CV.

Comparison with the control data (Figure 33(d)) further highlights the strong influence of dye induction. In the absence of dyes, both fungi exhibited low laccase production during the initial growth phase; however, enzyme secretion increased as the cultures aged under all culture conditions. Immobilized controls exhibited the highest baseline values. The enzyme activities in dye treatments were consistently far greater than in the corresponding controls for many culture conditions, demonstrating that dye exposure acted as a potent inducer of Laccase production along with growth conditions and immobilization. However, this raises questions regarding the mechanism of dye decolorization under conditions where laccase production was not significantly higher than the control, yet decolorization efficiencies exceeding 80% were still achieved.

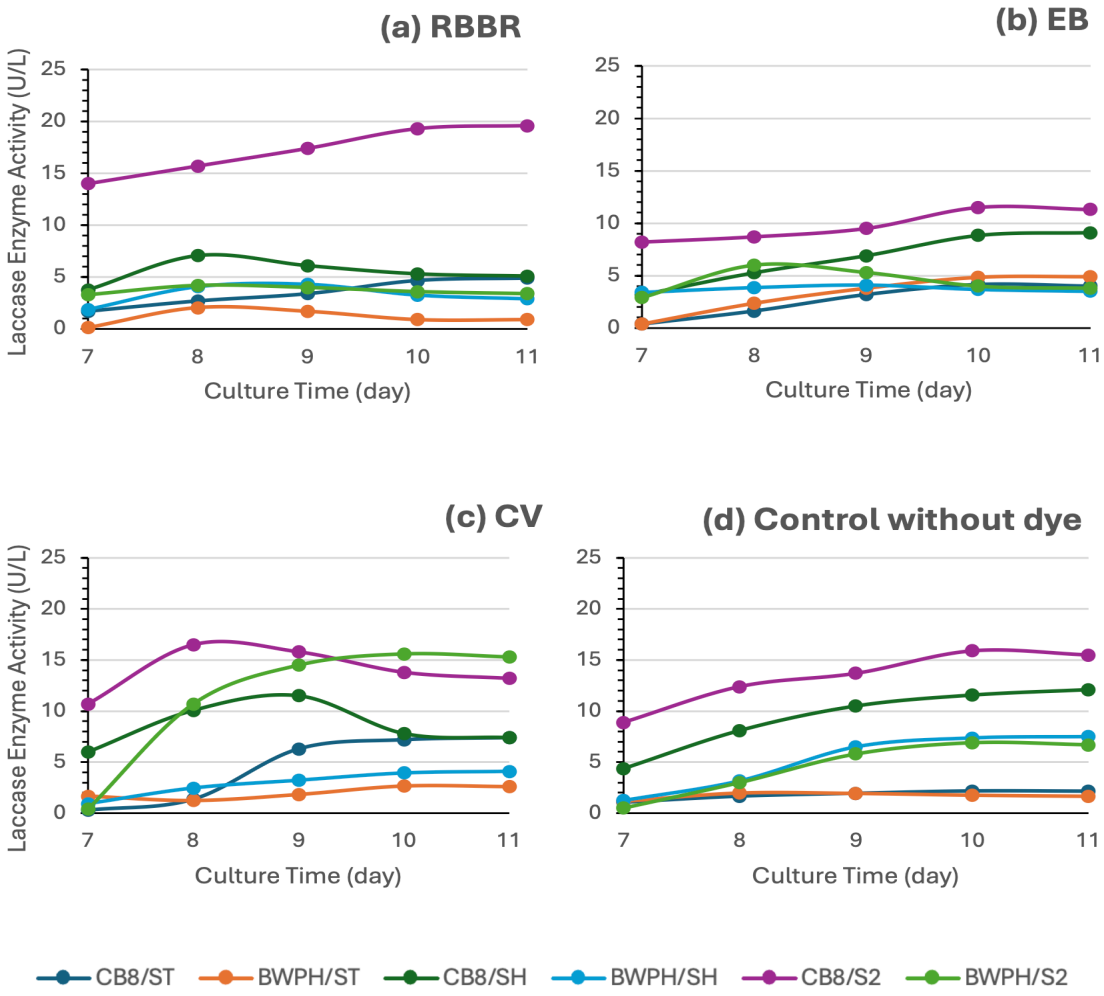

Figure 33. Laccase enzyme activity detected in static, shaking and sponge immobilized cultures of *T. versicolor* (CB8) and *P. ostreatus* (BWPH) during 5 days incubation with dye (a) Remazol Brilliant Blue R (b) Evans Blue (c) Crystal Violet and (d) fungal control without dye

5.5.2 Manganese Peroxidase

The production of manganese peroxidase (MnP) by *T. versicolor* (CB8) and *P. ostreatus* (BWPH) exhibited a distinct reliance on growth conditions and dye exposure, closely resembling the physiological patterns noted in laccase activity. As seen in Figure 34, among all investigated dyes, shaking cultures (SH) of CB8 exhibited the highest amounts of MnP, followed by sponge-immobilized cultures (S2), while static cultures (ST) demonstrated the lowest activity. This pattern aligns with established principles of fungal physiology, where agitation improves nutrient distribution and oxygen availability - both essential for peroxidase synthesis - while immobilization stabilizes mycelia and promotes oxidative metabolism, though it may limit oxygen diffusion deeper within the matrix. In contrast, static cultures exhibit metabolic limitations, yielding less MnP activity until the later stages of development. The significantly elevated MnP activities in CB8 relative to BWPH align with literature

indicating that *T. versicolor* is a robust generator of MnP, while *P. ostreatus* generally prefers laccase-dominant ligninolytic routes.

The exposure to dye served as an extra stimulus for MnP synthesis, although the degree of induction differed depending on the dye used. RBBR and Evans Blue elicited the most robust early-phase MnP responses in CB8, especially in shaking cultures, where concentrations surpassed 40-68 U/L within 24 hours of dye introduction (Figure 34(a) and (b)). This corroborates earlier research indicating that anthraquinone (RBBR) and azo dyes (Evans Blue) induce significant oxidative stress, resulting in the activation of peroxidases and laccases. Crystal Violet, despite its structural resilience, significantly stimulated MnP formation in CB8 under both shaking and immobilized conditions, demonstrating that MnP is involved in the oxidative degradation of triphenylmethane dyes (Figure 34(c)). Nevertheless, BWPH exhibited only limited MnP activity under the majority of circumstances, with the significant exception of CV during immobilized growth (BWPH/S2), where MnP concentrations exceeded 100 U/L by day 10. This selective induction implies a compensating enzymatic response in *P. ostreatus*, wherein MnP is more prominently expressed when laccase levels are inadequate to degrade a structurally complicated substrate such as CV.

The disparities in MnP production are closely associated with the previously documented dye-removal results. Elevated MnP activity in CB8/SH and CB8/S2, especially in the RBBR and EB treatments, corresponds with the fast decolorization noted under such conditions (section 5.4.1 and 5.4.4), generally surpassing 95% elimination within 72-96 hours (Figure 27 and 31) The simultaneous presence of elevated laccase and MnP elucidates why CB8 cultures, particularly under agitation and immobilization, exhibited the most rapid and thorough dye degradation. MnP broadens the spectrum of oxidizable substrates by producing Mn^{3+} chelates that can interact with phenolic and certain non-phenolic dye structures. Conversely, diminished MnP activity in static cultures is associated with reduced and incomplete decolorization, especially for RBBR, where CB8/ST attained merely ~50% elimination after 96 hours, while BWPH/ST exhibited even poorer performance as seen in Figure 27(a) (section 5.4.1). In Evans Blue, the elevated MnP peaks seen in CB8/SH and CB8/S2 correspond with nearly total decolorization (>98%) (Figure 27(b) and 31(b)), corroborating the involvement of peroxidases in the cleavage of azo linkages when functioning synergistically with laccases (section 5.4.1 and 5.4.4).

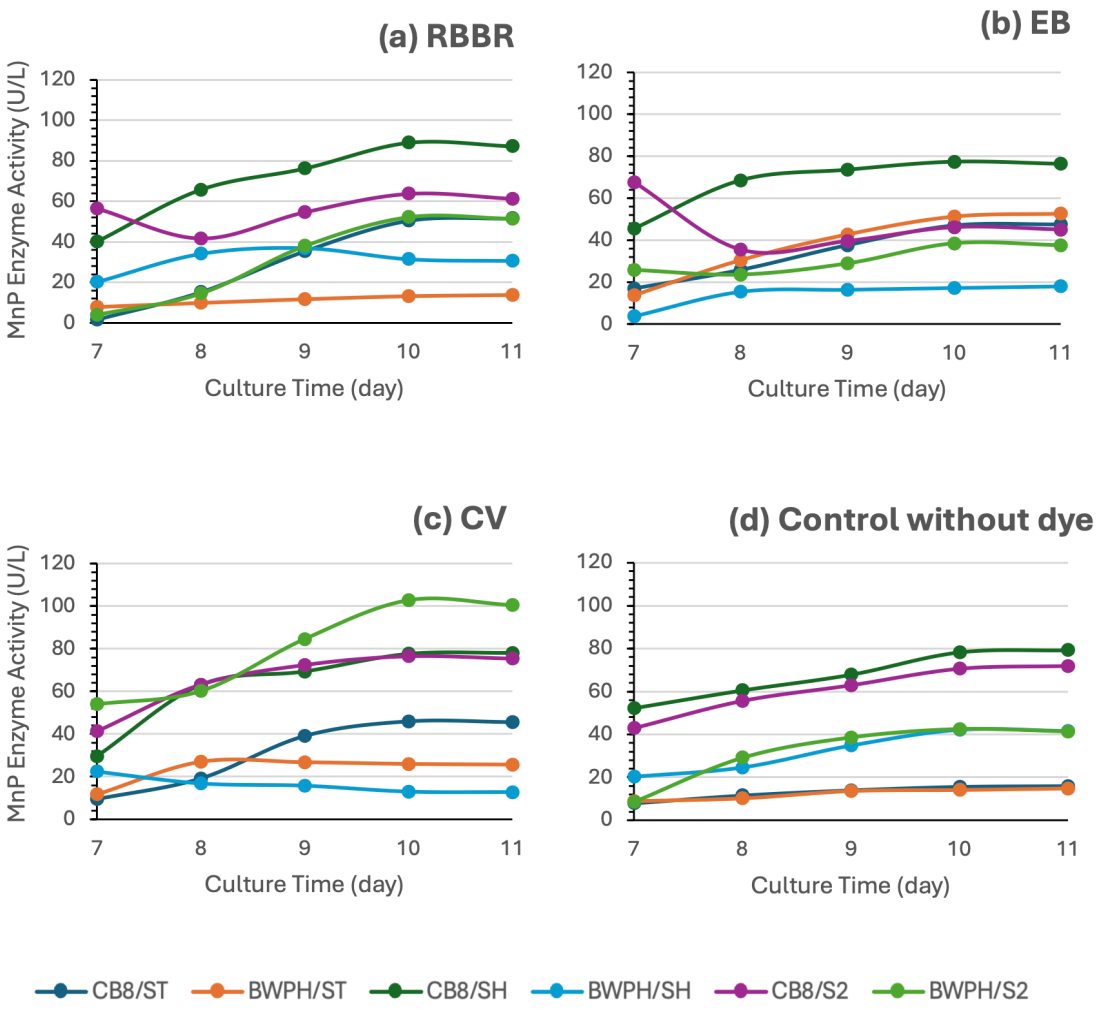

Figure 34. Manganese dependent Peroxidase (MnP) enzyme activity detected in static, shaking and sponge immobilized cultures of *T. versicolor* (CB8) and *P. ostreatus* (BWPH) during 5 days incubation with dye (a) Remazol Brilliant Blue R (b) Evans Blue (c) Crystal Violet and (d) fungal control without dye

Crystal Violet reveals a more intricate scenario. CB8, which generates moderate to high levels of MnP under SH and S2 conditions (Figure 34(c)), demonstrated effective CV deterioration (>90% in SH, around 88-89% in S2) (Figure 27(c) and 31(c)). BWPH, however, exhibited minimal MnP production under most settings but achieved exceptionally high MnP levels in BWPH/S2 by day 10; notably, CV degradation in BWPH/S2 reached approximately 83%, which is considerably greater than in other BWPH growth conditions (Figure 34(c) and 31(c)).

The MnP activity patterns indicate that enzyme synthesis is concurrently influenced by physiological parameters (aeration, agitation, immobilization), fungal species, and the chemical structure of the dye. Furthermore, the strong association between MnP levels and decolorization efficacy across several dyes substantiates that MnP, in conjunction with laccase, significantly contributes to fungal dye degradation. Elevated MnP production consistently correlated with high degradation rates, whereas delayed or minimum MnP expression was associated with slower and less thorough dye elimination. The reliance on two enzymes

highlights that enhancing fungal growth conditions and choosing suitable inducers are essential for maximizing bioremediation efficacy in dye-polluted wastewater.

5.5.3 Lignin Peroxidase

The activity of lignin peroxidase (LiP) in *T. versicolor* (CB8) and *P. ostreatus* (BWPH) was significantly affected by the introduction of synthetic dyes, duration of incubation, and method of cultivation, highlighting LiP's function as a stress- and substrate-inducible enzyme in ligninolytic metabolism (Figure 35). In control cultures devoid of dyes, both fungi demonstrated a progressive enhancement in LiP activity throughout incubation time, aligning with the initiation of secondary metabolism during the idiophase. The rise was notably more significant in static and sponge-immobilized conditions, where the integrity of the mycelium and extended metabolic activity enhanced enzyme secretion.

Under the influence of RBBR, the production of lignin peroxidase (LiP) exhibited substantial variation across different growing conditions and fungal strains as clearly seen in Figure 35(a). Under static conditions, CB8/ST exhibited exceptionally high LiP activity on day 7, which was then followed by a gradual drop in the following days (Figure 35(a)). This pattern indicates a fast enzymatic reaction to the anthraquinone configuration of RBBR, which closely resembles lignin subunits and is easily targeted by high-redox-potential enzymes like LiP. The ensuing decline in activity may be ascribed to partial dye decolorization, the accumulation of inhibiting degradation products, or enzyme inactivation over time. Conversely, *P. ostreatus* exhibited a lagged although continuous enhancement in LiP activity across all cultivation methods, attaining peak levels during later incubation phases. This signifies a more adaptive response in BWPH, wherein enzyme synthesis is progressively elevated as the fungus acclimates to the dye stress. Shaking and sponge-immobilized cultures facilitated more consistent LiP synthesis in both fungi, presumably due to enhanced oxygen transport and safeguarding the mycelium from severe stress. The enzyme patterns correspond well with previously reported dye decolorization trends in section 5.4.1 and 5.4.4. Treatments exhibiting the strongest LiP activity (CB8/ST and CB8/S2) linked to the most significant RBBR elimination (Figure 27(a) and 31(a)), underscoring that the anthraquinone structure of RBBR necessitates robust oxidative cleavage predominantly facilitated by LiP.

Evans Blue, an azo dye containing sulfonic substituents, produced a distinct pattern of enzyme induction as seen in Figure 35(b). CB8 under static conditions (CB8/ST) demonstrated the highest LiP activity at initial time intervals. Nonetheless, a progressive decrease from Day 7 to Day 11 indicates that extended exposure to Evans Blue may impose slight inhibitory effects or that the fungus alters its metabolic priorities as breakdown advances. In shaking cultures (CB8/SH) and immobilized cultures (CB8/S2), LiP activity was initially minimal but progressively increased over time. The postponed induction suggests that both aeration (SH) and immobilization (S2) necessitate an extended acclimatization phase prior to the optimal synthesis of LiP in the presence of sulfonated azo dyes. In BWPH, BWPH/ST exhibited modest amounts of LiP consistently, while BWPH/SH and BWPH/S2 had increasing trend over time. This pattern indicates that *P. ostreatus* has a superior response to dye exposure in dynamic (SH) or immobile (S2) conditions when confronted with azo dyes. The decolorization results

exhibit a strong correlation with the enzymatic tendencies. The elimination of EB significantly improved after Day 9 as mentioned in section 5.4.1 and 5.4.4, coinciding with the rise in LiP activity in CB8/SH, CB8/S2, and BWPH/S2 (Figure 27(b) and 31(b)). The oxidative breakage of azo linkages depends on peroxidase activity, elucidating the concurrent increase in enzyme production and decolorization efficacy.

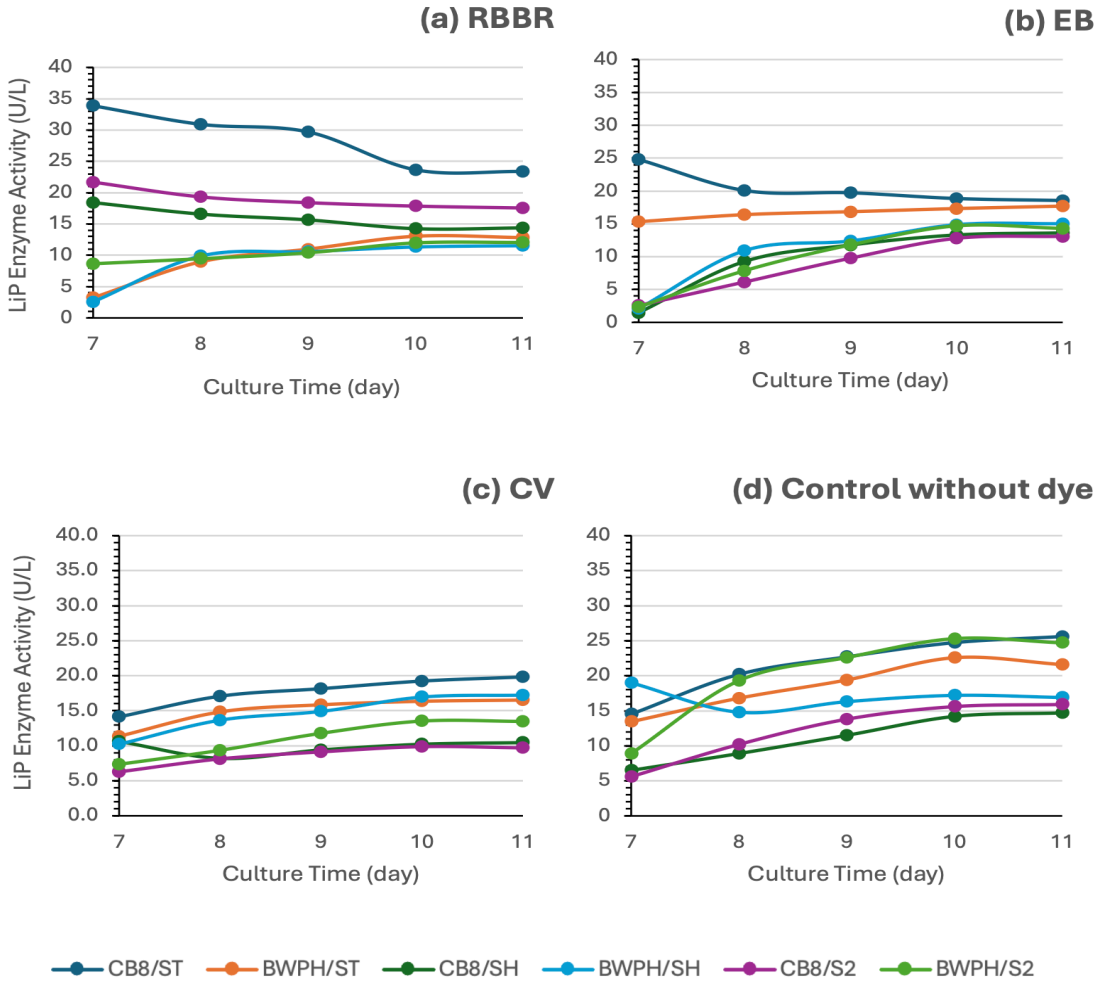

Figure 35. Lignin Peroxidase (LiP) enzyme activity detected in static, shaking and sponge immobilized cultures of *T. versicolor* (CB8) and *P. ostreatus* (BWPH) during 5 days incubation with dye (a) Remazol Brilliant Blue R (b) Evans Blue (c) Crystal Violet and (d) fungal control without dye

Crystal Violet, a triphenylmethane dye, elicited a prolonged and progressively escalating LiP response (Figure 35(c)). Crystal Violet (CV) induced a progressive enhancement of LiP activity in both fungi, especially under static conditions, suggesting that LiP production is predominantly linked to detoxification rather than direct substrate resemblance to lignin. CV is a hazardous triphenylmethane dye, and the increasing LiP activity indicates the activation of fungal defense mechanisms in reaction to chemical stress. *T. versicolor* exhibited elevated LiP levels during static cultivation, but *P. ostreatus* demonstrated greater efficiency under shaking

and sponge-immobilized conditions, indicating species-specific tolerance and metabolic strategies. The diminished LiP activity in certain immobilized CB8 cultures may be attributed to the partial adsorption of CV into the sponge matrix, which decreases the effective interaction between the dye and the enzyme. The treatments yielding the highest enzyme production-specifically CB8/ST, BWPH/ST, and BWPH/SH-were associated with the most effective dye removal efficiency (Figure 27(c)). This affirms that LiP significantly contributes to the degradation of complex aromatic dyes, with fungal physiology and cultivation technique directly affecting biodegradation efficiency.

To conclude this section, it was important to elucidate the contribution of extracellular ligninolytic enzymes to the decolorization of structurally diverse dyes (including anthraquinone, azo, and triphenylmethane classes), statistical analyses were conducted to determine the significance of each enzyme and to assess the correlation between enzyme activities and the observed decolorization percentages under static, shaking, and sponge-immobilized fungal biomass conditions. Shapiro-Wilk normality testing indicated non-normal distribution of laccase activity and RBBR dye decolorization percentage ($p < 0.05$). Therefore, Spearman's rank correlation was used to evaluate the association between enzyme activities and RBBR dye decolorization. Spearman correlation analysis revealed a strong positive association between laccase activity and RBBR dye decolorization ($\rho = 0.771$, $p = 0.072$), as well as between MnP activity and decolorization ($\rho = 0.771$, $p = 0.072$) (Appendices Table A2). In contrast, LiP activity showed a negligible correlation with dye removal efficiency ($\rho = 0.086$, $p = 0.872$). A significant positive correlation was observed between laccase and MnP activities ($\rho = 0.89$, $p < 0.05$), suggesting coordinated enzyme expression during dye degradation. Although correlations with decolorization did not reach statistical significance, likely due to the small sample size ($n = 6$), the observed trends indicate the predominant involvement of laccase and MnP in RBBR degradation. Machado et al. [217] evaluated extracellular extracts of 35 selected fungi grown on solid medium with sugar cane bagasse for RBBR decolorization and experimental analysis proved that RBBR decolorization was not directly correlated with laccase or MnP activities, as several fungi achieved high decolorization despite low or absent of MnP production, while others with strong ligninolytic enzyme activity showed limited decolorization.

The Spearman correlation analysis between enzyme activities and EB dye decolorization revealed that Laccase exhibited a moderate positive association with decolorization ($\rho = 0.667$), indicating that higher Laccase activity tends to enhance dye removal (Appendices Table A3). However, this correlation was not statistically significant ($p = 0.148$), likely due to the small sample size and variability in the data. MnP showed a weak positive correlation with decolorization ($\rho = 0.232$; $p = 0.658$), suggesting minimal influence on dye removal, while LiP displayed a moderate negative correlation ($\rho = -0.551$; $p = 0.257$), indicating that higher LiP activity may be associated with slightly lower decolorization, though this was also not significant. The overall Spearman correlation matrix showed similar trends, with Laccase and MnP positively correlated ($\rho = 0.657$) and Laccase and LiP negatively correlated ($\rho = -0.543$). The Shapiro-Wilk normality test indicated that all enzyme activities and decolorization percentages did not significantly deviate from normality, except Laccase, which was borderline

($p = 0.051$). These findings suggest that among the enzymes studied, Laccase may play the most influential role in dye decolorization, but the lack of statistically significant correlations emphasizes that conclusions are limited by the small dataset and potential experimental variability. Overall, the results support using non-parametric methods, such as Spearman correlation, for analysing these relationships.

The Spearman correlation analysis indicates that none of the individual enzymes (Laccase, MnP, or LiP), show a statistically significant relationship with CV dye decolorization, with correlation coefficients ranging from weakly negative (LiP, $\rho = -0.257$) to very weakly positive (Laccase $\rho = 0.143$; MnP $\rho = 0.029$) and all p-values well above 0.05 (Appendices Table A4). Examining the full correlation matrix reveals a strong positive correlation between Laccase and MnP ($\rho = 0.886$, $p = 0.019$), suggesting that these two enzymes tend to increase together, while both show moderate negative correlations with LiP ($\rho = -0.6$), though these are not statistically significant. Decolorization, however, does not exhibit any significant correlation with any of the enzymes, consistent with the individual enzyme analysis. The Shapiro-Wilk normality test shows that all variables-Laccase, MnP, LiP, and decolorization-have p-values greater than 0.05, indicating no strong evidence of deviation from normality.

Overall, these results suggest that despite the widespread acknowledgment of extracellular ligninolytic enzymes, such as laccase and manganese peroxidase (MnP), as pivotal catalysts in the oxidation and degradation of intricate synthetic dyes, their activity alone frequently proves inadequate for accurately predicting decolorization efficiency in complex biological systems. White-rot fungi demonstrate considerable variability in enzyme synthesis and dye degradation potential, influenced by species, dye composition, and environmental conditions; elevated enzyme concentrations may not necessarily correlate with optimal decolorization rates. Research indicates that many strains may utilize either laccase or manganese peroxidase, or mixtures thereof, to decolorize specific dyes, with the significance of a particular enzyme varying among dyes and organisms, lacking a definitive universal pattern [218,219].

Furthermore, extracellular enzyme activity assessed in culture supernatants represent just a fraction of the possible elimination pathways. Non-enzymatic and biomass-related processes-such as biosorption, cell surface interactions, dye absorption by mycelium, and the activity of other intracellular or cell-associated oxidative/reductive enzymes have been demonstrated to significantly enhance overall decolorization. For example, fungal biomass can directly adsorb dyes, contributing substantially to elimination in the absence of elevated extracellular enzyme activity [100]. Intracellular enzymes, including azoreductases, tyrosinases, and other oxidoreductases, may metabolize dyes post-uptake, particularly for azo and heterocyclic compounds where external oxidative enzymes exhibit diminished efficacy [220].

It is increasingly acknowledged that mediator compounds, radicals, and other auxiliary factors-including hydrogen peroxide essential for peroxidase activity, redox mediators facilitating electron transfer between enzymes and dye molecules, or the presence of metal ions-can significantly affect the catalytic efficacy of laccases and peroxidases. These parameters are

frequently overlooked by basic extracellular enzyme assays yet can substantially facilitate or impede decolorization in actual systems [221,222].

This intricacy underscores the need for systems-level techniques, including transcriptome and proteomic investigations, to elucidate the molecular pathways involved in dye decolorization. Transcriptomic profiling elucidates comprehensive gene expression alterations prompted by dye exposure, uncovering regulatory networks linked to xenobiotic metabolism, oxidative stress response, intracellular redox equilibrium, and transport mechanisms that are not just represented by extra-cellular enzyme assays. Additionally, proteomic investigations delineate the functional protein landscape, encompassing transporters, regulatory proteins, and post-translational changes that directly regulate dye uptake, transformation, and detoxification. The integration of transcriptomic and proteomic data facilitates a mechanistic and predictive comprehension of dye-microorganism interactions, considering biological regulation, dye structural complexity, and process-specific conditions, thereby establishing a solid basis for the rational optimization of fungal-based dye remediation systems.

5.6 Transcriptome Analysis of CB8 strain

5.6.1 Sequencing Quality Assessment and Data preprocessing

In this study, *T. versicolor* (CB8 strain) whole transcriptome sequencing was performed in order to examine the differentially expressed genes (DEG) profiles, and to perform gene annotation (GO) on set of useful genes based on gene ontology pathway information. The aim was to look for differentially expressed genes which may be not studied and corelated well with dye decolorization by white-rot fungi. In depth gene level study is merely available for azo, anthraquinone and triphenylmethane dye decolorization by *T. versicolor*. Nonetheless, transcriptome profiling that encompasses extensive gene expression alterations in reaction to dye exposure is still constrained. Such investigations are essential for elucidating the regulatory networks that control xenobiotic metabolism, oxidative stress response, intracellular redox equilibrium, and transport mechanisms-processes [223]. Consequently, DEG identification using transcriptomics is crucial for elucidating the molecular mechanisms of dye decolorization and for identifying new candidate genes for subsequent functional investigations. This study presents a novel and comprehensive transcriptomic investigation of white-rot fungal responses to RBBR and EB dye, with a particular focus on intracellular xenobiotic degradation and detoxification pathways rather than solely on extracellular ligninolytic enzymes. To the best of our knowledge, no previous report has described an in-depth transcriptomic analysis of RBBR and EB dye degradation by white-rot fungi, highlighting the originality and scientific significance of this research.

Analyses were successfully performed on all 9 paired-ends samples. The raw sequencing output from all nine samples demonstrated consistently high data quality and uniform yield, confirming the technical robustness of the experiment (Appendices Table A5). Figure A2 (Appendices) shows the throughput of raw data and trimmed data. A total of approximately 41-43 million reads per sample were generated, corresponding to roughly 6.2-6.5 Giga base pairs (Gbp) of sequence, except for sample 9CB8EB which yielded a slightly lower but

sufficient 37.9 million reads (~5.7 Gbp). All libraries exhibited stable GC content averaging 60.3%, which is consistent with the expected genomic composition of the studied organism.

The Phred assigns a Q score of 30 (Q30) to a base, this is equivalent to the probability of an incorrect base call 1 in 1000 times. This means that the base call accuracy (i.e., the probability of a correct base call) is 99.9%. When sequencing quality reaches Q30, virtually all the reads will be perfect, having zero errors and ambiguities. This is why Q30 is considered a benchmark for quality in next-generation sequencing. Whereas a lower base call accuracy of 99% (Q20) will have an incorrect base call probability of 1 in 100, meaning that every 100 bp sequencing read will likely contain an error. In our study, read quality metrics were excellent across the board: Q20 scores ranged from 97.84% to 98.66%, and Q30 scores, reflecting bases with an error probability ≤ 0%, were consistently high (94.36-96.05%). Critically, no systematic differences in sequencing depth or quality were observed between the control (CB8CONT), RBBR-treated (CB8RBBR), and EB-treated (CB8EB) groups, indicating that the experimental treatments did not introduce technical bias or degrade library integrity. This high-quality, uniform dataset provides a reliable foundation for subsequent bioinformatic analyses, including read alignment, transcript quantification, and differential expression testing. Figure 36 shows the Q30 percentage (% of bases with quality over Phred score 30) of each sample's raw and trimmed data.

Trimmomatic program was used to remove adapter sequences and bases with base quality lower than three from the ends. Also using sliding window method, bases of reads that does not qualify for window size 4, and mean quality 15 are trimmed. Afterwards, reads with length shorter than 36bp are dropped to produce trimmed data. The details of trimmed data have been presented in Figure 36 and Table 8.

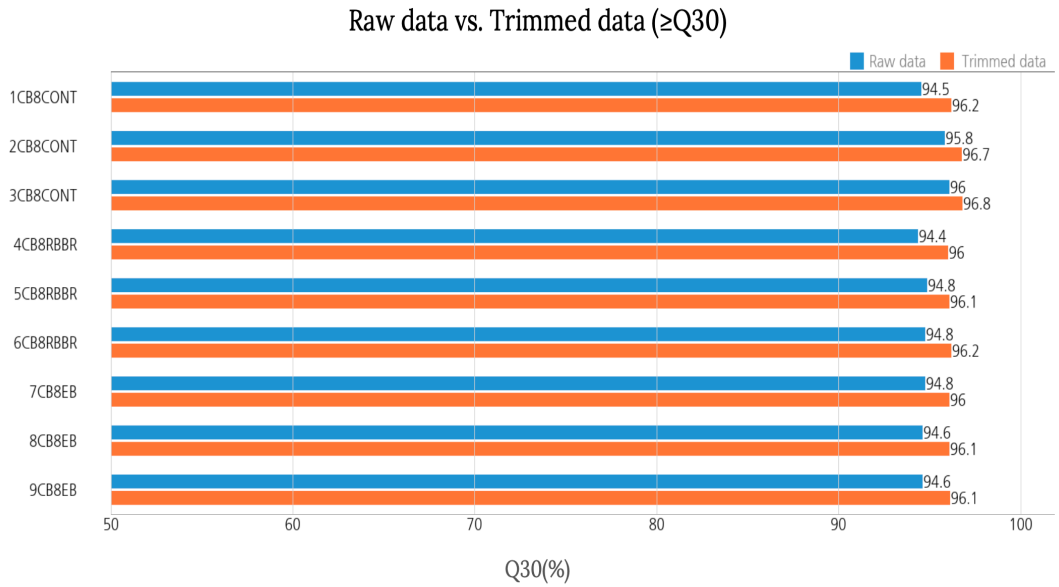

Figure 36. Q30 score of Raw and Trimmed data for control and dye treated samples of *T. versicolor*

Table 8. Trimming data statistics summary of read count and quality scores for control and dye treated samples of *T. versicolor*

Index	Sample ID	Total read bases	Total reads	GC (%)	Q20 (%)	Q30 (%)
1	1CB8CONT	5,898,357,098	41,219,506	60.41	98.84	96.17
2	2CB8CONT	5,935,248,501	40,769,878	60.31	99.06	96.74
3	3CB8CONT	6,010,321,800	40,831,744	60.58	99.07	96.77
4	4CB8RBBR	5,915,920,061	41,384,748	60.50	98.78	96.00
5	5CB8RBBR	6,061,859,603	41,164,618	60.82	98.80	96.06
6	6CB8RBBR	6,134,700,526	42,352,080	60.55	98.84	96.17
7	7CB8EB	5,962,591,307	40,735,504	60.59	98.80	96.05
8	8CB8EB	5,890,890,250	40,468,020	60.57	98.80	96.07
9	9CB8EB	5,388,968,120	37,514,040	60.76	98.82	96.12

(Note: Total read bases: Total number of read bases after trimming;
Total reads: Total number of reads after trimming;
GC (%): GC Content;
Q20 (%): Ratio of bases that have Phred quality score greater than or equal to 20;
Q30 (%): Ratio of bases that have Phred quality score greater than or equal to 30)

5.6.2 Read Mapping and Transcript Expression Profiling

Next step was to map trimmed reads with reference genome with HISAT2. HISAT2 is a fast and sensitive alignment program for mapping next-generation sequencing reads (both DNA and RNA) to a population of genomes as well as to a single reference genome. In order to map cDNA fragments obtained from RNA sequencing, *T. versicolor* GCF_000271585 was obtained from National Centre for Biotechnology Information (NCBI) and used as a reference genome. Table 9 shows the statistic obtained from HISAT2, which is known to handle spliced read mapping through Bowtie2 aligner. The table clearly showing information about the number and percentage of mapped reads and unmapped reads out of the total processed reads. Figure 37 shows the overall read mapping ratio, the ratio of mapped reads to trimmed reads. It illustrates the efficiency of trimmed RNA-seq reads aligning to the *T. versicolor* reference genome via HISAT2. The "overall read mapping ratio" denotes the proportion of reads that successfully mapped from the total high-quality (trimmed) reads preserved post-preprocessing. The bar plot illustrates mapping rates for nine samples under various experimental settings (CB8CONT, CB8RBBR, and CBEB). All samples exhibit a comparable mapping range of

approximately 44-49%, with the highest mapping ratio at 49.6% (3CB8CONT) and the lowest at 44.7% (4CB8RBBR). Approximately fifty percent of the sequenced reads matched either singularly or in a multi-mapped manner to the reference genome.

In fungal transcriptomics, particularly for non-model species such as *T. versicolor*, mapping rates often range from 40% to 60% due to reasons such as fungal genomes frequently exhibit partial or fragmented assemblies, numerous transcripts may remain unannotated or may originate from alternatively spliced variants absent in the reference. Environmental or dye-induced factors may activate the expression of secondary metabolism or stress-response genes that are either absent or minimally represented in the genome. The Figure 37 demonstrates that all samples attained consistent and satisfactory mapping ratios, signifying high-quality trimming and effective alignment appropriate for subsequent studies, including differential gene expression (DEG), GO enrichment, and pathway analysis.

Table 9. Mapped data statistics summary of control and dye treated samples of *T. versicolor*

Sample ID	Number of processed reads	Number of mapped reads (%)	Number of unmapped reads (%)
1CB8CONT	41,219,506	18,554,742 (45.01%)	22,664,764 (54.99%)
2CB8CONT	40,769,878	18,364,607 (45.04%)	22,405,271 (54.96%)
3CB8CONT	40,831,744	20,234,454 (49.56%)	20,597,290 (50.44%)
4CB8RBBR	41,384,748	18,485,764 (44.67%)	22,898,984 (55.33%)
5CB8RBBR	41,164,618	18,932,039 (45.99%)	22,232,579 (54.01%)
6CB8RBBR	42,352,080	19,642,218 (46.38%)	22,709,862 (53.62%)
7CB8EB	40,735,504	18,664,150 (45.82%)	22,071,354 (54.18%)
8CB8EB	40,468,020	18,421,246 (45.52%)	22,046,774 (54.48%)
9CB8EB	37,514,040	17,364,600 (46.29%)	20,149,440 (53.71%)

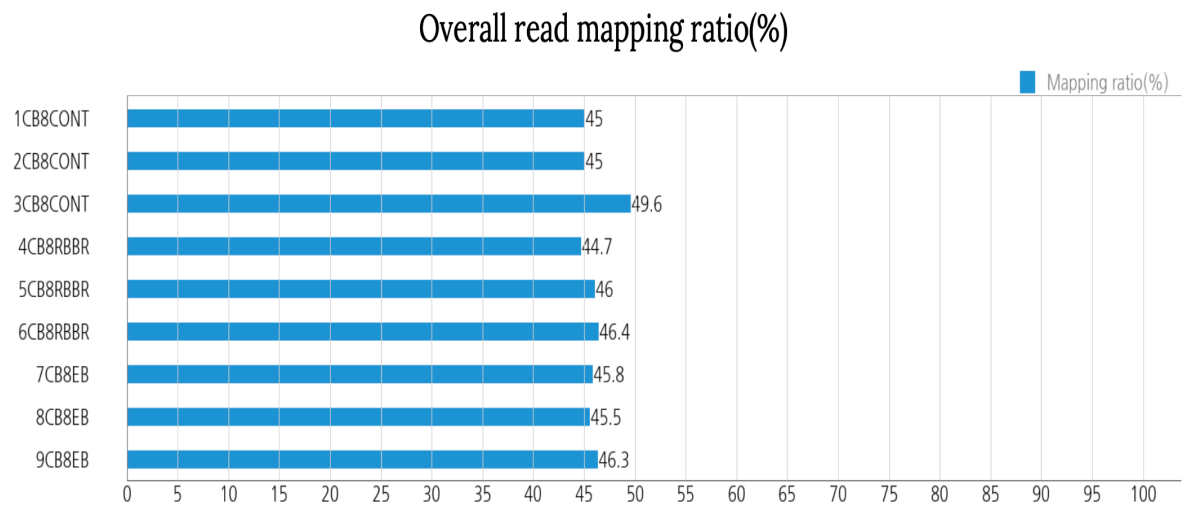

Figure 37. Overall read mapping ratio (%) of control and dye treated samples of *T. versicolor*

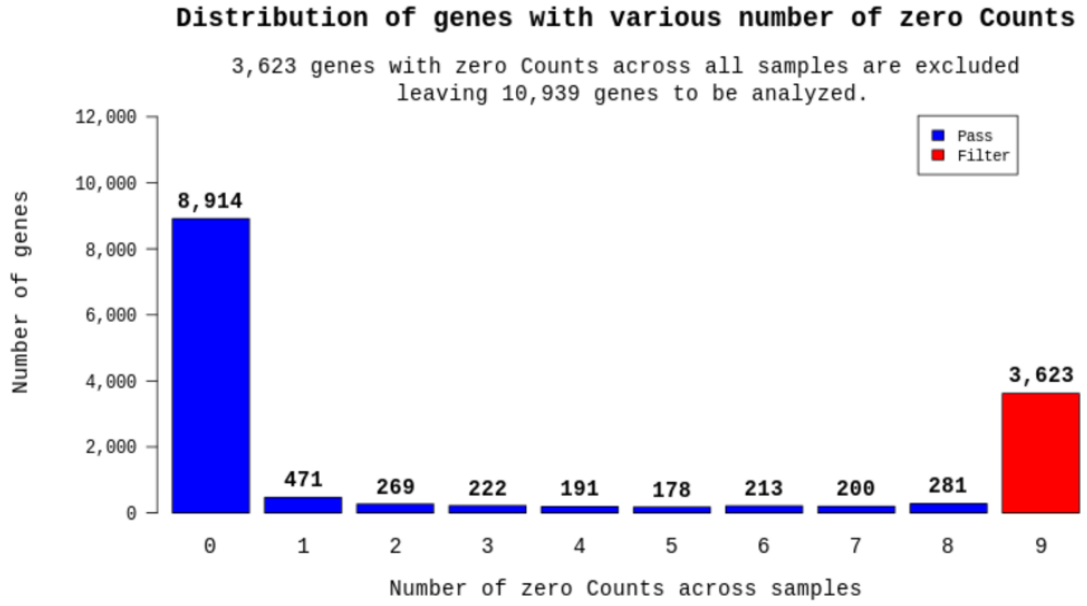

Figure 38. Distribution of genes with zero counts in control and dye treated samples of *T. versicolor*

After the read mapping, known genes and transcripts were assembled with StringTie based on reference genome model. StringTie is a widely used, highly efficient computational tool for transcript assembly from RNA-Seq data, assembling short reads into full-length transcripts using a network flow algorithm to reconstruct complex gene structures and quantify expression. After assembly, the abundance of gene/transcript is calculated in the read count and normalized values as FPKM (Fragments Per Kilobase of transcript per Million mapped reads) and TPM (Transcripts Per Kilobase Million) for a sample. Transcript Expression profile and gene

expression profile was calculated for each sample as a transcript/gene as read count, FPKM (Fragment per Kilobase of transcript per Million mapped reads) and TPM (Transcripts Per Kilobase Million). Transcript Expression profile check the entire set of RNA molecules (transcripts) present in a cell at a specific time, including messenger RNA (mRNA), non-coding RNA (ncRNA), microRNA (miRNA), etc. whereas gene expression profile typically focuses on the abundance of messenger RNA (mRNA) levels, as mRNA carries the code for protein synthesis.

After initial preprocessing, genes that exhibited no detectable expression across the dataset were removed to sorts differentially expressed gene among samples by read count value of known genes. Figure 38 represents distribution of genes with zero counts in control and dye treated samples of *T. versicolor*. Specifically, 3 623 genes showed zero read counts in all samples, indicating that no sequencing reads were mapped to these genes under any experimental condition. Genes with zero counts provide no information for downstream statistical analyses because they lack measurable variation and cannot contribute to estimates of expression differences or model dispersion. Retaining such genes would increase the multiple-testing burden and introduce unnecessary noise. Therefore, these genes were excluded, leaving 10 939 expressed genes for subsequent analysis.

5.6.3 Differential Gene Expression and Visualization

In order to reduce systematic bias, size factors were estimated from the read count data (estimate Size Factors method). Using them, the read count data was normalized with Relative Log Expression (RLE) method in DESeq2 R library. Then, statistical test was performed with the normalized data. log2(read count+1) and regularized log (rlog) transformed values were used for data visualization. rlog transformation is a method to minimize differences between samples for genes/transcripts in low expression. It transforms count data into log2 scale and normalizes them with a library size factor. rlog is robust in the case when the size factors vary widely. These logarithm figures were used only for visualization. To proceed a statistical test, RLE normalized count was adopted for negative binomial Wald Test (nbinomWaldTest) in DESeq2.

DEGs analysis was performed on 2 comparisons pairs using DESeq2, the one pair was CB8RBBR Vs CB8CONT and the second pair was CB8EB Vs CB8CONT. Initially, one criteria was applied as fold change value should be equal to or greater than two (|fc|>=2). As seen in below Figure 39(a), 2 455 genes were up/down regulated in CB8RBBR vs CB8CONT while 3 201 genes were up/down regulated in CB8EB vs CB8CONT. While applying stringent criteria of fold change value equal or greater than two (|fc|>=2) and nbinomWaldTest raw p-value <0.05 conditions in at least one of comparison pairs, the results showed 2 395 genes which satisfied criteria as seen in Figure 39(b). CB8RBBR vs CB8CONT showed 1 106 genes to be differentially expressed while CB8EB vs CB8CONT showed 1 830 genes to be differentially expressed. There were 318 genes which significantly up regulated during RBBR dye degradation by *T. versicolor* (CB8) fungi and high proportion of genes were down regulated in this condition. Similary during EB dye degradation, majority of genes were downregulated in dye treating condition of fungi.

The volcano plot (Figure 40(a) and (b)) indicates differential gene expression in the fungal strain CB8 between a control sample (CB8CONT) and the one subjected to dye RBBR and EB dye degradation respectively by *T. versicolor*. The graphic integrates fold change (effect size) with statistical significance to emphasize genes that are differentially expressed as a result of dye exposure, potentially activating stress responses, detoxification pathways, or degradation mechanisms in white-rot fungus such as *T. versicolor*. The differential gene expression profiles of *T. versicolor* (strain CB8) in response to Evans Blue (EB) and Remazol Brilliant Blue R (RBBR) dyes, illustrated in the corresponding volcano plots, demonstrate distinct transcriptional responses likely influenced by the chemical structures of the dyes-azo for EB and anthraquinone for RBBR. In the EB-treated samples (CB8EB vs. CB8CONT), the graph demonstrates a marked asymmetry favouring upregulation, characterized by a dense aggregation of orange points that signify significantly upregulated genes ($\log_2$ fold change > 1, raw $p < 0.05$) achieving substantial statistical significance ($-\log_{10}$ p-value up to 7.5) and considerable positive fold changes (up to +15), indicating a strong activation of adaptive pathways, including those related to ligninolytic enzymes for dye degradation. In contrast, downregulated genes (blue dots) are fewer and less significant ($-\log_{10}$ p-value up to around 5.5), indicating a more moderate repression of non-essential activities. Conversely, the RBBR-treated samples (CB8RBBR vs. CB8CONT) exhibit a pronounced tendency toward downregulation, characterized by a significant cluster of blue points with elevated significance ($-\log_{10}$ p-value reaching 8) and substantial negative fold changes (as low as -15), signifying enhanced stress-induced repression of metabolic or growth-related genes to alleviate toxicity. The upregulated genes in the RBBR plot are less abundant and less prominent, with fold changes often below +10, indicating a more defensive reaction rather than an offensive one. The distinctions highlight dye-specific bioremediation strategies in *T. versicolor*, where EB induces targeted enzyme activation for effective azo dye degradation, whereas RBBR exerts wider inhibitory effects, likely due to its resistant anthraquinone structure, guiding enhanced fungal applications in wastewater treatment.

Figure 40(c) and (d) illustrates the difference in gene expression levels between RBBR-treated samples (CB8RBBR) or EB-treated samples (CB8EB) and the untreated control (CB8CONT). The histogram depicts the distribution of genes across various $\log_2$ expression intervals, facilitating the evaluation of overall changes in transcriptional activity resulting from RBBR or EB exposure. In both scenarios, most genes are situated within the mid-range expression bins (4-6, 6-8, and 8-10), illustrating the standard unimodal distribution seen in normalized RNA-seq datasets. Significant disparities arise when contrasting the height of the bars between the two samples.

CB8CONT exhibits a greater frequency of genes than the RBBR or EB within high expression bins (6-8 and 8-10). But in moderate levels, dye treated samples show enhancement of transcriptional activity for a significant number of genes. The marginal decrease in the prevalence of low-expression genes (0-2 and 2-4 bins) in dye treated samples compared to CB8CONT further corroborates a transition towards elevated expression levels during dye-induced stress. The observed results indicate that the fungal system engages a wide array of

metabolic, detoxifying, oxidative stress, and ligninolytic pathways in reaction to RBBR and EB, leading to a comprehensive elevation of the transcriptome.

(a) (b)

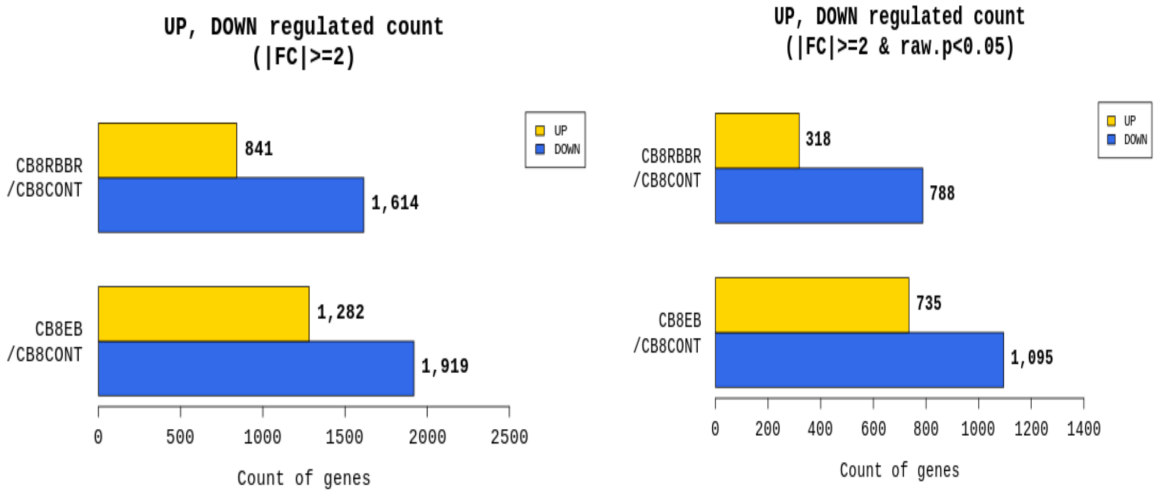

Figure 39. Up and down regulated genes based on (a) fold change and (b) fold change and p-value of comparison pair of control versus dye treated samples of *T. versicolor*

(a)

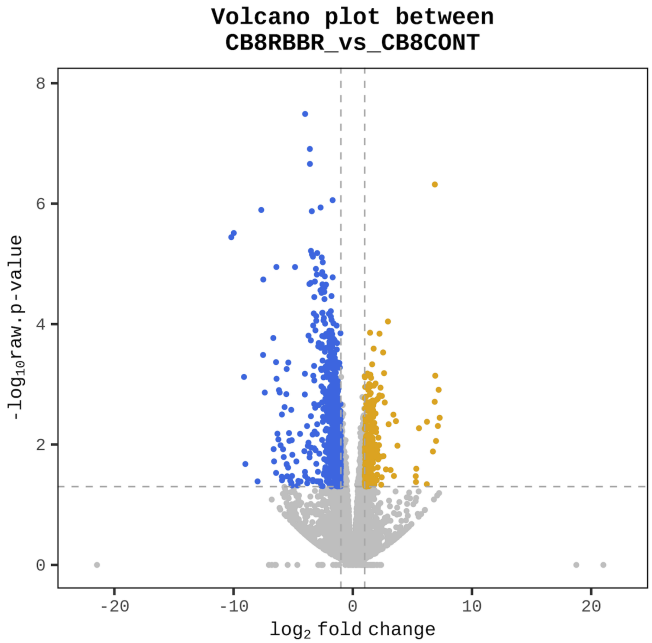

(b)

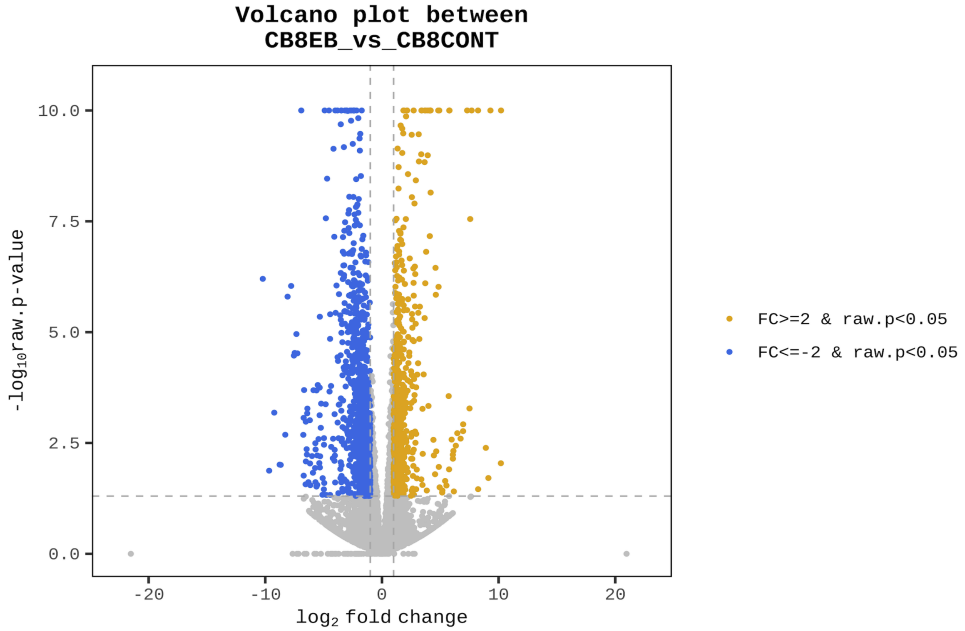
Volcano plot between
CB8EB_vs_CB8CONT
10.0
7.5
5.0
2.5
0.0
-log10raw.p-value
-20
-10
0
10
20
log2 fold change
FC>=2 & raw.p<0.05
FC<=-2 & raw.p<0.05

(c)

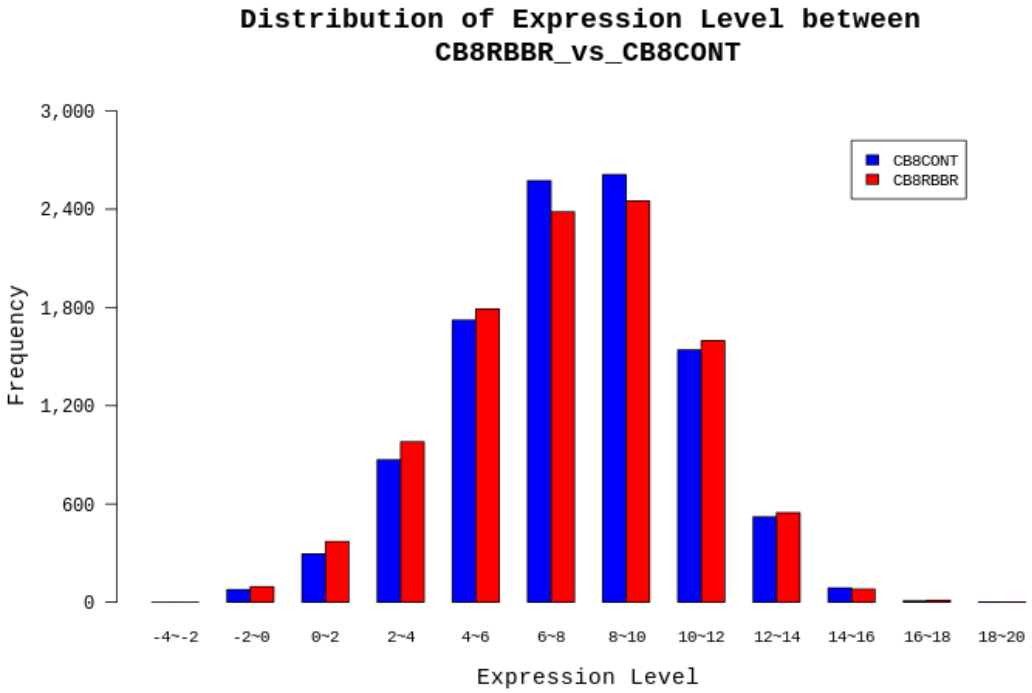
Distribution of Expression Level between
CB8RBBR_vs_CB8CONT
3,000
2,400
1,800
1,200
600
0
Frequency
CB8CONT
CB8RBBR
-4~-2
-2~0
0~2
2~4
4~6
6~8
8~10
10~12
12~14
14~16
16~18
18~20
Expression Level

(d)

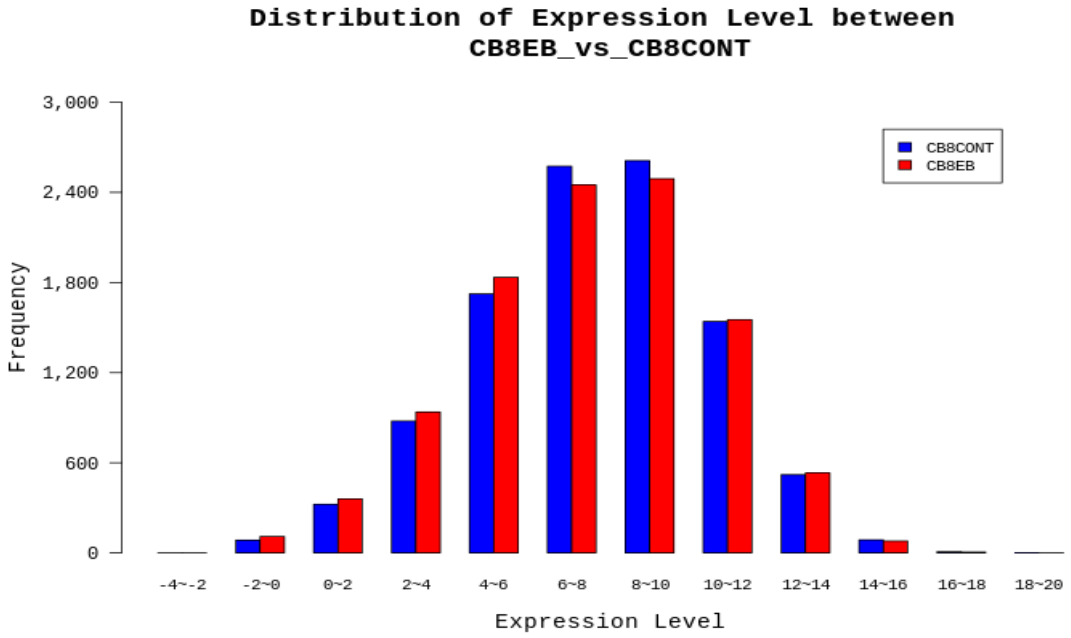

Figure 40. Volcano plot (a,b) and distribution of expression level (c,d) between comparison pair of control versus dye treated samples of *T. versicolor*

For further organization of genes and samples into related groups, a two-way hierarchical clustering heatmap (Figure 41) was derived from Z-score-scaled, log2-normalized expression values for the 2,395 differentially expressed genes (DEGs) found in *T. versicolor* under control (CB8CONT) and dye-exposed (CB8RBBR and CB8EB) conditions along with their replicates. Z-score transformation standardizes gene expression across samples, facilitating direct comparison of relative upregulation and downregulation irrespective of baseline expression levels. The color gradient from blue (indicating low relative expression) to yellow (indicating high relative expression) represents normalized deviations from the mean expression profile of each gene.

Hierarchical clustering of genes (rows) and samples (columns) uncovers distinct transcriptional modules specific to each experimental condition. The sample dendrogram illustrates distinct separation of CB8RBBR and CB8EB treatments from CB8CONT, indicating that dye exposure induces significant alterations in global transcriptional activity. Moreover, CB8RBBR and CB8EB constitute largely separate subclusters, suggesting that while both dyes elicit xenobiotic stress responses, they also activate dye-specific regulatory mechanisms. The gene dendrogram delineates clusters of co-expressed genes, many of which exhibit pronounced coordinated induction (yellow blocks) or repression (blue blocks) exclusively in RBBR- or EB-treated samples. These clusters likely represent functional groups associated with oxidative degradation, ligninolytic enzyme production, membrane transport, detoxifying mechanisms, or stress-response signalling, all of which are triggered during the fungal breakdown of resistant dyes.

The heatmap presented in Figure 41 elucidates the extent and organization of transcriptional reprogramming in *T. versicolor* in reaction to synthetic dyes, demonstrating that dye degradation is associated with meticulously regulated, condition-specific alterations in gene expression. This clustering methodology facilitates future pathway-level interpretation and functional annotation of the differentially expressed gene sets.

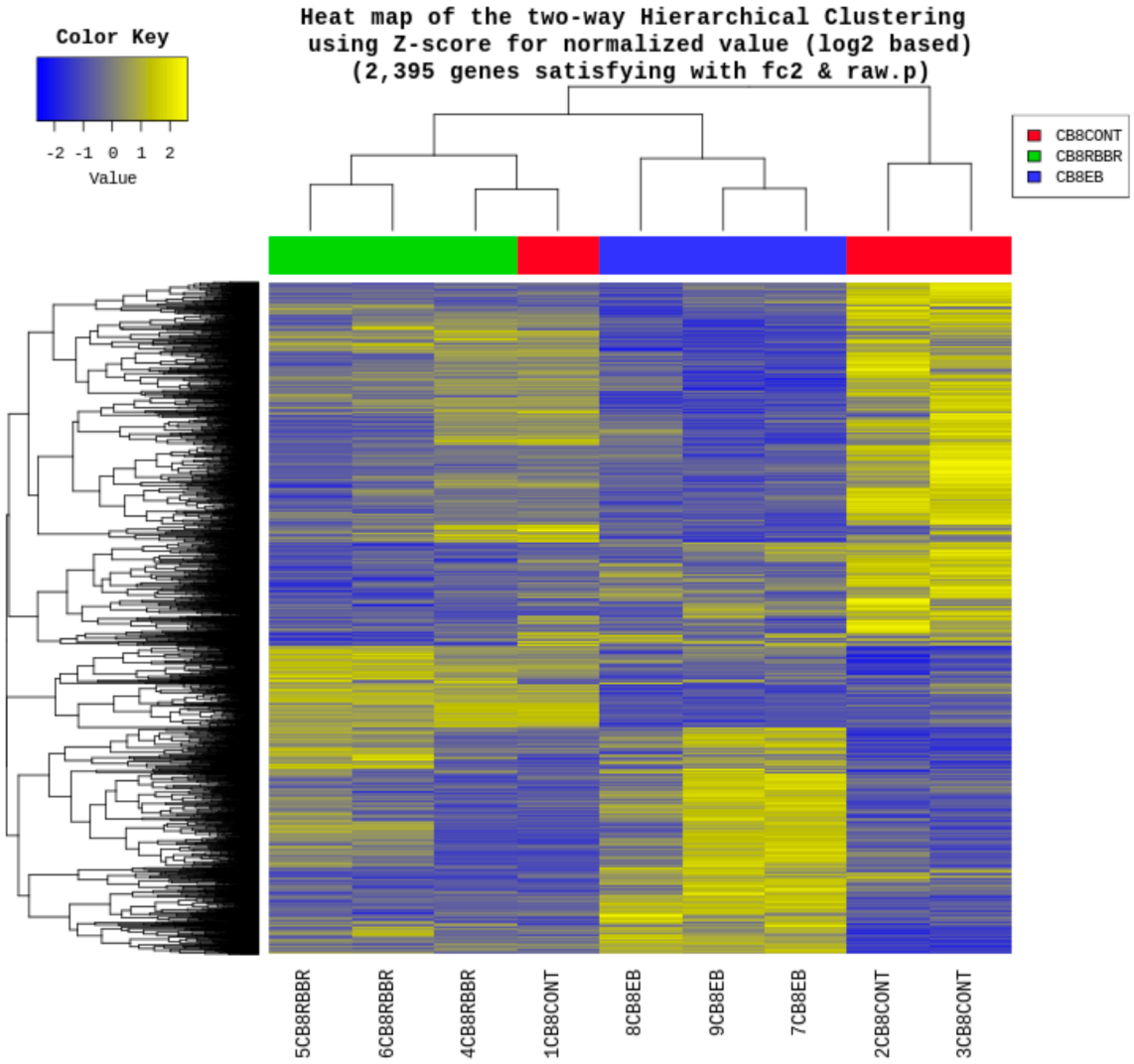

Figure 41. Heatmap of Differentially Expressed Genes (DEGs) in *T. versicolor* grown in optimized condition (CB8CONT) versus *T. versicolor* utilized for Remazol Brilliant Blue R (CB8RBBR) and Evans Blue (CB8EB) dye degradation

5.6.4 Functional Annotation and Enrichment Analysis

I. GO Enrichment Analysis for CB8RBBR-CB8CONT DEGs

Based on the list of differentially expressed genes, Gene ontology (GO) by functional orthologs was performed which resulted in GO annotations, clusters of orthologues genes (COG) classes, Kyoto Encyclopedia of Genes and Genomes orthology (KEGG-KO) for differentially

expressed genes of *T. versicolor* (CB8) utilized for Remazol Brilliant Blue R (RBBR) dye-degrading conditions compared to control cultures. Subsequently, top DEGs which were highly up and down regulated were selected further for detailed analysis of Gene Ontology Enrichment analysis. They were divided into three Enrichment categories such as Molecular Functions (MF), Biological Process (BP) and Cellular Components (CC) based on the selection of most suitable GO accession number for each gene. Table 10 represents top significantly up and down regulated genes, their protein ID, putative functions, COG function class, most suitable GO ID, GO description and fold change value.

Table 10. GO Enrichment, COG classification along with Fold change for differentially regulated genes during Remazol Brilliant Blue R dye degradation by *T. versicolor* versus control sample

Gene Ontology (GO) Enrichment category- Molecular Functions (MF)					
Protein ID	**Putative function**	**COG cate-gory**	**GO Description**	**GO ID**	**Fold Change**
39887	cytochrome P450	IQ	monooxygenase activity	4497	147.4
35158	Aldo keto reductase	C	Catalytic activity	3824	126.3
44572	D-lactaldehyde dehydrogenase	V	lactaldehyde dehydrogenase (NAD+) activity	8911	118
35161	DAHP synthetase	E	3-deoxy-7-phosphoheptulonate synthase activity	3849	117.2
36761	Belongs to NADPH quinone reductase and related Zn-dependent oxidoreductases	C	aldehyde dehydrogenase (NAD+) activity	4029	105.6
32836	D-isomer specific 2-hydroxyacid dehydrogenase	E	oxidoreductase activity	16616	74.6
37745	ARM repeat-containing protein	C	Catalytic activity	3824	38.8
41051	Glutathione S-transferase, C-terminal domain	O	transcription coregulator activity	3712	13.4
39257	Alcohol dehydrogenase GroES-like domain	C	alcohol dehydrogenase (NAD+) activity	4022	9
42209	3' exoribonuclease family, domain 1	J	3'-5'-RNA exonuclease activity	0175	4.0
34024	oxidoreductase	C	Catalytic activity	3824	4.0

38976	3,4-dihydroxy-2-butanone 4-phosphate synthase	H	Catalytic activity	3824	3.6
41123	S-adenosyl-L-methionine-dependent methyltransferase	Q	Catalytic activity	3824	3.3
40129	Nuclear pore complex scaffold, nucleoporins 186/192/205	S	structural molecule activity	5198	3.2
39879	Fatty acid hydroxylase superfamily	I	Catalytic activity	3824	3.2
34426	Iron hydrogenase	Y	Catalytic activity	3824	3
32719	Belongs to the mitochondrial carrier (TC 2.A.29) family	C	transporter activity	5215	3
32504	Cysteine proteinase	O	Catalytic activity	3824	3.0
32328	Udp-glucose 4-epimerase	M	Catalytic activity	3824	2.9
33116	mitochondrial Lipoyl synthase	H	Catalytic activity	3824	2.8
36733	MFS general substrate transporter	U	transporter activity	5215	2.8
42056	Manganese peroxidase isozyme MP2	T	Mn-dependent (NADH-oxidizing) peroxidase activity	16689	-2.1
44196	Lignin peroxidase	T	Diarylpropane peroxidase activity	16690	-2.1
32737	Laccase I	Q	Oxidoreductase activity	16682	-2.5
42420	DNA mismatch repair	L	nucleotide binding	0166	-4.9
41469	catalase	P	Catalytic activity	3824	-5.0
32773	Fungal specific transcription factor domain	K	transcription regulatory region nucleic acid binding	1067	-5.5
37827	Kinesin-domain-containing protein	Z	cytoskeletal motor activity	3774	-5.9
35701	Kinesin-domain-containing protein	Z	cytoskeletal motor activity	3774	-5.9
31813	Serine hydrolase involved in the detoxification of formaldehyde	S	Catalytic activity	3824	-5.9
36856	glutamate decarboxylase	E	Catalytic activity	3824	-10.8
33141	alpha-galactosidase	G	Catalytic activity	3824	-15.9
35886	GTP-binding protein	U	nucleotide binding	0166	-21.4
43999	Glycosyl hydrolase family 45	G	Catalytic activity	3824	-23.7

35299	arginyltransferase	O	Catalytic activity	3824	-62
39667	RF-1 domain	J	nucleic acid binding	3676	-84.3

Gene Ontology (GO) Enrichment Category: Biological Process (BP)					
Protein ID	**Putative function**	**COG cate-gory**	**GO Description**	**GO ID**	**Fold Change**
34348	FAD-binding domain	PQ	transition metal ion transport	0041	47.0
38116	Pkinase-domain-containing protein	T	cell cycle checkpoint signaling	0075	8.0
32739	NAF1-domain-containing protein	S	small nucleolar ribonucleoprotein complex assembly	0491	3
35910	glycoside hydrolase family 5 protein	G	polysaccharide catabolic process	0272	2.8
39551	Belongs to the cyclin family	D	regulation of cyclin-dependent protein serine/threonine kinase activity	0079	-4.9
38681	Microtubule binding	Z	mitotic spindle elongation	0022	-5.5
38247	Starch binding domain	G	polysaccharide catabolic process	0272	-5.6
43477	peptidase S28	O	tRNA wobble base modification	2097	-8.0
37580	SET domain	A	tRNA wobble base modification	2097	-20.9
33088	Tubulin-tyrosine ligase family	O	microtubule cytoskeleton organization	0226	-33.6
42724	DNA polymerase X family	L	DNA synthesis involved in DNA repair	0731	-46.8
41330	EG45-like domain containing protein	S	response to hypoxia	1666	-52.8
35077	DNA photolyase	LT	photoreactive repair	0719	-254.0
38385	ubiquitin carboxyl-terminal hydrolase	O	protein deneddylation	0338	-516.6

Gene Ontology (GO) Enrichment Category: Cellular Component (CC)					
Protein ID	**Putative function**	**COG cate-gory**	**GO Description**	**GO ID**	**Fold Change**
39411	Component of ribonuclease P, a protein complex that generates mature tRNA molecules by cleaving their 5'-ends.	J	ribonuclease MRP complex	0172	74.0
36633	Sec7-like domain is implicated in guanine nucleotide exchange function	U	Golgi cis cisterna	0137	3.0
38793	TPR-like protein	K	cellular component	5575	2.9
35989	Protein of unknown function (DUF3808)	S	cellular component	5575	2.8
39984	Expressed protein	L	cellular component	5575	-4.9
42250	Histone H2A	B	nuclear chromosome	0228	-5
43374	CFEM domain	S	cellular component	5575	-5.2
35739	Histone-fold-containing protein	B	nuclear chromosome	0228	-5.4
37884	Histone-like transcription factor (CBF/NF-Y) and archaeal histone	L	cellular component	5575	-6.0
32649	Protein of unknown function DUF89	S	intracellular anatomical structure	5622	-9.4
33614	Heat shock protein 9/12	S	cellular component	5575	-10
33014	RTA1-domain-containing protein	S	fungal-type vacuole	0324	-167.0

A notable characteristic of the dataset was the significant overexpression of genes that encode oxidative enzymes, especially cytochrome P450 monooxygenase, which exhibited the largest fold change among all differentially expressed genes. The enhancement of the Gene Ontology molecular function term monooxygenase activity (GO:0004497) substantiates the role of cytochrome P450 in the preliminary oxidative attack on the anthraquinone structure of RBBR. Cytochrome P450 enzymes facilitate hydroxylation and oxygen insertion processes that destabilize aromatic dye molecules, producing reactive intermediates that are more susceptible to subsequent degradation. This discovery aligns with earlier studies on white-rot fungi, including *P. chrysosporium* and *P. ostreatus*, wherein cytochrome P450 upregulation has been

associated with the intracellular breakdown of synthetic dyes subsequent to extracellular oxidative alteration [224–226].

Concurrently with P450 induction, numerous NAD(P)H-dependent oxidoreductases and dehydrogenases were markedly increased, including aldo-keto reductase, D-lactaldehyde dehydrogenase, quinone reductase-related proteins, and alcohol dehydrogenase. These genes were enriched under the Gene Ontology terms catalytic activity (GO:0003824) and oxidoreductase activity (GO:0016616), underscoring their involvement in redox processes. Their increased fold change indicates active detoxification of aldehydes, quinones, and other hazardous intermediates produced during dye oxidation. These enzymes are recognized for their role in the reductive phase of xenobiotic metabolism, transforming reactive chemicals into less toxic and more soluble metabolites, thus avoiding intracellular harm. The analogous increase of reductases during RBBR breakdown has been recorded in many white-rot fungus, corroborating a conserved intracellular detoxification mechanism [227,228].

Genes associated with glutathione-mediated detoxification were increased, including glutathione S-transferase, signifying the conjugation of dye metabolites with glutathione as a component of Phase II detoxification. This method improves solubility and aids in the elimination of breakdown products from the cell. The synchronized increase of monooxygenases, dehydrogenases, and glutathione-dependent enzymes indicates a meticulously regulated intracellular pathway for the metabolism of dye-derived intermediates [229,230].

Genes associated with transport exhibited moderate yet considerable upregulation, encompassing key facilitator superfamily transporters and mitochondrial carrier proteins, enriched under the Gene Ontology term transporter activity (GO:0005215). These transporters presumably facilitate the absorption of dye molecules or their degradation products, as well as the excretion of hazardous metabolites. The upregulation of genes associated with transition metal ion transport indicates a heightened requirement for metal cofactors necessary for heme-containing enzymes like cytochrome P450. Similarly, Thuillier et al [230]. Observed 25-fold increase in transporters of the main facilitator superfamily (MFS) when *P. chrysosporium* cultivated in acetone extractives from oak compared to minimum media devoid of extractives. Transporter induction is a recognized characteristic of dye-degrading fungus and is essential for sustaining intracellular homeostasis following exposure to hazardous xenobiotics [231].

Metabolic reprogramming was further demonstrated by the overexpression of DAHP synthase, a crucial enzyme in the shikimate pathway that provides precursors for aromatic amino acids and secondary metabolites. The augmented expression of this gene indicates elevated production of metabolites that facilitate redox equilibrium, enzymatic activity, and stress resilience during dye degradation. The upregulation of mitochondrial enzymes, such as lipoyl

synthase, indicates an enhancement in energy metabolism to satisfy the elevated energy requirements of oxidative and reductive detoxification activities. Differential transcriptome investigations have demonstrated that central metabolism is intricately regulated by the source and origin of substrates provided to white-rot fungi [232,233].

Conversely, a significant number of genes related to cell cycle regulation, cytoskeletal architecture, and DNA metabolism were downregulated in the presence of dye-degrading conditions. Negative fold change values were noted for cyclin family proteins, kinesin motor proteins, microtubule-binding proteins, histones, and genes associated with DNA polymerase. Gene Ontology terms associated with mitotic spindle elongation, cytoskeletal motor activity, and DNA synthesis were markedly enriched among downregulated genes, signifying a suppression of growth and cell division. This inhibition signifies a purposeful redistribution of cellular resources from proliferation to survival and detoxification, a process frequently observed in fungus subjected to environmental contaminants [234,235]. Despite increasing interest in xenobiotic biodegradation, in-depth investigations into the role of cell cycle regulation during xenobiotic compound degradation remain scarce, indicating a significant knowledge gap in this area.

Transcriptomic analysis indicated the down-regulation of essential ligninolytic genes, such as laccase, manganese peroxidase, and lignin peroxidase, during the breakdown of RBBR by *T. versicolor*. In comparison with the enzyme profiling results (Figure 33(a), 34(a) and 35(a)), laccase activity was lower under RBBR decolorization conditions than in the control, which is consistent with the downregulation observed in the transcriptomic analysis. In contrast, peroxidase activity exhibited a slight increase relative to the control, suggesting post transcription modifications and more prominent role of peroxidases during RBBR degradation. Nonetheless, numerous investigations have shown that efficient dye degradation by white-rot fungi does not inherently correspond with the transcriptional activation of these enzymes. The activities of lignin peroxidase (LiP), manganese peroxidase (MnP), RBBR-oxidizing activity (RBBROx), and laccase were investigated in *Irpex lacteus* cultures by Novotný et al [236]. The presence of the dyes Methyl Red, Congo Red, Reactive Blue 19 (RBBR), and Bromophenol Blue resulted in reduced MnP and laccase activities, with the decrease being more pronounced for laccase. In contrast, studies on *Pycnoporus cinnabarinus* and *Pleurotus sajor-caju* reported enhanced extracellular laccase activity in the presence of RBBR and anthraquinone-2-sulfonic acid, respectively [237]. These findings indicate that the regulation of ligninolytic enzymes in response to dye exposure is species-specific and strongly influenced by fungal physiology and environmental conditions. Dye elimination may occur via constitutively produced enzymes, post-transcriptional regulation, or alternate oxidative mechanisms, including cytochrome P450 systems and reductive enzymes which are highly expressive in our study. Moreover, the existence of xenobiotic dyes might induce metabolic stress, resulting in the suppression of

secondary metabolism genes while stimulating detoxification and stress-response pathways [238]. The downregulation of catalase and certain heat shock proteins indicates that *T. versicolor* depends less on traditional antioxidant defence mechanisms and more on specialized enzymatic pathways directly engaged in dye processing. This adaptive method may facilitate regulated oxidative processes essential for dye breakdown while reducing nonspecific oxidative harm.

A plausible mechanism for RBBR degradation in *T. versicolor* can be hypothesized based on the observed expression patterns. Initial dye alteration likely transpires via oxidative processes facilitated by cytochrome P450 monooxygenases, potentially in concert with extracellular ligninolytic enzymes. The oxidized dye intermediates are then processed through intracellular reduction and detoxification by dehydrogenases, reductases, and glutathione-dependent enzymes. Transport proteins enable the translocation of dye molecules and metabolites across cellular membranes, while metabolic pathways are adjusted to maintain redox equilibrium and fulfil energy demands. Concurrently, growth-related processes are inhibited to preserve resources for effective xenobiotic degradation.

The transcriptional response of *T. versicolor* to RBBR exposure exhibits a coordinated and complex degradation approach that includes oxidative initiation, intracellular detoxification, transporter-mediated metabolite management, and metabolic reprogramming. These results align well with previously established methods of RBBR breakdown in white-rot fungus and further underscore the ecological and biotechnological potential of *T. versicolor* for the remediation of dye-contaminated wastewater.

II. GO Enrichment Analysis for CB8EB-CB8CONT DEGs

Transcriptomic analysis of *T. versicolor* under circumstances of Evans Blue dye degradation, in comparison to control cultures, demonstrated significant differential gene expression, reflecting a substantial metabolic and physiological alteration linked to xenobiotic stress and dye degradation. Fold change values denote the extent of transcriptional induction or repression following Evans Blue exposure, with significantly positive values signifying robust upregulation of genes associated with dye transformation and stress adaptation, whereas markedly negative values indicate repression of non-essential growth and regulatory mechanisms. The same method was applied to DEGs of CB8EB-CB8CONT and GO functional annotations by orthology analysis was done using eggnog mapper. Top significantly up and down regulated genes were selected further for detailed analysis of Gene Ontology Enrichment analysis. As previously mentioned, they were divided into MF, BP and CC Enrichment categories based on the selection of most suitable GO accession number for each gene. Table 11 represents top significantly up and down regulated genes, their protein ID, putative

functions, COG function class, most suitable GO ID, GO description and fold change value for Evans Blue dye degrading condition.

Table 11. GO Enrichment, COG classification along with Fold change for differentially regulated genes during Evans Blue dye degradation by *T. versicolor* versus control sample

Gene Ontology (GO) Enrichment category- Molecular Functions (MF)					
Protein ID	**Putative Function**	**COG Cate-gory**	**GO Description**	**GO ID**	**Fold Change**
41848	NADH dehydrogenase (ubiquinone) Fe-S protein 5	S	NADH dehydrogenase (ubiquinone) activity	08137	303.5
44572	D-lactaldehyde dehydrogenase	V	lactaldehyde dehydrogenase (NADP+)	43892	189.5
32836	D-isomer specific 2-hydroxyacid dehydrogenase	E	oxidoreductase activity	16616	181.9
31737	MFS polyamine transporter	S	transporter activity	05215	158
42059	Belongs to the tannase family	G	tannase activity	50318	124.7
35161	DAHP synthetase	E	fructose-bisphosphate aldolase activity	04332	124
39887	cytochrome P450	IQ	monooxygenase activity	04497	106.9
37962	Alpha beta-hydrolase	S	hydrolase activity	16787	88.2
36626	Indoleamine 2,3-dioxygenase	S	dioxygenase activity	51213	67.6
39053	SNARE associated Golgi protein	S	SNAP receptor activity	05484	55
40915	Lysin motif	S	chitin binding	08061	42.8
37745	ARM repeat-containing protein	C	Catalytic activity	03824	36.2
34370	Heterokaryon incompatibility protein (HET)	S	protein binding	05515	35.9
39885	Iron permease	U	iron ion transmembrane transporter activity	05381	30.9
42454	Manganese dependent peroxidase	T	Mn-dependent (NADH-oxidizing) peroxidase activity	16689	-2.5
32737	Laccase I	Q	Oxidoreductase activity	16682	-2.4
44094	Aldo keto reductase	S	Catalytic activity	03824	-52.2

42834	other FunK1 protein kinase	S	protein kinase activity	04672	-60.2
35183	E3 ubiquitin-protein ligase RNF220	O	ubiquitin protein ligase activity	61630	-70.6
35146	Alpha beta-hydrolase	S	hydrolase activity	16787	-79.2
40160	Zinc-finger of C2H2 type	S	DNA binding	03677	-87.7
33733	Epoxide hydrolase	I	epoxide hydrolase activity	04301	-104.5
38951	glutathione transferase	O	glutathione transferase activity	04364	-312
40940	HNH endonuclease	S	endonuclease activity	04519	-409.5
37669	Epoxide hydrolase	I	epoxide hydrolase activity	04301	-813.6
37801	Glutathione S-transferase, C-terminal domain	O	transcription coregulator activity	03712	-1186.6

Gene Ontology (GO) Enrichment Category: Biological Process (BP)					
Protein ID	**Putative Function**	**COG Cate-gory**	**GO Description**	**GO ID**	**Fold Change**
34348	FAD-binding domain	PQ	transition metal ion transport	00041	63.0
34074	cytochrome P450	IQ	xenobiotic metabolic process	06805	54.7
44334	FAD NAD-P-binding domain-containing protein	C	transition metal ion transport	00041	54.0
38317	Glycolipid 2-alpha-mannosyltransferase	G	glycoprotein biosynthetic process	09101	29.4
35066	PUB domain	S	ubiquitin-dependent protein catabolic process	06511	-51.5
39647	cytochrome P450	IQ	secondary metabolic process	19748	-63.7
40656	pheromone	S	cell communication	07154	-72.5
39042	NAD-P-binding protein	V	transition metal ion transport	00041	-83.9
34292	Autophagy protein Apg6	T	autophagy	06914	-106.9
41338	Histidinol-phosphate aminotransferase	E	L-histidine biosynthetic process	00105	-152.0
35668	Glutathione S-transferase C-terminal-like protein	O	glutathione metabolic process	06749	-161.0
41088	hydrophobin	S	cell wall modification	42545	-186.5
42002	NAD-P-binding protein	Q	transition metal ion transport	00041	-435.5

Gene Ontology (GO) Enrichment Category: Cellular Component (CC)					
Protein ID	**Description**	**COG Cate-gory**	**GO Description**	**GO ID**	**Fold Change**
39983	SNARE associated Golgi protein	S	Golgi membrane	00139	1182.7
39411	Component of ribonuclease P	J	ribonuclease MRP complex	00172	479.7
33013	RTA1-domain-containing protein	S	fungal-type vacuole	00324	301.7
39979	Expressed protein	L	Cellular component	05575	206.6
33007	RTA1 like protein	S	fungal-type vacuole	00324	55.2
33863	AFG1-like ATPase	S	ATPase complex	1904949	-104.7

A significant characteristic of the dataset was the remarkably elevated expression of genes related to intracellular transport and organelle functionality. The gene with the highest upregulation encoded a SNARE-associated Golgi protein, situated at the Golgi membrane (GO:0000139; cellular component), exhibiting a fold change more than 1100. SNARE proteins govern vesicle fusion and intracellular transport, indicating improved trafficking of enzymes, transporters, or detoxifying systems during dye stress [239]. This response signifies that vesicle-mediated transport is crucial for the mobilization of proteins associated with dye processing and metabolite management. Comparable stimulation of vesicular transport mechanisms has been documented in white-rot fungi subjected to resistant dyes, wherein intracellular compartmentalization facilitates detoxification [240,241].

Genes associated with energy metabolism and redox equilibrium were significantly activated. NADH dehydrogenase (ubiquinone) Fe-S protein 5, enriched under the Gene Ontology molecular function NADH dehydrogenase (ubiquinone) activity (GO:0008137) and classified within COG category S, exhibited a fold change above 300. This enzyme is an essential element of the mitochondrial electron transport chain, and its overexpression indicates heightened respiratory activity to satisfy the elevated energy requirements for dye breakdown. Augmented mitochondrial respiration has been extensively linked to the oxidative breakdown of dyes, necessitating considerable reducing power and ATP. Furthermore, cofactors and redox intermediates generated during the degradation process play a vital role in supporting the reduction process. Flavin adenine dinucleotide (FAD) and nicotinamide adenine dinucleotide phosphate (NAD(P)H) are recognized as redox-active coenzyme intermediates [242]. They possess the capacity to accept electrons from an azo reductase and subsequently transfer electrons to an azo dye molecule. This results in the degradation of azo-bonds in the dyes, yielding aromatic amines as a consequence [243,244].

Oxidative and reductive detoxification enzymes represented another significant category of elevated genes. D-lactaldehyde dehydrogenase (GO:0043892; COG V) and D-isomer-specific 2-hydroxyacid dehydrogenase (GO:0016616; COG E) demonstrated significant fold increases, signifying the active oxidation of aldehydes and organic acids produced during dye

degradation. The significant enrichment of the GO keywords oxidoreductase activity and catalytic activity substantiates a redox-driven intracellular breakdown pathway. These dehydrogenases are recognized for their ability to detoxify reactive dye intermediates by transforming them into less harmful chemicals, a process aligned with previously documented intracellular stages of dye degradation in white-rot fungi [245,246]. Other oxidative enzymes, such as indoleamine 2,3-dioxygenase and alpha/beta hydrolases, were also increased, reinforcing the role of oxygen-dependent cleavage processes. The existence of these proteins exhibiting significant fold change suggests the ability to hydrolyse ester or phenolic linkages, perhaps aiding in the degradation of complicated dye substituents. Collectively, these enzymes indicate a complex oxidative attack on the dye molecule [247].

Cytochrome P450 monooxygenases were markedly elevated and enriched in the Gene Ontology terms monooxygenase activity (GO:0004497) and "xenobiotic metabolic process" (GO:0006805), classified under COG category IQ. As mentioned previously that Cytochrome P450 enzymes facilitate the introduction of oxygen into aromatic compounds, enabling the cleavage of intricate dye complexes like Evans Blue, which comprises numerous aromatic rings and azo linkages. The activation of many P450-related genes indicates a pivotal role for intracellular monooxygenation processes in the initiation of dye degradation. This observation is consistent with published research on white-rot fungus, wherein cytochrome P450 systems enhance extracellular oxidative enzymes in the breakdown of azo and anthraquinone dyes [248,249].

Genes associated with transport exhibited significant induction, especially major facilitator superfamily (MFS) transporters and iron permease proteins, which were enriched under transporter activity (GO:0005215) and iron ion transmembrane transporter activity (GO:0005381). The overexpression of these transporters indicates the active absorption of dye molecules or their breakdown products, together with the control of intracellular iron concentrations. Iron serves as an essential cofactor for heme-containing enzymes, including cytochrome P450 and other oxidoreductases, suggesting a strong correlation between metal homeostasis and dye degradation efficacy [229,248].

Genes linked to fungal vacuoles, especially proteins containing the RTA1 domain, were significantly elevated. Vacuolar enrichment denotes the sequestration of harmful dye intermediates or the preservation of degradation products, a method frequently employed by fungi to alleviate intracellular toxicity. This compartmentalization mechanism has been documented in other white-rot fungi that degrade synthetic dyes, underscoring the significance of vacuolar detoxification routes [121].

In contrast to the robust activation of detoxification and transport pathways, numerous genes associated with regulation, signalling, and cellular homeostasis were significantly downregulated. Glutathione S-transferases, generally engaged in the conjugation of hazardous substances, exhibited significant negative fold alterations. This indicates that, with exposure to Evans Blue, *T. versicolor* may depend more significantly on oxidative and dehydrogenase-mediated detoxification instead of glutathione conjugation. The downregulation of epoxide hydrolases, ubiquitin-related proteins, and autophagy-related genes suggests a reduction in

protein turnover and recycling mechanisms, potentially aimed at conserving energy for primary breakdown pathways [233,234]. In case of Evans Blue dye decolorization, the extracellular enzymes such as laccase and MnP were detected during transcriptomic but they were slightly downregulated in comparison to their control samples and the same have been reflected during enzyme profiling (Figure 33(b), 34(b) and 35(b)).

Transcriptional regulators, such as zinc-finger proteins, together with genes linked to DNA binding and endonuclease activity, were repressed, indicating diminished focus on transcriptional remodelling and DNA processing. The downregulation of hydrophobin and pheromone-related genes further signifies the inhibition of cell-cell communication and cell wall remodelling, aligning with a stress-adapted, non-proliferative physiological condition. These patterns combined indicate that the fungus favours metabolic detoxification above growth, development, and signalling in response to dye stress [250].

A potential mechanism for the breakdown of Evans Blue dye in *T. versicolor* can be inferred from the observed transcriptional alterations. Exposure to dye stimulates increased absorption and intracellular movement via transporter systems and Golgi-mediated vesicular transport. The initial oxidative alteration of the dye is predominantly facilitated by cytochrome P450 monooxygenases and other oxygen-dependent enzymes, leading to the instability of the aromatic dye structure. The resultant intermediates undergo additional processing by dehydrogenases and oxidoreductases, culminating in detoxification and partial mineralization [251]. Vacuolar sequestration and regulated transit of metabolites prevent intracellular toxicity, while enhanced mitochondrial respiration provides the energy and reducing equivalents necessary for continuous breakdown. The simultaneous downregulation of growth-related and regulatory pathways indicates a purposeful reallocation of cellular resources towards effective dye breakdown.

These findings provide novel insights into dye degradation by white-rot fungi by uncovering the roles of genes, proteins, and transporters that were largely overlooked in earlier studies, emphasizing the synergistic action of intracellular enzymatic pathways and extracellular oxidative systems. The robust induction of cytochrome P450, dehydrogenases, and transporters highlights the efficacy of *T. versicolor* as a biocatalyst for the remediation of dye-contaminated wastewater.

While a comparative investigation of the transcriptome responses of *T. versicolor* during the degradation of Remazol Brilliant Blue R (RBBR) and Evans Blue indicates a conserved but dye-specific adaptation approach that mirrors the chemical complexity of both synthetic dyes. In both dye systems, fold change patterns demonstrate significant activation of genes associated with oxidative metabolism, intracellular detoxification, and transport, underscoring a common core degradation mechanism characteristic of white-rot fungi. It should be emphasized that Cytochrome P450 monooxygenases demonstrated significant positive fold changes in response to both RBBR and Evans Blue treatment, highlighting their pivotal function in commencing intracellular dye transformation via monooxygenation and aromatic ring instability. This aligns with other studies indicating that P450-mediated hydroxylation serves as a supplementary pathway to extracellular ligninolytic enzymes in the breakdown of anthraquinone and azo dyes.

In both scenarios, the upregulation of NAD(P)H-dependent dehydrogenases and oxidoreductases, such as aldo-keto reductases and lactaldehyde dehydrogenases, signifies active detoxification of reactive intermediates produced during oxidative dye cleavage, thereby endorsing a conserved Phase II-like reductive metabolism. Evans Blue exposure resulted in significantly greater fold changes in genes related to intracellular trafficking, Golgi vesicle transport, vacuolar compartmentalization, and mitochondrial respiration, indicating an increased dependence on intracellular sequestration, vesicle-mediated transport, and energy-demanding processes, likely due to the higher molecular weight and dual azo structure of Evans Blue in comparison to RBBR. In contrast, RBBR degradation exhibited a relatively greater activation of shikimate pathway enzymes and redox-associated metabolic genes, suggesting augmented metabolic facilitation for the processing of aromatic compounds characteristic of anthraquinone dyes. In all dye systems, transporter genes, especially those from the MFS family and metal ion transporters, were consistently increased, enhancing dye absorption, metabolite efflux, and cofactor availability for heme-dependent enzymes. Concurrently, both RBBR and Evans Blue conditions exhibited significant downregulation of genes associated with cell cycle progression, cytoskeletal architecture, DNA replication, and signalling, indicating growth arrest and a deliberate reallocation of energy towards detoxification. Significantly, traditional antioxidant mechanisms like catalase and glutathione S-transferases were diminished in both datasets, indicating that *T. versicolor* predominantly utilizes specific oxidative and reductive enzymatic systems instead of broad stress responses during dye breakdown, with the relative focus on intracellular trafficking, energy metabolism, and metabolic pathway activation being adjusted based on dye structure and complexity, thereby underscoring the ecological adaptability and biotechnological potential of this white-rot fungus for the treatment of structurally diverse textile dyes.

5.7 Proteome Analysis of CB8 strain

5.7.1 Differential protein expression and visualization

To obtain a more profound mechanistic understanding of dye bioremediation by white-rot fungi, transcriptome analysis was complemented with proteome profiling. Transcriptomics offers insights into gene expression, but proteome analysis facilitates the direct evaluation of functional protein abundance, thereby encompassing post-transcriptional regulation and enzymatic responses related to dye degradation [252]. A comparative proteomic analysis was undertaken to investigate differences in protein abundance between treatment and control conditions. Due to the exploratory nature of the work and the lack of biological replicates, a fold-change technique was utilized to discover differentially abundant proteins. This exploratory proteomics research is essential for elucidating significant metabolic pathways, stress response mechanisms, and dye-degrading enzymes that facilitate fungal-mediated bioremediation, as well as for formulating hypotheses for subsequent targeted validation experiments [253].

Protein quantification and preliminary differential protein identification were conducted via MaxQuant. The Figure 42(a) depicts the proteomic data processing pipeline for identifying differentially abundant proteins in *T. versicolor* during RBBR dye degradation (CB8RBBR)

relative to the control condition (CB8CONT). Starting from the proteinGroups.txt file, a total of 65 differential proteins were initially detected for this comparison. Subsequent analysis in Perseus software involved the removal of reverse hits, potential contaminants, and proteins identified solely by site modifications, yielding 32 high-confidence proteins. The raw intensities for CB8RBBR and CB8CONT were log2-transformed, and log2 fold changes were computed as log2(Intensity CB8RBBR) - log2(Intensity CB8CONT). In the absence of biological replicates, statistical significance via p-values was not assessed; instead, a threshold of log2 fold change ≥ 0.3 was applied to select 29 proteins as differentially abundant, likely representing those up or down regulated in the dye degradation condition to facilitate enzymatic responses. Figure 43 provides data regarding the quantity of upregulated and downregulated proteins during the breakdown of RBBR dye. Among 29 differentially expressed proteins, 16 were upregulated and 13 were downregulated after RBBR dye decolorization.

Similarly, the Figure 42(b) illustrates the workflow for proteomic analysis of Evans Blue dye degradation (CB8EB) versus the control (CB8CONT). From the proteinGroups.txt file, 51 differential proteins were originally identified. After filtering in Perseus to exclude reverse hits, potential contaminants, and site-only identifications, 28 high-confidence proteins remained. Log2 transformation was applied to the intensities of CB8EB and CB8CONT, with log2 fold changes calculated accordingly. Without biological replicates, no p-value filtering was employed, and 7 proteins exhibiting a log2 fold change ≥ 0.3 were designated as differentially abundant, indicating a more selective induction of proteins potentially involved in azo dye breakdown compared to other dyes. Among 28 differentially expressed proteins during EB dye degradation, 2 were up regulated while majority of proteins were down regulated (Figure 43).

The Figure 42(c) also outlines the data processing for Crystal Violet (CV) dye degradation (CB8CV) compared to the control (CB8CONT). Initially, 66 differential proteins were noted in the proteinGroups.txt file for this pairwise analysis. Processing in Perseus eliminated reverse hits, potential contaminants, and proteins identified only by site, resulting in 29 high-confidence proteins. Intensities were converted to log2 values, and fold changes were determined as log2(Intensity CB8CV) - log2(Intensity CB8CONT). Given the lack of replicates, p-value criteria were omitted, and a log2 fold change threshold of ≥ 0.3 was used to identify 12 differentially abundant proteins, suggesting moderate proteomic reconfiguration tailored to triarylmethane dye remediation. Out of 29 high confidence proteins, 9 were up regulated while 20 were down regulated during CV dye degradation by CB8 (Figure 43).

In the realm of fungal dye degradation, proteins that are up-regulated during treatment typically indicate the activation of particular metabolic and stress-response pathways that facilitate the fungus's ability to decompose resistant dye molecules and manage toxic stress. Fungi that decompose complex aromatic dyes frequently exhibit heightened expression of extracellular oxidative enzymes, including laccases, manganese peroxidases, and other oxidoreductases, which facilitate critical processes in the depolymerization and oxidative degradation of dye structures, and these enzymes have consistently been associated with efficient dye removal in white-rot and saprotrophic fungi [254]. Their upregulation is indicative of active biodegradation processes. Conversely, down-regulated proteins often signify pathways that are

less essential during stress circumstances, such as fundamental biosynthesis, growth-related metabolism, or housekeeping functions, as the fungus reallocates resources towards stress tolerance and breakdown pathways. This pattern of proteome rebalancing, wherein energy and cellular resources are redirected from growth to breakdown and detoxification, aligns with the general stress responses documented in proteomic studies of fungi subjected to external stressors [255]. The elevated quantity of up-regulated proteins in certain comparisons such as CB8RBBR/CB8CONT likely signifies a more robust activation of degradative mechanisms, while the increased number of down-regulated proteins in other comparisons (CB8EB/CB8CONT) implies a more significant inhibition of non-essential processes as the organism acclimatizes to exposure. These data correspond with extensive mycoremediation studies, wherein the equilibrium between up- and down-regulated proteins signifies a dynamic reconfiguration of fungal metabolism that facilitates dye decolorization and tolerance to environmental stress [256].

(a)

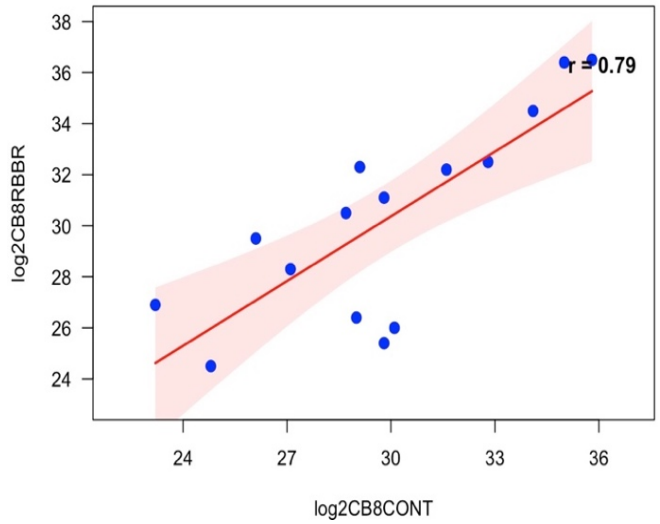

(b)

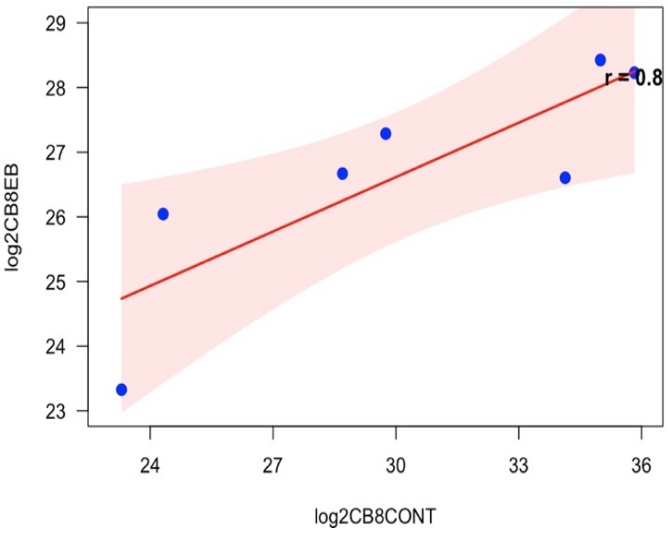

(c)

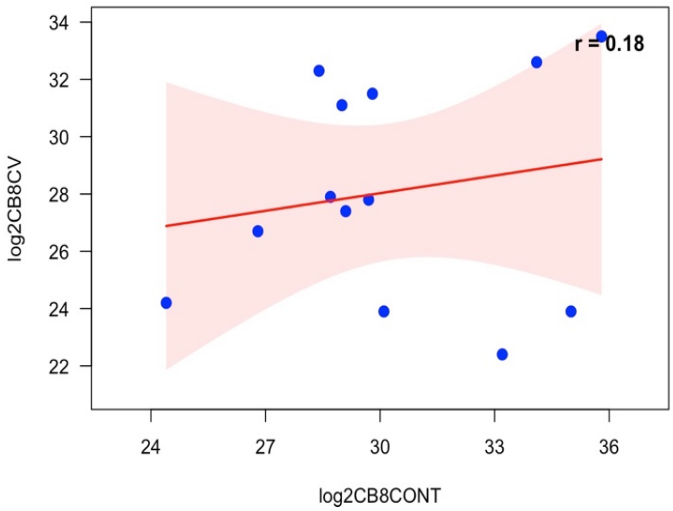

Figure 42. Scatter plots representing the log_2 fold change for (a) CB8RBBR vs. CB8CONT, (b) CB8EB vs. CB8CONT, and (c) CB8CV vs. CB8CONT

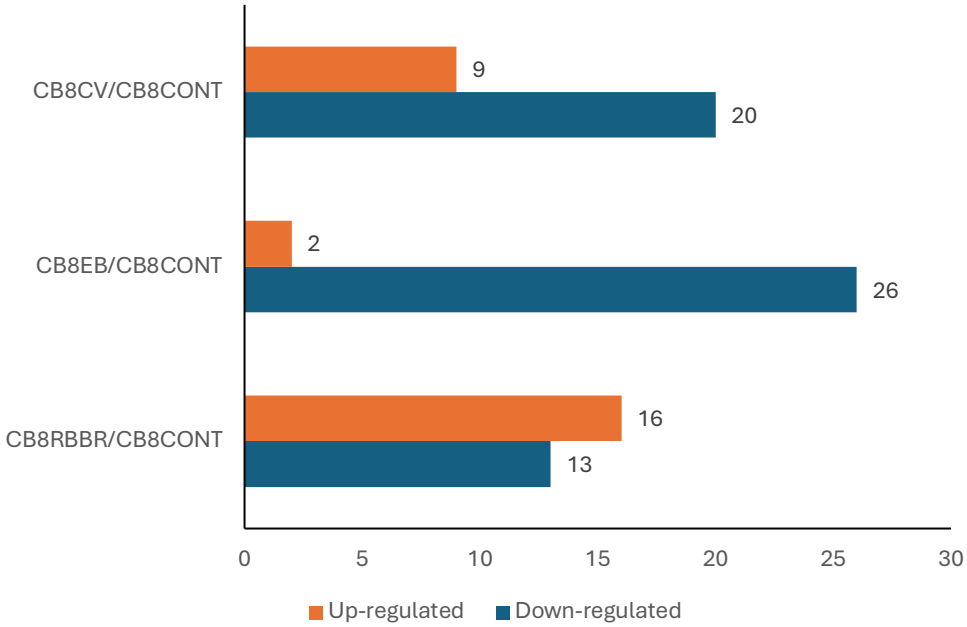

Figure 43. Up and down regulated proteins based on log2 fold change value of comparison pair of control versus dye treated samples of *T. versicolor*

The two-way hierarchical clustering heatmap presented in Figure 43 provides a comprehensive visualization of proteomic variations in *T. versicolor* (CB8) under control growth conditions (CB8CONT) and during the degradation of synthetic dyes (CB8RBBR, CB8EB, and CB8CV). This analytical tool integrates a color-coded matrix representing normalized protein expression levels, ranging from 1.5 (dark blue, indicating upregulation) to -1.5 (light blue to white,

indicating downregulation), with hierarchical clustering applied to both rows (individual proteins) and columns (experimental conditions). The dendrograms on the left and top illustrate similarity relationships based on Euclidean distance and linkage methods, reorganizing the data to highlight co-regulated protein groups and condition-specific responses. In this study, the heatmap elucidates how CB8 adapts its proteome to bioremediate dyes such as RBBR, EB and CV compared to baseline growth without dye exposure.

The column clustering reveals distinct proteomic profiles across the conditions, underscoring the fungus's tailored response to different dye chemistries. Notably, CB8EB and CB8CV cluster closely together, suggesting highly similar enzymatic inductions for azo and triarylmethane dyes, possibly involving shared oxidative pathways like laccase-mediated decolorization. The control condition (CB8CONT) branches adjacently to this pair, indicating moderate overlap with baseline metabolism but clear deviations under dye stress. In contrast, CB8RBBR forms a separate branch, implying a more unique proteomic shift, likely due to the recalcitrant anthraquinone structure requiring enhanced peroxidase activity or greater oxidative stress tolerance [257]. These patterns demonstrate that while dye exposure generally perturbs the proteome away from control levels, the extent and specificity of changes depend on dye type, with RBBR eliciting the most divergent response [258].

Row clustering groups 46 proteins - identified by accession codes such as A0A502UQV7 and R7S8R3 - into coherent modules based on expression patterns, facilitating the identification of functional pathways. The top cluster exhibits downregulation (lighter shades) in CB8EB and CB8CV relative to CB8CONT, with variable responses in CB8RBBR, potentially encompassing dye-inducible oxidoreductases critical for EB and CV breakdown. A middle cluster shows activation (darker shades) in CB8CONT and CB8RBBR but repression in CB8EB and CB8CV, suggesting proteins specialized for anthraquinone metabolism. These clusters highlight co-expressed protein sets, enriching for ligninolytic enzymes like manganese peroxidases and versatile peroxidases in upregulated modules.

Similarities across dye conditions point to a conserved stress response, including cytochrome P450 and ABC transporter involvement for dye uptake and detoxification, whereas differences emphasize adaptive flexibility - such as heightened peroxidase reliance for RBBR [122]. These findings have implications for optimizing fungal-based wastewater treatment, as understanding proteomic shifts can guide strain engineering or condition optimization to enhance dye removal efficiency [259]. Further annotation of protein IDs via databases like UniProt would confirm specific enzyme roles, strengthening the mechanistic insights derived from this visualization.

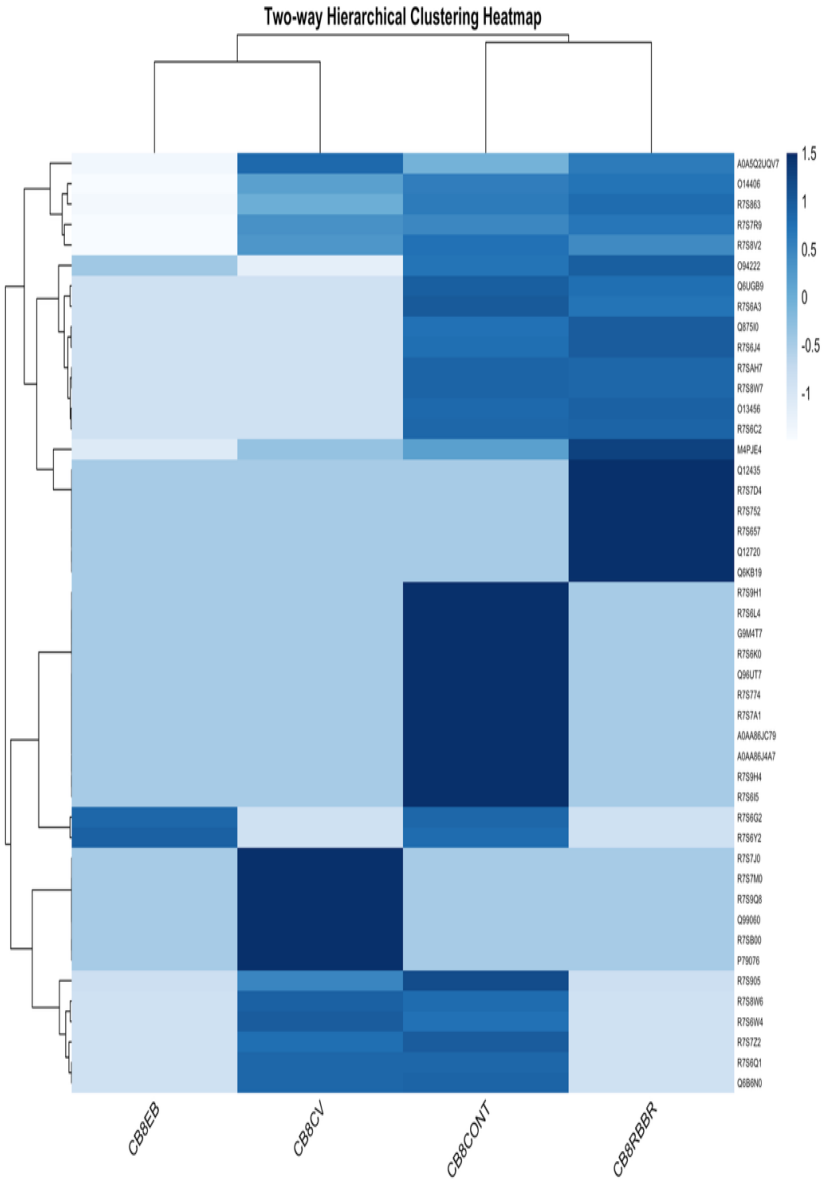

Figure 43. Heatmap of differentially abundant proteins based on log2 protein intensity of *Trametes versicolor* in dye degrading condition vs control condition

5.7.2 Functional annotation and enrichment analysis of proteins

The processed and refined dataset was subsequently used for Gene Ontology (GO) annotation. Proteins showing zero intensity in both treated and control samples were excluded from the GO annotation analysis. Final protein ID lists of differentially abundant proteins were generated for each comparison, including CB8RBBR-CB8CONT (29 proteins), CB8EB-CB8CONT (28 proteins), and CB8CV-CB8CONT (29 proteins). Corresponding protein FASTA sequences were retrieved from the UniProt database. These sequences were uploaded to the usegalaxy.eu platform, where functional annotation was performed using the eggNOG-mapper orthology-based tool to assign GO terms, COG functional categories, and KEGG pathway annotations.

I. GO Enrichment Analysis for CB8RBBR-CB8CONT DEPs

A comparative proteome investigation of *T. versicolor* utilized for RBBR dye-degrading conditions demonstrated significant metabolic reprogramming, marked by pronounced activation of ligninolytic and oxidative stress-related enzymes, alongside the concurrent inhibition of growth-associated metabolic pathways as shown in Table 12. This expression pattern signifies that the fungus emphasizes extracellular oxidative breakdown of the dye rather than primary metabolism when confronted with the resistant anthraquinone structure of RBBR.

The most significantly upregulated proteins included heme-dependent peroxidases, exhibiting substantial positive $\log_2$ fold changes and enrichment in molecular function categories such as heme binding and peroxidase activity, alongside biological process categories associated with cellular oxidant detoxification and responses to oxidative stress. These enzymes conduct one-electron oxidation processes utilizing hydrogen peroxide, producing reactive radicals that can target the aromatic and quinone structures of synthetic colors [260]. In the context of RBBR degradation, these peroxidases presumably commence the oxidative cleavage of the anthraquinone chromophore, resulting in the rupture of the conjugated π-electron system that imparts dye color. The robust induction of these enzymes indicates that peroxidase-mediated oxidation serves as the principal catalyst for RBBR decolorization in *T. versicolor* and the same has been reflected in enzyme profiling (Figure 34(a), 35(a)). Xu et al. described the role of Dye decoloring peroxidases (DyPs) which have remarkable efficacy in decolorizing and degrading various dyes. DyPs are a category of heme peroxidases that significantly differ from established heme peroxidases regarding amino acid sequences, protein architecture, catalytic residues, and their physical and chemical characteristics. DyPs catalyze the oxidation of polycyclic dyes and phenolic chemicals [261].

Laccases exhibited variable expression, with multiple isoforms demonstrating moderate overexpression, especially in the biological process category related to lignin catabolism. Laccases, as multicopper oxidases, facilitate the oxidation of many phenolic and non-phenolic substrates and are recognized for their function in lignin and dye degradation. In RBBR-exposed cultures, laccases presumably function synergistically with peroxidases by directly oxidizing the dye or via redox mediators, producing unstable radical intermediates that enhance the degradation of the dye molecule. The finding that certain copper-binding laccase isoforms were downregulated while others were upregulated indicates isoform-specific regulation, preferentially enhancing the enzymes most efficient in degrading anthraquinone-type dyes [218,219]. The laccase enzyme profiling indicated reduced overall laccase activity under RBBR decolorization conditions compared to the control. However, conventional enzyme activity assays quantify total laccase activity and are unable to distinguish between individual laccase isoforms. Since white-rot fungi produce multiple laccase isoenzymes with distinct regulatory and functional properties, changes at the isoform level may not be accurately reflected by bulk activity measurements. Oxidative ability towards aromatic compounds varied substantially among the isoforms [262]. Proteomic analysis therefore provided a more precise molecular-level understanding by differentiating between individual laccase isoforms and revealing isoform-specific regulation during RBBR degradation.

The enhancement of proteins linked with the extracellular region reinforces the idea that RBBR breakdown primarily takes place outside the fungal cell, thus reducing intracellular toxicity. The activation of oxidant detoxification pathways simultaneously indicates the necessity for stringent regulation of reactive oxygen species produced during enzymatic oxidation [263]. This equilibrium enables *T. versicolor* to utilize oxidative chemistry for pollutant breakdown while safeguarding cellular components from oxidative harm.

Conversely, numerous proteins associated with primary metabolism and biosynthesis were significantly downregulated under dye-degrading conditions. These encompassed enzymes related to fatty acid metabolism, deoxyribonucleotide biosynthesis, glycoprotein degradation, and carbohydrate-processing hydrolases. The suppression of these pathways signifies a decline in growth and biosynthetic activity, implying that cellular resources and energy are reallocated towards stress adaptation and secondary metabolic processes, including the creation of ligninolytic enzymes. The downregulation of oxalate decarboxylase suggests that pH modulation and organic acid-mediated processes are less significant under these conditions, with enzyme-driven oxidative reactions prevailing in the breakdown process.

Table 12. GO Enrichment, COG classification along with log2 Fold change for differentially expressed proteins in CB8RBBR-CBRCONT (Dark blue, dark orange and dark green highlighted cells show upregulated proteins; Light blue, light orange and light green highlighted cells show downregulated proteins)

Protein ID	Putative Protein Function	COG Category	GO Description	GO ID	log2 Fold Change
Gene Ontology (GO) Enrichment category- Molecular Functions (MF)					
Q12435	Peroxidase	T	heme binding	20037	34.2
Q6KB19	Peroxidase	T	peroxidase activity	4601	26.1
A0A481SVG9	Laccase (Lcc1)	Q	oxidoreductase activity	16491	1.5
Q96UT7	Laccase (lacc3)	Q	copper ion binding	05507	-25.3
G9M4T7	Laccase (lacc3)	Q	copper ion binding	05507	-26.0
R7S6Q1	FAD-binding domain-containing protein	C	flavin adenine dinucleotide binding	50660	-26.8
R7S9H1	Fungalysin metallopeptidase (M36)	O	metalloendopeptidase activity	4222	-26.8

Gene Ontology (GO) Enrichment category- Cellular Component (CC)					
M4PJE4	Immunomodulatory protein	S	extracellular region	05576	1.8
Gene Ontology (GO) Enrichment category- Biological Process (BP)					
Q12720	Peroxidase	T	cellular oxidant detoxification	98869	31.1
Q875I0	Laccase	Q	lignin catabolic process	46274	3.7
A0A144KZJ7	Laccase	Q	lignin catabolic process	46274	1.3
O13456	Laccase (CVLG1)	Q	lignin catabolic process	46274	1.2
O14406	Peroxidase (mrp)	T	response to oxidative stress	06979	0.3
R7S8W7	Ribonucleoside-diphosphate reductase	F	deoxyribonucleotide biosynthetic process	09263	-0.3
Q6UGB9	Oxalate Decarboxylase	G	oxalate metabolic process	33609	-2.5
R7S6A3	RNA splicing	S	endoplasmic reticulum to Golgi vesicle-mediated transport	06888	-4.4
R7S9H4	acetyl-CoA synthetase-like protein	I	fatty acid metabolic process	06631	-26.6
R7S8W6	Glycosyl hydrolase family 92	G	glycoprotein catabolic process	06516	-29.0
R7S905	Glycosyl hydrolase family 92	G	glycoprotein catabolic process	06516	-33.2

II. GO Enrichment Analysis for CB8EB-CB8CONT DEPs

The breakdown of Evans Blue dye by *T. versicolor* reveals differently expressed proteins that signify substantial reorganization of oxidative, metabolic, and regulatory processes. Numerous essential ligninolytic oxidoreductases, comprising various laccase isoforms (lcc3, lcc13) and peroxidases, exhibited substantial downregulation (log_2 fold change -2.5 to -27.1) as seen in Table 13, although their recognized function in dye and lignin degradation [219]. Likewise reflected in enzyme profiling (Figure 33- 35). This downregulation presumably indicates a time shift among transcription, secretion, and extracellular accumulation of these enzymes, rather than a loss of functional significance. The molecular activities associated with oxidoreductase

activity, copper and iron ion binding, FAD binding, and monooxygenase activity highlights the role of redox-active enzymes such cytochrome P450s in the transformation and detoxification of aromatic compounds [264]. The simultaneous inhibition of protein kinases and metallopeptidases indicates diminished signaling and proteolytic activity when the system shifts from a stress response to prolonged extracellular enzymatic function.

The differential expression underscores modifications in intracellular structure, metabolism, and stress response at the cellular and biological process levels. Proteins linked to the extracellular region and vacuolar membrane signify active protein trafficking and compartmentalization during dye exposure, whereas the enrichment of oxidative stress response, lignin catabolism, and oxalate and fatty acid metabolism illustrates the metabolic expense of dye degradation. The DEPs related to oxidative stress response, lignin catabolism and peroxidases are corelating well with DEGs.The downregulation of glycosyl hydrolases and oxalate decarboxylase indicates modified carbon use and organic acid metabolism under dye stress [265]. These findings collectively endorse a concept wherein *T. versicolor* initially activates ligninolytic machinery, thereafter demonstrating diminished intracellular levels of these proteins as stable, post-translationally changed enzymes accumulate extracellularly and facilitate dye decolorization. The decoupling between intracellular protein levels and extracellular catalytic activity is a defining characteristic of white-rot fungal biodegradation systems.

Table 13. GO Enrichment, COG classification along with log2 Fold change for differentially expressed proteins in CB8REB-CBRCONT

Protein ID	Putative Protein Function	COG Cate-gory	GO Description	GO ID	log2 Fold Change
Gene Ontology (GO) Enrichment category- Molecular Functions (MF)					
A0A5Q2UQV7	Laccase (lcc13)	Q	hydroquinone:oxygen oxidoreductase activity	52716	-2.5
O94222	Laccase (lcc3)	Q	oxidoreductase	16491	-6.6
G9M4T7	Laccase (lcc3)	Q	copper ion binding	05507	-23.5
R7S6Q1	FAD-binding domain-containing protein	C	flavin adenine dinucleotide binding	50660	-25.7
A0AA86J4A7	cytochrome P450	IQ	iron ion binding	05506	-26.5
A0AA86JC79	cytochrome p450	Q	monooxygenase activity	04497	-26.5
R7S9H1	Fungalysin metallopeptidase (M36)	O	metalloendopeptidase activity	04222	-26.8
R7S6L4	Pkinase-domain-containing protein	T	protein kinase activity	04672	-28.5

Gene Ontology (GO) Enrichment category- Cellular Component (CC)					
R7S6Y2	Mrna splicing factor	S	post-mRNA release spliceosomal complex	71014	1.7
M4PJE4	Immunomodulatory protein	S	extracellular region	05576	-2.0
R7S7Z2	Vacuolar membrane-associated protein Iml1	T	vacuolar membrane	05774	-31.3
Gene Ontology (GO) Enrichment category- Biological Process (BP)					
O14406	Peroxidase	T	response to oxidative stress	06979	-7.5
Q875I0	Laccase (lcc3)	Q	lignin catabolic process	46274	-23.2
R7S9H4	acetyl-CoA synthetase-like protein	I	fatty acid metabolic process	06631	-26.6
Q50JG3	Laccase (lcc3)	Q	lignin catabolic process	46274	-27.1
Q6UGB9	Oxalate Decarboxylase	G	oxalate metabolic process	33609	-28.9
R7S8W6	Glycosyl hydrolase family 92	G	glycoprotein catabolic process	06516	-29.0
R7S905	Glycosyl hydrolase family 92	G	glycoprotein catabolic process	06516	-33.1

III. GO Enrichment Analysis for CB8CV-CB8CONT DEPs

Table 14 represents differentially expressed proteins during CV dye degradation. *T. versicolor* demonstrated significant overexpression of oxidative and carbohydrate-active enzymes that directly promote the decomposition of Crystal Violet. Proteins linked to pyranose oxidase activity, general oxidoreductase activity, and hydrolase activity exhibited significant positive $\log_2$ fold increases, signifying an increased production of hydrogen peroxide and redox equivalents necessary for the oxidative breakdown of the dye's aromatic structure. The enhancement of FAD-binding proteins and hydroquinone:oxygen oxidoreductase activity further substantiates the role of flavin-dependent redox cycling and quinone transformation, which are crucial for destabilizing triphenylmethane dyes like Crystal Violet [266]. The upregulation of the lignin catabolic process indicates that ligninolytic pathways are utilized for synthetic dye degradation, emphasizing the functional similarities between lignin and dye oxidation mechanisms.

In contrast, several copper-binding oxidoreductases, metalloendopeptidases, and proteins associated with lipid metabolism, oxalate metabolism, vesicle-mediated transport, and glycoprotein catabolism were downregulated, indicating metabolic reallocation during prolonged dye stress. The diminished expression of copper-binding proteins, such as laccase-

associated components, likely indicates a temporal transition from intracellular production to dependence on previously secreted and stable external enzymes. The downregulation of fatty acid and oxalate metabolism signifies a reduction in secondary carbon fluxes, enabling the reallocation of cellular resources towards oxidative detoxification [267]. Collectively, these expression patterns indicate that *T. versicolor* emphasizes redox-driven ligninolytic and oxidoreductive pathways while minimizing energy-intensive metabolic and transport processes, thus enhancing Crystal Violet decolorization efficiency [268].

Table 14. GO Enrichment, COG classification along with log2 Fold change for differentially expressed proteins in CB8CV-CBRCONT

Protein ID	Putative Protein Function	COG_ category	GO Description	GO ID	log2 Fold Change
Gene Ontology (GO) Enrichment category- Molecular Functions (MF)					
P79076	Pyranose 2-oxidase (P2Ox)	E	pyranose oxidase activity	50233	33.5
R7S7M0	Alpha/beta-hydrolase	E	hydrolase activity	16787	26.0
R7S7J0	Aryl-alcohol oxidase-like protein	E	oxidoreductase activity	16491	23.4
R7S6W4	Aprataxin zinc finger domain-containing protein	S	flavin adenine dinucleotide binding	50660	4.0
A0A5Q2UQV7	Laccase(Lcca)	Q	hydroquinone: oxygen oxidoreductase activity	52716	1.6
O94222	Laccase(Lcc2)	Q	oxidoreductase	16491	-11.1
Q96UT7	Laccase(Lcc1)	Q	copper ion binding	5507	-25.3
G9M4T7	Laccase(Lcc5)	Q	copper ion binding	5507	-26.0
R7S9H1	Extracellular metalloproteinase (Fungalysin)	O	Metallo-endopeptidase activity	04222	-26.8
Gene Ontology (GO) Enrichment category- Cellular Component (CC)					
M4PJE4	Immunomodulatory protein	S	extracellular region	5576	-0.8
R7S7Z2	Vacuolar membrane-associated protein IML1	T	vacuolar membrane	5774	-1.9

Gene Ontology (GO) Enrichment category- Biological Process (BP)					
Q99060	Peroxidase (PGVII mnp2)	T	lignin catabolic process	46274	30.5
R7S8W6	Glycoside hydrolase family 92 protein	G	glycoprotein catabolic process	6516	2.1
Q6B6N0	Glycoside hydrolase family 92 protein (cmp3)	T	cellular oxidant detoxification	98869	-0.2
O14406	Peroxidase (mrp)	T	response to oxidative stress	06979	-1.5
R7S905	Glycoside hydrolase family 92 protein	G	glycoprotein catabolic process	6516	-10.7
Q875I0	Laccase	Q	lignin catabolic process	46274	-23.2
R7S9H4	Acetyl-CoA synthetase-like protein	I	fatty acid metabolic process	6631	-26.6
R7S6A3	CENP-V/GFA domain-containing protein	S	endoplasmic reticulum to Golgi vesicle-mediated transport	6888	-28.0
Q6UGB9	Oxalate decarboxylase	G	oxalate metabolic process	33609	-28.8

5.7.3 Mechanistic insights into dye degradation

The proposed mechanism for *T. versicolor*-mediated degradation of dyes such as Remazol Brilliant Blue R and Evans Blue begins with the interaction of these dyes at the fungal cell surface or in the extracellular environment as seen in Figure 44. Major Facilitator Superfamily (MFS) transporters play a key role by facilitating the uptake of essential metal ions like iron, zinc, and copper, which act as cofactors for oxidative enzymes. These transporters may also indirectly aid in dye entry or the efflux of degradation byproducts. Extracellular oxidative enzymes, including laccases and peroxidases (such as heme peroxidases), initiate the degradation process by oxidizing the dyes. Laccases, which are multicopper oxidases, and peroxidases utilize molecular oxygen or hydrogen peroxide to cleave aromatic rings and chromophoric groups in the azo (Evans Blue) and anthraquinone (RBBR) structures, producing reactive dye intermediates like quinones, radicals, or partially degraded fragments. Proteins such as laccase, peroxidase, heme peroxidase, and FAD-binding domain-containing proteins directly support this initial oxidation, making it an energy-efficient step that minimizes intracellular exposure to intact, toxic dyes.

Following the generation of reactive intermediates, which can be cytotoxic, these compounds are rapidly transported intracellularly for further processing to prevent oxidative stress. NADH/PH-dependent dehydrogenases help reduce or modify these intermediates through hydride transfer, stabilizing radicals and converting them into less reactive forms. FAD-binding domain-containing proteins, often linked to dehydrogenase activity, and aldo-keto reductases, which perform NADPH-dependent reductions on carbonyl groups in dye fragments, are crucial here. Additionally, ribonucleoside-diphosphate reductase contributes to maintaining nucleotide pools for cellular repair amid the oxidative stress induced by these intermediates.

Intracellular detoxification and metabolism then take over to break down the intermediates into non-toxic metabolites. Cytochrome P450 enzymes catalyze monooxygenation reactions, incorporating oxygen into dye fragments to facilitate further cleavage or conjugation. Phase II detoxification involves conjugation enzymes like glutathione S-transferase (GST), which attaches glutathione to electrophilic sites on the metabolites, enhancing their solubility and preparing them for excretion. Supporting metabolic pathways provide the necessary energy and precursors: acetyl-CoA synthetase-like proteins produce acetyl-CoA for energy or biosynthesis, while DHAP synthetase connects to glycolysis and glycerol metabolism for reducing equivalents like NADH. Oxalate decarboxylase breaks down oxalate byproducts from peroxidase activity to avoid accumulation, and glycosyl hydrolase family enzymes may hydrolyse glycosylated conjugates or assist in cell wall remodelling under stress. Key upregulated components here include cytochrome P450, glutathione S-transferase, aldo-keto reductase, acetyl-CoA synthetase-like protein, DHAP synthetase, oxalate decarboxylase, and glycosyl hydrolase family proteins.

To manage the intracellular handling of these compounds without cytoplasmic buildup, degraded intermediates and metabolites are trafficked through the endomembrane system. The Golgi apparatus and vacuoles are involved in sorting, modifying, and sequestering detoxified products, with vacuoles serving as storage sinks for conjugated metabolites. Vesicular transport ensures efficient movement between organelles, such as from the endoplasmic reticulum to the Golgi. Upregulated genes for endoplasmic reticulum to Golgi vesicle-mediated transport and general vesicular transport support this compartmentalization. Mitochondria also play a role by supplying ATP and NADH for these energy-demanding processes.

Finally, the detoxified metabolites - such as smaller organic acids, amines, or even fully mineralized products like carbon dioxide and water - are exported from the cell via MFS transporters or exocytosis. This export may involve positioning at the extracellular wall or regulatory feedback to downregulate the pathway once the dyes are cleared. Overall, this mechanism reflects *T. versicolor*'s adaptive bioremediation capabilities, where the ligninolytic enzyme system, strengthen by upregulated genes, enables efficient decolorization and detoxification of industrial dyes. However, transcriptomic and proteomic analyses also identified several uncharacterized genes and proteins with currently unassigned functions, indicating that a more complete understanding of dye degradation mechanisms will be achieved as the roles of these components are elucidated.

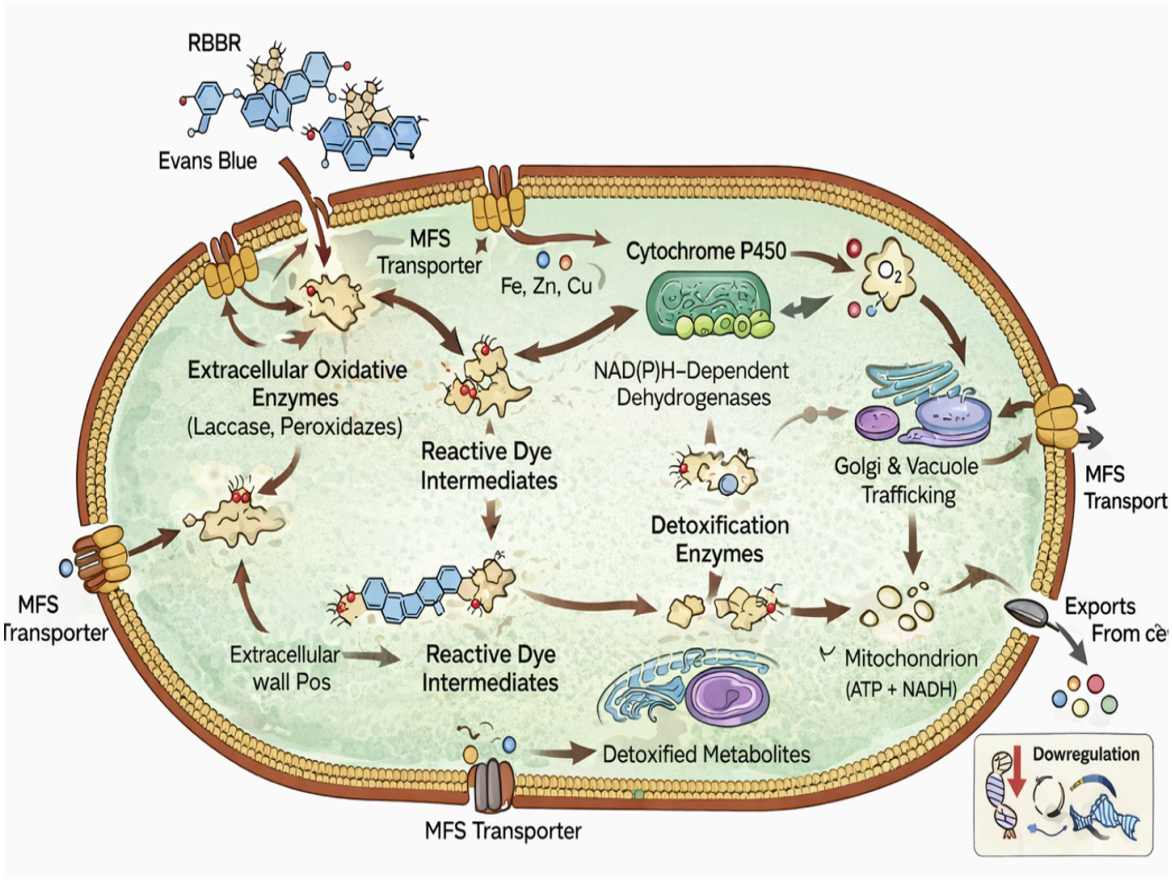

Figure 44. Proposed mechanistic way of Remazol Brilliant Blue R and Evans Blue dye degradation by *Trametes versicolor* (CB8) strain (Figure by R. Upadhyay with help of AI)

The difference noted between transcriptomic and proteomic profiles mostly stem from variations in sampling period (24 hours versus 48 hours) and the biological compartment studied (whole cells versus extracellular media). The transcriptomic analysis of whole fungal cells 24 hours post-dye treatment primarily elucidates the initial cellular response to stress, wherein *T. versicolor* engages signalling pathways, redox balancing mechanisms, transport systems, and metabolic reprogramming. As a result, genes associated with energy metabolism, NADH/NADPH regeneration, transporters, cytochrome P450 enzymes, dioxygenases, and stress-response regulators are significantly identified [269]. Currently, transcription indicates cellular preparation and adaptive readiness rather than continuous enzyme production, and transcripts for ligninolytic enzymes like laccases and peroxidases may be ephemeral or temporally misaligned, leading to modest expression levels despite their subsequent functional significance.

Conversely, proteome examination of the extracellular media at 48 hours specifically identifies secreted and accumulated enzymes linked to secondary metabolism, notably ligninolytic oxidoreductases. At this stage, enzymes like laccases, manganese peroxidases, and versatile peroxidases have been completely synthesized, secreted, post-translationally changed, and stabilized extracellularly, enabling their persistence and accumulation despite a decrease in

intracellular transcription. Proteomics thus represents the functional enzymatic apparatus engaged in dye degradation, but transcriptomics does not account for secretion dynamics, extracellular stability, or post-translational maturation. The combined temporal and geographical variations elucidate the observed discrepancy between mRNA and protein levels, highlighting the complementary roles of transcriptomics in intracellular adaptive responses and proteomics in external degradative processes. Hence, this gap can be empirically validated as a deliberate and complementary multi-omics approach. To the best of my knowledge, no research articles to date have reported an in-depth multi-omics analysis of the degradation of Remazol Brilliant Blue R, Evans Blue, and Crystal Violet dyes by *Trametes versicolor*. This PhD research is therefore novel, as it not only optimizes dye decolorization conditions but also elucidates the underlying molecular mechanisms involved in the degradation process.

5.8 Ecotoxicological evaluation of dye and post-treated samples

As mentioned previously, the aim of this study was not only to decolorize dye-containing wastewater but also to reduce the toxicity of the dyes after fungal treatment compared to the untreated (pure) dyes. Therefore, *Daphnia magna* and *Spirodela polyrhiza* were selected as model organisms for toxicity assessment. These bioassays provide insight into the environmental safety of the treated water, its suitability for safe discharge into water bodies, and its potential for reuse in specific applications.

5.8.1 Assessment of Zootoxicity

The zootoxic effects of pure dyes (Remazol Brilliant Blue R, Evans Blue, and Crystal Violet) and their respective fungal-treated effluents were assessed using *Daphnia magna* as a bioindicator species for ecotoxicology test. Toxicity was quantified using half maximal effective concentration (EC_{50}), Toxicity Unit (TU), and classified according to the Persoone toxicity classification system (Table 15).

The pure RBBR dye demonstrated substantial toxicity at 24 hours of exposure (EC_{50} = 33.60%, TU = 3.00; Class III), which escalated considerably after 48 hours (EC_{50} = 9.20%, TU = 10.87), transitioning to very hazardous Class IV. This indicates a distinct temporal escalation in the toxicity of the untreated dye. After fungal bioremediation, both *T. versicolor* (CB8) and *P. ostreatus* (BWPH) markedly diminished the toxicity of RBBR. After 48 hours, the EC_{50} rose to 15.92% (TU = 6.28) with CB8 and 14.23% (TU = 7.03) with BWPH, reverting the toxicity classification to Class III. At 24 hours, BWPH exhibited the most effective detoxifying performance, characterized by the greatest EC_{50} (45.21%) and the lowest TU (2.21). The results validate that both fungi successfully detoxified RBBR, with *P. ostreatus* (BWPH) demonstrating enhanced early-stage detoxification efficacy. Thus, the objective was successfully achieved for Remazol Brilliant Blue R dye-containing wastewater, as maximum decolorization was attained along with a significant reduction in toxicity.

Pure Evans Blue exhibited considerable toxicity at 24 hours (EC_{50} = 35.36%, TU = 2.83; Class III), but toxicity significantly escalated after 48 hours (EC_{50} = 7.10%, TU = 14.08), classifying it as very hazardous (Class IV). A notable decrease in toxicity was seen following fungal

treatment. The EC_{50} for *T. versicolor* (CB8) rose to 52.50% at 24 hours and 25.00% at 48 hours, while the TU diminished to 1.90 and 4.00, respectively, keeping the effluent within Class III. Likewise, *P. ostreatus* (BWPH) elevated the EC_{50} to 53.45% (24 h) and 15.97% (48 h), with TU values of 1.87 and 6.26, respectively. CB8 demonstrated somewhat superior detoxifying effectiveness compared to BWPH for Evans Blue, especially after extended exposure durations.

Crystal Violet was identified as the most hazardous dye among those examined. The pure dye exhibited severe toxicity at both 24-hour and 48-hour exposure intervals, with EC_{50} values significantly lower than 6.25% and TU values over 100, aligning with Persoone Class V (very poisonous). Treatment with *T. versicolor* (CB8) markedly diminished the toxicity of Crystal Violet, elevating EC_{50} to 9.93% at 24 hours and 5.27% at 48 hours, with TU values of 10.07 and 18.97, respectively. This led to a decrease in toxicity classification from Class V to Class IV, signifying a significant detoxifying impact. Conversely, *P. ostreatus* (BWPH) did not diminish the toxicity of Crystal Violet, as the treated effluents consistently remained in Class V across both exposure durations. This illustrates the clear superiority of *T. versicolor* (CB8) in the biodegradation of very poisonous triphenylmethane dyes, including Crystal Violet.

The dye-free fungal growth medium demonstrated low to moderate toxicity. The extracellular medium in which CB8 was cultivated exhibited EC_{50} values of 58.4% and 24.1% at 24 hours and 48 hours, respectively, but the medium cultivated with BWPH demonstrated superior EC_{50} values of 76.44% and 70.71%. The associated TU values remained modest (1.31-4.15), all within Class III, indicating that the fungus did not generate highly hazardous compounds. This confirms that the observed reductions in toxicity in dye-treated effluents result from dye breakdown rather than by-products from fungi.

The research unequivocally indicates that pure dyes displayed markedly more toxicity to *D. magna* compared to their respective fungal-treated effluents. The toxicity escalated with prolonged exposure to untreated dyes, especially RBBR and Evans Blue, which transitioned from moderate (Class III) to highly toxic (Class IV). Conversely, fungal bioremediation successfully stabilized or diminished toxicity over time. Of the two fungi, *T. versicolor* (CB8) shown a greater detoxifying capability for Evans Blue and Crystal Violet, whereas *P. ostreatus* (BWPH) demonstrated notable efficacy in diminishing RBBR toxicity. The significant decrease in Crystal Violet toxicity from Class V to Class IV by CB8 signifies a substantial enhancement in environmental safety. These findings validate that white-rot fungi are very efficient biological agents for the detoxification of synthetic dye-laden wastewaters, markedly diminishing their ecological threat to aquatic life.

Table 15. Assessment of zootoxic effects on *Daphnia magna* exposed to pure dyes (Remazol Brilliant Blue R, Evans Blue, and Crystal Violet), dye-treated samples using *Trametes versicolor* (CB8) and *Pleurotus ostreatus* (BWPH), and pure fungal cultures without dye, based on exposure duration, EC_{50} values, toxicity units (TUa), and Persoone toxicity classes

Dye	Fungal bioremediation treatment	Exposure Time (h)	Half maximal effective concentration EC_{50} [%]	Toxicity Unit (TUa)	Persoone Toxicity Class
Remazol Brilliant Blue R	Pure dye	24	33.60	3	III
		48	9.20	10.87	IV
	Effluent treated with *T. versicolor* (CB8)	24	22.11	4.52	III
		48	15.92	6.28	III
	Effluent treated with *P. ostreatus* (BWPH)	24	45.21	2.21	III
		48	14.23	7.03	III
Evans Blue	Pure dye	24	35.36	2.83	III
		48	7.10	14.08	IV
	Effluent treated with *T. versicolor* (CB8)	24	52.50	1.90	III
		48	25	4.00	III
	Effluent treated with *P. ostreatus* (BWPH)	24	53.45	1.87	III
		48	15.97	6.26	III
Crystal Violet	Pure dye	24	<<6.25	>100	V
		48	<<6.25	>70	IV
	Effluent treated with *T. versicolor* (CB8)	24	9.93	10.07	IV
		48	5.27	18.97	IV
	Effluent treated with *P. ostreatus* (BWPH)	24	<6.25	>70	IV
		48	<<6.25	>70	IV
No dye	Growth medium with *T. versicolor* (CB8)	24	58.4	1.71	III
		48	24.1	4.15	III
	Growth medium with *P. ostreatus* (BWPH)	24	76.44	1.31	III
		48	70.71	1.41	III

5.8.2 Assessment of Phytotoxicity

The phyto-toxicity was tested on *Spirodela polyrhiza*. The toxicity profile of RBBR exhibited distinct dye-strain specificity in reaction to fungal bioremediation. The pure dye demonstrated

significant toxicity to *Spirodela* polyrhiza (toxicity class IV), highlighting the established environmental hazards associated with sulfonated anthraquinone dyes. Treatment with *T. versicolor* and *P. ostreatus* resulted in a significant rise in EC_{50} and a decrease in TUa, altering the overall toxicity classification from class IV to III. This corresponds with prior research indicating that certain white-rot fungi may proficiently detoxify anthraquinone dyes via enzymatic cleavage of chromophoric rings, but the efficacy of detoxification is heavily influenced by the ligninolytic enzyme profile of each strain [270].

Evans Blue, an azo dye, exhibited moderate toxicity in its unprocessed state (class III). Both fungi enhanced their toxicity profiles; however, *P. ostreatus* attained the most significant detoxifying effect, increasing EC_{50} to over 93.8% and lowering toxicity to class II. This result aligns with prior studies indicating that the degradation of azo dyes by white-rot fungus typically produces less hazardous metabolites through the reductive breakage of azo bonds and subsequent mineralization via ligninolytic pathways. *T. versicolor* also diminished toxicity, while the treated sample persisted in class III. The literature similarly delineates strain-dependent heterogeneity, wherein certain fungi generate aromatic amines during azo dye degradation that retain residual toxicity, while others further metabolize these intermediates into less deleterious chemicals. The robust detoxification capacity of *P. ostreatus* in our investigation corroborates its established efficacy as a biological agent for azo dye cleanup.

Crystal Violet had the greatest intrinsic toxicity among the evaluated dyes, characterized by exceedingly low EC_{50} values and classified within the most hazardous group, possessing the highest TUa. This is anticipated, as triphenylmethane dyes such as CV are recognized for their durability, mutagenic properties, and ability to significantly limit growth in aquatic vegetation. The fungal treatment yielded divergent results: *T. versicolor* markedly diminished toxicity (class IV to III), whereas *P. ostreatus* failed to effectuate considerable detoxification, maintaining toxicity in class IV. The observed differences correspond to trends documented in prior investigations, wherein *T. versicolor*, owing to its robust laccase activity, may efficiently oxidize triphenylmethane compounds, resulting in less hazardous byproducts. Conversely, several fungal strains metabolize CV incompletely, yielding intermediates that maintain significant toxicity. The continued presence of toxicity after *P. ostreatus* treatment in our findings indicates either inadequate degradation or the generation of detrimental transformation products, aligning with recognized difficulties in the bioremediation of triphenylmethane dyes.

Collectively, these data underscore a fundamental problem prevalent in the mycoremediation literature: decolorization does not inherently imply detoxification. Although white-rot fungi are well-known for their capacity to decompose a variety of dyes via ligninolytic enzymes, including laccases, peroxidases, and oxidases, their efficacy in reducing ecotoxicity is significantly influenced by (1) the chemical structure of the dye, (2) the metabolic capabilities of the fungal strain, and (3) the characteristics of the degradation intermediates generated. Numerous published research indicate instances of significant color removal accompanied by persistent residual toxicity, frequently attributed to stable aromatic by-products. Our findings substantiate this observation and illustrate the essential importance of integrating ecotoxicity assays, such as *Spirodela* growth inhibition tests, into wastewater remediation research.

The decreased toxicity observed, especially for RBBR and Evans Blue by *P. ostreatus* and for Crystal Violet by *T. versicolor*, highlights the efficacy of fungal bioremediation in alleviating ecological risks linked to dye-laden effluents. These enhancements correspond with a growing corpus of research underscoring fungal treatment as a viable, environmentally sustainable alternative to chemical and physical wastewater treatment approaches, particularly where detoxification, rather than mere decolorization, is the objective.

Table 16. Assessment of phytotoxic effects on *Spirodela polyrhiza* exposed to pure dyes (Remazol Brilliant Blue R, Evans Blue, and Crystal Violet), dye-treated samples using *Trametes versicolor* (CB8) and *Pleurotus ostreatus* (BWPH), and pure fungal cultures without dye, based on EC_{50} values, toxicity units (TUa), and Persoone toxicity classes

Dye	Fungal bioremediation treatment	EC_{50} [%]	TUa (Class)	Level of toxic effect
Remazol Brilliant Blue R	Pure dye	8.11	12.31	IV
	Effluent treated with *T. versicolor* (CB8)	15.94	6.27	III
	Effluent treated with *P. ostreatus* (BWPH)	44.04	2.27	III
Evans Blue	Pure dye	18.62	5.37	III
	Effluent treated with *T. versicolor* (CB8)	82.23	1.21	III
	Effluent treated with *P. ostreatus* (BWPH)	>93.8	0.34	II
Crystal Violet	Pure dye	1.31	76.33	IV
	Effluent treated with *T. versicolor* (CB8)	10.13	9.86	III
	Effluent treated with *P. ostreatus* (BWPH)	<5.86	>70	IV
No dye	Effluent with *T. versicolor* (CB8)	67.34	1.48	III
	Effluent with *P. ostreatus* (BWPH)	96.81	1.033	II

5.9 Evaluation of impact of different light conditions on dye degradation

Light is a significant environmental component that can affect fungal physiology, metabolism, and enzyme synthesis. Despite the fact that most white-rot fungi are non-photosynthetic, exposure to various light wavelengths has been documented to influence secondary metabolism, oxidative stress responses, and the expression of ligninolytic enzymes, including laccase, manganese peroxidase, and lignin peroxidase, which are pivotal in the degradation of xenobiotics and dyes [271]. Light serves as a regulatory signal that impacts fungal growth patterns and redox balance, therefore indirectly regulating the breakdown efficiency of recalcitrance chemicals, such as synthetic dyes [272]. Thus, examining the influence of light

conditions on dye decolorization yields valuable insights for enhancing fungal-based bioremediation systems.

This study assessed the impact of various light conditions (dark, white, blue, green, and red light) on the decolorization of RBBR dye by *T. versicolor* (CB8) and *P. ostreatus* (BWPH) under Treatment 1, in which dye was introduced to a 7-day-old actively growing fungal culture. Both fungal strains demonstrated significant RBBR decolorization efficiency (>93%) under all examined light conditions at both 24 and 72 hours, reflecting substantial degradation capability and metabolic resilience (Figure 45(a)). For *T. versicolor*, decolorization at 24 hours varied from 96.2% to 97.8%, with only slight changes among light treatments, indicating that initial RBBR removal was predominantly unaffected by light exposure. At 72 hours, a minor reduction was noted under dark conditions (93.3%), but white and blue light preserved elevated decolorization levels (~97%), suggesting that light exposure may enhance enzyme activity during extended incubation. *P. ostreatus* exhibited a slight enhancement in RBBR decolorization with time, attaining 98.1% at 72 hours under darkness, whereas alternative light treatments also facilitated consistently elevated removal rates exceeding 97%. The results indicate that both fungi can effectively decolorize RBBR irrespective of light conditions, while light may boost long-term breakdown efficiency by promoting oxidative enzyme regulation.

A comparable trend was noted for EB dye, with exceptionally high decolorization efficiency (>98%) documented for both fungi under all light conditions and incubation durations (Figure 45(b)). *T. versicolor* accomplished nearly total EB elimination within 24 hours, with percentages varying from 98.9% to 99.6%, and these levels were sustained or somewhat enhanced at 72 hours. The most significant decolorization was typically noted under white and green light, suggesting a possible stimulatory influence of these wavelengths on the enzymatic mechanisms associated with EB breakdown. *P. ostreatus* exhibited remarkable EB decolorization, while somewhat reduced values were observed under blue and green light at 24 hours, subsequently improving at 72 hours. The continuously elevated elimination of EB relative to RBBR indicates that EB is more readily biodegradable, perhaps owing to its simpler molecular structure and greater vulnerability to oxidative degradation by fungal enzymes.

The findings demonstrate that the introduction of dyes into a mature (7-day-old) fungal culture resulted in both *T. versicolor* and *P. ostreatus* displaying significant and swift decolorization capabilities, which are only little affected by light conditions. This indicates that the existing enzymatic apparatus and biomass exert a greater influence on dye removal efficiency than light exposure. Nonetheless, minor enhancements or stabilization at particular light wavelengths indicate the possibility for light-mediated modulation of fungal metabolism, which might be utilized to optimize large-scale fungal bioremediation efforts.

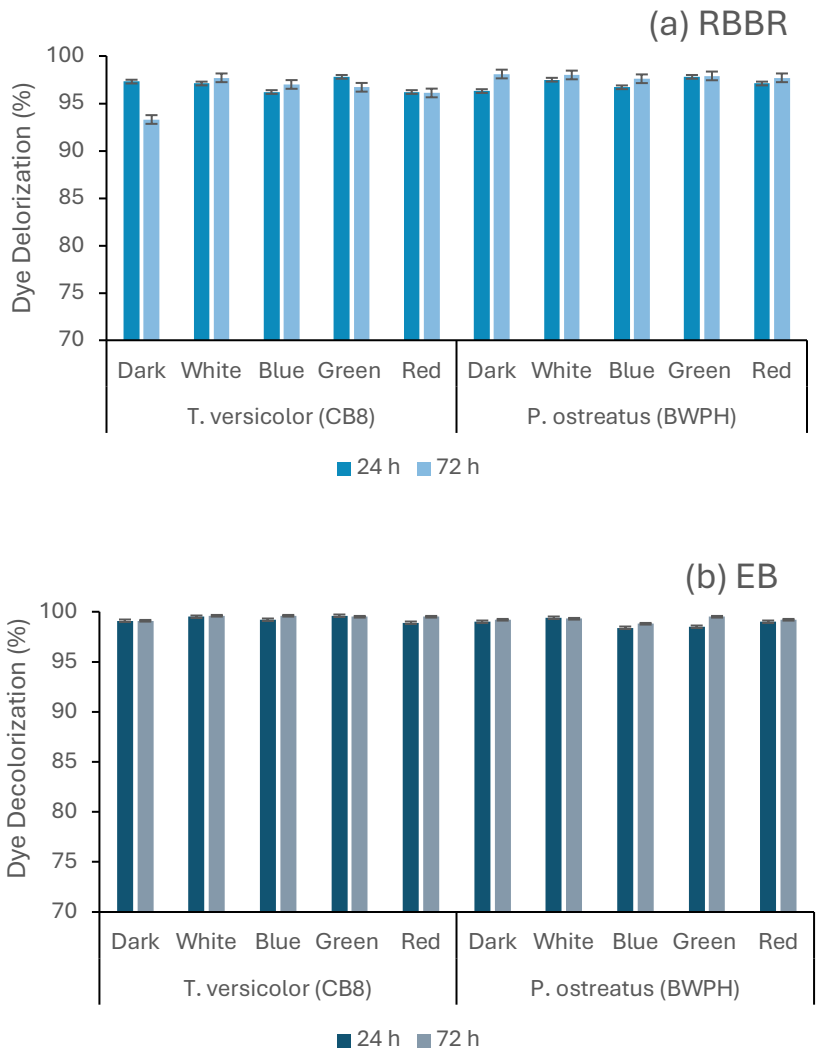

Figure 45. Decolorization of (a) Remazol Brilliant Blue R and (b) Evans Blues dyes under different light conditions using Treatment 1- dye added to 7 day old pre-grown mycelia

The impact of varying light conditions on the decolorization of RBBR and Evans Blue dyes by *T. versicolor* (CB8) and *P. ostreatus* (BWPH) was assessed when the dye and fungus inoculum were introduced concurrently on day zero. Decolorization consistently increased with incubation time across all light conditions, demonstrating that dye removal was a time-dependent biological process linked to fungal growth and the gradual generation of ligninolytic enzymes. In the case of RBBR, *T. versicolor* exhibited significant decolorization at 48 hours (about 90-93%) across all light conditions, and these levels were persistently elevated at 120 hours, indicating that the degradation of RBBR by this fungus was predominantly unaffected by light (Figure 46(a)). Marginally increased decolorization under green and red light at 120 hours suggests a potential stimulatory influence of these wavelengths on enzyme activity. Conversely, *P. ostreatus* exhibited more variability at 48 hours, with less decolorization under white and blue light; yet, by 120 hours, RBBR removal surpassed 91% across all conditions, suggesting that the initial impacts of light diminished with extended incubation.

Evans Blue decolorization was more significantly affected by light conditions than RBBR (Figure 46(b)). At 48 hours, both fungi exhibited less EB decolorization under blue and white light, especially *P. ostreatus*, indicating an early suppression of fungal metabolism or enzyme production under these wavelengths. Dark, green, and red lighting settings facilitated relatively greater EB elimination in the initial period. By 120 hours, decolorization significantly increased for both fungi, with *T. versicolor* attaining over 92% clearance across all light conditions and demonstrating optimal effectiveness under green light. *P. ostreatus* shown enhanced EB decolorization at 120 hours; nevertheless, its efficacy was inferior to that of *T. versicolor*, particularly under blue light, suggesting heightened light sensitivity. The findings indicate that *T. versicolor* exhibits greater tolerance to light fluctuations and superior efficacy in dye decolorization, but *P. ostreatus* is more influenced by light quality, especially in the first incubation phase. Green and red light typically promoted dye decolorization, while blue light shown an inhibitory effect, particularly on the more intricate Evans Blue dye.

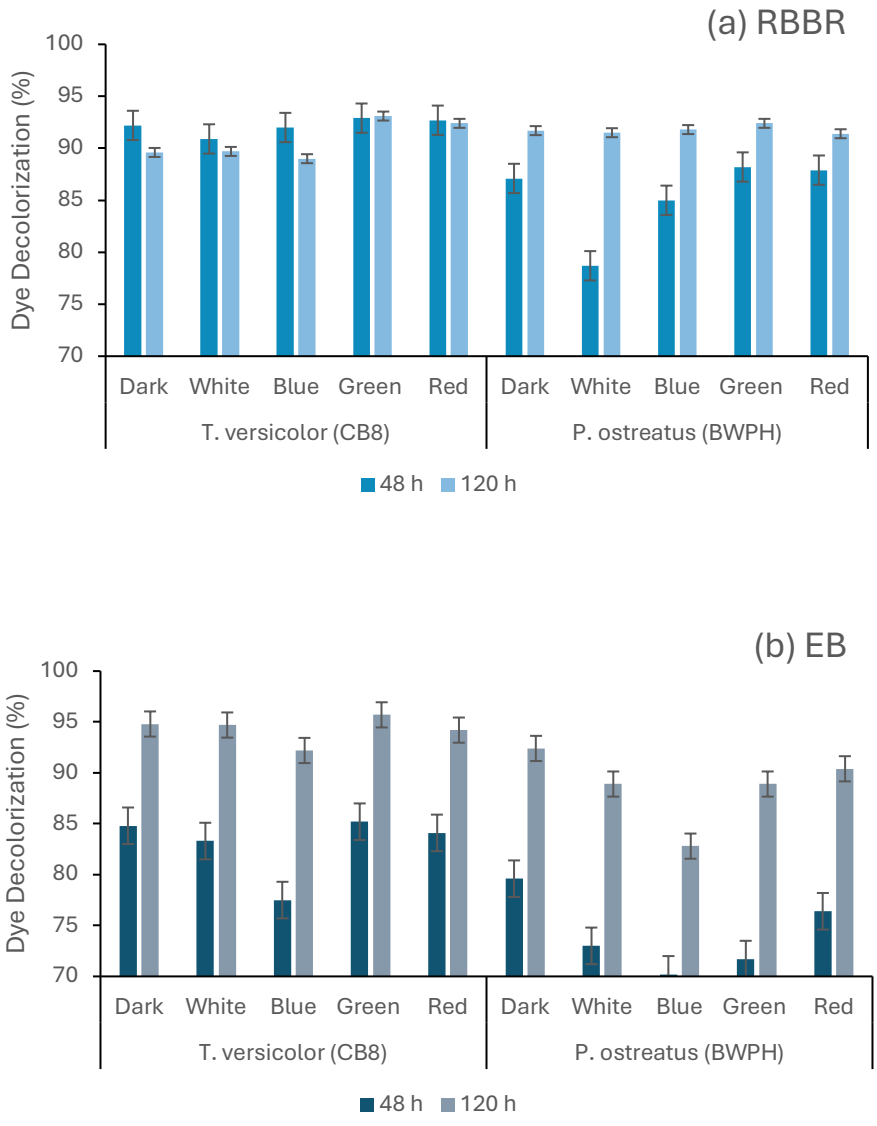

Figure 46. Decolorization of Remazol Brilliant Blue R dyes under different light conditions using Treatment 2 where dye and fungal inoculum added simultaneously

5.10 Evaluation of Triphenylmethane Dye decolorization by biosorption

The experimental aspect of this research work examined the biosorption capabilities of selected fungal species (CB8 and BWPH) for two triphenylmethane dyes-Brilliant Green and Crystal Violet-has been published as **Publication 3**.

5.10.1 Effect of Immobilization on dye sorption potential

The principal studies were designed to evaluate the biosorption efficacy of developed biosorbents from CB8 and BWPH strains in both self-immobilized and sponge-immobilized forms. Table 17 demonstrates that, at initial concentrations of BG and CV dye at 200 mg/L, the greatest decolorization was attained by live immobilized fungal biomass in contrast to non-immobilized fungal biomass. The sorption capacity for both examined dyes was increased by a minimum of three fold with the application of CB8/S2-BS and BWPH/S2-BS. The BG dye was eliminated up to 90.3% via CB8/S2-BS within a 6 hours, demonstrating exceptional removal effectiveness and rapidity. Sponge cubes were covered with live fungal biomass, facilitating interaction between dye molecules and the functional groups of the fungal hyphae. The principal process by which living biomass eliminates dyes is the compound's bioaccumulation in the cytoplasm and cell wall. The utilization of sponges may lead to an increased surface area, hence facilitating improved dye sorption by living fungal biomass. During the evaluation of autoclaved-dead biomass of CB8/S2-BS-A, it eliminated 48.4% of BG and 22.8% of CV dye. This rate exceeds that of self-immobilized biomass, although is less effective than that of live biomass. In a similar manner, the dead immobilized *P. ostreatus* biosorbent was not as efficient as the living biomass.

Both dyes are classified under the triarylmethane group; nevertheless, variations in functional groups and their interactions with fungal mycelium may lead to differences in sorption capability. The BG dye comprises an organic hydrogen sulfate salt, while the CV dye consists of an organic chloride salt. Iqbal and Saeed [112] obtained comparable results, demonstrating that the immobilization of *Phanerochaete chrysosporium* fungal biomass on loofa sponge improved the sorption of Remazol Brilliant Blue R dye by 18.60% relative to non-immobilized fungal biomass. A recent work shown that a loofah sponge manufactured with Ca-alginate achieved a methylene dye sorption capacity of 180 mg/g [273], but the zinc nanoparticle-loofah sponge composite was not significantly efficient in improving the sorption of trypan blue [274]. Consequently, it is essential to investigate various sponge fabrications to improve dye sorption capability. Our discovery is significant, as it introduces an eco-friendly, economical sponge modification that facilitates waste disposal.

Table 17. Biosorption capacities of *T. versicolor* and *P. ostreatus* variants for Brilliant Green and Crystal Violet in batch treatment (conditions: C_0= 200 mg/L, biomass dose of self-immobilized biomass= 0.5 g wet/ 10 mL, biomass dose of sponge-immobilized biomass= 1 piece/ 10 mL, Biomass type= Live/Autoclaved-Dead, T = 22.5 °C, t = 6 h) (Published in **Publication 3**)

Biosorbent	Biomass Type	Brilliant Green Sorption (%)	Crystal Violet Sorption (%)
Trametes versicolor (CB8-BS)	Live	14.2	15.6
Immobilized *Trametes versicolor* (CB8/S2-BS)	Live	90.3 ****	43.9 **
Immobilized *Trametes versicolor* (CB8/S2-BS-A)	Autoclaved dead	48.4 ***	22.8 *
Pleurotus ostreatus (BWPH-BS)	Live	23.9	12.1
Immobilized *Pleurotus ostreatus* (BWPH/S2-BS)	Live	81.7 *	39.3 *
Immobilized *Pleurotus ostreatus* (BWPH/S2-BS-A)	Autoclaved dead	30.3^{-}	18.9^{-}
Sponge (S2)	No fungal biomass	49.9 ***	6.5^{-}

(Note: **** $p \leq 0.0001$, *** $p \leq 0.001$, ** $p \leq 0.01$, * $p \leq 0.05$, $^{-}p \geq 0.05$ for one tail *t*-test compared with self-immobilized biomass;[275]).

5.10.2 Brilliant Green sorption by live biosorbent: Role of dye concentration and contact time

This part of research work have been published as **Publication 3.** Biosorption tests for the BG dye were conducted using a concentration range of 100 mg/L to 400 mg/L, an adsorbent dosage of 0.5 g of wet *T. versicolor* CB8-BS or *P. ostreatus* BWPH-BS biosorbent, and a single piece of sponge-immobilized biosorbent. Figure 47 illustrates that the *T. versicolor* CB8 strain biosorbent successfully eliminated 46.9% of BG dye within 6 hours at an initial concentration of 100 mg/L. With an increase in dye concentration to 200 mg/L, the dye removal capability was reduced by half. At elevated dye concentrations, fungal biomass was unable to absorb significant quantities of BG dye. The experimental results indicate that an unstable interaction between the dye and CB8-BS fungal biomass was observed from 0 to 2 hours. Bioaccumulation, physisorption, and chemisorption are primarily responsible for the removal of dye from the aqueous media [276]. Conversely, sponge-immobilized *T. versicolor* biosorbent did not confront this issue, since it commenced dye absorption immediately upon contact with the dye-laden medium. It is observed that the amount of BG absorbed by sponge-immobilized *T. versicolor* CB8/S2-BS biosorbent in just one hour was more than the amount absorbed by CB8-BS by end of 24 h (Figure 47(a)). At the maximum BG dye concentration of 400 mg/L, CB8/S2-BS effectively sorbed about 90% of the dye from the medium. The greatest

dye adsorption capacity of CB8/S2-BS is notable at 379.4 mg/g for Brilliant Green dye within approximately 6 hours (Figure 48).

Table 18 clearly demonstrates that our biosorbent exhibits a significantly higher capacity in comparison to the findings of other researchers who have explored other biological or physicochemical sorbents for the elimination of BG dye. Our study is distinguished by its superior efficiency and rapid removal rate compared to previous fungal sorbents developed for the sorption of several dyes. The loofa sponge-immobilized *Phanerochaete chrysosporium* absorbed Remazol Brilliant Blue R dye, with a capacity of 101.06 mg/g [113]. Nouri et al. [277] attained a maximum biosorption capacity of 58.48 mg/g for Remazol Black dye using dried *Sarocladium* sp. biomass. Chew and Ting [278] employed free-cells and alginate-immobilized forms in bio-sorption research to examine the dye-removal efficacy of *Trichoderma asperellum* on four triarylmethane dyes. In comparison to free cells, *T. asperellum* demonstrated superior dye removal efficacy when utilizing alginate-immobilized forms. Free cells absorbed 12.97, 12.54, 14.34, and 11.44 mg/g of CV, methyl violet, cotton blue, and malachite green, whereas immobilized forms absorbed 60.64, 50.29, 49.91, and 16.61 mg/g, respectively. The augmentation of dye sorption with increasing dye concentration is ascribed to the diminished resistance to dye uptake, hence enhancing dye diffusion [279]. This is highly advantageous for the large-scale treatment of dye-laden wastewater, which necessitates substantial removal efficiency in the shortest possible timeframe.

Figure 47(b) illustrates the sorption of BG dye by *P. ostreatus* BWPH fungus biosorbent at different dye concentrations (100-400 mg/L). During the initial hours (0-5 h), BG dye sorption markedly increases, particularly at reduced dye concentrations (100-200 mg/L). This trend aligns with research on fungal biosorption, indicating that the initial phase is governed by surface adsorption, attributed to the plentiful binding sites on fungal biomass. Electrostatic interactions between dye molecules and constituents of the fungal cell wall, including proteins, glucans, and chitin, facilitate the initial rapid adsorption [280]. The sorption rate diminishes following the initial rapid phase due to the saturation of active binding sites and the reduced diffusion of dye molecules into the deeper layers of fungal biomass. Figure 47(b) indicates that elevated dye concentrations (300-400 mg/L) lead to diminished total dye sorption percentages, contrary to the behaviour observed with *T. versicolor* fungus. The curves demonstrate that BWPH/S2-BS at reduced dye concentrations (100, 200 mg/L) exhibit more dye absorption compared to BWPH-BS alone, with dye sorption amounts of 246.7 mg/g and 302.5 mg/g at their respective initial dye concentrations (Figure 48). This may be ascribed to the augmented surface area or more availability of functional groups in the BWPH/S2-BS condition, presumably enhancing the functional characteristics of the fungal biomass.

(a)

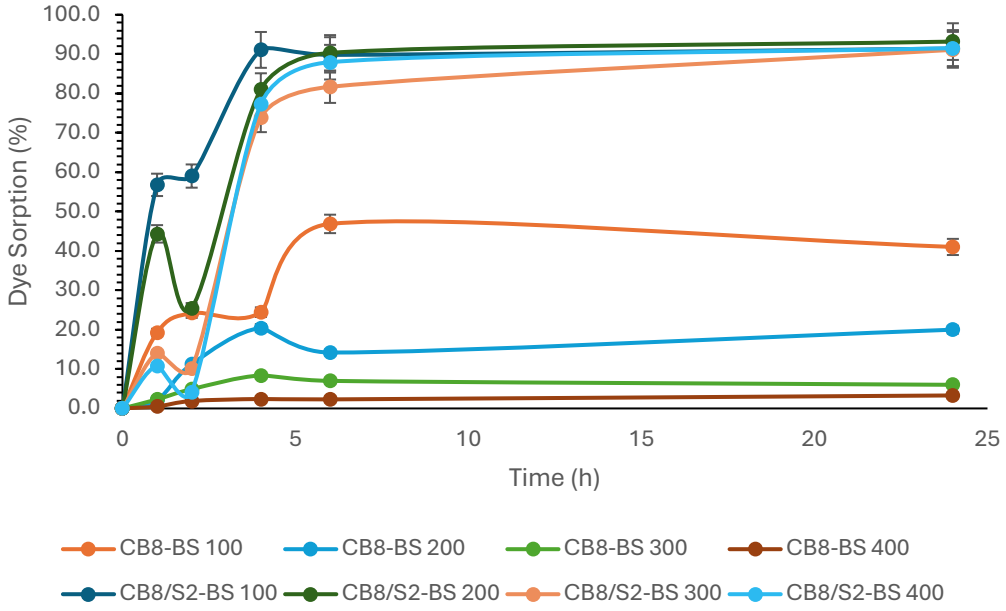

(b)

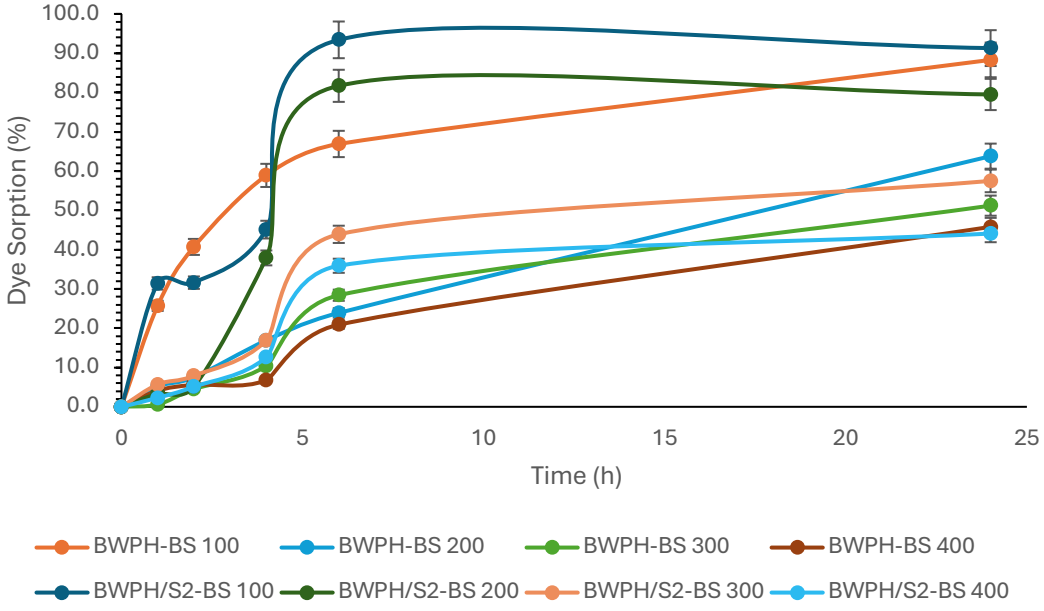

Figure 47. Effect of Brilliant Green dye concentration on dye removal efficiency by live biosorbents of (**a**) *Trametes versicolor* (CB8-BS and CB8/S2-BS) and (**b**) *Pleurotus ostreatus* (BWPH-BS and BWPH/S2-BS) (conditions: C_0 = 100-400 mg/L, biomass dose of self-immobilized biomass = 0.5 g wet/ 10 mL, biomass dose of sponge-immobilized biomass = 1 piece/ 10 mL, T = 22.5 °C, t = 0,1,2,6,24 h) (Published in **Publication 3**).

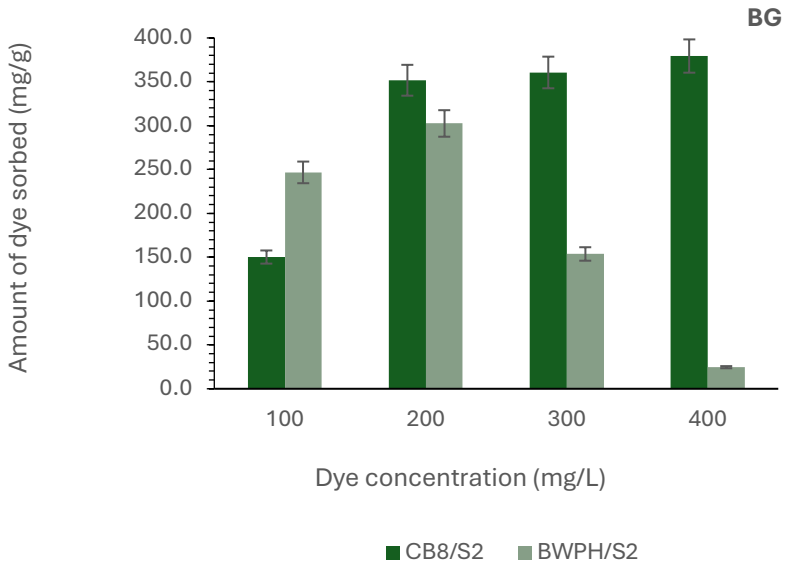

Figure 48. Maximum sorption capacity of Brilliant Green by immobilized *T. versicolor* (CB8/S2-BS) and *P. ostreatus* (BWPH/S2-BS) at varying dye concentrations. (Published in **Publication 3**).

Table 18. Literature comparison of Brilliant Green dye sorption by different physicochemical and biological sorbents (Published in **Publication 3**).

Sorbent (Physicochemical or Biological)	**Optimized Condition: Initial Dye Concentration (mg/L), Time (min), Sorbent Amount (g), pH, Temperature (°C)**	**Biosorption Capacity (mg/g), Decolorization (%)**	**Adsorption Kinetics**	**Reference**
Poly(acrylic acid) hydrogel composite (PAA-K hydrogel) with kaolin clay conventional method	30, 250, 1, 7, 35	6.25, 50%	Pseudo-second-order model, Freundlich and Langmuir Model	[281]
Poly(acrylic acid) hydrogel composite (PAA-K hydrogel) with kaolin clay ultrasound method	30, 375, 1, 7, 35	12.5, 84%	Pseudo-second-order model, Freundlich and Langmuir isotherm	

Activated carbon(AC) derived from guava tree wood	25, 20, 0.8, 7, -	90, 99%	Pseudo-second-order model, Freundlich isotherm	[282]
Trichoderma asperellum- free cells	100, 350, 0.25 5, 30 ± 2	12.97, -	-	[278]
Trichoderma asperellum alginate-immobilized forms	100, 350, 0.25, 5, 30 ± 2	60.64, -	-	
Salix alba leaves (SAL)	50, 210 0.15, 6, 25	15.89, 95.2%	Pseudo-second-order model, Langmuir isotherm	[283]
Sponge-immobilized *Trametes versicolor* (CB8/S2-BS)	**400, 360, 0.5, 4.3, 22.5**	**379.4, 88%**	-	**Our study [275]**
Sponge-immobilized *Pleurotus ostreatus* (BWPH/S2-BS)	**200, 360, 0.5, 4.3, 22.5**	**302.5, 80%**	-	**Our study [275]**

5.10.3 Crystal Violet sorption by live biosorbent: Role of concentration and contact time

This part of research work have been published as **Publication 3.** Correspondingly, as illustrated in Figure 49(a) and (b), there was a pronounced increase in dye sorption over the initial 5 hours, particularly at reduced dye concentrations (100-200 mg/L). The self-immobilized biosorbents of *T. versicolor* CB8 and *P. ostreatus* BWPH exhibited superior efficacy in the removal of Crystal Violet dye relative to Brilliant Green. The disparity in removal can be ascribed to the variance in molecular weight of the two dyes. CB8/S2-BS and BWPH/S2-BS eliminated over 60% of CV dye at reduced dye concentrations. However, per gram of biosorbent, the maximum amount of CV was quite good even at higher dye concentration (Figure 50). Table 19 compares various physicochemical and biological methods for the removal of CV dye. *Ceriporia lacerata* (CLB) powdered mycelial biomass had a biosorption capacity of 239.25 mg/g for CV at a lower initial dye concentration of 100 mg/L [284], while the fungal sorbents CB8/S2-BS and BWPH/S2-BS shown equivalent sorption for

CV dye at elevated concentrations. Moturi and Singara Charya attained comparable decolorization of Crystal Violet and Malachite Green dyes via WRF, requiring roughly 15 days for decolorization through biodegradation [285]. In our study, the biosorption process facilitated dye removal in a shorter timeframe. The biosorption mechanism did not achieve full equilibrium after 24 hours for lower dye concentrations. Longer contact durations may be necessary due to the slow occupancy of particularly active sites at a low driving force (concentration gradient). While this does not diminish the biosorbent's efficacy, it suggests that, in practical applications, extended treatment durations or continuous-flow systems may be necessary to enhance dye removal efficiency, particularly for diluted wastewater streams. Consequently, it may be relevant in the initial phases of wastewater treatment, where a significant portion of the dye can be absorbed by the immobilized biomass. The immobilized biomass offers a significant benefit for the facile separation of biomass during wastewater treatment.

(a)

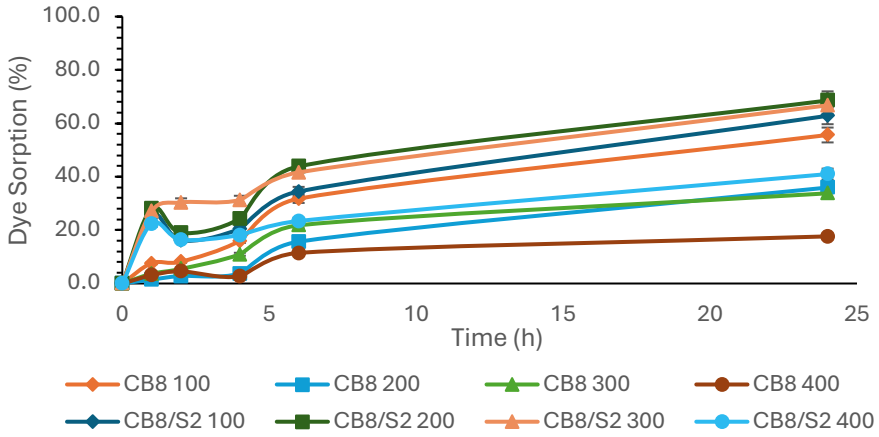

(b)

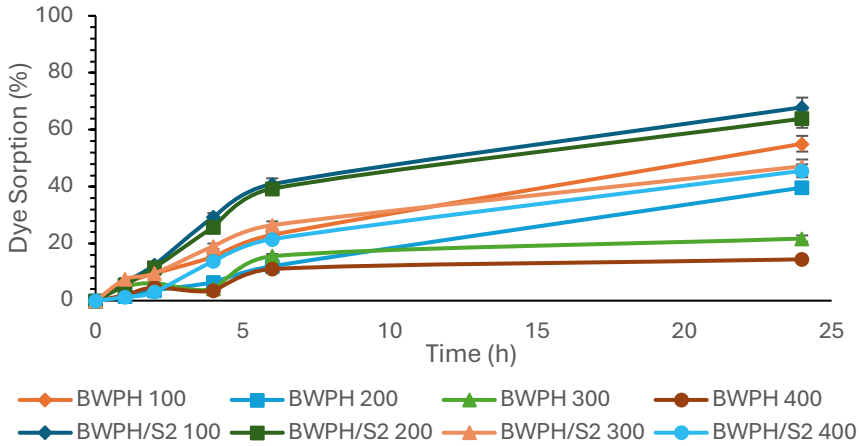

Figure 49. Effect of Crystal Violet dye concentration on dye removal efficiency by live biosorbents of (**a**) *Trametes versicolor* (CB8-BS and CB8/S2-BS) and (**b**) *Pleurotus ostreatus* (BWPH-BS and BWPH/S2-BS) (conditions: C0= 100-400 mg/L, biomass dose of self-immobilized biomass= 0.5 g wet/ 10 mL, biomass dose of sponge-immobilized biomass = 1 piece/ 10 mL, T = 22.5 °C, t = 0,1,2,6,24 h) (Published in **Publication 3**)

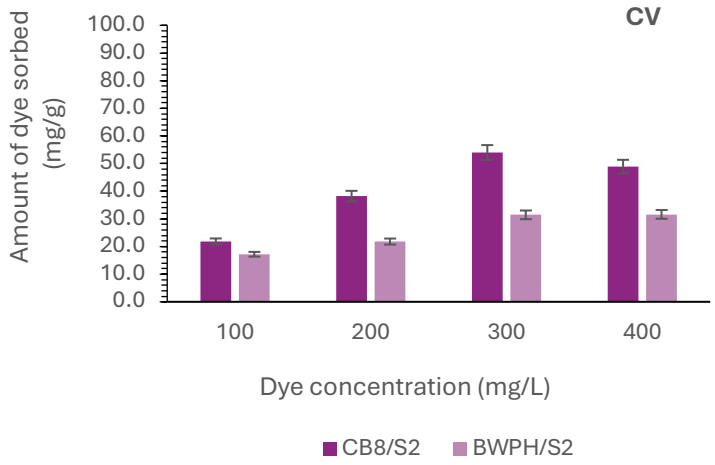

Figure 50. Maximum sorption capacity of Crystal Violet by immobilized *T. versicolor* (CB8/S2-BS) and *P. ostreatus* (BWPH/S2-BS) at varying dye concentrations (Published in **Publication 3**)

Table 19. Literature comparison of Crystal Violet dye sorption by different physicochemical and biological sorbents (Published in **Publication 3**).

Sorbent (Physicochemical or Biological)	Optimized Condition: Initial Dye Concentration (mg/L), Time (min), Sorbent Amount (g), pH, Temperature (°C)	Biosorption Capacity (mg/g), Decolorization (%)	Adsorption Kinetics	Reference
Coriolopsis sp. (1c3) filamentous fungi-free-mycelium forms	100, 2880, 1, 5, -	-, 58.3%	-	[286]
Coriolopsis sp. (1c3) filamentous fungi-filamentous biofilm	100, 2880, 1 g biomass on muslin cloth, 5, -	-, 85.1%	-	
Biochar derived from palm kernel shell (BC-PKS)	50-500, 1440, 0.5, - 25	24.45, -	Pseudo-second-order model, Langmuir isotherm	[287]
Ceriporia lacerata (CLB)- powdered mycelial biomass	100, 780, 0.01, - 20	239.25, -	Pseudo-second-order model, Koble-Corrigan model	[284]

Adiantum capillus-veneris plant leaves	30, 90, 0.06, 3, -	9.05, 90.36%	Pseudo-second-order model, Freundlich isotherm	[288]
Sponge-immobilized *Trametes versicolor* (CB8/S2-BS)	**300, 360, 0.5, 4.3, 22.5**	**54, 40%**	**-**	**Our study [275]**
Sponge-immobilized *Pleurotus ostreatus* (BWPH/S2-BS)	**400, 360, 0.5, 4.3, 22.5**	**31.6, 21%**	**-**	**Our study [275]**

5.10.4 Principal Component Analysis for dye sorption

This part of research work has been published as **Publication 3**. This research was validated by principal component analysis utilizing R version 4.5.0. The PCA biplot (Figures 51 and 52) illustrates the correlations across contact times (T1, T2, T4, T6, and T24), biomass types, and immobilization methods (CB8-BS, CB8/S2-BS, BWPH-BS, BWPH/S2-BS), alongside their respective dye removal percentages at different beginning dye concentrations (100-400 mg/L).

In Figure 51(a), Principal Component 1 (Dim1) explains 85.9% of the total variance, indicating the dataset's predominant trends. The relationship between contact time and starting dye concentration is strongly correlated with Dim1, as seen by their vector orientations and magnitudes. The significant connection between contact time and initial dye concentration vectors with Dim1 suggests that this axis mostly reflects the combined effect of dye availability and exposure duration on fungal biosorption capability. Biologically, increased initial dye concentrations amplify the mass transfer driving force, while prolonged contact times ensure more complete occupation of binding sites, both of which are critical parameters affecting biosorption effectiveness in fungal systems. A comparable trend was observed in Figure 51(b). Extended vectors indicate that these variables significantly affect sample differentiation, in conjunction with Dim1. Increased dye concentrations and extended contact durations are likely responsible for the observed variance in sorption efficiency. The CB8-BS (free-fungal) and CB8/S2-BS (immobilized) clusters are significantly differentiated by Dim1. CB8/S2-BS samples (e.g., score: 76.7) are positioned further along the positive axis of Dim1 compared to CB8 (e.g., score: 72.4), indicating enhanced Brilliant Green dye sorption efficacy under sponge-immobilized experimental circumstances.

The PCA biplot analysis (Figure 50(b)) similarly illustrates the efficacy of immobilizing *P. ostreatus* (BWPH/S2-BS) for the removal of BG dye. Dim1 (84.7% variation) illustrates the substantial influence of contact duration and starting dye concentration on sorption effectiveness, with BWPH/S2-BS surpassing BWPH-BS under high-stress circumstances. In both fungal species, the immobilization matrix (S2) seems to mitigate the constraints imposed

by elevated dye concentrations, since the CB8/S2-BS and BWPH/S2-BS clusters are situated nearer to areas linked with effective sorption, despite differing dye levels. Extended contact duration positively correlates with sorption efficiency in both strains, although CB8/S2-BS demonstrates superior efficiency at shorter intervals, indicating more rapid saturation kinetics. CB8/S2-BS and BWPH/S2-BS exhibit diminished sensitivity to increased dye concentrations, presumably attributable to enhanced stability and accessibility of the active site resulting from immobilization. A comparative examination of *P. ostreatus* (BWPH/S2-BS) and *T. versicolor* (CB8/S2-BS) demonstrates consistent advantages of immobilization among fungal species, but species-specific metabolic characteristics may influence matrix interactions. This enhancement is ascribed to the protective properties of the S2 matrix, which presumably stabilizes the fungal biomass and improves reusability.

The PCA biplots (Figure 52(a) and (b)) depict the correlation among contact time, initial CV dye concentration, and sorption efficiency for two fungus species: *T. versicolor* (CB8-BS and CB8/S2-BS) and *P. ostreatus* (BWPH-BS and BWPH/S2-BS). Both biplots are predominantly influenced by Dim1, which accounts for 91% of the total variation in *T. versicolor* (CB8-BS) and 91.8% in *P. ostreatus* (BWPH-BS), respectively, signifying that the principal patterns in the data are significantly governed by experimental circumstances (contact time and dye concentration). Dim2 accounts for about 6.6-6.7% of the variance, indicating minimal secondary effects of self-immobilized biomass on dye removal percentage, since it was distinctly separated from sponge-immobilized biomass. The key factors influencing sample separation are contact duration and initial CV dye concentration, as well as Dim1, demonstrated by their significant correlation with this axis. Immobilized strains (CB8/S2-BS and BWPH/S2-BS) are clearly differentiated from their free counterparts (CB8-BS and BWPH-BS), with Dim1 occupying locations linked to enhanced sorption efficiency. This distinction indicates that immobilization augments dye absorption, presumably owing to enhanced structural stability, greater availability of active sites, and increased resistance to dye toxicity. *P. ostreatus* (BWPH/S2-BS) exhibits a somewhat greater Dim1 variance, indicating a somewhat more predictable sorption behavior compared to *T. versicolor* (CB8/S2-BS). Consequently, immobilization markedly improves CV dye sorption for both fungal species, perhaps offering protection against dye toxicity and enhancing mechanical stability [289]. Immobilization is strongly advised for enhancing the scalability of fungal bioremediation of CV dye. Both CB8/S2-BS and BWPH/S2-BS are viable options, exhibiting minor performance differences that may inform species selection according to particular industrial requirements. These data support immobilization as a scalable approach to improve fungal bioremediation in dye-contaminated effluents [290,291].

(a)

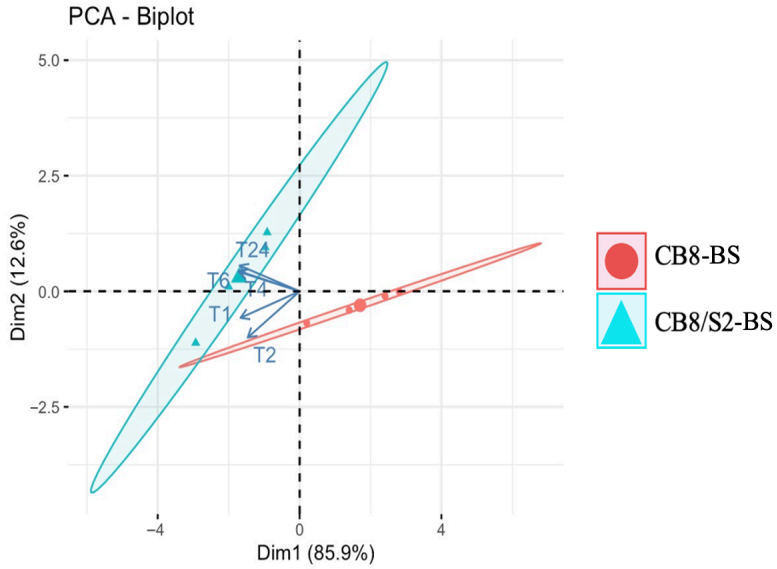

(b)

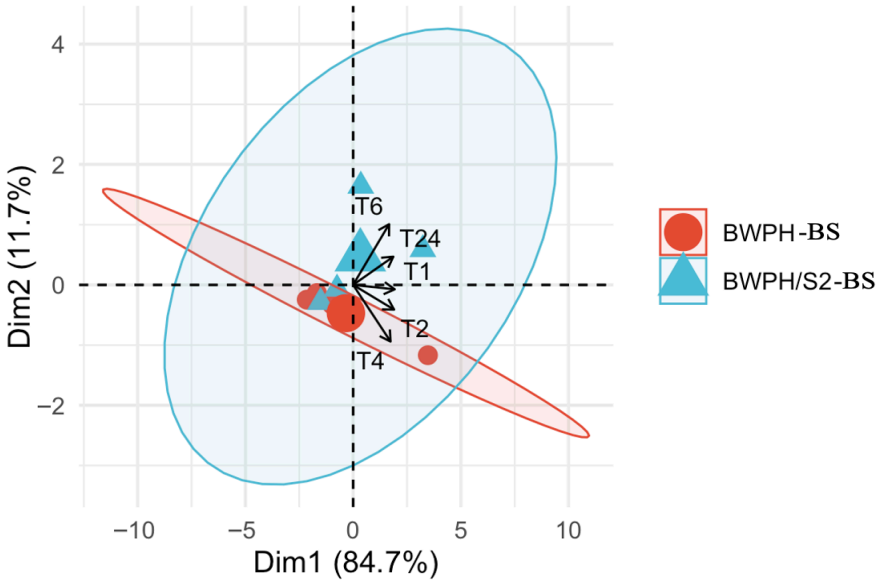

Figure 51. PCA visualization of the combined effects of sorption time and dye concentration on Brilliant Green removal by free and immobilized fungal strains (**a**) *Trametes versicolor* (CB8 and CB8/S2) (**b**) *Pleurotus ostreatus* (BWPH and BWPH/S2) (conditions: C_0 = 100-400 mg/L, biomass dose = 0.5 g wet/10 mL, biomass type = live, T = 22.5 °C, t = 0,1,2,6,24 h) (Published in **Publication 3**)

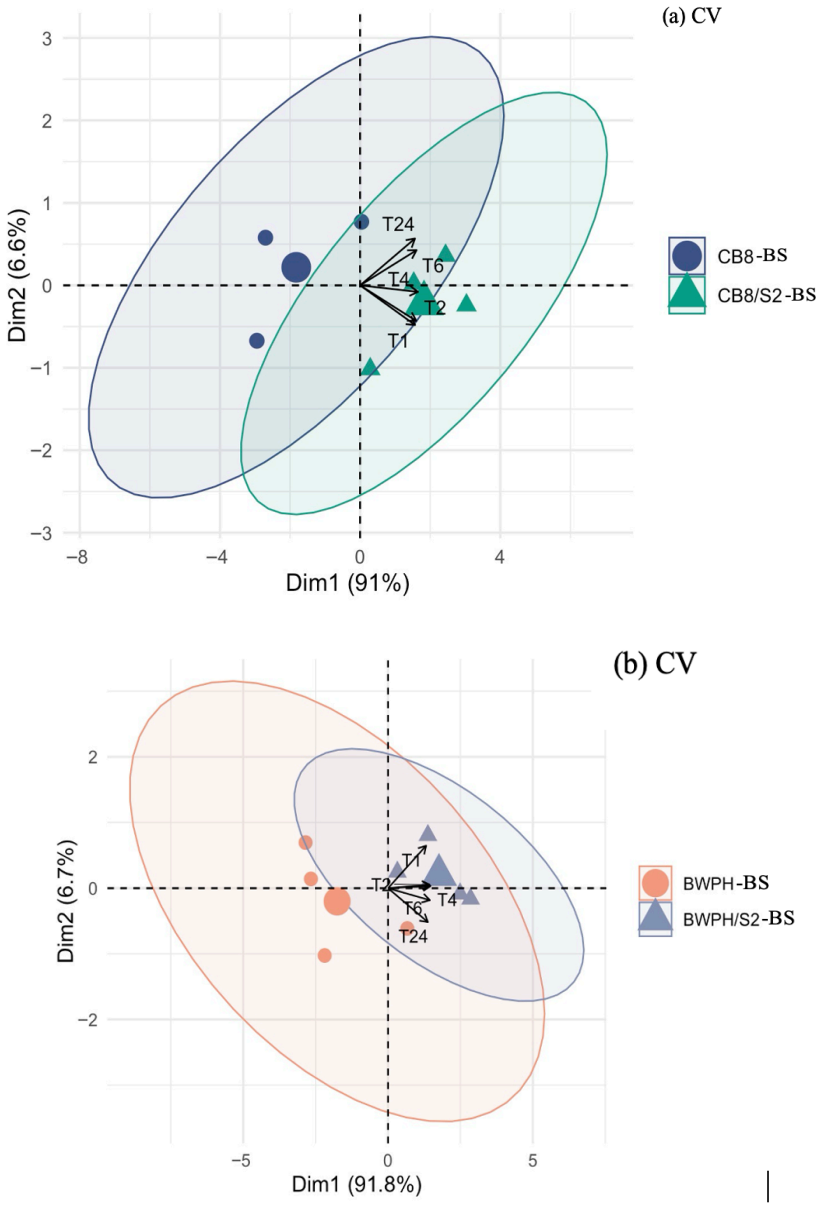

Figure 52. PCA visualization of the combined effects of sorption time and dye concentration on Crystal Violet removal by free and immobilized fungal strains (**a**) *Trametes versicolor* (CB8-BS and CB8/S2-BS) (**b**) *Pleurotus ostreatus* (BWPH-BS and BWPH/S2-BS) (conditions: C_0 = 100-400 mg/L, biomass dose = 0.5 g wet/10 mL, biomass type = live, T = 22.5 °C, t = 0,1,2,6,24 h) (Published in **Publication 3**)

5.10.5 Impact of Autoclaved-Dead Biomass on Triphenylmethane dyes removal

This part of research work has been published as **Publication 3**. The thermally inactivated *T. versicolor* (CB8/S2-BS-A) immobilized biomass was incubated with BG or CV dye solutions at varying dye concentrations. In contrast to live biomass, the autoclaved biomass exhibited no desorption throughout the initial time. The absorption of dye exhibited a progressive rise with extended contact duration. The maximum dye removal for both dyes occurred at the lowest dye concentration. Autoclaved CB8/S2-BS-A successfully eliminated 73% of BG (Figure 53(a))

and 63.1% of CV (Figure 53(b)). Upon autoclaving, self-immobilized CB8-BS-A and BWPH-BS-A biomass had a significant drop in fungal biomass. No significant sorption of dye (less than 8%) was discovered when it was employed for dye removal. Consequently, it was terminated for additional trials, and the sponge-immobilized variant was selected instead.

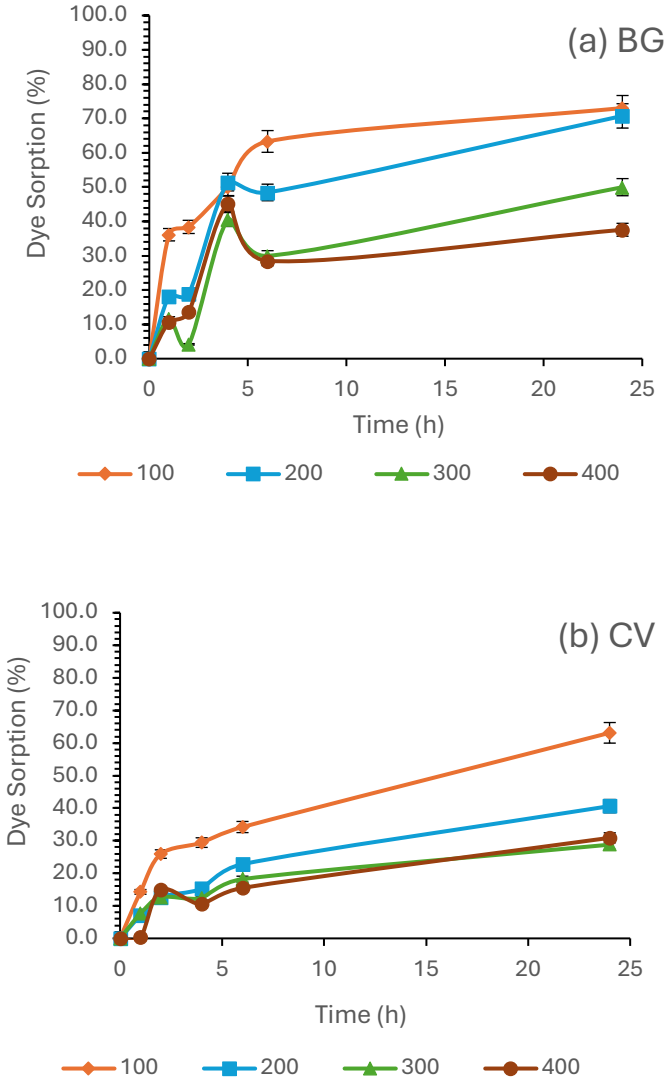

Figure 53. Decolorization potential of autoclaved - immobilized *T. versicolor* (CB8/S2-BS-A) biomass on (**a**) Brilliant Green and (**b**) Crystal Violet (conditions: C_0 = 100–400 mg/L, biomass dose of sponge-immobilized biomass=1 piece/ 10 mL, T = 22.5 °C, t = 0,1,2,6,24 h) **(**published **Publication 3)**

Autoclaving may affect the functional groups on the surface of fungal biomass, resulting in modifications to its biosorption capacity. This may also lead to alterations in the porosity of the sponge, resulting in varied dye-sorption behaviors. In contrasts to the obtained result, the highest Congo Red eliminations (95.37-100%) against live pellets and pellets that have been acid and alkali pretreatment are demonstrated by the autoclaved pellets of *T. versicolor* [292,293].

5.10.6 Effect of biomass grown at static condition on dyes sorption

This part of research work has been published as well in **Publication 3**. The fungal biomass was grown in static condition to compare and contrast the effect of aeration on fungal dye sorption efficiency. A piece of biomass was exposed to dye, demonstrating the fungal biomass's ability to sorb the colour. After seven days of growth, autoclaved biomass was prepared to compare dye sorption by live and autoclaved biomass. CB8 live and autoclaved biomass grown under static conditions showed comparable clearance percentages when dye removal was assessed at 6 hours. Since these strains were proficient at removing their respective dyes, CB8 was tested for BG and BWPH for CV. About 30% of the BG dye was eliminated by CB8 in 6 hours when the original dye concentration was 200 mg/L (Figure 54). In contrast, BWPH static biomass was not very effective at removing CV dye. Distinct fungal growth conditions result in distinct mycelium structures. For example, mycelium grew into a single layer when biomass was generated under static conditions. A tiny, spherical fungal structure developed when the fungus was shaken constantly. The dye sorption capacity was clearly altered by the difference in surface area between the spherical and flattened surfaces [275].

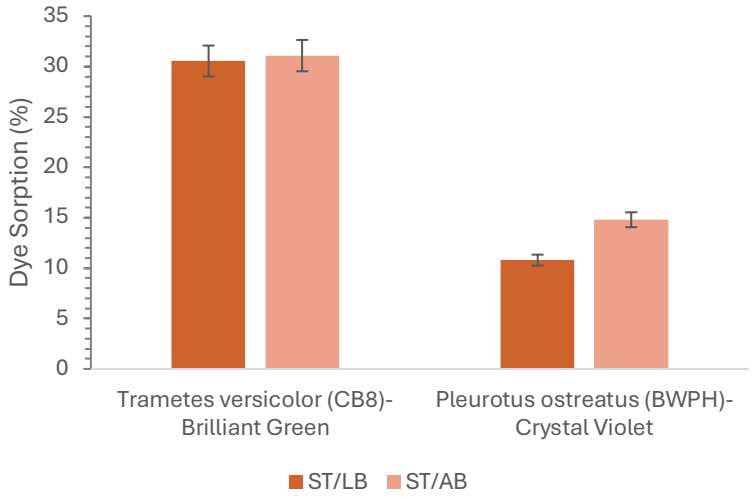

Figure 54. Effect of static (ST) growth condition of live (LB) and autoclaved biomass (AB) of (a) *Trametes versicolor* (CB8) and (b) *Pleurotus ostreatus* (BWPH) respectively on BG and CV dye removal (conditions: C_0 = 200 mg/L, biomass dose = 0.5 g $_{wet}$/10ml, biomass type= Live biomass (LB), Autoclaved Biomass (AB), T = 22.5 °C, t = 6 h)

5.10.7 Influence of Temperature and pH on Brilliant Green sorption

This part of research work has been published as **Publication 3**. Temperature and pH are two essential physicochemical parameters that influence WRF's capacity to absorb dyes. The interaction between dye molecules and the functional groups on the mycelial surface may be affected by the pH level. Likewise, temperature influences membrane fluidity, enzyme kinetics, and the rate of dye molecule absorption by fungi. We employed a central composite design to conduct an experiment assessing the interactive effects of temperature and pH on dye sorption.

Figure 55 S(a), C(a) illustrates the interaction influence of pH and temperature on the biosorption efficiency of Brilliant Green dye by immobilized *T. versicolor* (contour plot). The response surface indicates a substantial dependence on dye removal percentage on both factors. The experimental data aligned closely with the quadratic model ($p < 0.05$), and ANOVA indicated that the lack of fit was non-significant. The anticipated R^2 of 0.9484 aligns reasonably with the corrected R^2 of 0.9825; specifically, the disparity is under 0.2. The biosorption capacity of *T. versicolor* was much greater at lower to moderate temperatures (20.85-32.17 °C) and at moderately acidic to neutral pH levels (pH 3.4-6), reaching a maximum of approximately 50%. This indicates that moderately acidic and mesophilic conditions are optimal for CB8/S2 enzymatic and surface activity. The lower left quadrant of the contour plot (low pH, low temperature) exhibited the most dye removal, indicating optimal sorption efficiency under these conditions. Conversely, the efficacy of biosorption markedly diminished at temperatures over 37 °C, and the pH shifted towards alkaline conditions (>7.3). The rightmost region of the contour plot, indicative of elevated temperatures (up to 49.15 °C) and high pH levels (up to 8.6), exhibited minimal dye elimination (<10%), likely due to the degradation of fungal cell surfaces and the denaturation or inhibition of enzymes responsible for dye binding and degradation. The concept that both excessively low and high extremes of pH and temperature might hinder biosorption efficacy is substantiated by the transition zone illustrated in the central region of Figure 55 S(a), C(a) (pH ~6, temperature ~32-37 °C), where significant dye removal (30-40%) is observed. The results indicate that maintaining moderate temperatures (25-35 °C) and slightly acidic conditions (pH 4.0-6.0) is essential for optimizing the biosorption of Brilliant Green dye using *T. versicolor*. Utilizing BWPH/S2-BS for BG dye sorption adhered to the 2FI model, revealing that optimal dye sorption (approximately 50%) occurred at low pH levels (3.4-4.7) and reduced temperatures (20.85-26.5 °C), suggesting that acidic conditions and diminished thermal energy enhance dye absorption by *P. ostreatus* (Figure 55 S(b), C(b)). These conditions likely facilitate increased surface binding or electrostatic attraction between the fungal biomass and the cationic Brilliant Green molecules, as fungal cell walls exhibit a higher negative charge under acidic pH levels. Analogous to the *T. versicolor* strain, elevated temperature and pH resulted in a gradual decrease in dye removal, with sorption effectiveness dropping below 30% at pH levels exceeding 6 and temperatures surpassing 32 °C. The minimal biosorption efficacy (<10%) was observed in the extreme top-right quadrant of the plot, characterized by elevated pH (8.6) and high temperature (49.15 °C), indicating that the thermal and chemical circumstances are detrimental to dye interaction and fungal metabolism.

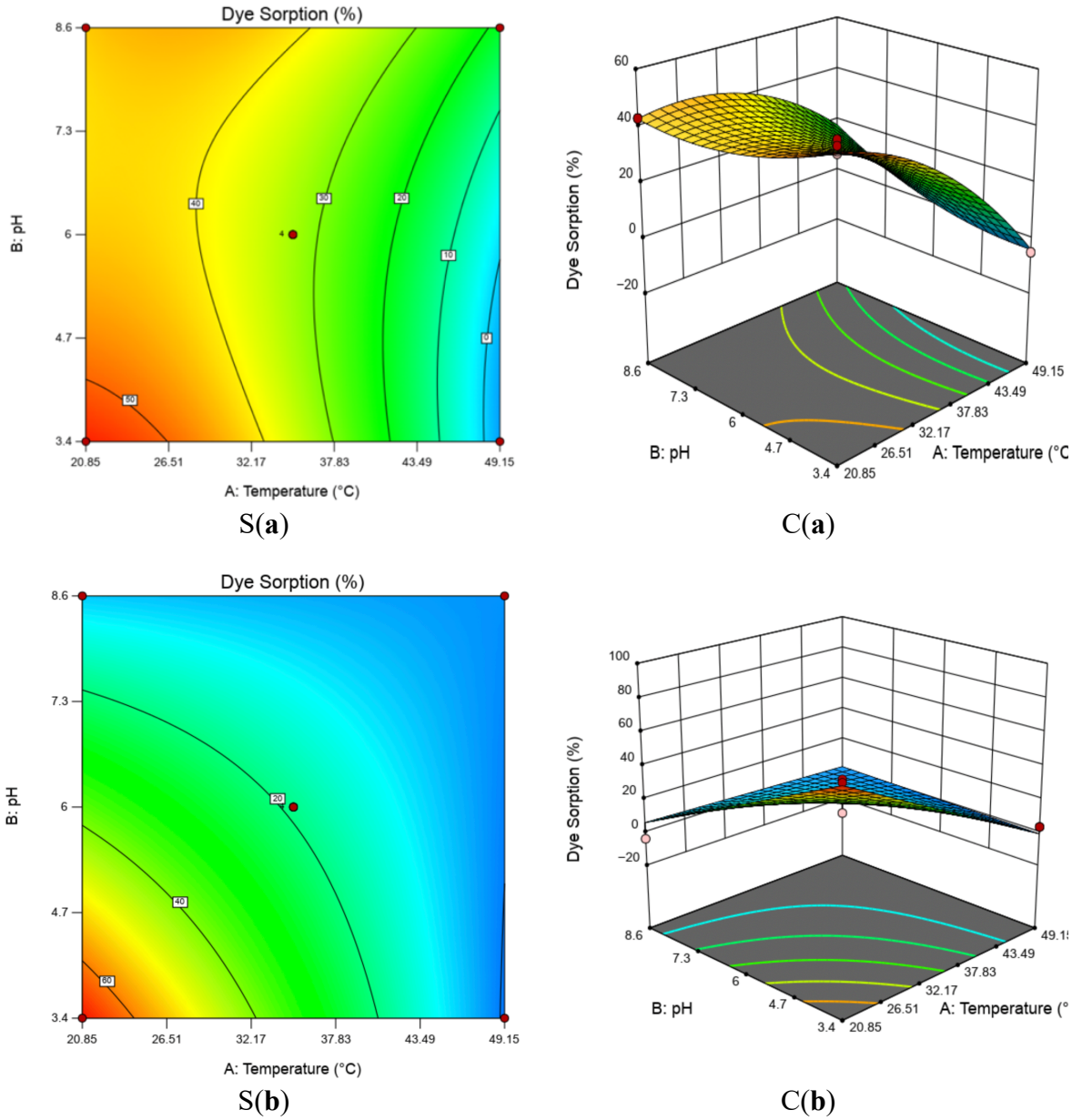

Figure 55. Combined influence of pH and temperature on Brilliant Green sorption capacity of immobilized (a) *T. versicolor* (CB8/S2-BS) and (b) *P. ostreatus* (BWPH/S2-BS): surface and contour visualization (Published in **Publication 3**)

5.10.8 Influence of Temperature and pH on Crystal Violet sorption

This part of research work has been published as **Publication 3**. The CV biosorption by immobilized *T. versicolor* and *P. ostreatus* are visible in Figures 56(c) and (d). Likewise, BG dye, several pH and temperature ranges were investigated to ascertain the optimal conditions for fungal dye sorption. The maximum dye sorption (~40%) for CV dye removal by CB8/S2-BS is observed at a pH of 6.5-7.5 and a temperature of approximately 30 °C, as indicated by the analysis of the plot's surface morphology. Sorption significantly decreases at elevated temperatures and reduced pH levels, resulting in a descending gradient on the three-dimensional surface. Negative or near-zero values indicate minimal activity or desorption

phenomena under harsh conditions. The fit summary for CB8/S2 indicated that the quadratic model was appropriate for the data ($p < 0.05$), whereas the ANOVA test showed a non-significant lack of fit ($p > 0.05$). The predicted R^2 and adjusted R^2 values diverged by over 0.2, indicating a restriction in the model's predictive efficacy, despite its utility in identifying the optimal conditions for dye removal. Simultaneously, the 2FI model was markedly favored by immobilized *P. ostreatus* (p value = 0.0003) in comparison to the linear model (p value= 0.1296). An ANOVA test of the developed model indicated a non-significant lack of fit ($p > 0.05$). Moreover, the disparity between the Adjusted R^2 of 0.8451 and the Predicted R^2 of 0.7042 was within 0.2, signifying a commendable concordance.

As a cationic dye, CV binds to negatively charged entities on the fungal cell wall, including phosphate, carboxyl, or hydroxyl groups. Protonation of functional groups diminishes electrostatic interactions at low pH levels (<5), resulting in reduced dye uptake. Deprotonated sites enhance binding efficacy at elevated pH levels (~7). Membrane fluidity is a crucial determinant of dye sorption, as biosorption involves both chemisorption and physisorption. A moderate temperature enhances dye absorption and degradation by augmenting membrane fluidity and enzyme kinetics. Elevated temperatures (>40 °C) can diminish biosorption by denaturing enzymes, compromising membranes, and obstructing metabolic processes. The phenomena can be elucidated by a progressive decline in sorption as the temperature exceeds around 35 °C. Our results align with those of Lin et al. [284] and Grassi et al. [294]. The absorption of CV from aqueous solution has utilized powdered mycelial biomass of the basidiomycetous fungus *Ceriporia lacerata*. Within a pH range of 2-10, the quantity of absorbed CV per unit biomass weight by *C. lacerata* increased with the elevation of the dye solution's pH, particularly up to pH 6. No significant increase in dye sorption was seen between pH 6 and pH 10. According to Grassi et al., dye sorption increased with pH, achieving around 87% dye removal at pH 6 [294]. The removal rate sustained at 87% within the pH range of 6 to 10.

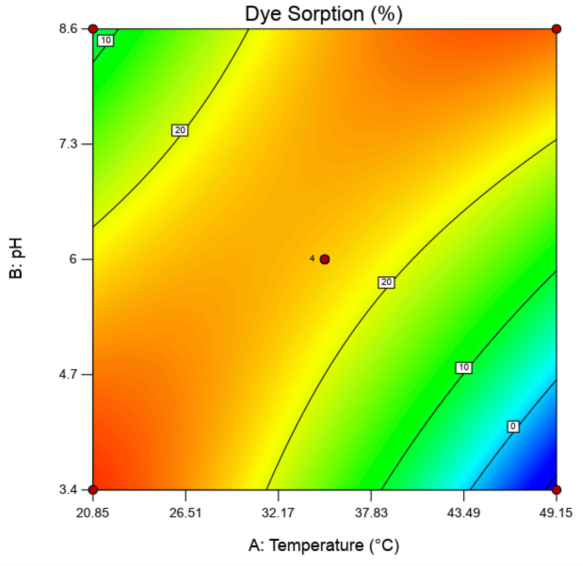

S(c)

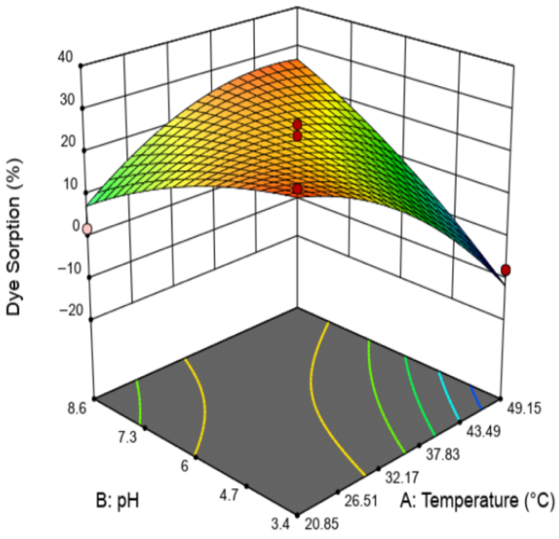

C(c)

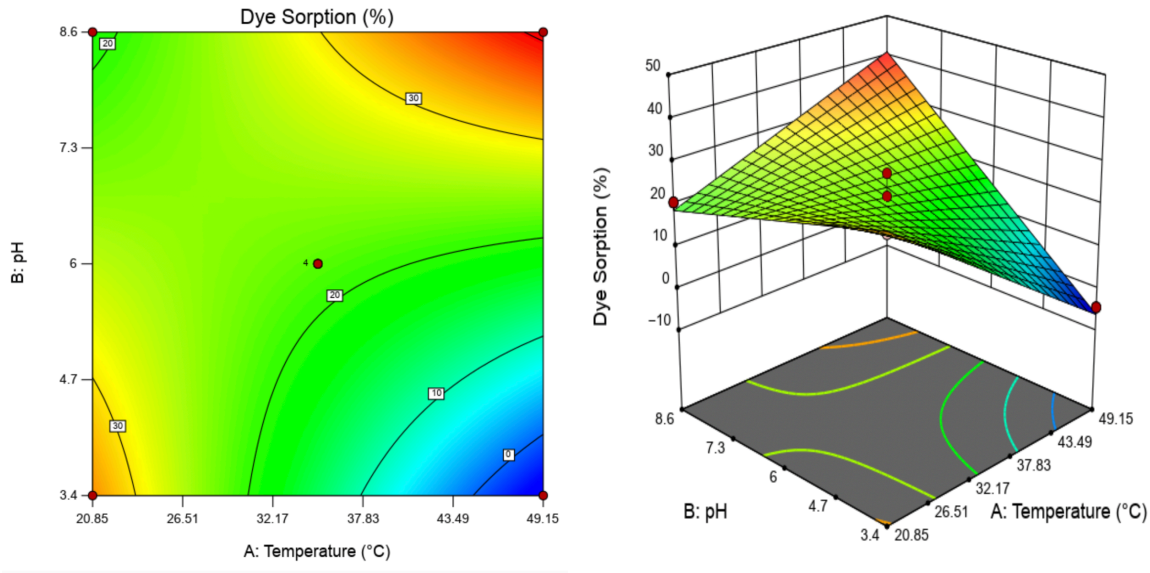

S(d) C(d)

Figure 56. Combined influence of pH and temperature on Crystal Violet sorption capacity of immobilized (c) *T. versicolor* (CB8/S2-BS) and (d) *P. ostreatus* (BWPH/S2-BS): surface and contour visualization (Published in **Publication 3**)

5.10.9 Characterization of Mycelial Matrix and Dye Sorption

Most of this part of research work has been published as **Publication 3**. The FT-IR data and SEM images connected with CB8/S2 and BWPH/S2 after BG and CV dye sorption have not been included in publication.

I. Fourier Transform Infrared Spectroscopy

The absorption mechanism of triarylmethane dyes entails various potential non-covalent interactions between dye molecules and fungal mycelium peptides and polysaccharides, including dipole-dipole, dipole-induced dipole, charge-charge, charge-dipole, charge-π electron, and π-π stacking of aromatic rings [295]. The FT-IR spectra in Figures 57(a) and (b) illustrate the functional groups implicated in the dye biosorption process by the fungi *T. versicolor* (CB8-BS) and *P. ostreatus* (BWPH-BS). A prominent peak was observed in both plots, approximately between 3200 and 3500 cm^{-1}, suggesting the possible participation of hydroxyl (-OH) and amino (-NH) groups. In dye-sorbed fungal samples (CB8-BS-BG, CB8-BS-CV, BWPH-BS-BG, and BWPH-BS-CV), a subtle shift and reduction in intensity were noted in this region, indicating that the fungal mycelium and dye molecules were interacting through hydrogen bonds and electrostatic interactions with the hydroxyl and amino groups of the fungal mycelium [141]. Additionally, C-H stretching was seen between 2800 and 3000 cm^{-1}, which corresponds to the weak van der Waals interaction [296]. In contrast to *P. ostreatus* (BWPH-BS), *T. versicolor* (CB8-BS) exhibited a more pronounced shift between 1600 and 1700 cm^{-1}, indicating C=O stretching and maybe ion exchange interactions with dye molecules [297]. The presence of C-N or C-O functional groups is signified by a distinct signal near 1100

cm^{-1}, suggesting complexation with dye molecules [109]. The negatively charged carboxyl and hydroxyl groups on fungal biomass are crucial for dye adsorption, as both BG and CV are triarylmethane cationic dyes [280]. Significant alterations are evident in the spectra of CV-absorbed fungal samples (BWPH-BS-CV and CB8-BS-CV), where the aromatic ring stretching at 1332 cm^{-1} and the out-of-plane C-H vibration of the aromatic ring at 700 cm^{-1} of the absorbed dye are readily noticeable. No clear evidence of dye absorption from its molecules was seen in the BWPH-BS-BG and CB8-BS-BG spectra following BG absorption, as previously documented in several absorption investigations of green dyes [298–300]. The observed alterations in peak position and intensity are regarded as evidence of the interaction between fungal mycelium and absorbed dyes. Significant peak alterations and the emergence of supplementary peaks after dye sorption suggest a distinctive interaction between the dye and fungus biomass. The immobilization of fungal biomasses (CB8/S2-BS and BWPH/S2-BS) onto sponge (S2) (Figure 58) matrices has been validated by the enhanced intensity and breadth of the O-H/N-H band (~3300 cm^{-1}), signifying the incorporation of fungal hydroxyl and amino groups (Figure 57). New peaks emerged at 1650 cm^{-1} and 1540 cm^{-1} in immobilized fungal biomass, matching to the Amide I (C=O) and Amide II (N-H) bands of fungal proteins. Increased intensity was noted between 1200 and 1000 cm^{-1}, linked to the C-O stretching of fungal polysaccharides (glucans, chitin). The supplementary functional groups may account for the increased biosorption ability of immobilized fungal biomass.

(a)

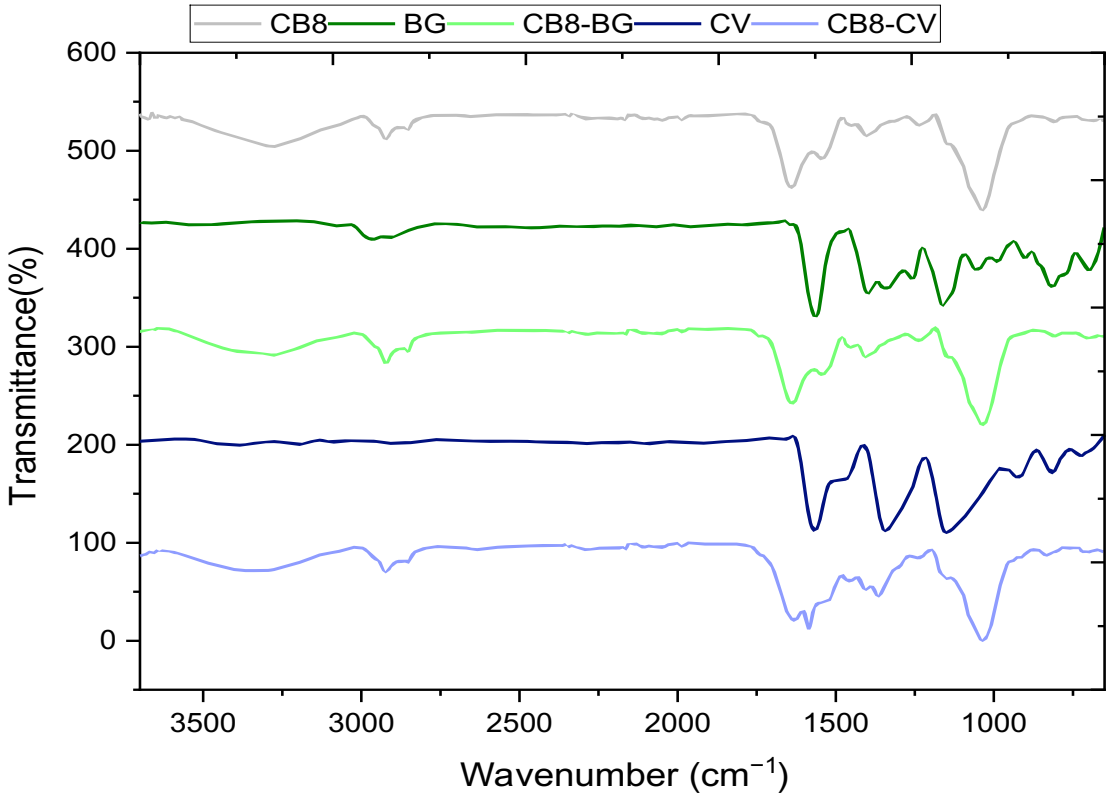

(b)

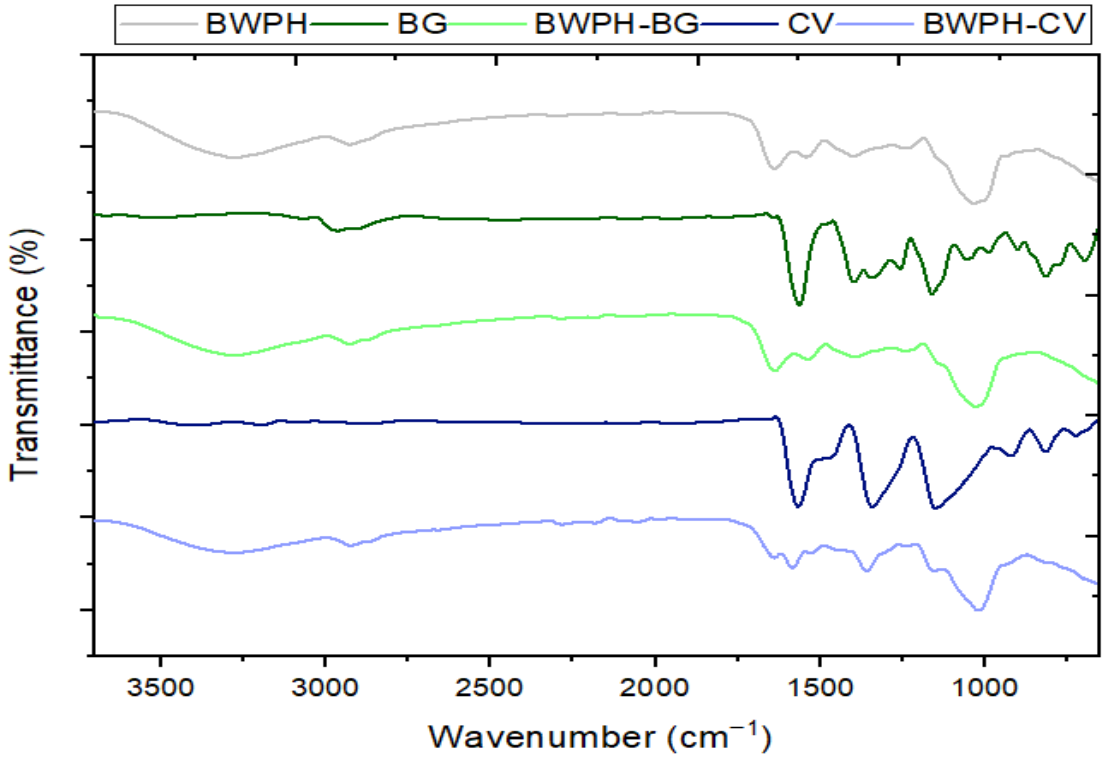

Figure 57. FT-IR spectrum of (**a**) *Trametes versicolor* (CB8-BS) and (**b**) *Pleurotus ostreatus* (BWPH-BS) biosorbents before and after Brilliant Green and Crystal Violet dye sorption (Published in **Publication 3**)

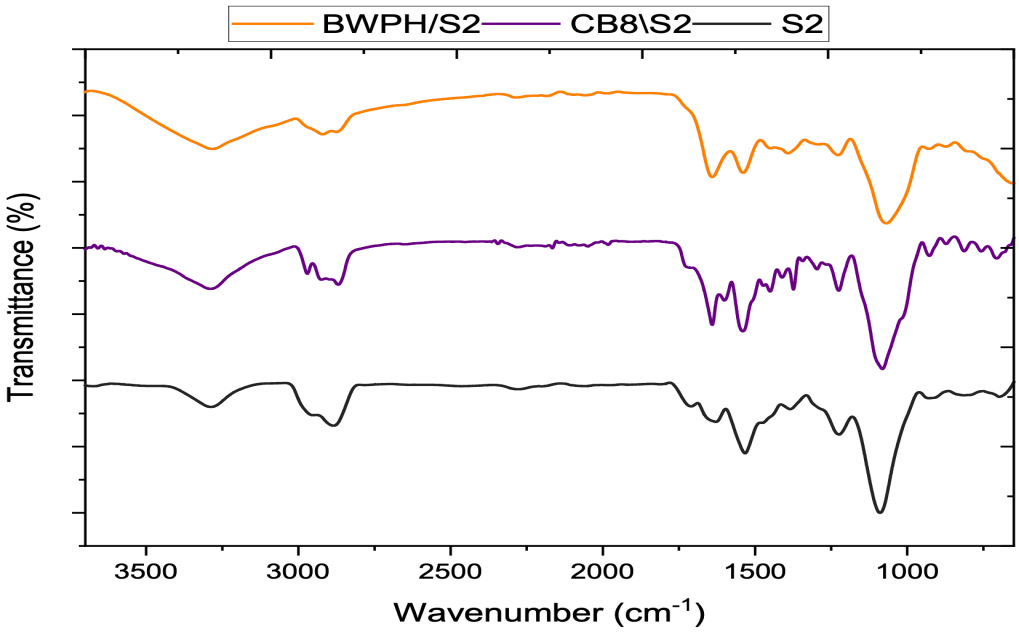

Figure 58. FT-IR spectrum of immobilized support-sponge (S2), *Trametes versicolor* (CB8/S2-BS) and *Pleurotus ostreatus* (BWPH/S2-BS) biosorbents before dye sorption (Published in **Publication 3- Supplementary material**)

III. Scanning Electron Microscopy

The scanning electron microscopy (SEM) image (Figure 59) of the polyurethane sponge (S2) reveals a highly porous and interconnected three-dimensional structure, ideal for microbial immobilization [273]. The sponge's fibrous composition provides a substantial surface area for fungal attachment and growth, while its structural integrity ensures durability throughout bioprocessing. The open pores facilitate efficient nutrient transport and oxygen transfer, crucial for maintaining fungal metabolic activity. The hyphae are intricately interwoven throughout the sponge matrix, forming a fibrous surface [301]. The sponge's structure appears to promote even hyphal distribution, minimizing diffusion limitations and enhancing dye absorption effectiveness, as demonstrated by the results.

The SEM images (Figure 60(a) and (b)) of CB8/S2-BS and BWPH/S2-BS demonstrate successful fungal colonization prior to and following their exposure to Brilliant Green and Crystal Violet dyes. Before dye sorption (a and b), both immobilized systems exhibit a porous, fibrous network created by the fungal mycelia interwoven with the sponge matrix, offering an extensive surface area and numerous attachment sites conducive to dye binding. Following the sorption of Brilliant Green (Figure 60(c) and (d)), significant surface changes are evident. In *T. versicolor*, the formerly exposed and coarse mycelial surfaces are now covered by a thin, uniform layer of dye, signifying a robust interaction between the dye molecules and fungal biomass. A comparable pattern is observed in *P. ostreatus*, where the mycelial strands exhibit increased smoothness and are partially obscured by the deposited dye, indicating absorption onto both the fungal surface and the sponge architecture.

After exposure to Crystal Violet (Figure 60(e) and (f)), more significant structural modifications are evident. In the *T. versicolor* system, the mycelium is enveloped by dense particulate and aggregated deposits, indicative of significant buildup of the cationic dye on the surfaces of the fungus and sponge. The micrograph of *P. ostreatus* reveals significant accumulation of crystalline or granular dye clusters, accompanied by partial obstruction of the porosity network, indicating a robust binding affinity of CV to the components of the fungal cell wall. The before-and-after comparisons demonstrate that both fungi undergo substantial morphological alterations following dye absorption, with surface coatings, occluded pores, and accumulated dye aggregates serving as definitive visual proof of the successful sorption of both Brilliant Green and Crystal Violet by the sponge-immobilized fungal systems.

The SEM picture of CB8 (Figure 61(a)) reveals a dense, fibrous network of hyphae exhibiting a uniform surface morphology, indicative of filamentous fungal growth. The mycelial structure is intact and hence, indicating robust pre-sorption conditions. In the meantime, BWPH hyphae (Figure 61(b)) exhibit a loosely structured yet extensive network, marked by noticeable pores and channels that suggest a substantial surface area for potential dye interaction. After BG and CV dye absorption (Figure 61(c-f)), CB8 and BWPH hyphae demonstrate a significant reduction in pore size, facilitating dye infiltration. CB8 demonstrates superior dye-binding capacity, which is mitigated by possible structural stress, while BWPH offers a balanced interplay between efficacy and stability. Utilization of supports (e.g., sponge S2) may mitigate morphological changes and enhance reusability.

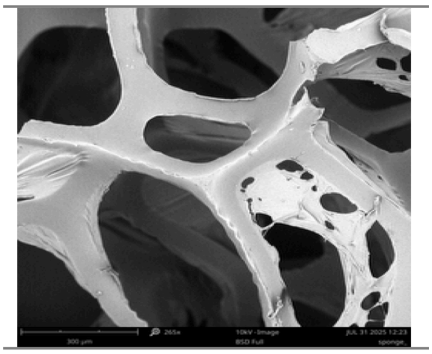

(a) Support- Sponge (S2)

Figure 59. SEM characterization of (a) native sponge matrix (S2) at 265x magnification (Published in **Publication 3**)

	Before	**After Brilliant Green dye sorption**	**After Crystal Violet dye sorption**
	(a)	(c)	(e)
Immobilized *Trametes versicolor* (CB8/S2-BS)		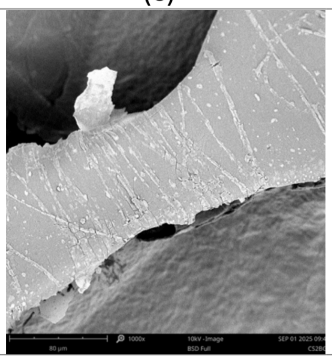	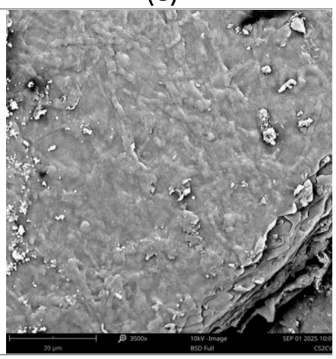
	(b)	(d)	(f)
Immobilized *Pleurotus ostreatus* (BWPH/S2-BS)	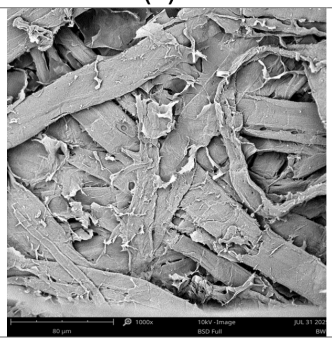	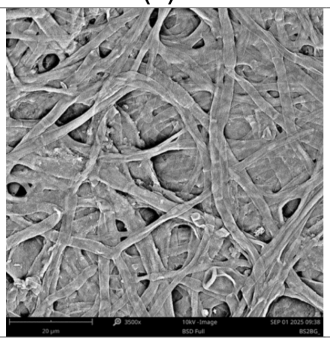	

Figure 60. Scanning electron micrographs showing morphological changes in immobilized biosorbents of *Trametes versicolor* (CB8/S2-BS) and *Pleurotus ostreatus* (BWPH/S2-BS) before dye exposure (a-b), after Brilliant Green absorption (c-d), and after Crystal Violet absorption (e-f) with 1000x-3500x magnification (Partially published in **Publication 3**)

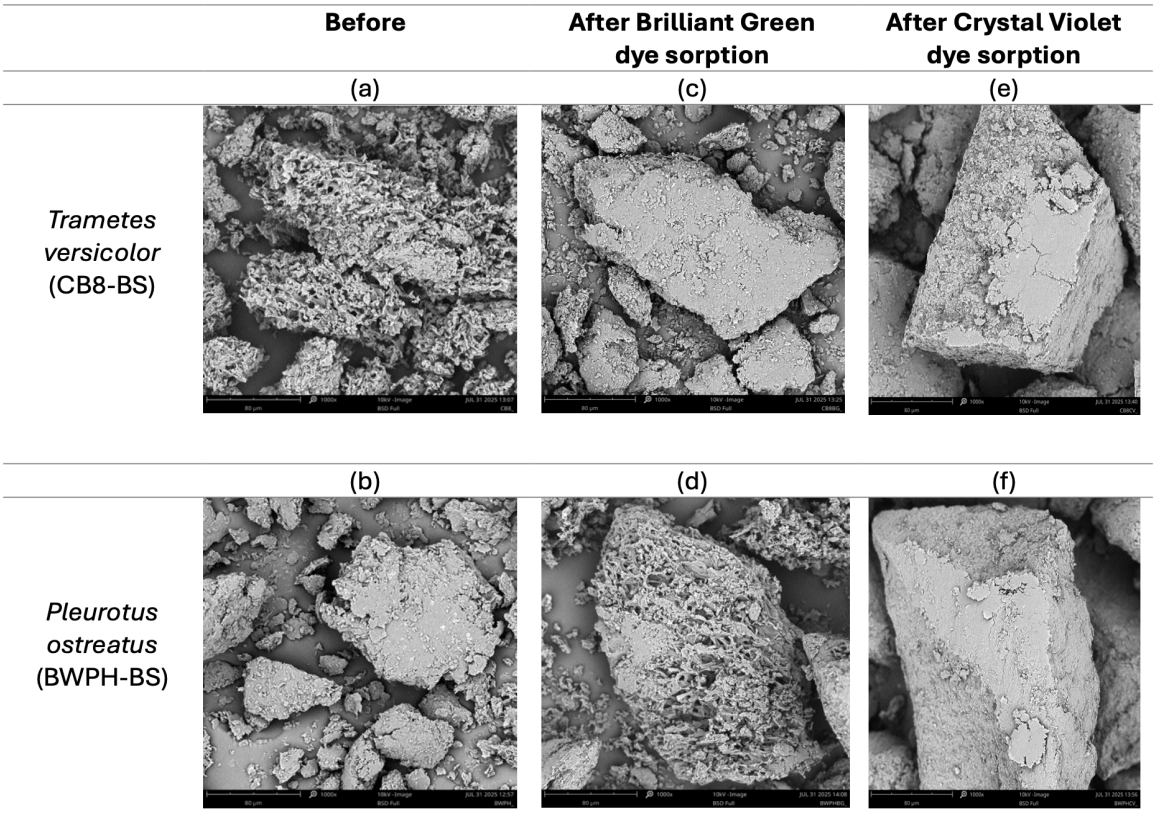

Figure 61. Scanning electron micrographs showing morphological changes in biosorbents of Trametes versicolor (CB8-BS) and Pleurotus ostreatus (BWPH-BS) before dye exposure (a-b), after Brilliant Green absorption (c-d), and after Crystal Violet absorption (e-f) with 1000x magnification (Published in **Publication 3**)

5.10.10 Reusability of Immobilized Mycelial Pellets

This part of research work has been published as **Publication 3**. Figure 62(a) and (b) illustrates the elimination of BG and CV dyes, respectively, utilizing immobilized biosorbents of *T. versicolor* (CB8/S2-BS) and *P. ostreatus* (BWPH/S2-BS) fungal mycelial pellets. In the initial cycle of sorption investigations, mycelial pellets were subjected to dye solution for six hours under standardized conditions. Both fungi exhibited an exceptionally high dye absorption efficiency (almost 40-80%) during the initial cycle. CB8/S2-BS exhibited a robust sorption capacity for both dyes in the second round following the overnight immersion of the pellets in water and their subsequent reuse. In the second cycle, the BWPH/S2-BS variant's capacity for BG dye sorption was reduced by fifty percent, indicating a decline in binding sites or saturation of fungal biomass. Nonetheless, it exhibited a significantly high capacity for CV sorption. After methanol treatment of fungal pellets, the dye sorption effectiveness of both fungal strains dramatically diminished (about 10-15%), indicating that the functional groups implicated in biosorption may have been altered or damaged by methanol exposure. The reduction in sorption during the second cycle aligns with previous studies that identified diminished biosorption efficacy during biomass reutilization, primarily due to site saturation or structural

modifications of the fungal surface [302]. The significant reduction in sorption after methanol pre-treatment suggests alterations in the composition of the fungal cell wall, potentially due to the depletion of lipids and proteins, as methanol serves as a denaturing agent [99]. Fungal pellets immersed in water exhibited greater reusability than those subjected to methanol treatment, rendering them more suitable for repeated dye biosorption applications. The biomass structure was presumably modified by methanol exposure, reducing its ability to retain dye molecules in subsequent cycles.

(a)

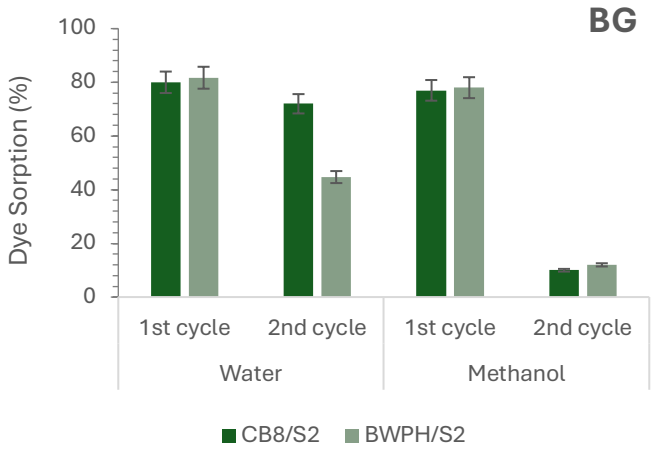

(b)

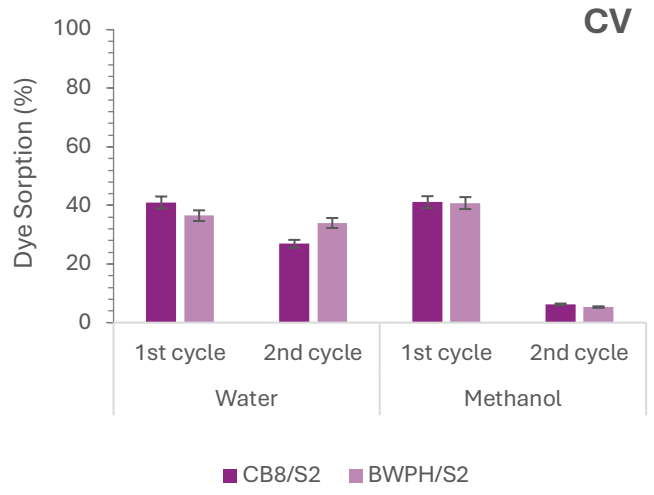

Figure 62. Evaluation of reusability of immobilized *Trametes versicolor* (CB8) and *Pleurotus ostreatus* (BWPH) fungal pellets for (**a**) Brilliant Green and (**b**) Crystal Violet dye sorption (Published in **Publication 3**)

As a concluding remark of research connected with biosorption of triphenylmethane dyes by developed fungal biosorbents, the significant performance of sponge-immobilized fungal biosorbent, *T. versicolor* (CB8/S2-BS) and *P. ostreatus* (BWPH/S2-BS) were noted for faster and effective biosorption of triarylmethane dyes, including Brilliant Green and Crystal Violet.

Among the evaluated configurations, immobilized live biomass surpassed self-immobilized and dead forms, attaining over 90% dye elimination within six hours. The primary parameters affecting sorption were dye concentration and contact time, as validated by PCA, with optimal performance noted at moderately acidic pH levels and temperatures of 30°C. The reusability of sponge pellets underscores a practical, cost-effective, biodegradable, and environmentally friendly alternative to conventional physicochemical methods. It is appropriate for application in both centralized facilities and decentralized treatment units. The findings indicate that fungal immobilization is a dependable, eco-friendly, and scalable approach to mitigating the adverse impacts of dye-contaminated industrial effluents on the environment, thereby fostering cleaner water resources and advancing sustainable wastewater treatment methods.

5.11 Bioreactor Study

According to previous bench-scale research of biodegradation of dyes, self-immobilized and sponge-immobilized *T. versicolor* (CB8/SH and CB8/S2) demonstrated the highest and most quick decolorization efficiency for Remazol Brilliant Blue R under optimized conditions. Consequently, these biomasses were chosen for the ensuing bioreactor studies. The decolorization efficacy of the CB8 strain in a bioreactor was assessed under optimal conditions during four successive dye-addition cycles. Each cycle entailed the incorporation of 125 mg/L of RBBR dye to evaluate the persistent decolorization capability and operational stability of the fungal reactors relative to abiotic controls. Distinct variations were noted among the two reactor setups throughout the four successive dye-addition cycles as seen in Figure 63. The abiotic control comprising solely sponge fragments (C/S2) exhibited negligible removal throughout the investigation, with values between 2.4% and 8.2%, indicating that the sponge provided only minimal physical absorption and emphasizing the necessity of fungal activity for true decolorization.

Conversely, both fungal systems demonstrated exceptionally high degrading efficiency from the initial cycle onward. In the initial cycle, the shaken culture of *T. versicolor* (CB8/SH) eliminated 95.3% of the dye within 48h, but the sponge-immobilized biomass (CB8/S2) had a somewhat superior removal rate of 96.0%. The elevated initial performance signifies a swift enzymatic reaction and robust metabolic activity in both systems. During the second cycle, both fungal reactors exhibited elevated decolorization efficiency, with CB8/SH and CB8/S2 attaining 90.1% and 95.7% elimination, respectively, indicating that successive dye addition did not promptly compromise fungal degradation capability. In the third cycle, a significant reduction in dye removal was observed in both fungal reactors, with CB8/SH achieving a decolorization rate of 82.1% and CB8/S2 dropping to 75.1%. This decrease likely indicates physiological stress resulting from nutrient deprivation, buildup of dye metabolites, or partial downregulation of ligninolytic enzymes following successive dye exposures. Notwithstanding this reduction, both systems persisted in eliminating the bulk of the dye, sustaining significantly superior performance compared to the abiotic control. During the fourth cycle, the abiotic control decreased to a mere 2.4% removal, but the fungal reactors either stabilized or exhibited minor recovery. The CB8/SH culture achieved an 83.1% clearance rate, while the sponge-immobilized biomass increased to 80.2%, indicating a potential partial recovery of enzymatic

activity or ongoing adaption of the immobilized fungus. The results indicate that *T. versicolor* maintained significant decolorization efficacy across all cycles, with sponge immobilization yielding equivalent or enhanced performance, particularly in the first phases of operation.

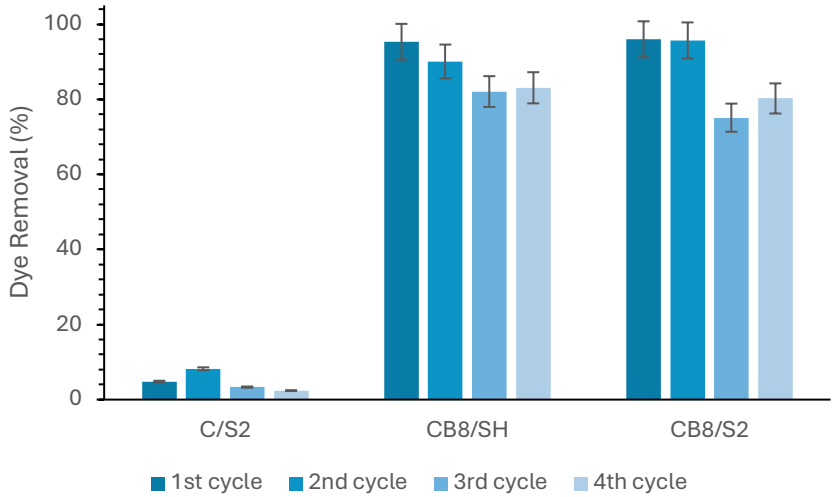

Figure 63. RBBR dye removal percentage in bioreactors containing self-immobilized and sponge immobilized biomass of *T. versicolor* (CB8/SH and CB8/S2)

Susana Rodríguez-Cuoto [303] investigated the decolorization of RBBR dye (133.33 mg/L) using *Trametes pubescens* grown on sunflower seed shells under solid-state fermentation in temporary immersion bioreactors operated over five successive batches. RBBR decolorization exceeded 55% within 4 h and reached approximately 70% after 24 h in all batches. In comparison, the biosorbent developed in the present study demonstrated superior performance, maintaining decolorization efficiencies above 95% for up to two cycles even at higher dye loadings, with the lowest observed decolorization being 75%. Palmieri et al. [304] reported approximately 70% decolorization in a fixed-bed bioreactor using laccase extracted from *Pleurotus ostreatus* and immobilized via entrapment in copper alginate beads. Unlike enzyme-based systems, our approach does not require enzyme extraction or immobilization, which are technically demanding and cost-intensive. Instead, whole-cell immobilization on an inexpensive support material (sponge) is employed, making the developed biosorbent more economically viable, simpler to implement, and easier to operate.

CHAPTER 6
CONCLUSION

This PhD research identifies White-rot fungi, specifically *Trametes versicolor* (CB8) strain, as highly efficient and mechanistically intricate biological agents for the treatment of wastewater contaminated with synthetic dyes. The central hypothesis of this study addresses existing knowledge gaps by proposing that *T. versicolor* and *P. ostreatus* have potential for dye degradation can be substantially enhanced through optimization of key physicochemical parameters and effectively implemented in compact, decentralized bioreactor systems tailored to specific dye classes. Furthermore, the treatment is capable of producing effluents with minimal ecotoxicological impact, thereby establishing its environmental sustainability. The mechanism behind xenobiotic pollutant degradation by white-rot fungi is still not fully understood. In this context, multi-omics approaches offer critical insight into the relationship between enzyme activity profiles and gene expression patterns, providing a robust foundation for predictive modelling of interactions between fungal enzymes and different classes of synthetic dyes and help to decipher fungal mediated dye degradation pathway.

The key findings of PhD research are as follows:

- **Successful immobilization:** Whole fungal cell immobilization was more successful (70-100% sponge coated with fungal mycelium) on cost effective carrier material-sponge (S2).
- **Broad-spectrum activity:** *T. versicolor* and *P. ostreatus* effectively degraded structurally diverse dyes from different classes such as azo, triphenylmethane and anthraquinone group with efficiency higher than 57%.
- **High dye removal efficiency at higher dye load:** *T. versicolor* achieved up to ~98%, 91%, 98%, 97%, 97% dye removal and *P. ostreatus* achieved up to ~88%, 57%, 92%, 84%, 97% at higher dye load (400 mg/L) for Evans Blue, Congo Red, Brilliant Green, Crystal Violet and Remazol Brilliant Blue R respectively.
- **Enhanced performance via immobilization:** Sponge-immobilized live fungal_biomass improved biosorption, biodegradation, operational stability, and biomass reusability. The findings indicate that dye removal efficiencies of approximately 96% can be attained by optimized fungal systems with sponge-immobilized biomass, which improves both biodegradation and biosorption efficacy.
- **Impact of physicochemical parameters:** Optimization studies showed agitation, growth medium composition, and fungal species significantly influence decolorization. Statistical analysis demonstrated that nitrogen source, carbon source, greatly influence decolorization results, with nitrogen source having the most pronounced effect.
- **Optimized biodegradation condition:** shaking, sponge immobilized biomass or self-immobilized biomass, ambient temperature, regular medium (5 g/L Glucose, 1g/L Peptone,

1 g/L KH_2PO_4, 1 g/L MgSO4.7H2O), *T. versicolor* live biomass - confirmed Tukey's post hoc test ($p<0.05$).

- **Ability to decolorize dye mixture:** Both *T. versicolor* and P. *ostreatus* showed up to 70% decolorization when RBBR, EB and CV were mixed in equal proportion.
- **Enzyme activity insights:** Extracellular laccase, manganese peroxidase (MnP), and lignin peroxidase (LiP) activities were evaluated, and their relationships with RBBR, EB and CV dye decolorization were analysed statistically. Spearman correlation showed a strong positive association between RBBR decolorization and both laccase and MnP activities ($\rho = 0.771$, $p = 0.072$), whereas LiP exhibited a negligible correlation ($\rho = 0.086$, $p = 0.872$). These findings indicate that although extracellular ligninolytic enzymes are important for dye oxidation, enzyme activity alone is insufficient to reliably predict decolorization efficiency in complex fungal systems.
- **Multi-omics findings:** Integrated transcriptome and proteomic investigations indicated that intracellular detoxification pathways, primarily involving cytochrome P450 monooxygenases, oxidoreductases, dehydrogenases, glutathione-dependent enzymes, and membrane transporters collectively mediate dye transformation, detoxification, and metabolite transport. Intracellular pathways are major contributors to dye degradation. Downregulation of cell division and cytoskeletal genes indicates growth suppression to prioritize detoxification and stress tolerance. Several genes and proteins with unassigned functions may contribute to dye degradation.
- **Ecotoxicology test:** Zootoxicity tests using *Daphnia magna* showed that pure RBBR, EB, and CV dyes were classified as class IV after 48 h exposure, which decreased to class III following bioremediation by *T. versicolor* and *P. ostreatus*. Phytotoxicity assays with *Spirodela polyrhiza* indicated that pure RBBR, EB, and CV were classified as IV, III, and IV, respectively, and their toxicity was reduced to classes III, II, and II after *P. ostreatus* treatment.
- **Environmental safety:** Fungal treatment reduced residual toxicity, confirming ecotoxicological safety of treated effluents.
- **Rapid and high-capacity biosorption:** The biosorption aspect of this study revealed that sponge-immobilized live fungal biomass provides quick, high-capacity, and reusable dye removal, especially for triphenylmethane dyes, greatly surpassing traditional self-immobilized biosorbents. Maximum sorption in 6 h-379.4 mg/g for BG and 48.9 mg/g for CV at 400 mg/L.
- **Optimized biosorption conditions:** Research on the optimization of the sorption process has shown that BG removal is the highest at 20.85-32.17 °C, pH 3.4-6 and for CV sorption is the most efficient at 30 °C, pH 6.5-7.5; sorption data fit quadratic model ($p < 0.05$).
- **Scalability demonstrated:** Laboratory-scale findings successfully translated to bioreactor-scale, showing feasibility for compact, decentralized treatment systems.
- **Framework for future application:** The results of research provides a basis for developing customized fungal-based systems tailored to specific dye types and wastewater characteristics.

In conclusion, this study confirms that *T. versicolor* is an ecologically robust and biotechnologically viable agent for synthetic dye remediation, operating through a synergistic combination of biosorption, extracellular oxidation, and intracellular detoxification processes. By integrating optimization strategies, immobilization techniques, multi-omics analyses, and bioreactor-scale validation, this work advances fungal wastewater treatment beyond traditional paradigms. The findings strongly support the incorporation of white-rot fungi into sustainable wastewater management strategies and align with the United Nations Sustainable Development Goals 6 (Clean Water and Sanitation), 12 (Responsible Consumption and Production), and 14 (Life Below Water).

CHAPTER 7
FUTURE PROSPECTS OF RESEARCH

The findings of this study open several promising avenues for advancing fungal-based remediation of dye-containing wastewater toward full-scale industrial implementation. From an engineering perspective, future work should focus on the development and optimization of continuous-flow and modular bioreactor systems employing immobilized white-rot fungal biomass. Scale-up studies incorporating real industrial effluents, fluctuating hydraulic loads, and mixed dye compositions will be essential to evaluate long-term operational stability, mass transfer limitations, and biofilm durability. Integration of fungal bioreactors with existing physicochemical or biological treatment units could further enhance overall treatment efficiency while reducing energy consumption and sludge generation. Additionally, monitoring gene expression, enzyme production, and enzymatic activity in these scenarios will be essential for optimizing the process and unlocking the full potential of this promising strain for efficient and adaptable dye bioremediation.

The mechanistic insights generated through transcriptomic and proteomic analyses provide a strong foundation for targeted genetic and metabolic engineering of fungal strains. Future research may explore overexpression or regulatory enhancement of key detoxification pathways, including cytochrome P450 monooxygenases, NAD(P)H-dependent oxidoreductases, and membrane transporters, to improve dye uptake, intracellular degradation, and tolerance to high dye concentrations. Genome editing tools such as CRISPR/Cas systems could be applied to selectively suppress growth-inhibitory responses while maintaining detoxification capacity, thereby improving treatment efficiency under industrial conditions. Strain engineering strategies informed by dye-specific proteomic signatures could enable the development of customized fungal consortia or “designer strains” tailored to particular dye classes or wastewater profiles. The biotechnological potential of White-rot fungi is unlocked not only for dye degradation but omics-guided insights into WRF metabolism may facilitate the development of sustainable bioprocesses, including lignin and dye-derived aromatic bioconversion into value-added products, thereby supporting the transition toward a low-carbon, bio-based circular economy.

From an environmental and sustainability perspective, future studies should extend life-cycle assessment (LCA) of fungal-based treatment systems to quantify environmental benefits relative to conventional methods. Long-term ecotoxicological evaluations, including chronic toxicity, mutagenicity, and endocrine disruption assays, will be critical to confirm the environmental safety of treated effluents and degradation by-products. The reuse and regeneration potential of immobilized fungal biomass also warrants further investigation, particularly in the context of circular bioeconomy approaches, such as coupling dye remediation with biomass valorization or enzyme recovery.

Overall, the integration of advanced bioreactor engineering, strain-level optimization, and comprehensive environmental assessment represents a logical and impactful pathway for translating fungal dye remediation from experimental systems to sustainable wastewater treatment infrastructure. These future directions will not only enhance treatment efficiency and reliability but also strengthen the role of white-rot fungi as key biotechnological tools in addressing global challenges associated with industrial dye pollution.

REFERENCES

1. Vikrant, K.; Giri, B.S.; Raza, N.; Roy, K.; Kim, K.-H.; Rai, B.N.; Singh, R.S. Recent Advancements in Bioremediation of Dye: Current Status and Challenges. *Bioresour. Technol.* **2018**, *253*, 355–367, doi:10.1016/j.biortech.2018.01.029.
2. Farhana, K.; Mahamude, A.S.F.; Mica, M.T. The Scenario of Textile Industry in Malaysia: A Review for Potentiality. *Mater. Circ. Econ.* **2022**, 4(1), 20, doi:10.1007/s42824-022-00063-5.
3. Rows, F.M. The Life and Work of Sir William Henry Perkin. *J. Soc. Dye. Colour.* **1938**, *54*, 551–562, doi:10.1111/j.1478-4408.1938.tb01996.x.
4. Blaszczyk, R.L. *The Color Revolution*; MIT Press, **2012**; ISBN 0-262-30442-2.
5. Lin, J.; Ye, W.; Xie, M.; Seo, D.H.; Luo, J.; Wan, Y.; Van Der Bruggen, B. Environmental Impacts and Remediation of Dye-Containing Wastewater. *Nat. Rev. Earth Environ.* **2023**, *4*, 785–803, doi:10.1038/s43017-023-00489-8.
6. Sosa-Martínez, J.D.; Balagurusamy, N.; Montañez, J.; Peralta, R.A.; Moreira, R.D.F.P.M.; Bracht, A.; Peralta, R.M.; Morales-Oyervides, L. Synthetic Dyes Biodegradation by Fungal Ligninolytic Enzymes: Process Optimization, Metabolites Evaluation and Toxicity Assessment. *J. Hazard. Mater.* **2020**, *400*, 123254, doi:10.1016/j.jhazmat.2020.123254.
7. Jegatheesan, V.; Shu, L.; Jegatheesan, L. Producing Fit-for-purpose Water and Recovering Resources from Various Sources: An Overview. *Environ. Qual. Manag.* **2021**, *31*, 9–28, doi:10.1002/tqem.21780.
8. Ewuzie, U.; Saliu, O.D.; Dulta, K.; Ogunniyi, S.; Bajeh, A.O.; Iwuozor, K.O.; Ighalo, J.O. A Review on Treatment Technologies for Printing and Dyeing Wastewater (PDW). *J. Water Process Eng.* **2022**, *50*, 103273, doi:10.1016/j.jwpe.2022.103273.
9. Tkaczyk, A.; Mitrowska, K.; Posyniak, A. Synthetic Organic Dyes as Contaminants of the Aquatic Environment and Their Implications for Ecosystems: A Review. *Sci. Total Environ.* **2020**, *717*, 137222, doi:10.1016/j.scitotenv.2020.137222.
10. Routoula, E.; Patwardhan, S.V. Degradation of Anthraquinone Dyes from Effluents: A Review Focusing on Enzymatic Dye Degradation with Industrial Potential. *Environ. Sci. Technol.* **2020**, *54*, 647–664, doi:10.1021/acs.est.9b03737.
11. Rahimi, S.; Poormohammadi, A.; Salmani, B.; Ahmadian, M.; Rezaei, M. Comparing the Photocatalytic Process Efficiency Using Batch and Tubular Reactors in Removal of Methylene Blue Dye and COD from Simulated Textile Wastewater. *J. Water Reuse Desalination* **2016**, *6*, 574–582, doi:10.2166/wrd.2016.190.
12. Paraschiv, D.; Tudor, C.; Petrariu, R. The Textile Industry and Sustainable Development: A Holt–Winters Forecasting Investigation for the Eastern European Area. *Sustainability* **2015**, *7*, 1280–1291, doi:10.3390/su7021280.
13. Breitenmoser, L.; Cuadrado Quesada, G.; N, A.; Bassi, N.; Dkhar, N.B.; Phukan, M.; Kumar, S.; Naga Babu, A.; Kierstein, A.; Campling, P.; et al. Perceived Drivers and Barriers in the Governance of Wastewater Treatment and Reuse in India: Insights from a Two-Round Delphi Study. *Resour. Conserv. Recycl.* **2022**, *182*, 106285, doi:10.1016/j.resconrec.2022.106285.
14. Long, X.; Pan, Q.; Wang, C.; Wang, H.; Li, H.; Li, X. Microbial Fuel Cell-Photoelectrocatalytic Cell Combined System for the Removal of Azo Dye Wastewater. *Bioresour. Technol.* **2017**, *244*, 182–191, doi:10.1016/j.biortech.2017.07.088.
15. Robinson, T.; Chandran, B.; Nigam, P. Studies on the Production of Enzymes by White-Rot Fungi for the Decolourisation of Textile Dyes. *Enzyme Microb. Technol.* **2001**, *29*, 575–579, doi:10.1016/s0141-0229(01)00430-6.
16. Al-Tohamy, R.; Ali, S.S.; Li, F.; Okasha, K.M.; Mahmoud, Y.A.-G.; Elsamahy, T.; Jiao, H.; Fu, Y.; Sun, J. A Critical Review on the Treatment of Dye-Containing Wastewater:

Ecotoxicological and Health Concerns of Textile Dyes and Possible Remediation Approaches for Environmental Safety. *Ecotoxicol. Environ. Saf.* **2022**, *231*, 113160, doi:10.1016/j.ecoenv.2021.113160.
17. Wang, K.; Zhang, S.; Xu, Q.; Lian, T.; Xu, Z.; Jiang, M.; Liu, P. Fabrication of Salt-Tolerant Chitosan-Based Polyelectrolyte Flocculant through Enhancing H-Bond Hydration Effect for Treating and Recycling of Highly Saline Dyeing Wastewater. *Sep. Purif. Technol.* **2023**, *307*, 122786, doi:10.1016/j.seppur.2022.122786.
18. González, T.; Terrón, M.C.; Yagüe, S.; Junca, H.; Carbajo, J.M.; Zapico, E.J.; Silva, R.; Arana-Cuenca, A.; Téllez, A.; González, A.E. Melanoidin-Containing Wastewaters Induce Selective Laccase Gene Expression in the White-Rot Fungus Trametes Sp. I-62. *Res. Microbiol.* **2008**, *159*, 103–109, doi:10.1016/j.resmic.2007.10.005.
19. Ghosh, A.; Dastidar, M.G.; Sreekrishnan, T.R. Bioremediation of Chromium Complex Dyes and Treatment of Sludge Generated during the Process. *Int. Biodeterior. Biodegrad.* **2017**, *119*, 448–460, doi:10.1016/j.ibiod.2016.08.013.
20. Tortella, G.; Durán, N.; Rubilar, O.; Parada, M.; Diez, M.C. Are White-Rot Fungi a Real Biotechnological Option for the Improvement of Environmental Health? *Crit. Rev. Biotechnol.* **2015**, *35*, 165–172, doi:10.3109/07388551.2013.823597.
21. Negi, A. Environmental Impact of Textile Materials: Challenges in Fiber–Dye Chemistry and Implication of Microbial Biodegradation. *Polymers* **2025**, *17*, 871, doi:10.3390/polym17070871.
22. Alegbe, E.O.; Uthman, T.O. A Review of History, Properties, Classification, Applications and Challenges of Natural and Synthetic Dyes. *Heliyon* **2024**, *10* (13), doi:10.1016/j.heliyon.2024.e33646.
23. Shyla, H.; Saha, P.; Rao, K.V.B. Biodegradation and Decolorization of Two Different Azo Dyes, Reactive Blue 221 and Direct Black 38, and Assessment of the Degraded Dye Metabolites. *Desalination Water Treat.* **2018**, *123*, 338–347, doi:10.5004/dwt.2018.22624.
24. Ancient (Pre-Historic and Historic) Indian and European Dye Pigments: A Case Study. In *Sustainable Textiles: Production, Processing, Manufacturing & Chemistry*; Springer Nature Switzerland: Cham, **2025**; pp. 197–211 ISBN 978-3-031-91216-0.
25. Aragaw, T.A.; Bogale, F.M. Biomass-Based Adsorbents for Removal of Dyes From Wastewater: A Review. *Front. Environ. Sci.* **2021**, *9*, 764958, doi:10.3389/fenvs.2021.764958.
26. Armah, L.; Adjei, D.A.; Menetey, B.K.; William, K.D. Emblematic Interpretation of the Designs of Selected Kente Fabrics among Ashanti People of Ghana. *Art Des. Rev.* **2023**, *11*, 263–280, doi:10.4236/adr.2023.113020.
27. Grierson, S.; Duff, D.G.; Sinclair, R.S. Natural Dyes of the Scottish Highlands. *Text. Hist.* **1985**, *16*, 23–43, doi:10.1179/004049685793701223.
28. McGovern, P.E.; Michel, R.H. Royal Purple Dye: The Chemical Reconstruction of the Ancient Mediterranean Industry. *Acc. Chem. Res.* **1990**, *23*, 152–158, doi:10.1021/ar00173a006.
29. Sotiropoulou, S.; Karapanagiotis, I.; Andrikopoulos, K.S.; Marketou, T.; Birtacha, K.; Marthari, M. Review and New Evidence on the Molluscan Purple Pigment Used in the Early Late Bronze Age Aegean Wall Paintings. *Heritage* **2021**, *4*, 171–187, doi:10.3390/heritage4010010.
30. Deveoglu, O. A Review on Cochineal (Dactylopius Coccus Costa) Dye. *Research Journal of Recent Sciences*, **2020**, *9*, 2277, 2502
31. Yadav, S.; Tiwari, K.S.; Gupta, C.; Tiwari, M.K.; Khan, A.; Sonkar, S.P. A Brief Review on Natural Dyes, Pigments: Recent Advances and Future Perspectives. *Results Chem.* **2023**, *5*, 100733, doi:10.1016/j.rechem.2022.100733.

32. Extraction and Application of Natural Dyes. In *Sustainable Practices in the Textile Industry*; Wiley, **2021**; pp. 1–40 ISBN 978-1-119-81888-5.
33. Repon, Md.R.; Islam, T.; Islam, T.; Ghorab, A.E.; Rahman, M.M. Cleaner Pathway for Developing Bioactive Textile Materials Using Natural Dyes: A Review. *Environ. Sci. Pollut. Res.* **2023**, *30*, 48793–48823, doi:10.1007/s11356-023-26131-0.
34. Kamboj, A.; Medha, K.; Gupta, V.; Jose, S. Ultraviolet Protection of Textiles with Herbal Dyes: A Contemporary Review. *Sustain. Chem. Pharm.* **2024**, *41*, 101689, doi:10.1016/j.scp.2024.101689.
35. Melo Miranda, B.; Vilela Junior, O.; Santos Fernandes, S.; Mendes Lemos, G.R.; Schwan, C.L.; Aliaño-González, M.J.; Fernández Barbero, G.; Murowaniecki Otero, D. Potential of New Plant Sources as Raw Materials for Obtaining Natural Pigments/Dyes. *Agronomy* **2025**, *15(2)*, 405, doi:10.3390/agronomy15020405.
36. Vázquez-Ortega, F.; Lagunes, I.; Trigos, Á. Cosmetic Dyes as Potential Photosensitizers of Singlet Oxygen Generation. *Dyes Pigments* **2020**, *176*, 108248, doi:10.1016/j.dyepig.2020.108248.
37. Lellis, B.; Fávaro-Polonio, C.Z.; Pamphile, J.A.; Polonio, J.C. Effects of Textile Dyes on Health and the Environment and Bioremediation Potential of Living Organisms. *Biotechnol. Res. Innov.* **2019**, *3*, 275–290, doi:10.1016/j.biori.2019.09.001.
38. Mirjalili, M.; Nazarpoor, K.; Karimi, L. Eco-Friendly Dyeing of Wool Using Natural Dye from Weld as Co-Partner with Synthetic Dye. *J. Clean. Prod.* **2011**, *19*, 1045–1051, doi:10.1016/j.jclepro.2011.02.001.
39. Mabuza, L.; Sonnenberg, N.; Marx-Pienaar, N. Natural versus Synthetic Dyes: Consumers' Understanding of Apparel Coloration and Their Willingness to Adopt Sustainable Alternatives. *Resour. Conserv. Recycl. Adv.* **2023**, *18*, 200146, doi:10.1016/j.rcradv.2023.200146.
40. Srivastava, D.R.; Singh, N. Importance of Natural Dye over Synthetic Dye: A Critical Review. *International Journal of Home Science*, **2019**, 5(2), 148-150.
41. Upadhyay, R.; Przystaś, W.; Dave, B. Myco-Remediation of Synthetic Dyes: A Comprehensive Review on Contaminant Alleviation Mechanism, Kinetic Study and Toxicity Analysis. *Int. J. Environ. Sci. Technol.* **2024**, 22(1), 521-538, doi:10.1007/s13762-024-05793-4.
42. Rápó, E.; Tonk, S. Factors Affecting Synthetic Dye Adsorption; Desorption Studies: A Review of Results from the Last Five Years (2017–2021). *Molecules* **2021**, *26*, 5419, doi:10.3390/molecules26175419.
43. Chung, K.-T. Azo Dyes and Human Health: A Review. *J. Environ. Sci. Health Part C* **2016**, *34*, 233–261, doi:10.1080/10590501.2016.1236602.
44. Benkhaya, S.; M'rabet, S.; El Harfi, A. Classifications, Properties, Recent Synthesis and Applications of Azo Dyes. *Heliyon* **2020**, *6*(1), doi:10.1016/j.heliyon.2020.e03271.
45. Kusumlata; Ambade, B.; Kumar, A.; Gautam, S. Sustainable Solutions: Reviewing the Future of Textile Dye Contaminant Removal with Emerging Biological Treatments. *Limnol. Rev.* **2024**, *24*, 126–149, doi:10.3390/limnolrev24020007.
46. Shahid, M.; Wertz, J.; Degano, I.; Aceto, M.; Khan, M.I.; Quye, A. Analytical Methods for Determination of Anthraquinone Dyes in Historical Textiles: A Review. *Anal. Chim. Acta* **2019**, *1083*, 58–87, doi:10.1016/j.aca.2019.07.009.
47. Cheriaa, J.; Khaireddine, M.; Rouabhia, M.; Bakhrouf, A. Removal of Triphenylmethane Dyes by Bacterial Consortium. *Sci. World J.* **2012**, *2012*, 1–9, doi:10.1100/2012/512454.
48. Shedbalkar, U.; Dhanve, R.; Jadhav, J. Biodegradation of Triphenylmethane Dye Cotton Blue by Penicillium Ochrochloron MTCC 517. *J. Hazard. Mater.* **2008**, *157*, 472–479, doi:10.1016/j.jhazmat.2008.01.023.

49. Božič, M.; Kokol, V. Ecological Alternatives to the Reduction and Oxidation Processes in Dyeing with Vat and Sulphur Dyes. *Dyes Pigments* **2008**, *76*, 299–309, doi:10.1016/j.dyepig.2006.05.041.
50. Faria, P.C.C.; Órfão, J.J.M.; Pereira, M.F.R. Adsorption of Anionic and Cationic Dyes on Activated Carbons with Different Surface Chemistries. *Water Res.* **2004**, *38*, 2043–2052, doi:10.1016/j.watres.2004.01.034.
51. Azam, K.; Shezad, N.; Shafiq, I.; Akhter, P.; Akhtar, F.; Jamil, F.; Shafique, S.; Park, Y.-K.; Hussain, M. A Review on Activated Carbon Modifications for the Treatment of Wastewater Containing Anionic Dyes. *Chemosphere* **2022**, *306*, 135566, doi:10.1016/j.chemosphere.2022.135566.
52. Lewis, D.M. Developments in the Chemistry of Reactive Dyes and Their Application Processes. *Color. Technol.* **2014**, *130*, 382–412, doi:10.1111/cote.12114.
53. Carneiro, P.A.; Umbuzeiro, G.A.; Oliveira, D.P.; Zanoni, M.V.B. Assessment of Water Contamination Caused by a Mutagenic Textile Effluent/Dyehouse Effluent Bearing Disperse Dyes. *J. Hazard. Mater.* **2010**, *174*, 694–699, doi:10.1016/j.jhazmat.2009.09.106.
54. Treu, R.; Falandysz, J. Mycoremediation of Hydrocarbons with Basidiomycetes—a Review. *J. Environ. Sci. Health Part B* **2017**, *52*, 148–155, doi:10.1080/03601234.2017.1261536.
55. Landrigan, P.J.; Stegeman, J.J.; Fleming, L.E.; Allemand, D.; Anderson, D.M.; Backer, L.C.; Brucker-Davis, F.; Chevalier, N.; Corra, L.; Czerucka, D.; et al. Human Health and Ocean Pollution. *Ann. Glob. Health* **2020**, *86(1)*, 151, doi:10.5334/aogh.2831.
56. Sharma, J.; Sharma, S.; Soni, V. Classification and Impact of Synthetic Textile Dyes on Aquatic Flora: A Review. *Reg. Stud. Mar. Sci.* **2021**, *45*, 101802, doi:10.1016/j.rsma.2021.101802.
57. Saravanan, P.; Josephraj, J.; Pushpa Thillainayagam, B. A Comprehensive Analysis of Biosorptive Removal of Basic Dyes by Different Biosorbents. *Environ. Nanotechnol. Monit. Manag.* **2021**, *16*, 100560, doi:10.1016/j.enmm.2021.100560.
58. Vigiak, O.; Grizzetti, B.; Udias-Moinelo, A.; Zanni, M.; Dorati, C.; Bouraoui, F.; Pistocchi, A. Predicting Biochemical Oxygen Demand in European Freshwater Bodies. *Sci. Total Environ.* **2019**, *666*, 1089–1105, doi:10.1016/j.scitotenv.2019.02.252.
59. Concerns and Threats of Contamination on Aquatic Ecosystems. In *Bioremediation and Biotechnology*; Springer International Publishing: Cham, 2020; pp. 1–26 ISBN 978-3-030-35690-3.
60. Belpaire, C.; Reyns, T.; Geeraerts, C.; Van Loco, J. Toxic Textile Dyes Accumulate in Wild European Eel Anguilla Anguilla. *Chemosphere* **2015**, *138*, 784–791, doi:10.1016/j.chemosphere.2015.08.007.
61. Poopal, R.-K.; Ashwini, R.; Ramesh, M.; Li, B.; Ren, Z. Triphenylmethane Dye (C52H54N4O12) Is Potentially a Hazardous Substance in Edible Freshwater Fish at Trace Level: Toxicity, Hematology, Biochemistry, Antioxidants, and Molecular Docking Evaluation Study. *Environ. Sci. Pollut. Res.* **2022**, *30*, 28759–28779, doi:10.1007/s11356-022-24206-y.
62. Hocini, I.; Benabbas, K.; Khellaf, N.; Djelal, H.; Amrane, A. Can Duckweed Be Used for the Biomonitoring of Textile Effluents? *Euro-Mediterr. J. Environ. Integr.* **2019**, *4*, doi:10.1007/s41207-019-0126-9.
63. Ardila-Leal, L.D.; Poutou-Piñales, R.A.; Pedroza-Rodríguez, A.M.; Quevedo-Hidalgo, B.E. A Brief History of Colour, the Environmental Impact of Synthetic Dyes and Removal by Using Laccases. *Mol. Basel Switz.* **2021**, *26*, 3813, doi:10.3390/molecules26133813.
64. Heibati, B.; Rodriguez-Couto, S.; Al-Ghouti, M.A.; Asif, M.; Tyagi, I.; Agarwal, S.; Gupta, V.K. Kinetics and Thermodynamics of Enhanced Adsorption of the Dye AR 18 Using

Activated Carbons Prepared from Walnut and Poplar Woods. *J. Mol. Liq.* **2015**, *208*, 99–105, doi:10.1016/j.molliq.2015.03.057.
65. Park, H.; Lee, M.; Kim, B.; Lee, K.; Roh, J.; Moon, Y.; Hong, C. Clinical and Immunologic Evaluations of Reactive Dye-Exposed Workers. *J. Allergy Clin. Immunol.* **1991**, *87(3)*, 639–649, doi:10.1016/0091-6749(91)90382-x.
66. Rovira, J.; Domingo, J.L. Human Health Risks Due to Exposure to Inorganic and Organic Chemicals from Textiles: A Review. *Environ. Res.* **2019**, *168*, 62–69, doi:10.1016/j.envres.2018.09.027.
67. *Environmental Deterioration and Human Health: Natural and Anthropogenic Determinants*; Malik, A., Grohmann, E., Akhtar, R., Eds.; Springer Netherlands: Dordrecht, 2014; ISBN 978-94-007-7889-4.
68. Miller, M.D.; Steinmaus, C.; Golub, M.S.; Castorina, R.; Thilakartne, R.; Bradman, A.; Marty, M.A. Potential Impacts of Synthetic Food Dyes on Activity and Attention in Children: A Review of the Human and Animal Evidence. *Environ. Health* **2022**, *21(1),45*, doi:10.1186/s12940-022-00849-9.
69. Littlefield, N. Chronic Toxicity and Carcinogenicity Studies of Gentian Violet in Mice. *Fundam. Appl. Toxicol.* **1985**, *5(5)*, 902–912, doi:10.1016/0272-0590(85)90172-1.
70. Holkar, C.R.; Jadhav, A.J.; Pinjari, D.V.; Mahamuni, N.M.; Pandit, A.B. A Critical Review on Textile Wastewater Treatments: Possible Approaches. *J. Environ. Manage.* **2016**, *182*, 351–366, doi:10.1016/j.jenvman.2016.07.090.
71. Donkadokula, N.Y.; Kola, A.K.; Naz, I.; Saroj, D. A Review on Advanced Physico-Chemical and Biological Textile Dye Wastewater Treatment Techniques. *Rev. Environ. Sci. Biotechnol.* **2020**, *19(3)*, 543–560, doi:10.1007/s11157-020-09543-z.
72. Yogalakshmi, K.N.; Das, A.; Rani, G.; Jaswal, V.; Randhawa, J.S. Nano-Bioremediation: A New Age Technology for the Treatment of Dyes in Textile Effluents. In *Bioremediation of Industrial Waste for Environmental Safety*; Saxena, G., Bharagava, R.N., Eds.; Springer Singapore: Singapore, 2020; pp. 313–347 ISBN 978-981-13-1890-0.
73. Tomei, M.C.; Soria Pascual, J.; Mosca Angelucci, D. Analysing Performance of Real Textile Wastewater Bio-Decolourization under Different Reaction Environments. *J. Clean. Prod.* **2016**, *129*, 468–477, doi:10.1016/j.jclepro.2016.04.028.
74. Ćurić, I.; Dolar, D.; Karadakić, K. Textile Wastewater Reusability in Knitted Fabric Washing Process Using UF Membrane Technology. *J. Clean. Prod.* **2021**, *299*, 126899, doi:10.1016/j.jclepro.2021.126899.
75. Xue, F.; Tang, B.; Bin, L.; Ye, J.; Huang, S.; Fu, F.; Li, P.; Cui, J. Residual Micro Organic Pollutants and Their Biotoxicity of the Effluent from the Typical Textile Wastewater Treatment Plants at Pearl River Delta. *Sci. Total Environ.* **2019**, *657*, 696–703, doi:10.1016/j.scitotenv.2018.12.008.
76. Ramos, R.O.; Albuquerque, M.V.C.; Lopes, W.S.; Sousa, J.T.; Leite, V.D. Degradation of Indigo Carmine by Photo-Fenton, Fenton, H2O2/UV-C and Direct UV-C: Comparison of Pathways, Products and Kinetics. *J. Water Process Eng.* **2020**, *37*, 101535, doi:10.1016/j.jwpe.2020.101535.
77. Yurtsever, A.; Sahinkaya, E.; Çınar, Ö. Performance and Foulant Characteristics of an Anaerobic Membrane Bioreactor Treating Real Textile Wastewater. *J. Water Process Eng.* **2020**, *33*, 101088, doi:10.1016/j.jwpe.2019.101088.
78. Castillo-Suárez, L.A.; Sierra-Sánchez, A.G.; Linares-Hernández, I.; Martínez-Miranda, V.; Teutli-Sequeira, E.A. A Critical Review of Textile Industry Wastewater: Green Technologies for the Removal of Indigo Dyes. *Int. J. Environ. Sci. Technol.* **2023**, *20(9)*, 10553–10590, doi:10.1007/s13762-023-04810-2.

79. Wang, X.; Jiang, J.; Gao, W. Reviewing Textile Wastewater Produced by Industries: Characteristics, Environmental Impacts, and Treatment Strategies. *Water Sci. Technol.* **2022**, *85(7)*, 2076–2096, doi:10.2166/wst.2022.088.
80. Kamati, S.N.; Yan, J.; Fan, J. A Review on Progresses in Reactive Dye-Containing Wastewater Treatment. *Water Pract. Technol.* **2024**, *19(7)*, 2712–2733, doi:10.2166/wpt.2024.142.
81. Azari, A.; Nabizadeh, R.; Nasseri, S.; Mahvi, A.H.; Mesdaghinia, A.R. Comprehensive Systematic Review and Meta-Analysis of Dyes Adsorption by Carbon-Based Adsorbent Materials: Classification and Analysis of Last Decade Studies. *Chemosphere* **2020**, *250*, 126238, doi:10.1016/j.chemosphere.2020.126238.
82. Madhav, S.; Ahamad, A.; Singh, P.; Mishra, P.K. A Review of Textile Industry: Wet Processing, Environmental Impacts, and Effluent Treatment Methods. *Environ. Qual. Manag.* **2018**, *27(3)*, 31–41, doi:10.1002/tqem.21538.
83. Sarkar, B. Micellar Enhanced Ultrafiltration in the Treatment of Dye Wastewater: Fundamentals, State-of-the-Art and Future Perspectives. *Groundw. Sustain. Dev.* **2022**, *17*, 100730, doi:10.1016/j.gsd.2022.100730.
84. Moradihamedani, P. Recent Advances in Dye Removal from Wastewater by Membrane Technology: A Review. *Polym. Bull.* **2022**, *79*, 2603–2631, doi:10.1007/s00289-021-03603-2.
85. Dotto, J.; Fagundes-Klen, M.R.; Veit, M.T.; Palácio, S.M.; Bergamasco, R. Performance of Different Coagulants in the Coagulation/Flocculation Process of Textile Wastewater. *J. Clean. Prod.* **2019**, *208*, 656–665, doi:10.1016/j.jclepro.2018.10.112.
86. Ihaddaden, S.; Aberkane, D.; Boukerroui, A.; Robert, D. Removal of Methylene Blue (Basic Dye) by Coagulation-Flocculation with Biomaterials (Bentonite and Opuntia Ficus Indica). *J. Water Process Eng.* **2022**, *49*, 102952, doi:10.1016/j.jwpe.2022.102952.
87. Núñez, J.; Yeber, M.; Cisternas, N.; Thibaut, R.; Medina, P.; Carrasco, C. Application of Electrocoagulation for the Efficient Pollutants Removal to Reuse the Treated Wastewater in the Dyeing Process of the Textile Industry. *J. Hazard. Mater.* **2019**, *371*, 705–711, doi:10.1016/j.jhazmat.2019.03.030.
88. Güyer, G.T.; Nadeem, K.; Dizge, N. Recycling of Pad-Batch Washing Textile Wastewater through Advanced Oxidation Processes and Its Reusability Assessment for Turkish Textile Industry. *J. Clean. Prod.* **2016**, *139*, 488–494, doi:10.1016/j.jclepro.2016.08.009.
89. Li, S.; Zhang, C.; Li, F.; Hua, T.; Zhou, Q.; Ho, S.-H. Technologies towards Antibiotic Resistance Genes (ARGs) Removal from Aquatic Environment: A Critical Review. *J. Hazard. Mater.* **2021**, *411*, 125148, doi:10.1016/j.jhazmat.2021.125148.
90. Wang, J.; Tang, J. Fe-Based Fenton-like Catalysts for Water Treatment: Catalytic Mechanisms and Applications. *J. Mol. Liq.* **2021**, *332*, 115755, doi:10.1016/j.molliq.2021.115755.
91. Lotfi, S.; Fischer, K.; Schulze, A.; Schäfer, A.I. Photocatalytic Degradation of Steroid Hormone Micropollutants by TiO2-Coated Polyethersulfone Membranes in a Continuous Flow-through Process. *Nat. Nanotechnol.* **2022**, *17*, 417–423, doi:10.1038/s41565-022-01074-8.
92. Qin, X.; Jing, L.; Tian, G.; Qu, Y.; Feng, Y. Enhanced Photocatalytic Activity for Degrading Rhodamine B Solution of Commercial Degussa P25 TiO2 and Its Mechanisms. *J. Hazard. Mater.* **2009**, *172*, 1168–1174, doi:10.1016/j.jhazmat.2009.07.120.
93. Qattan, S.Y.A. Harnessing Bacterial Consortia for Effective Bioremediation: Targeted Removal of Heavy Metals, Hydrocarbons, and Persistent Pollutants. *Environ. Sci. Eur.* **2025**, *37(1)*, 85, doi:10.1186/s12302-025-01103-y.
94. Ayub, A.; Wani, A.K.; Chopra, C.; Sharma, D.K.; Amin, O.; Wani, A.W.; Singh, A.; Manzoor, S.; Singh, R. Advancing Dye Degradation: Integrating Microbial Metabolism,

Photocatalysis, and Nanotechnology for Eco-Friendly Solutions. *Bacteria* **2025**, *4(1)*, 15, doi:10.3390/bacteria4010015.
95. Sun, J.; Hu, Y.; Li, W.; Zhang, Y.; Chen, J.; Deng, F. Sequential Decolorization of Azo Dye and Mineralization of Decolorization Liquid Coupled with Bioelectricity Generation Using a pH Self-Neutralized Photobioelectrochemical System Operated with Polarity Reversion. *J. Hazard. Mater.* **2015**, *289*, 108–117, doi:10.1016/j.jhazmat.2015.02.010.
96. Guo, G.; Tian, F.; Zhao, Y.; Tang, M.; Liu, W.; Liu, C.; Xue, S.; Kong, W.; Sun, Y.; Wang, S. Aerobic Decolorization and Detoxification of Acid Scarlet GR by a Newly Isolated Salt-Tolerant Yeast Strain Galactomyces Geotrichum GG. *Int. Biodeterior. Biodegrad.* **2019**, *145*, 104818, doi:10.1016/j.ibiod.2019.104818.
97. Dinakarkumar, Y.; Ramakrishnan, G.; Gujjula, K.R.; Vasu, V.; Balamurugan, P.; Murali, G. Fungal Bioremediation: An Overview of the Mechanisms, Applications and Future Perspectives. *Environ. Chem. Ecotoxicol.* **2024**, *6*, 293–302, doi:10.1016/j.enceco.2024.07.002.
98. Latif, W.; Ciniglia, C.; Iovinella, M.; Shafiq, M.; Papa, S. Role of White Rot Fungi in Industrial Wastewater Treatment: A Review. *Appl. Sci.* **2023**, *13*, 8318, doi:10.3390/app13148318.
99. Kaushik, P.; Malik, A. Mycoremediation of Synthetic Dyes: An Insight into the Mechanism, Process Optimization and Reactor Design. In *Microbial Degradation of Synthetic Dyes in Wastewaters*; Singh, S.N., Ed.; Environmental Science and Engineering; Springer International Publishing: Cham, 2015; pp. 1–25 ISBN 978-3-319-10941-1.
100. Srinivasan, A.; Viraraghavan, T. Decolorization of Dye Wastewaters by Biosorbents: A Review. *J. Environ. Manage.* **2010**, *91(10)*, 1915–1929, doi:10.1016/j.jenvman.2010.05.003.
101. Grainger, S.; Fu, G.Y.; Hall, E.R. Biosorption of Colour-Imparting Substances in Biologically Treated Pulp Mill Effluent Using Aspergillus Niger Fungal Biomass. *Water. Air. Soil Pollut.* **2011**, *217(1)*, 233–244, doi:10.1007/s11270-010-0582-y.
102. Crini, G.; Badot, P.-M. Application of Chitosan, a Natural Aminopolysaccharide, for Dye Removal from Aqueous Solutions by Adsorption Processes Using Batch Studies: A Review of Recent Literature. *Prog. Polym. Sci.* **2008**, *33(4)*, 399–447, doi:10.1016/j.progpolymsci.2007.11.001.
103. Kaushik, P.; Malik, A. Comparative Performance Evaluation of Aspergillus Lentulus for Dye Removal through Bioaccumulation and Biosorption. *Environ. Sci. Pollut. Res.* **2013**, *20(5)*, 2882–2892, doi:10.1007/s11356-012-1190-8.
104. Mathur, M.; Gola, D.; Panja, R.; Malik, A.; Ahammad, S.Z. Performance Evaluation of Two Aspergillus Spp. for the Decolourization of Reactive Dyes by Bioaccumulation and Biosorption. *Environ. Sci. Pollut. Res.* **2018**, *25(1)*, 345–352, doi:10.1007/s11356-017-0417-0.
105. Rajhans, G.; Barik, A.; Sen, S.K.; Raut, S. Degradation of Dyes by Fungi: An Insight into Mycoremediation. *BioTechnologia* **2021**, *102(4)*, 445–455, doi:10.5114/bta.2021.111109.
106. Asgher, M.; Kamal, S.; Iqbal, H.M.N. Improvement of Catalytic Efficiency, Thermo-Stability and Dye Decolorization Capability of Pleurotus ostreatusIBL-02 Laccase by Hydrophobic Sol Gel Entrapment. *Chem. Cent. J.* **2012**, *6(1),110*, doi:10.1186/1752-153x-6-110.
107. Jureczko, M.; Przystaś, W. Removal of Two Cytostatic Drugs: Bleomycin and Vincristine by White-Rot Fungi – a Sorption Study. *J. Environ. Health Sci. Eng.* **2021**, *19(1)*, 651–662, doi:10.1007/s40201-021-00635-8.

108. Przystaś, W.; Zabłocka-Godlewska, E.; Grabińska-Sota, E. Biological Removal of Azo and Triphenylmethane Dyes and Toxicity of Process By-Products. *Water. Air. Soil Pollut.* **2012**, *223(4)*, 1581–1592, doi:10.1007/s11270-011-0966-7.
109. Pecková, V.; Legerská, B.; Chmelová, D.; Horník, M.; Ondrejovič, M. Comparison of Efficiency for Monoazo Dye Removal by Different Species of White-Rot Fungi. *Int. J. Environ. Sci. Technol.* **2021**, *18(1)*, 21–32, doi:10.1007/s13762-020-02806-w.
110. Santaeufemia, S.; Torres, E.; Mera, R.; Abalde, J. Bioremediation of Oxytetracycline in Seawater by Living and Dead Biomass of the Microalga Phaeodactylum Tricornutum. *J. Hazard. Mater.* **2016**, *320*, 315–325, doi:10.1016/j.jhazmat.2016.08.042.
111. Torres, E. Biosorption: A Review of the Latest Advances. *Processes* **2020**, *8(12)*, 1584, doi:10.3390/pr8121584.
112. Enayatizamir, N.; Tabandeh, F.; Rodríguez-Couto, S.; Yakhchali, B.; Alikhani, H.A.; Mohammadi, L. Biodegradation Pathway and Detoxification of the Diazo Dye Reactive Black 5 by Phanerochaete Chrysosporium. *Bioresour. Technol.* **2011**, *102(22)*, 10359–10362, doi:10.1016/j.biortech.2011.08.130.
113. Iqbal, M.; Saeed, A. Biosorption of Reactive Dye by Loofa Sponge-Immobilized Fungal Biomass of Phanerochaete Chrysosporium. *Process Biochem.* **2007**, *42*, 1160–1164, doi:10.1016/j.procbio.2007.05.014.
114. Crespão, L.P.; Rosenberger, A.G.; Lima, F.D.S.; Delgado Bertéli, M.B.; Dragunski, D.C.; Colauto, N.B.; Linde, G.A.; Celso Gonçalves, A.; Caetano, J. Sugarcane Biomass Colonized by *Pleurotus Ostreatus* for Red 4B Dye Removal: A Sustainable Alternative. *Environ. Technol.* **2021**, *42(17)*, 2611–2623, doi:10.1080/09593330.2019.1708975.
115. Sun, S.; Xie, S.; Cheng, Y.; Yu, H.; Zhao, H.; Li, M.; Li, X.; Zhang, X.; Yuan, J.S.; Dai, S.Y. Enhancement of Environmental Hazard Degradation in the Presence of Lignin: A Proteomics Study. *Sci. Rep.* **2017**, *7(1),11356*, doi:10.1038/s41598-017-10132-4.
116. Rawat, D.; Sharma, R.S.; Karmakar, S.; Arora, L.S.; Mishra, V. Ecotoxic Potential of a Presumably Non-Toxic Azo Dye. *Ecotoxicol. Environ. Saf.* **2018**, *148*, 528–537, doi:10.1016/j.ecoenv.2017.10.049.
117. Danouche, M.; El Arroussi, H.; El Ghachtouli, N. Mycoremediation of Synthetic Dyes by Yeast Cells: A Sustainable Biodegradation Approach. *Environ. Sustain.* **2021**, *4(1)*, 5–22, doi:10.1007/s42398-020-00150-w.
118. Ceretta, M.B.; Nercessian, D.; Wolski, E.A. Current Trends on Role of Biological Treatment in Integrated Treatment Technologies of Textile Wastewater. *Front. Microbiol.* **2021**, *12*, 651025, doi:10.3389/fmicb.2021.651025.
119. Obaideen, K.; Shehata, N.; Sayed, E.T.; Abdelkareem, M.A.; Mahmoud, M.S.; Olabi, A.G. The Role of Wastewater Treatment in Achieving Sustainable Development Goals (SDGs) and Sustainability Guideline. *Energy Nexus* **2022**, *7*, 100112, doi:10.1016/j.nexus.2022.100112.
120. Park, H.; Choi, I.-G. Genomic and Transcriptomic Perspectives on Mycoremediation of Polycyclic Aromatic Hydrocarbons. *Appl. Microbiol. Biotechnol.* **2020**, *104(16)*, 6919–6928, doi:10.1007/s00253-020-10746-1.
121. Das, S.; Cherwoo, L.; Singh, R. Decoding Dye Degradation: Microbial Remediation of Textile Industry Effluents. *Biotechnol. Notes* **2023**, *4*, 64–76, doi:10.1016/j.biotno.2023.10.001.
122. Kijpornyongpan, T.; Schwartz, A.; Yaguchi, A.; Salvachúa, D. Systems Biology-Guided Understanding of White-Rot Fungi for Biotechnological Applications: A Review. *iScience* **2022**, *25(7)*, 104640, doi:10.1016/j.isci.2022.104640.
123. Ijoma, G.N.; Heri, S.M.; Matambo, T.S.; Tekere, M. Trends and Applications of Omics Technologies to Functional Characterisation of Enzymes and Protein Metabolites Produced by Fungi. *J. Fungi* **2021**, *7(9)*, 700, doi:10.3390/jof7090700.

124. Ali, S.S.; Al-Tohamy, R.; Mahmoud, Y.A.-G.; Kornaros, M.; Sun, S.; Sun, J. Recent Advances in the Life Cycle Assessment of Biodiesel Production Linked to Azo Dye Degradation Using Yeast Symbionts of Termite Guts: A Critical Review. *Energy Rep.* **2022**, *8*, 7557–7581, doi:10.1016/j.egyr.2022.05.240.
125. Przystaś, W.; Zabłocka-Godlewska, E.; Grabińska-Sota, E. Efficiency of Decolorization of Different Dyes Using Fungal Biomass Immobilized on Different Solid Supports. *Braz. J. Microbiol.* **2018**, *49(2)*, 285–295, doi:10.1016/j.bjm.2017.06.010.
126. Vasconcelos, M.R.S.; Vieira, G.A.L.; Otero, I.V.R.; Bonugli-Santos, R.C.; Rodrigues, M.V.N.; Rehder, V.L.G.; Ferro, M.; Boaventura, S.; Bacci, M.; Sette, L.D. Pyrene Degradation by Marine-Derived Ascomycete: Process Optimization, Toxicity, and Metabolic Analyses. *Environ. Sci. Pollut. Res.* **2019**, *26(1)*, 12412–12424, doi:10.1007/s11356-019-04518-2.
127. Yanto, D.H.Y.; Chempaka, R.M.; Nurhayat, O.D.; Argo, B.D.; Watanabe, T.; Wibisono, Y.; Hung, Y.-T. Optimization of Dye-Contaminated Wastewater Treatment by Fungal Mycelial-Light Expanded Clay Aggregate Composite. *Environ. Res.* **2023**, *231*, 116207, doi:10.1016/j.envres.2023.116207.
128. Paul, M.; Pandey, N.K.; Banerjee, A.; Shroti, G.K.; Tomer, P.; Gazara, R.K.; Thatoi, H.; Bhaskar, T.; Hazra, S.; Ghosh, D. An Insight into Omics Analysis and Metabolic Pathway Engineering of Lignin-Degrading Enzymes for Enhanced Lignin Valorization. *Bioresour. Technol.* **2023**, *379*, 129045, doi:10.1016/j.biortech.2023.129045.
129. McGregor, N.G.S.; De Boer, C.; Santos, M.; Haon, M.; Navarro, D.; Schroder, S.; Berrin, J.-G.; Overkleeft, H.S.; Davies, G.J. Activity-Based Protein Profiling Reveals Dynamic Substrate-Specific Cellulase Secretion by Saprotrophic Basidiomycetes. *Biotechnol. Biofuels Bioprod.* **2022**, *15*, doi:10.1186/s13068-022-02107-z.
130. Ata, Ö.; Mattanovich, D. Into the Metabolic Wild: Unveiling Hidden Pathways of Microbial Metabolism. *Microb. Biotechnol.* **2024**, *17(8),e14548*, doi:10.1111/1751-7915.
131. Pratap, B.; Kumar, S.; Nand, S.; Azad, I.; Bharagava, R.N.; Romanholo Ferreira, L.F.; Dutta, V. Wastewater Generation and Treatment by Various Eco-Friendly Technologies: Possible Health Hazards and Further Reuse for Environmental Safety. *Chemosphere* **2023**, *313*, 137547, doi:10.1016/j.chemosphere.2022.137547.
132. Jureczko, M.; Krawczyk, T.; López De Alda, M.; Garcia-Vara, M.; Banach-Wiśniewska, A.; Przystaś, W. Removal of the Cytostatic Drugs Bleomycin and Vincristine by White-Rot Fungi under Various Conditions, and Determination of Enzymes Involved, Degradation by-Products, and Toxicity. *Sci. Total Environ.* **2024**, *954*, 176420, doi:10.1016/j.scitotenv.2024.176420.
133. Nagraj; Chaurasia, P.K.; Bharati, S.L.; Sharma, N.; Kumar, J.; Sivalingam, A.M. Degradation of Dyes by Fungi: An Overview on Recent Updates. *The Microbe* **2025**, *6*, 100232, doi:10.1016/j.microb.2024.100232.
134. Przystaś, W.; Zabłocka-Godlewska, E.; Grabińska-Sota, E. Pleurotus Ostreatus as a Species with Potentially High Effectiveness in the Removal of Synthetic Dyes Belonging to Different Classes. *Desalination Water Treat.* **2019**, *161*, 376–386, doi:10.5004/dwt.2019.24314.
135. Jureczko, M.; Przystaś, W.; Krawczyk, T.; Gonciarz, W.; Rudnicka, K. White-Rot Fungi-Mediated Biodegradation of Cytostatic Drugs - Bleomycin and Vincristine. *J. Hazard. Mater.* **2021**, *407*, 124632, doi:10.1016/j.jhazmat.2020.124632.
136. Tolerance to Cytostatic Drugs Bleomycin and Vincristine by White Rot Fungi. *Arch. Environ. Prot.* **2023**, 46(3), doi:10.24425/aep.2020.134540.
137. Bilal, M.; Asgher, M.; Parra-Saldivar, R.; Hu, H.; Wang, W.; Zhang, X.; Iqbal, H.M.N. Immobilized Ligninolytic Enzymes: An Innovative and Environmental Responsive

Technology to Tackle Dye-Based Industrial Pollutants – A Review. *Sci. Total Environ.* **2017**, *576*, 646–659, doi:10.1016/j.scitotenv.2016.10.137.
138. Girijan, S.; Kumar, M. Immobilized Biomass Systems: An Approach for Trace Organics Removal from Wastewater and Environmental Remediation. *Curr. Opin. Environ. Sci. Health* **2019**, *12*, 18–29, doi:10.1016/j.coesh.2019.08.005.
139. Jun, L.Y.; Yon, L.S.; Mubarak, N.M.; Bing, C.H.; Pan, S.; Danquah, M.K.; Abdullah, E.C.; Khalid, M. An Overview of Immobilized Enzyme Technologies for Dye and Phenolic Removal from Wastewater. *J. Environ. Chem. Eng.* **2019**, *7*, 102961, doi:10.1016/j.jece.2019.102961.
140. Zheng, Z.; Ali, A.; Su, J.; Zhang, S.; Fan, Y.; Sun, Y. Self-Immobilized Biochar Fungal Pellet Combined with Bacterial Strain H29 Enhanced the Removal Performance of Cadmium and Nitrate. *Bioresour. Technol.* **2021**, *341*, 125803, doi:10.1016/j.biortech.2021.125803.
141. Wu, K.; Pan, X.; Zhang, J.; Zhang, X.; Salah zene, A.; Tian, Y. Biosorption of Congo Red from Aqueous Solutions Based on Self-Immobilized Mycelial Pellets: Kinetics, Isotherms, and Thermodynamic Studies. *ACS Omega* **2020**, *5(38)*, 24601–24612, doi:10.1021/acsomega.0c03114.
142. Puchana-Rosero, M.J.; Lima, E.C.; Ortiz-Monsalve, S.; Mella, B.; Da Costa, D.; Poll, E.; Gutterres, M. Fungal Biomass as Biosorbent for the Removal of Acid Blue 161 Dye in Aqueous Solution. *Environ. Sci. Pollut. Res.* **2017**, *24(4)*, 4200–4209, doi:10.1007/s11356-016-8153-4.
143. Upadhyay, R.; Khan, I.U.-H.; Przystaś, W. An Evaluation of Decolorization Mechanism of Synthetic Dyes Belonging to the Azo, Anthraquinone and Triphenylmethane Group, as a Sustainable Approach, by Immobilized CB8 Strain (Trametes Versicolor). *Desalination Water Treat.* **2023**, *284*, 268–277, doi:10.5004/dwt.2023.29270.
144. Sun, S.; Xie, S.; Chen, H.; Cheng, Y.; Shi, Y.; Qin, X.; Dai, S.Y.; Zhang, X.; Yuan, J.S. Genomic and Molecular Mechanisms for Efficient Biodegradation of Aromatic Dye. *J. Hazard. Mater.* **2016**, *302*, 286–295, doi:10.1016/j.jhazmat.2015.09.071.
145. Rybczyńska-Tkaczyk, K.; Korniłłowicz-Kowalska, T. Biosorption Optimization and Equilibrium Isotherm of Industrial Dye Compounds in Novel Strains of Microscopic Fungi. *Int. J. Environ. Sci. Technol.* **2016**, *13*, 2837–2846, doi:10.1007/s13762-016-1111-3.
146. Ghanaim, A.M.; Mahdy, O.M.E.; Mohamed, H.I. Biodegradation of Azo Dyes by Aspergillus Flavus and Its Bioremediation Potential Using Seed Germination Efficiency. *BMC Microbiol.* **2025**, *25(1),7*, doi:10.1186/s12866-024-03703-9.
147. Prabhakar, T.; Giaretta, J.; Zulli, R.; Rath, R.J.; Farajikhah, S.; Talebian, S.; Dehghani, F. Covalent Immobilization: A Review from an Enzyme Perspective. *Chem. Eng. J.* **2025**, *503*, 158054, doi:10.1016/j.cej.2024.158054.
148. He, H.; Li, Y.; Fang, M.; Li, T.; Liang, Y.; Mei, Y. Carbon Source Affects Synthesis, Structures, and Activities of Mycelial Polysaccharides from Medicinal Fungus Inonotus Obliquus. *J. Microbiol. Biotechnol.* **2021**, *31(6)*, 855–866, doi:10.4014/jmb.2102.02006.
149. Sabuda, M.C.; Mejia, J.; Wedal, M.; Kuester, B.; Xu, T.; Santelli, C.M. The Effect of Organic Carbon Form and Concentration on Fungal Selenite Reduction. *Appl. Geochem.* **2022**, *136*, 105163, doi:10.1016/j.apgeochem.2021.105163.
150. Zhang, X.; Hou, X.; Xu, D.; Xue, M.; Zhang, J.; Wang, J.; Yang, Y.; Lai, D.; Zhou, L. Effects of Carbon, Nitrogen, Ambient pH and Light on Mycelial Growth, Sporulation, Sorbicillinoid Biosynthesis and Related Gene Expression in Ustilaginoidea Virens. *J. Fungi* **2023**, *9(4)*, 390, doi:10.3390/jof9040390.

151. Itoo, Z.A.; Reshi, Z.A. Effect of Different Nitrogen and Carbon Sources and Concentrations on the Mycelial Growth of Ectomycorrhizal Fungi under In-Vitro Conditions. *Scand. J. For. Res.* **2014**, *29(7)*, 619–628, doi:10.1080/02827581.2014.964756.
152. Li, F.; Di, L.; Liu, Y.; Xiao, Q.; Zhang, X.; Ma, F.; Yu, H. Carbaryl Biodegradation by Xylaria Sp. BNL1 and Its Metabolic Pathway. *Ecotoxicol. Environ. Saf.* **2019**, *167*, 331–337, doi:10.1016/j.ecoenv.2018.10.051.
153. Di Lonardo, D.P.; Van Der Wal, A.; Harkes, P.; De Boer, W. Effect of Nitrogen on Fungal Growth Efficiency. *Plant Biosyst. - Int. J. Deal. Asp. Plant Biol.* **2020**, *154(4)*, 433–437, doi:10.1080/11263504.2020.1779849.
154. Kumar, Y.; Ramesh, H.; Dhabade, K.; Shahare, M.; Kalra, B. Structural Study and Molecular Docking Insights into Laccase-Mediated Dye Degradation. *Sustain. Chem. Environ.* **2024**, *8*, 100175, doi:10.1016/j.scenv.2024.100175.
155. Janusz, G.; Kucharzyk, K.H.; Pawlik, A.; Staszczak, M.; Paszczynski, A.J. Fungal Laccase, Manganese Peroxidase and Lignin Peroxidase: Gene Expression and Regulation. *Enzyme Microb. Technol.* **2013**, *52*, 1–12, doi:10.1016/j.enzmictec.2012.10.003.
156. De Jong, E.; Cazemier, A.E.; Field, J.A.; De Bont, J.A.M. Physiological Role of Chlorinated Aryl Alcohols Biosynthesized De Novo by the White Rot Fungus *Bjerkandera* Sp. Strain BOS55. *Appl. Environ. Microbiol.* **1994**, *60(1)*, 271–277, doi:10.1128/aem.60.1.271-277.1994.
157. Bilal, M.; Zdarta, J.; Jesionowski, T.; Iqbal, H.M.N. Manganese Peroxidases as Robust Biocatalytic Tool — An Overview of Sources, Immobilization, and Biotechnological Applications. *Int. J. Biol. Macromol.* **2023**, *234*, 123531, doi:10.1016/j.ijbiomac.2023.123531.
158. Moreira, M. Oxidation of Lignin in Eucalyptus Kraft Pulp by Manganese Peroxidase from Bjerkandera Sp. Strain BOS55. *Bioresour. Technol.* **2001**, *78(1)*, 71–79, doi:10.1016/s0960-8524(00)00161-9.
159. Zhang, Z.; Wen, J.; Li, J.; Ma, X.; Yu, Y.; Tan, X.; Wang, Q.; Liu, B.; Li, X.; Li, Y.; et al. The Evolution of Genomic and Epigenomic Features in Two Pleurotus Fungi. *Sci. Rep.* **2018**, *8(1), 8313*, doi:10.1038/s41598-018-26619-7.
160. Park, H.; Min, B.; Jang, Y.; Kim, J.; Lipzen, A.; Sharma, A.; Andreopoulos, B.; Johnson, J.; Riley, R.; Spatafora, J.W.; et al. Comprehensive Genomic and Transcriptomic Analysis of Polycyclic Aromatic Hydrocarbon Degradation by a Mycoremediation Fungus, Dentipellis Sp. KUC8613. *Appl. Microbiol. Biotechnol.* **2019**, *103(19)*, 8145–8155, doi:10.1007/s00253-019-10089-6.
161. Persoone, G.; Marsalek, B.; Blinova, I.; Törökne, A.; Zarina, D.; Manusadzianas, L.; Nalecz-Jawecki, G.; Tofan, L.; Stepanova, N.; Tothova, L.; et al. A Practical and User-friendly Toxicity Classification System with Microbiotests for Natural Waters and Wastewaters. *Environ. Toxicol.* **2003**, *18(6)*, 395–402, doi:10.1002/tox.10141.
162. Tomaszewski, M.; Cema, G.; Ziembińska-Buczyńska, A. Significance of pH Control in Anammox Process Performance at Low Temperature. *Chemosphere* **2017**, *185*, 439–444, doi:10.1016/j.chemosphere.2017.07.034.
163. Tomaszewski, M.; Cema, G.; Ziembińska-Buczyńska, A. Influence of Temperature and pH on the Anammox Process: A Review and Meta-Analysis. *Chemosphere* **2017**, *182*, 203–214, doi:10.1016/j.chemosphere.2017.05.003.
164. Munagapati, V.S.; Wen, H.-Y.; Wen, J.-C.; Gutha, Y.; Tian, Z.; Reddy, G.M.; Garcia, J.R. Anionic Congo Red Dye Removal from Aqueous Medium Using Turkey Tail (*Trametes Versicolor*) Fungal Biomass: Adsorption Kinetics, Isotherms, Thermodynamics, Reusability, and Characterization. *J. Dispers. Sci. Technol.* **2021**, *42(12)*, 1785–1798, doi:10.1080/01932691.2020.1789468.

165. Hasanien, Y.A.; Zaki, A.G.; Abdel-Razek, A.S. Employment of Collective Physical Pretreatment and Immobilization of Actinomucor Biomass for Prospective Crystal Violet Remediation Efficiency. *Biomass Convers. Biorefinery* **2025**, *15(2)*, 3235–3249, doi:10.1007/s13399-023-04991-3.
166. Przystaś, W. Decolourisation of a Mixture of Dyes from Different Classes Using a Bioreactor with Immobilised Pleurotus Ostreatus Mycelium. *Water* **2025**, *17(15)*, 2314, doi:10.3390/w17152314.
167. Chakraborty, S.; Basak, B.; Dutta, S.; Bhunia, B.; Dey, A. Decolorization and Biodegradation of Congo Red Dye by a Novel White Rot Fungus Alternaria Alternata CMERI F6. *Bioresour. Technol.* **2013**, *147*, 662–666, doi:10.1016/j.biortech.2013.08.117.
168. Basak, B.; Bhunia, B.; Mukherjee, S.; Dey, A. Optimization of Physicochemical Parameters for Phenol Biodegradation by Candida Tropicalis PHB5 Using Taguchi Methodology. *Desalination Water Treat.* **2013**, *51*, 6846–6862, doi:10.1080/19443994.2013.770638.
169. Asses, N.; Ayed, L.; Hkiri, N.; Hamdi, M. Congo Red Decolorization and Detoxification by *Aspergillus Niger*: Removal Mechanisms and Dye Degradation Pathway. *BioMed Res. Int.* **2018**, *2018(1)*, 1–9, doi:10.1155/2018/3049686.
170. Kumar, C.G.; Mongolla, P.; Joseph, J.; Sarma, V.U.M. Decolorization and Biodegradation of Triphenylmethane Dye, Brilliant Green, by Aspergillus Sp. Isolated from Ladakh, India. *Process Biochem.* **2012**, *47*, 1388–1394, doi:10.1016/j.procbio.2012.05.015.
171. Asgher, M.; Bhatti, H.N.; Ashraf, M.; Legge, R.L. Recent Developments in Biodegradation of Industrial Pollutants by White Rot Fungi and Their Enzyme System. *Biodegradation* **2008**, *19(6)*, 771–783, doi:10.1007/s10532-008-9185-3.
172. Kumar, C.G.; Mongolla, P.; Basha, A.; Joseph, J.; Sarma, V.U.M.; Kamal, A. Decolorization and Biotransformation of Triphenylmethane Dye, Methyl Violet, by Aspergillus Sp. Isolated from Ladakh, India. *J. Microbiol. Biotechnol.* **2011**, *21(3)*, 267–273, doi: 10.4014/jmb.1011.11010.
173. Abhisek, K.; Vhatkar, S.S.; Mathew, H.T.; Singh, P.; Oraon, R. A Critical Review on the Challenges and Techno-Economic Assessment of Dyes Removal Technologies from Waste Water. *Discov. Chem.* **2025**, *2(1)*, 41, doi:10.1007/s44371-025-00111-4.
174. Wang, N.; Chu, Y.; Wu, F.; Zhao, Z.; Xu, X. Decolorization and Degradation of Congo Red by a Newly Isolated White Rot Fungus, Ceriporia Lacerata, from Decayed Mulberry Branches. *Int. Biodeterior. Biodegrad.* **2017**, *117*, 236–244, doi:10.1016/j.ibiod.2016.12.015.
175. Saroj, S.; Dubey, S.; Agarwal, P.; Prasad, R.; Singh, R.P. Evaluation of the Efficacy of a Fungal Consortium for Degradation of Azo Dyes and Simulated Textile Dye Effluents. *Sustain. Water Resour. Manag.* **2015**, *1*, 233–243, doi:10.1007/s40899-015-0027-2.
176. Namasivayam, C.; Dinesh Kumar, M.; Selvi, K.; Ashruffunissa Begum, R.; Vanathi, T.; Yamuna, R.T. 'Waste' Coir Pith—a Potential Biomass for the Treatment of Dyeing Wastewaters. *Biomass Bioenergy* **2001**, *21*, 477–483, doi:10.1016/S0961-9534(01)00052-6.
177. Asfour, H.M.; Nassar, M.M.; Fadali, O.A.; El-Geundi, M.S. Colour Removal from Textile Effluents Using Hardwood Sawdust as an Absorbent. *J. Chem. Technol. Biotechnol. Chem. Technol.* **1985**, *35*, 28–35, doi:10.1002/jctb.5040350106.
178. Yu, J.-X.; Chi, R.-A.; Guo, J.; Zhang, Y.-F.; Xu, Z.-G.; Xiao, C.-Q. Desorption and Photodegradation of Methylene Blue from Modified Sugarcane Bagasse Surface by Acid TiO2 Hydrosol. *Appl. Surf. Sci.* **2012**, *258*, 4085–4090, doi:10.1016/j.apsusc.2011.12.106.
179. Daneshvar, E.; Vazirzadeh, A.; Niazi, A.; Kousha, M.; Naushad, Mu.; Bhatnagar, A. Desorption of Methylene Blue Dye from Brown Macroalga: Effects of Operating

Parameters, Isotherm Study and Kinetic Modeling. *J. Clean. Prod.* **2017**, *152*, 443–453, doi:10.1016/j.jclepro.2017.03.119.
180. Biria, D.; Zarrabi, A.; Khosravi, A. The Application of Corrugated Parallel Bundle Model to Immobilized Cells in Porous Microcapsule Membranes. *J. Membr. Sci.* **2008**, *311(1-2)*, 159–164, doi:10.1016/j.memsci.2007.12.022.
181. Zhuo, R.; Fan, F. A Comprehensive Insight into the Application of White Rot Fungi and Their Lignocellulolytic Enzymes in the Removal of Organic Pollutants. *Sci. Total Environ.* **2021**, *778*, 146132, doi:10.1016/j.scitotenv.2021.146132.
182. Chen, M.; Shang, T.; Fang, W.; Diao, G. Study on Adsorption and Desorption Properties of the Starch Grafted P-Tert-Butyl-Calix[n]Arene for Butyl Rhodamine B Solution. *J. Hazard. Mater.* **2011**, *185(2-3)*, 914–921, doi:10.1016/j.jhazmat.2010.09.107.
183. Singh, G.B.; Vinayak, A.; Mudgal, G.; Kesari, K.K. Azo Dye Bioremediation: An Interdisciplinary Path to Sustainable Fashion. *Environ. Technol. Innov.* **2024**, *36*, 103832, doi:10.1016/j.eti.2024.103832.
184. Eichlerová, I.; Homolka, L.; Lisá, L.; Nerud, F. Orange G and Remazol Brilliant Blue R Decolorization by White Rot Fungi Dichomitus Squalens, Ischnoderma Resinosum and Pleurotus Calyptratus. *Chemosphere* **2005**, *60*, 398–404, doi:10.1016/j.chemosphere.2004.12.036.
185. Sk, R.; Rk, S. Optimization of Physiochemical Parameters for Decolorization of Reactive Black HFGR Using Soil Fungus, Aspergillus Allhabadii MTCC 9988. *J. Bioremediation Biodegrad.* **2012**, *03(6),153-157*, doi:10.4172/2155-6199.1000153.
186. Liu, W.; Chao, Y.; Yang, X.; Bao, H.; Qian, S. Biodecolorization of Azo, Anthraquinonic and Triphenylmethane Dyes by White-Rot Fungi and a Laccase-Secreting Engineered Strain. *J. Ind. Microbiol. Biotechnol.* **2004**, *31(3)*, 127–132, doi:10.1007/s10295-004-0123-z.
187. C. R. Costa, F.; S. L. Brito, F.; R. De Grandi, M.J.; F. S. Daniel, J. White Rot Fungi for Biodegradation of Dyes: Potential for Industrial Uses - A Review. *J. Braz. Chem. Soc.* **2025**, 36(6), e-20250024, doi:10.21577/0103-5053.20250024.
188. Wang, F.; Xu, L.; Zhao, L.; Ding, Z.; Ma, H.; Terry, N. Fungal Laccase Production from Lignocellulosic Agricultural Wastes by Solid-State Fermentation: A Review. *Microorganisms* **2019**, *7*, 665, doi:10.3390/microorganisms7120665.
189. Thozhukattu Valliyaparambil, P.; Alagapuram Kaliyaperumal, K.; Gopakumaran, N. Pleurotus Ostreatus Laccase Decolorization of Remazol Brilliant Violet 5R Dye: Statistical Optimization and Toxicity Studies on Microbes and Its Kinetics. *J. Appl. Biotechnol. Rep.* **2019**, *6*, 88–95, doi:10.29252/JABR.06.03.02.
190. Daly, P.; Peng, M.; Di Falco, M.; Lipzen, A.; Wang, M.; Ng, V.; Grigoriev, I.V.; Tsang, A.; Mäkelä, M.R.; de Vries, R.P. Glucose-Mediated Repression of Plant Biomass Utilization in the White-Rot Fungus Dichomitus Squalens. *Appl. Environ. Microbiol.* **2019**, *85*, e01828-19, doi:10.1128/AEM.01828-19.
191. Kobakhidze, A.; Asatiani, M.; Kachlishvili, E.; Elisashvili, V. Induction and Catabolite Repression of Cellulase and Xylanase Synthesis in the Selected White-Rot Basidiomycetes. *Ann. Agrar. Sci.* **2016**, *14(3)*, 169–176, doi:10.1016/j.aasci.2016.07.001.
192. Ahamed, A.; Vermette, P. Effect of Mechanical Agitation on the Production of Cellulases by Trichoderma Reesei RUT-C30 in a Draft-Tube Airlift Bioreactor. *Biochem. Eng. J.* **2010**, *49(3)*, 379–387, doi:10.1016/j.bej.2010.01.014.
193. Abrashev, R.; Krumova, E.; Petrova, P.; Eneva, R.; Dishliyska, V.; Gocheva, Y.; Engibarov, S.; Miteva-Staleva, J.; Spasova, B.; Kolyovska, V.; et al. Glucose Catabolite Repression Participates in the Regulation of Sialidase Biosynthesis by Antarctic Strain Penicillium Griseofulvum P29. *J. Fungi* **2024**, *10(4)*, 241, doi:10.3390/jof10040241.

194. Alfaro, M.; Majcherczyk, A.; Kües, U.; Ramírez, L.; Pisabarro, A.G. Glucose Counteracts Wood-Dependent Induction of Lignocellulolytic Enzyme Secretion in Monokaryon and Dikaryon Submerged Cultures of the White-Rot Basidiomycete Pleurotus Ostreatus. *Sci. Rep.* **2020**, *10*, 12421, doi:10.1038/s41598-020-68969-1.
195. Garrido-Bazán, V.; Téllez-Téllez, M.; Herrera-Estrella, A.; Díaz-Godínez, G.; Nava-Galicia, S.; Villalobos-López, M.Á.; Arroyo-Becerra, A.; Bibbins-Martínez, M. Effect of Textile Dyes on Activity and Differential Regulation of Laccase Genes from Pleurotus Ostreatus Grown in Submerged Fermentation. *AMB Express* **2016**, *6*, 93, doi:10.1186/s13568-016-0263-3.
196. Jiao, X.; Li, G.; Wang, Y.; Nie, F.; Cheng, X.; Abdullah, M.; Lin, Y.; Cai, Y. Systematic Analysis of the Pleurotus Ostreatus Laccase Gene (PoLac) Family and Functional Characterization of PoLac2 Involved in the Degradation of Cotton-Straw Lignin. *Molecules* **2018**, *23(4)*, 880, doi:10.3390/molecules23040880.
197. Cuamatzi-Flores, J.; Nava-Galicia, S.; Esquivel-Naranjo, E.U.; Lopez Munguia, A.; Arroyo-Becerra, A.; Villalobos-López, M.A.; Bibbins-Martínez, M. Regulation of Dye-Decolorizing Peroxidase Gene Expression in Pleurotus Ostreatus Grown on Glycerol as the Carbon Source. *PeerJ* **2024**, *12*, e17467, doi:10.7717/peerj.17467.
198. Larrondo, L.F.; Vicuña, R.; Cullen, D. Phanerochaete Chrysosporium Genomics. In *Applied Mycology and Biotechnology*; Elsevier, 2005; Vol. 5, pp. 315–352 ISBN 978-0-444-51808-8.
199. Dong, J.L.; Zhang, Y.W.; Zhang, R.H.; Huang, W.Z.; Zhang, Y.Z. Influence of Culture Conditions on Laccase Production and Isozyme Patterns in the White-rot Fungus *Trametes Gallica*. *J. Basic Microbiol.* **2005**, *45(3)*, 190–198, doi:10.1002/jobm.200410511.
200. Levin, L.; Melignani, E.; Ramos, A.M. Effect of Nitrogen Sources and Vitamins on Ligninolytic Enzyme Production by Some White-Rot Fungi. Dye Decolorization by Selected Culture Filtrates. *Bioresour. Technol.* **2010**, *101(12)*, 4554–4563, doi:10.1016/j.biortech.2010.01.102.
201. Aghaie-Khouzani, M.; Forootanfar, H.; Moshfegh, M.; Khoshayand, M.R.; Faramarzi, M.A. Decolorization of Some Synthetic Dyes Using Optimized Culture Broth of Laccase Producing Ascomycete Paraconiothyrium Variabile. *Biochem. Eng. J.* **2012**, *60*, 9–15, doi:10.1016/j.bej.2011.09.002.
202. Tien, M.; Kirk, T.K. Lignin Peroxidase of Phanerochaete Chrysosporium. In *Methods in Enzymology*; Elsevier, 1988; Vol. 161, pp. 238–249 ISBN 978-0-12-182062-6.
203. Asgher, M.; Kausar, S.; Bhatti, H.N.; Hassan Shah, S.A.; Ali, M. Optimization of Medium for Decolorization of Solar Golden Yellow R Direct Textile Dye by Schizophyllum Commune IBL-06. *Int. Biodeterior. Biodegrad.* **2008**, *61*, 189–193, doi:10.1016/j.ibiod.2007.07.009.
204. Balachandran, B.; Sabumon, P.C. A Comprehensive Review on Biodegradation of Azo Dye Mixtures, Metabolite Profiling with Health Implications and Removal Strategies. *J. Hazard. Mater. Adv.* **2025**, *19*, 100834, doi:10.1016/j.hazadv.2025.100834.
205. Andrade, M.V.F.; Silva, K.M.L.D.; Siqueira, J.P.D.S.; Wanderley, C.R.P.; Araújo, R.D.S.; Marinho, G.; Rodrigues, K. Azo Dye Degradation by Phanerochaete Chrysosporium in the Medium Enriched with Nitrogen in the Presence of Primary Co-Substrate. *Braz. Arch. Biol. Technol.* **2013**, *56*, 867–874, doi:10.1590/S1516-89132013000500019.
206. Li, Q.; Feng, Y.; Zhuang, S.; Kang, L.; Yang, Y. Decolorization and Detoxification of Azo and Triphenylmethane Dyes Damaging Human Health by Crude Laccase from White-Rot Fungus Pleurotus Ostreatus Yang1 and Molecular Docking Between Laccase and Structurally Diverse Dyes. *Int. J. Mol. Sci.* **2025**, *26*, 8363, doi:10.3390/ijms26178363.

207. Verma, A.K.; Raghukumar, C.; Verma, P.; Shouche, Y.S.; Naik, C.G. Four Marine-Derived Fungi for Bioremediation of Raw Textile Mill Effluents. *Biodegradation* **2010**, *21(2)*, 217–233, doi:10.1007/s10532-009-9295-6.
208. Tudzynski, B. Nitrogen Regulation of Fungal Secondary Metabolism in Fungi. *Front. Microbiol.* **2014**, *5*, 656, doi:10.3389/fmicb.2014.00656.
209. Zhang, J.; Zhuo, X.; Wang, Q.; Ji, H.; Chen, H.; Hao, H. Effects of Different Nitrogen Levels on Lignocellulolytic Enzyme Production and Gene Expression under Straw-State Cultivation in Stropharia Rugosoannulata. *Int. J. Mol. Sci.* **2023**, *24(12)*, 10089, doi:10.3390/ijms241210089.
210. Rodríguez Couto, S.; Sanromán, M.A.; Hofer, D.; Gübitz, G.M. Stainless Steel Sponge: A Novel Carrier for the Immobilisation of the White-Rot Fungus Trametes Hirsuta for Decolourization of Textile Dyes. *Bioresour. Technol.* **2004**, *95(1)*, 67–72, doi:10.1016/j.biortech.2003.05.002.
211. Carabajal, M.; Perullini, M.; Jobbágy, M.; Ullrich, R.; Hofrichter, M.; Levin, L. Removal of Phenol by Immobilization of *Trametes Versicolor* in Silica–Alginate–Fungus Biocomposites and Loofa Sponge. *CLEAN – Soil Air Water* **2016**, *44(2)*, 180–188, doi:10.1002/clen.201400366.
212. González-Morales, E.; Peula-Ruiz, E.; Newman-Portela, A.M.; López-Tercero, L.; Medina-Castillo, A.L.; Lopez-Lopez, M.T.; Merroun, M.L.; Ruiz-Fresneda, M.A. Enhancing Se(IV) Bioremediation Efficiency via Immobilization of Filamentous Fungi and Yeasts in Eco-Friendly Alginate Bead Hydrogels. *Chemosphere* **2025**, *370*, 144020, doi:10.1016/j.chemosphere.2024.144020.
213. Voběrková, S.; Solčány, V.; Vršanská, M.; Adam, V. Immobilization of Ligninolytic Enzymes from White-Rot Fungi in Cross-Linked Aggregates. *Chemosphere* **2018**, *202*, 694–707, doi:10.1016/j.chemosphere.2018.03.088.
214. Fayyaz, I.; Saddick, S.; Mahmood, R.T.; Asad, M.J.; Hussain, M.A.; Hu, J.; Awais, M.; Khan, M.I.; Saydaxmetova, S. Biodegradation of Azo and Disperse Dyes by Trametes Versicolor: Process Optimization and MnP Enzyme Dynamics. *Results Eng.* **2025**, *25*, 103980, doi:10.1016/j.rineng.2025.103980.
215. Diorio, L.A.; Fréchou, D.M.S.; Levin, L.N. Removal of Dyes by Immobilization of Trametes Versicolor in a Solid-State Micro-Fermentation System. *Rev. Argent. Microbiol.* **2021**, *53(1)*, 3–10, doi:10.1016/j.ram.2020.04.007.
216. Uber, T.M.; Novi, D.M.P.; Murase, L.Y.; Cheute, V.M.S.; Kagueyama, S.S.; Contato, A.G.; Peralta, R.A.; Bracht, A.; Peralta, R.M. Decolorization and Detoxification of Synthetic Dyes by Trametes Versicolor Laccase Under Salt Stress Conditions. *Reactions* **2025**, *6(4)*, 53, doi:10.3390/reactions6040053.
217. Machado, K.M.G.; Matheus, D.R.; Bononi, V.L.R. Ligninolytic Enzymes Production and Remazol Brilliant Blue R Decolorization by Tropical Brazilian Basidiomycetes Fungi. *Braz. J. Microbiol.* **2005**, *36*, 246–252, doi:10.1590/S1517-83822005000300008.
218. Eichlerová, I.; Baldrian, P. Ligninolytic Enzyme Production and Decolorization Capacity of Synthetic Dyes by Saprotrophic White Rot, Brown Rot, and Litter Decomposing Basidiomycetes. *J. Fungi* **2020**, *6(4)*, 301, doi:10.3390/jof6040301.
219. Jeyabalan, J.; Veluchamy, A.; V, V.P.; Kumar, A.; Chandrasekar, R.; Narayanasamy, S. A Review on the Laccase Assisted Decolourization of Dyes: Recent Trends and Research Progress. *J. Taiwan Inst. Chem. Eng.* **2023**, *151*, 105081, doi:10.1016/j.jtice.2023.105081.
220. Prawitasari, D.A.; Kardena, E. Biotransformation of the Textile Dye Reactive Black 5 with *Aspergillus Niger* and Analysis of Ligninolytic Enzyme Activity. *HAYATI J. Biosci.* **2025**, *33*, 297–309, doi:10.4308/hjb.33.2.297-309.

221. Cantarella, G.; Galli, C.; Gentili, P. Free Radical versus Electron-Transfer Routes of Oxidation of Hydrocarbons by Laccase/Mediator Systems. *J. Mol. Catal. B Enzym.* **2003**, *22*, 135–144, doi:10.1016/S1381-1177(03)00014-6.
222. Unuofin, J.O.; Okoh, A.I.; Nwodo, U.U. Aptitude of Oxidative Enzymes for Treatment of Wastewater Pollutants: A Laccase Perspective. *Molecules* **2019**, *24(11)*, 2064, doi:10.3390/molecules24112064.
223. Kijpornyongpan, T.; Schwartz, A.; Yaguchi, A.; Salvachúa, D. Systems Biology-Guided Understanding of White-Rot Fungi for Biotechnological Applications: A Review. *iScience* **2022**, *25*, 104640, doi:10.1016/j.isci.2022.104640.
224. Syed, K.; Yadav, J.S. P450 Monooxygenases (P450ome) of the Model White Rot Fungus *Phanerochaete Chrysosporium*. *Crit. Rev. Microbiol.* **2012**, *38(4)*, 339–363, doi:10.3109/1040841X.2012.682050.
225. Khan, M.F. Recent Progress and Challenges in Microbial Defluorination and Degradation for Sustainable Remediation of Fluorinated Xenobiotics. *Processes* **2025**, *13(7)*, 2017, doi:10.3390/pr13072017.
226. Guengerich, F.P.; Waterman, M.R.; Egli, M. Recent Structural Insights into Cytochrome P450 Function. *Trends Pharmacol. Sci.* **2016**, *37(8)*, 625–640, doi:10.1016/j.tips.2016.05.006.
227. Barski, O.A.; Tipparaju, S.M.; Bhatnagar, A. The Aldo-Keto Reductase Superfamily and Its Role in Drug Metabolism and Detoxification. *Drug Metab. Rev.* **2008**, *40(4)*, 553–624, doi:10.1080/03602530802431439.
228. Aragaw, T.A.; Bogale, F.M.; Tesfaye, E.L. Oxidative Ligninolytic Enzymes and Their Role in Textile Dye Biodegradation: A Comprehensive Review. *Water Pract. Technol.* **2024**, *19*, 3598–3630, doi:10.2166/wpt.2024.229.
229. Miyauchi, S.; Kiss, E.; Kuo, A.; Drula, E.; Kohler, A.; Sánchez-García, M.; Morin, E.; Andreopoulos, B.; Barry, K.W.; Bonito, G.; et al. Large-Scale Genome Sequencing of Mycorrhizal Fungi Provides Insights into the Early Evolution of Symbiotic Traits. *Nat. Commun.* **2020**, *11(1)*, 5125, doi:10.1038/s41467-020-18795-w.
230. Thuillier, A.; Chibani, K.; Belli, G.; Herrero, E.; Dumarçay, S.; Gérardin, P.; Kohler, A.; Deroy, A.; Dhalleine, T.; Bchini, R.; et al. Transcriptomic Responses of Phanerochaete Chrysosporium to Oak Acetonic Extracts: Focus on a New Glutathione Transferase. *Appl. Environ. Microbiol.* **2014**, *80(20)*, 6316–6327, doi:10.1128/AEM.02103-14.
231. Iwata, M.; Gutiérrez, A.; Marques, G.; Sabat, G.; Kersten, P.J.; Cullen, D.; Bhatnagar, J.M.; Yadav, J.; Lipzen, A.; Yoshinaga, Y.; et al. Omics Analyses and Biochemical Study of Phlebiopsis Gigantea Elucidate Its Degradation Strategy of Wood Extractives. *Sci. Rep.* **2021**, *11*, 12528, doi:10.1038/s41598-021-91756-5.
232. Marinović, M.; Aguilar-Pontes, M.V.; Zhou, M.; Miettinen, O.; De Vries, R.P.; Mäkelä, M.R.; Hildén, K. Temporal Transcriptome Analysis of the White-Rot Fungus Obba Rivulosa Shows Expression of a Constitutive Set of Plant Cell Wall Degradation Targeted Genes during Growth on Solid Spruce Wood. *Fungal Genet. Biol.* **2018**, *112*, 47–54, doi:10.1016/j.fgb.2017.07.004.
233. Martinez, D.; Larrondo, L.F.; Putnam, N.; Gelpke, M.D.S.; Huang, K.; Chapman, J.; Helfenbein, K.G.; Ramaiya, P.; Detter, J.C.; Larimer, F.; et al. Genome Sequence of the Lignocellulose Degrading Fungus Phanerochaete Chrysosporium Strain RP78. *Nat. Biotechnol.* **2004**, *22*, 695–700, doi:10.1038/nbt967.
234. Gao, D.; Du, L.; Yang, J.; Wu, W.-M.; Liang, H. A Critical Review of the Application of White Rot Fungus to Environmental Pollution Control. *Crit. Rev. Biotechnol.* **2010**, *30(1)*, 70–77, doi:10.3109/07388550903427272.

235. Matsuzaki, F.; Shimizu, M.; Wariishi, H. Proteomic and Metabolomic Analyses of the White-Rot Fungus *Phanerochaete Chrysosporium* Exposed to Exogenous Benzoic Acid. *J. Proteome Res.* **2008**, *7(6)*, 2342–2350, doi:10.1021/pr700617s.
236. Novotný, Č.; Rawal, B.; Bhatt, M.; Patel, M.; Šašek, V.; Molitoris, H.P. Capacity of Irpex Lacteus and Pleurotus Ostreatus for Decolorization of Chemically Different Dyes. *J. Biotechnol.* **2001**, *89(2-3)*, 113–122, doi:10.1016/S0168-1656(01)00321-2.
237. Wesenberg, D. White-Rot Fungi and Their Enzymes for the Treatment of Industrial Dye Effluents. *Biotechnol. Adv.* **2003**, *22(1-2)*, 161–187, doi:10.1016/j.biotechadv.2003.08.011.
238. Hori, C.; Ishida, T.; Igarashi, K.; Samejima, M.; Suzuki, H.; Master, E.; Ferreira, P.; Ruiz-Dueñas, F.J.; Held, B.; Canessa, P.; et al. Analysis of the Phlebiopsis Gigantea Genome, Transcriptome and Secretome Provides Insight into Its Pioneer Colonization Strategies of Wood. *PLoS Genet.* **2014**, *10*, e1004759, doi:10.1371/journal.pgen.1004759.
239. Zhu, Y.; Zhou, D.; Bai, N.; Liu, Q.; Zhao, N.; Yang, J. SNARE Protein AoSec22 Orchestrates Mycelial Growth, Vacuole Assembly, Trap Formation, Stress Response, and Secondary Metabolism in Arthrobotrys Oligospora. *J. Fungi* **2023**, *9(1)*, 75, doi:10.3390/jof9010075.
240. Adnan, M.; Islam, W.; Waheed, A.; Hussain, Q.; Shen, L.; Wang, J.; Liu, G. SNARE Protein Snc1 Is Essential for Vesicle Trafficking, Membrane Fusion and Protein Secretion in Fungi. *Cells* **2023**, *12*, 1547, doi:10.3390/cells12111547.
241. Han, Z.; Luo, Z.; Li, X.; Xiong, D.; Tian, C. SNARE Genes CcSec22 and CcSso1 Coordinate Fungal Growth, Sporulation, Cell Wall Stress Tolerance, Endocytosis and Full Virulence in Cytospora Chrysosperma. *Sci. Rep.* **2025**, *15*, 5034, doi:10.1038/s41598-025-88584-2.
242. Aragaw, T.A. Potential and Prospects of Reductases in Azo Dye Degradation: A Review. *The Microbe* **2024**, *4*, 100162, doi:10.1016/j.microb.2024.100162.
243. Balachandran, B.; Sabumon, P.C. A Comprehensive Review on Biodegradation of Azo Dye Mixtures, Metabolite Profiling with Health Implications and Removal Strategies. *J. Hazard. Mater. Adv.* **2025**, *19*, 100834, doi:10.1016/j.hazadv.2025.100834.
244. Selvaraj, V.; Swarna Karthika, T.; Mansiya, C.; Alagar, M. An over Review on Recently Developed Techniques, Mechanisms and Intermediate Involved in the Advanced Azo Dye Degradation for Industrial Applications. *J. Mol. Struct.* **2021**, *1224*, 129195, doi:10.1016/j.molstruc.2020.129195.
245. Zhong, Z.; Li, L.; Chang, P.; Xie, H.; Zhang, H.; Igarashi, Y.; Li, N.; Luo, F. Differential Gene Expression Profiling Analysis in Pleurotus Ostreatus during Interspecific Antagonistic Interactions with Dichomitus Squalens and Trametes Versicolor. *Fungal Biol.* **2017**, *121(12)*, 1025–1036, doi:10.1016/j.funbio.2017.08.008.
246. Khan, M.F.; Hof, C.; Niemcová, P.; Murphy, C.D. Recent Advances in Fungal Xenobiotic Metabolism: Enzymes and Applications. *World J. Microbiol. Biotechnol.* **2023**, *39(11)*, 296, doi:10.1007/s11274-023-03737-7.
247. Ekanayaka, A.H.; De Silva, N.T.; Tarafder, E.; Chen, X.-M.; Dai, D.-Q.; Stephenson, S.L.; Asad, S.; Tibpromma, S.; Karunarathana, S.C. Linking the Metabolic Activity of Plastic-Degrading Fungi to Their Taxonomy and Evolution. *J. Fungi* **2025**, *11(5)*, 378, doi:10.3390/jof11050378.
248. Jurak, E.; Suzuki, H.; Van Erven, G.; Gandier, J.A.; Wong, P.; Chan, K.; Ho, C.Y.; Gong, Y.; Tillier, E.; Rosso, M.-N.; et al. Dynamics of the Phanerochaete Carnosa Transcriptome during Growth on Aspen and Spruce. *BMC Genomics* **2018**, *19*, 815, doi:10.1186/s12864-018-5210-z.
249. Hori, C.; Ishida, T.; Igarashi, K.; Samejima, M.; Suzuki, H.; Master, E.; Ferreira, P.; Ruiz-Dueñas, F.J.; Held, B.; Canessa, P.; et al. Analysis of the Phlebiopsis Gigantea

Genome, Transcriptome and Secretome Provides Insight into Its Pioneer Colonization Strategies of Wood. *PLoS Genet.* **2014**, *10*, e1004759, doi:10.1371/journal.pgen.1004759.
250. Gonzalez Ramos, V.M.; Mueller, A.; Peng, M.; Pawlowski, M.; Lipzen, A.; Ng, V.; Singan, V.; Wang, M.; De Vries, R.P.; Grigoriev, I.V.; et al. Transcriptional Response of the White-Rot Fungus Dichomitus Squalens to Polysaccharides Reveals a Co-Expression Network of Plant Biomass Conversion Related Genes. *Curr. Res. Biotechnol.* **2024**, *7*, 100198, doi:10.1016/j.crbiot.2024.100198.
251. Yu, X.; Mao, C.; Zong, S.; Khan, A.; Wang, W.; Yun, H.; Zhang, P.; Shigaki, T.; Fang, Y.; Han, H.; et al. Transcriptome Analysis Reveals Self-Redox Mineralization Mechanism of Azo Dyes and Novel Decolorizing Hydrolases in Aspergillus Tabacinus LZ-M. *Environ. Pollut.* **2023**, *325*, 121459, doi:10.1016/j.envpol.2023.121459.
252. Xie, M.; Wang, J.; Wang, F.; Wang, J.; Yan, Y.; Feng, K.; Chen, B. A Review of Genomic, Transcriptomic, and Proteomic Applications in Edible Fungi Biology: Current Status and Future Directions. *J. Fungi* **2025**, *11(6)*, 422, doi:10.3390/jof11060422.
253. Vogel, C.; Marcotte, E.M. Insights into the Regulation of Protein Abundance from Proteomic and Transcriptomic Analyses. *Nat. Rev. Genet.* **2012**, *13*, 227–232, doi:10.1038/nrg3185.
254. Sun, S.; Xie, S.; Cheng, Y.; Yu, H.; Zhao, H.; Li, M.; Li, X.; Zhang, X.; Yuan, J.S.; Dai, S.Y. Enhancement of Environmental Hazard Degradation in the Presence of Lignin: A Proteomics Study. *Sci. Rep.* **2017**, *7*, 11356, doi:10.1038/s41598-017-10132-4.
255. Gao, X.; Wang, C.; Dai, W.; Ren, S.; Tao, F.; He, X.; Han, G.; Wang, W. Proteomic Analysis Reveals Large Amounts of Decomposition Enzymes and Major Metabolic Pathways Involved in Algicidal Process of Trametes Versicolor F21a. *Sci. Rep.* **2017**, *7*, 3907, doi:10.1038/s41598-017-04251-1.
256. Cuamatzi-Flores, J.; Nava-Galicia, S.; Esquivel-Naranjo, E.U.; Lopez Munguia, A.; Arroyo-Becerra, A.; Villalobos-López, M.A.; Bibbins-Martínez, M. Regulation of Dye-Decolorizing Peroxidase Gene Expression in Pleurotus Ostreatus Grown on Glycerol as the Carbon Source. *PeerJ* **2024**, *12*, e17467, doi:10.7717/peerj.17467.
257. Bibi, M.; Yasmin, A.; Murtza, I.; Saeed, A.; Jamil, M.A.; Syed, S.S.; Banat, F.; Hai, A. Degradation of Anthraquinone Dye Remazol Brilliant Blue R through Geobacillus Laccase: Simulation of Molecular Docking and Process Optimization by Artificial Neural Network. *Results Eng.* **2025**, *27*, 106908, doi:10.1016/j.rineng.2025.106908.
258. Lee, A.H.; Jang, Y.; Kim, G.-H.; Kim, J.-J.; Lee, S.-S.; Ahn, B.-J. Decolorizing an Anthraquinone Dye by Phlebia Brevispora: Intra-Species Characterization. *Eng. Life Sci.* **2017**, *17(2)*, 125–131, doi:10.1002/elsc.201600059.
259. Attrill, G.; Boddy, L.; Dudley, E.; Greenfield, B.; Eastwood, D.C. Transcriptomic and Protein Analysis of Trametes Versicolor Interacting with a Hypholoma Fasciculare Mycelium Foraging in Soil. *Fungal Ecol.* **2024**, *72*, 101385, doi:10.1016/j.funeco.2024.101385.
260. Adamo, M.; Comtet-Marre, S.; Büttner, E.; Kellner, H.; Luis, P.; Vallon, L.; Prego, R.; Hofrichter, M.; Girlanda, M.; Peyret, P.; et al. Fungal Dye-Decolorizing Peroxidase Diversity: Roles in Either Intra- or Extracellular Processes. *Appl. Microbiol. Biotechnol.* **2022**, *106(8)*, 2993–3007, doi:10.1007/s00253-022-11923-0.
261. Xu, L.; Sun, J.; Qaria, M.A.; Gao, L.; Zhu, D. Dye Decoloring Peroxidase Structure, Catalytic Properties and Applications: Current Advancement and Futurity. *Catalysts* **2021**, *11(8)*, 955, doi:10.3390/catal11080955.
262. Yuan, X.; Tian, G.; Zhao, Y.; Zhao, L.; Wang, H.; Ng, T.B. Biochemical Characteristics of Three Laccase Isoforms from the Basidiomycete Pleurotus Nebrodensis. *Molecules* **2016**, *21(2)*, 203, doi:10.3390/molecules21020203.

263. Li, D.; Ding, Z.; Du, K.; Ye, X.; Cheng, S. Reactive Oxygen Species as a Link between Antioxidant Pathways and Autophagy. *Oxid. Med. Cell. Longev.* **2021**, *2021*, 5583215, doi:10.1155/2021/5583215.
264. Bissaro, B.; Várnai, A.; Røhr, Å.K.; Eijsink, V.G.H. Oxidoreductases and Reactive Oxygen Species in Conversion of Lignocellulosic Biomass. *Microbiol. Mol. Biol. Rev.* **2018**, *82*, e00029-18, doi:10.1128/MMBR.00029-18.
265. Dey, P.; Malik, A.; Singh, D.K.; Haange, S.-B.; Von Bergen, M.; Jehmlich, N. Unveiling Fungal Strategies: Mycoremediation in Multi-Metal Pesticide Environment Using Proteomics. *Sci. Rep.* **2024**, *14*, 23171, doi:10.1038/s41598-024-74517-y.
266. Deller, S.; Macheroux, P.; Sollner, S. Flavin-Dependent Quinone Reductases. *Cell. Mol. Life Sci. CMLS* **2008**, *65*, 141–160, doi:10.1007/s00018-007-7300-y.
267. Presley, G.N.; Zhang, J.; Schilling, J.S. A Genomics-Informed Study of Oxalate and Cellulase Regulation by Brown Rot Wood-Degrading Fungi. *Fungal Genet. Biol.* **2018**, *112*, 64–70, doi:10.1016/j.fgb.2016.08.004.
268. Peng, Q.; Zheng, H.; Xu, H.; Cheng, S.; Yu, C.; Wu, J.; Meng, K.; Xie, G. Response of Soil Fungi to Textile Dye Contamination. *Environ. Pollut.* **2024**, *359*, 124577, doi:10.1016/j.envpol.2024.124577.
269. Črešnar, B.; Petrič, Š. Cytochrome P450 Enzymes in the Fungal Kingdom. *Biochim. Biophys. Acta BBA - Proteins Proteomics* **2011**, *1814*, 29–35, doi:10.1016/j.bbapap.2010.06.020.
270. Eichlerová, I.; Homolka, L.; Benada, O.; Kofronová, O.; Hubálek, T.; Nerud, F. Decolorization of Orange G and Remazol Brilliant Blue R by the White Rot Fungus Dichomitus Squalens: Toxicological Evaluation and Morphological Study. *Chemosphere* **2007**, *69*, 795–802, doi:10.1016/j.chemosphere.2007.04.083.
271. Janusz, G.; Sulej, J.; Jaszek, M.; Osińska-Jaroszuk, M. Effect of Different Wavelengths of Light on Laccase, Cellobiose Dehydrogenase, and Proteases Produced by Cerrena Unicolor, Pycnoporus Sanguineus and Phlebia Lindtneri. *Acta Biochim. Pol.* **2016**, *63(2)*, 223–228, doi:10.18388/abp.2015_1235.
272. Idnurm, A.; Heitman, J. Light Controls Growth and Development via a Conserved Pathway in the Fungal Kingdom. *PLoS Biol.* **2005**, *3*, e95, doi:10.1371/journal.pbio.0030095.
273. Qiang, X.; Guo, X.; Quan, Q.; Su, H.; Huang, D. Improving the Adsorption Performance of Loofah Sponge towards Methylene Blue by Coating Ca2+ Crosslinked Sodium Alginate Layers on Its Fiber Surface. *Coatings* **2020**, *10(9)*, 814, doi:10.3390/coatings10090814.
274. Nadaroglu, H.; Cicek, S.; Gungor, A.A. Removing Trypan Blue Dye Using Nano-Zn Modified Luffa Sponge. *Spectrochim. Acta. A. Mol. Biomol. Spectrosc.* **2017**, *172*, 2–8, doi:10.1016/j.saa.2016.08.052.
275. Upadhyay, R.; Przystaś, W.; Turczyn, R.; Jureczko, M. Enhanced Biosorption of Triarylmethane Dyes by Immobilized Trametes Versicolor and Pleurotus Ostreatus: Optimization, Kinetics, and Reusability. *Water* **2025**, *17(17)*, 2600, doi:10.3390/w17172600.
276. Azin, E.; Moghimi, H. Efficient Mycosorption of Anionic Azo Dyes by Mucor Circinelloides: Surface Functional Groups and Removal Mechanism Study. *J. Environ. Chem. Eng.* **2018**, *6*, 4114–4123, doi:10.1016/j.jece.2018.06.002.
277. Nouri, H.; Azin, E.; Kamyabi, A.; Moghimi, H. Biosorption Performance and Cell Surface Properties of a Fungal-Based Sorbent in Azo Dye Removal Coupled with Textile Wastewater. *Int. J. Environ. Sci. Technol.* **2021**, *18*, 2545–2558, doi:10.1007/s13762-020-03011-5.

278. Chew, S.Y.; Ting, A.S.Y. Common Filamentous Trichoderma Asperellum for Effective Removal of Triphenylmethane Dyes. *Desalination Water Treat.* **2016**, *57(29)*, 13534–13539, doi:10.1080/19443994.2015.1060173.
279. Terangpi, P.; Chakraborty, S. Adsorption Kinetics and Equilibrium Studies for Removal of Acid Azo Dyes by Aniline Formaldehyde Condensate. *Appl. Water Sci.* **2017**, *7(7)*, 3661–3671, doi:10.1007/s13201-016-0510-4.
280. Drumm, F.C.; Franco, D.S.P.; Georgin, J.; Grassi, P.; Jahn, S.L.; Dotto, G.L. Macro-Fungal (Agaricus Bisporus) Wastes as an Adsorbent in the Removal of the Acid Red 97 and Crystal Violet Dyes from Ideal Colored Effluents. *Environ. Sci. Pollut. Res.* **2021**, *28(1)*, 405–415, doi:10.1007/s11356-020-10521-9.
281. Shirsath, S.R.; Patil, A.P.; Patil, R.; Naik, J.B.; Gogate, P.R.; Sonawane, S.H. Removal of Brilliant Green from Wastewater Using Conventional and Ultrasonically Prepared Poly(Acrylic Acid) Hydrogel Loaded with Kaolin Clay: A Comparative Study. *Ultrason. Sonochem.* **2013**, *20(3)*, 914–923, doi:10.1016/j.ultsonch.2012.11.010.
282. Mansour, R.A.; El Shahawy, A.; Attia, A.; Beheary, M.S. Brilliant Green Dye Biosorption Using Activated Carbon Derived from Guava Tree Wood. *Int. J. Chem. Eng.* **2020**, *2020*, 1–12, doi:10.1155/2020/8053828.
283. Fiaz, R.; Hafeez, M.; Mahmood, R. Removal of Brilliant Green (BG) from Aqueous Solution by Using Low Cost Biomass Salix Alba Leaves (SAL): Thermodynamic and Kinetic Studies. *J. Water Reuse Desalination* **2020**, *10*, 70–81, doi:10.2166/wrd.2020.054.
284. Lin, Y.; He, X.; Han, G.; Tian, Q.; Hu, W. Removal of Crystal Violet from Aqueous Solution Using Powdered Mycelial Biomass of Ceriporia Lacerata P2. *J. Environ. Sci.* **2011**, *23(12)*, 2055–2062, doi:10.1016/S1001-0742(10)60643-2.
285. Moturi, B.; Singara Charya, M. Decolourisation of Crystal Violet and Malachite Green By Fungi. *Sci. World J.* **2010**, *4(4)*, doi:10.4314/swj.v4i4.53585.
286. Munck, C.; Thierry, E.; Gräßle, S.; Chen, S.H.; Ting, A.S.Y. Biofilm Formation of Filamentous Fungi Coriolopsis Sp. on Simple Muslin Cloth to Enhance Removal of Triphenylmethane Dyes. *J. Environ. Manage.* **2018**, *214*, 261–266, doi:10.1016/j.jenvman.2018.03.025.
287. Kyi, P.P.; Quansah, J.O.; Lee, C.-G.; Moon, J.-K.; Park, S.-J. The Removal of Crystal Violet from Textile Wastewater Using Palm Kernel Shell-Derived Biochar. *Appl. Sci.* **2020**, *10(7)*, 2251, doi:10.3390/app10072251.
288. Gul, S.; Gul, S.; Gul, H.; Khitab, F.; Khattak, R.; Khan, M.; Ullah, R.; Ullah, R.; Wasil, Z.; Krauklis, A.; et al. Dried Leaves Powder of Adiantum Capillus-Veneris as an Efficient Biosorbent for Hazardous Crystal Violet Dye from Water Resources. *Separations* **2023**, *10(3)*, 165, doi:10.3390/separations10030165.
289. Bhatia, D.; Sharma, N.R.; Singh, J.; Kanwar, R.S. Biological Methods for Textile Dye Removal from Wastewater: A Review. *Crit. Rev. Environ. Sci. Technol.* **2017**, *47(19)*, 1836–1876, doi:10.1080/10643389.2017.1393263.
290. Ejaz, U.; Zehra, U.E.; Javed, H.; Sohail, M. Removal of Triphenylmethane Azo Dye by Immobilized Fungus: A Comparative Study with Physical Adsorption Processes. *Arab. J. Sci. Eng.* **2025**,1-11, doi:10.1007/s13369-025-10099-9.
291. Sintakindi, A.; Ankamwar, B. Fungal Biosorption as an Alternative for the Treatment of Dyes in Waste Waters: A Review. *Environ. Technol. Rev.* **2021**, *10*, 26–43, doi:10.1080/21622515.2020.1869322.
292. Legorreta-Castañeda, A.; Lucho-Constantino, C.; Beltrán-Hernández, R.; Coronel-Olivares, C.; Vázquez-Rodríguez, G. Biosorption of Water Pollutants by Fungal Pellets. *Water* **2020**, *12(4)*, 1155, doi:10.3390/w12041155.

293. Kaushik, P.; Malik, A. Alkali, Thermo and Halo Tolerant Fungal Isolate for the Removal of Textile Dyes. *Colloids Surf. B Biointerfaces* **2010**, *81(1)*, 321–328, doi:10.1016/j.colsurfb.2010.07.034.
294. Grassi, P.; Reis, C.; Drumm, F.C.; Georgin, J.; Tonato, D.; Escudero, L.B.; Kuhn, R.; Jahn, S.L.; Dotto, G.L. Biosorption of Crystal Violet Dye Using Inactive Biomass of the Fungus Diaporthe Schini. *Water Sci. Technol.* **2019**, *79(4)*, 709–717, doi:10.2166/wst.2019.091.
295. Sukla Baidya, K.; Kumar, U. Adsorption of Brilliant Green Dye from Aqueous Solution onto Chemically Modified Areca Nut Husk. *South Afr. J. Chem. Eng.* **2021**, *35*, 33–43, doi:10.1016/j.sajce.2020.11.001.
296. Du, L.-N.; Wang, B.; Li, G.; Wang, S.; Crowley, D.E.; Zhao, Y.-H. Biosorption of the Metal-Complex Dye Acid Black 172 by Live and Heat-Treated Biomass of Pseudomonas Sp. Strain DY1: Kinetics and Sorption Mechanisms. *J. Hazard. Mater.* **2012**, *205–206*, 47–54, doi:10.1016/j.jhazmat.2011.12.001.
297. Bairagi, H.; Khan, Md.M.R.; Ray, L.; Guha, A.K. Adsorption Profile of Lead on Aspergillus Versicolor: A Mechanistic Probing. *J. Hazard. Mater.* **2011**, *186*, 756–764, doi:10.1016/j.jhazmat.2010.11.064.
298. Tang, H.; Zhou, W.; Zhang, L. Adsorption Isotherms and Kinetics Studies of Malachite Green on Chitin Hydrogels. *J. Hazard. Mater.* **2012**, *209–210*, 218–225, doi:10.1016/j.jhazmat.2012.01.010.
299. Dolphen, R.; Thiravetyan, P. Adsorption of Melanoidins by Chitin Nanofibers. *Chem. Eng. J.* **2011**, *166*, 890–895, doi:10.1016/j.cej.2010.11.063.
300. Adsorption of Remazol Brillant Green 6B (RBG 6B) on Chitin: Process Optimization Using Response Surface Methodology. *Glob. NEST J.* **2018**, *20*, 257–268, doi:10.30955/gnj.002507.
301. Iqbal, M.; Saeed, A.; Edyvean, R.G.J.; O'Sullivan, B.; Styring, P. Production of Fungal Biomass Immobilized Loofa Sponge (FBILS)-Discs for the Removal of Heavy Metal Ions and Chlorinated Compounds from Aqueous Solution. *Biotechnol. Lett.* **2005**, *27*, 1319–1323, doi:10.1007/s10529-005-0477-y.
302. Ayangbenro, A.; Babalola, O. A New Strategy for Heavy Metal Polluted Environments: A Review of Microbial Biosorbents. *Int. J. Environ. Res. Public. Health* **2017**, *14*, 94, doi:10.3390/ijerph14010094.
303. Rodríguez-Couto, S. Production of Laccase and Decolouration of the Textile Dye Remazol Brilliant Blue R in Temporary Immersion Bioreactors. *J. Hazard. Mater.* **2011**, *194*, 297–302, doi:10.1016/j.jhazmat.2011.07.098.
304. Palmieri, G.; Giardina, P.; Sannia, G. Laccase-Mediated Remazol Brilliant Blue R Decolorization in a Fixed-Bed Bioreactor. *Biotechnol. Prog.* **2005**, *21*, 1436–1441, doi:10.1021/bp050140i.

APPENDICES

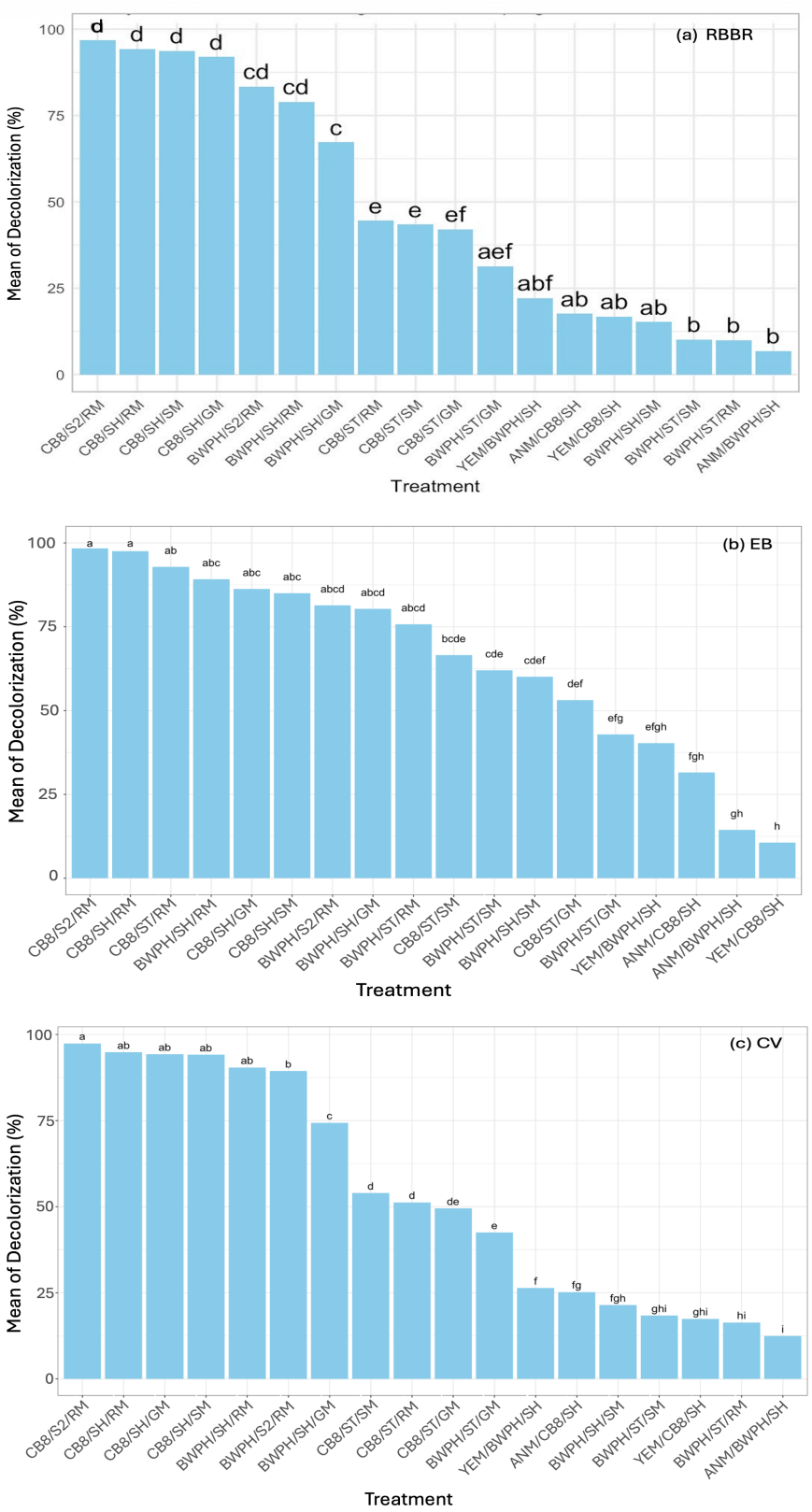

Figure A1. Tukey's post hoc significant grouping test for choosing optimal dye decolorization condition among agitation, immobilization and nutrient source for (a) Remazol Brilliant Blue R (b) Evans Blue and (c) Crystal Violet by *T. versicolor* (CB8) and *P. ostreatus* (BWPH) (presented in section **5.4.4**)

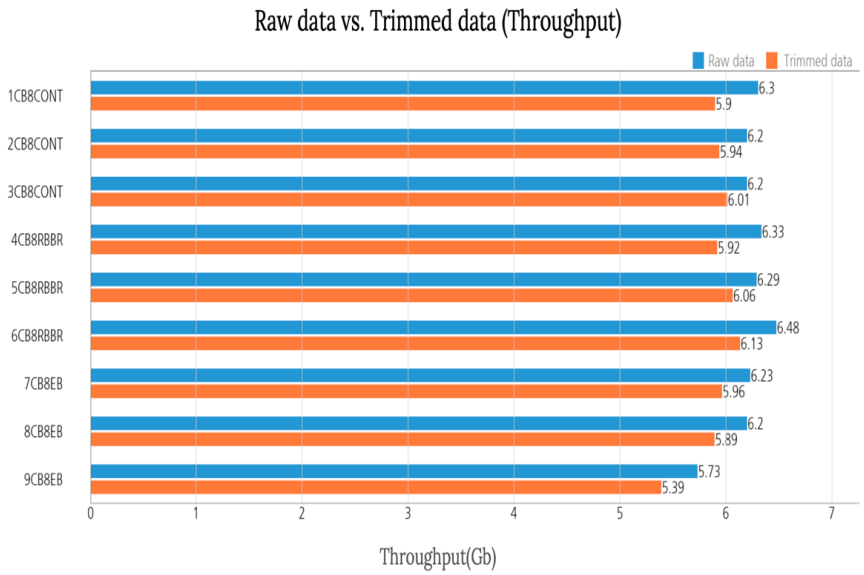

Figure A2. Throughput output of Raw and Trimmed data for *T. versicolor* in control and dye treated condition (presented in section **5.6.1**)

Table A1. Three-factor ANOVA to check effect of carbon source, nitrogen source and fungal biomass type on dye decolorization (presented in section **5.4.4**)

Source of variation	df	Sum of Squares	Mean Square	F value	p-value	Significance
Carbon source	2	559	279	4.81	0.0125	*
Nitrogen source	2	26358	13179	226.64	<0.001	***
Fungus	1	1096	1096	18.85	<0.001	***
Residuals	48	2791	58			

(Note: **** $p \leq 0.0001$, *** $p \leq 0.001$, ** $p \leq 0.01$, * $p \leq 0.05$, $\bar{p} \geq 0.05$)

Table A2. Spearman correlation of Enzyme activity with RBBR dye decolorization (presented in section **5.5.3**)

Enzyme	Spearman ρ	p-value	Strength
Laccase	0.771	0.072	Strong (not significant)
MnP	0.771	0.072	Strong (not significant)
LiP	0.086	0.872	Very weak
Total enzyme activity	**0.714**	**0.111**	**Strong (not significant)**

Table A3. Spearman correlation of Enzyme activity with EB dye decolorization (presented in section **5.5.3**)

Enzyme	Spearman ρ	p-value	Strength
Laccase	0.667	0.148	Strong
MnP	0.232	0.658	Weak
LiP	−0.551	0.257	Moderate negative
Total enzyme activity	**0.348**	**0.499**	Weak

Table A4. Spearman correlation of Enzyme activity with CV dye decolorization (presented in section **5.5.3**)

Enzyme	Spearman ρ	p-value	Strength
Laccase	0.143	0.787	Very weak
MnP	0.029	0.957	Very weak
LiP	−0.257	0.623	Weak negative
Total enzyme activity	**−0.086**	**0.872**	**Very weak**

Table A5. Raw data stats of read count and quality scores for control and dye treated samples of *T. versicolor* (presented in section **5.6.1**)

Index	Sample ID	Total read bases*	Total reads	GC (%)	Q20 (%)	Q30 (%)
1	1CB8CONT	6,301,273,790	41,730,290	60.12	97.89	94.53
2	2CB8CONT	6,197,750,304	41,044,704	60.12	98.53	95.83
3	3CB8CONT	6,197,305,458	41,041,758	60.42	98.66	96.05
4	4CB8RBBR	6,333,365,216	41,942,816	60.29	97.84	94.36
5	5CB8RBBR	6,287,189,718	41,67,018	60.73	98.10	94.84
6	6CB8RBBR	6,475,747,042	42,885,742	60.38	98.03	94.75
7	7CB8EB	6,226,401,044	41,234,444	60.45	98.06	94.75
8	8CB8EB	6,198,374,236	41,048,836	60.45	97.95	94.60
9	9CB8EB	5,728,816,180	37,939,180	60.44	97.94	94.59

(Note: * Total read bases = Total reads x Read length;
Total read bases: Total number of bases sequenced;
Total reads: Total number of reads;
GC (%): GC content;
Q20 (%): Ratio of bases that have Phred quality score greater than or equal to 20;
Q30 (%): Ratio of bases that have Phred quality score greater than or equal to 30)

List of Figures

List of Appendix Figures

List of Tables

List of Appendix Tables